Dipeptidyl Peptidase−4 in Cardiometabolic Disease

Natasha A. Trzaskalski

A thesis submitted in partial fulfillment of the requirements for the

Doctorate in Philosophy degree in Biochemistry

Department of Biochemistry, Microbiology and Immunology

Faculty of Medicine

University of Ottawa

Abstract

The cardiovascular implications of modulating cell specific expression of the serine protease dipeptidyl peptidase-4 (DPP4) were investigated in a series of murine models of metabolic dysfunction-associated steatotic liver disease (MASLD), cardiometabolic disease and myocardial infarction. *In vivo* experiments were conducted using several genetic models, including systemic *Dpp4* knockout mice (*Dpp4*$^{-/-}$), hepatocyte-specific knockout mice (*Dpp4*$^{hep-/-}$) and endothelial cell-specific knockout mice (*Dpp4*$^{EC-/-}$), which were challenged with high-fat, high cholesterol (HFHC) feeding, to induce MASLD and heart failure (HF), and exacerbate surgical myocardial infarction (MI). Pharmaceutical modulation of DPP4 was also performed by adding the DPP4 inhibitor (DPP4i) sitagliptin, and/or metformin, to drinking water. Molecular studies were then performed to evaluate the role of DPP4 in hepatic steatosis, hepatic glucose production (HGP), inflammation and fibrosis, together with echocardiography to evaluate cardiac function. Genetic ablation of hepatocyte-derived DPP4 increased incretin hormone bioactivity in the portal vein, which was associated with reduced HGP. Liver fibrosis and gene expression of immune-related pathways were increased in aged, obese *Dpp4*$^{-/-}$ mice, however liver steatosis and plasma lipids were unchanged. Conversely, expression of immune-related pathways was unchanged in *Dpp4*$^{hep-/-}$ mice. Additionally, in a lean model of MASLD, DPP4 activity increased, dissociating its enzymatic activity from obesity, while DPP4 protein decreased with viral clearance in patients with HCV treated with antiviral drugs. Within the heart of HFHC-diet fed aged mice, immune-related pathways in *Dpp4*$^{hep-/-}$ were reduced in ventricular tissue. Despite these molecular changes in the heart, there were no functional changes in systolic and diastolic parameters. Lastly, *Dpp4*$^{-/-}$, *Dpp4*$^{hep-/-}$ and *Dpp4*$^{EC-/-}$ mice were treated with sitagliptin, metformin or a combination of these drugs (dual therapy) to investigate the clinical cardioprotective outcomes. Four weeks after left anterior descending (LAD) coronary artery-ligation, cardiac function demonstrated via left ventricular ejection fraction (LVEF) was significantly increased in *Dpp4*$^{hep-/-}$ mice compared to controls with dual therapy treatment, both pre- and post-MI. This was not associated with a higher prevalence of fully kinetic myocardia, however *Dpp4*$^{EC-/-}$ mice did indeed have more fully kinetic hearts without changes in LVEF. Evaluating DPP4 activity and protein over time revealed a dissociated relationship between these measurements, where activity decreased 7 days after infarct, while protein continued to rise until endpoint. Overall, this thesis highlights the complexity of DPP4 biology in multiple diseases, and its utility as a therapeutic target.

Dedicated to the most important and inspiring woman in my life,
Mom, I owe all my success to you, and your belief in me,
I love you.

Acknowledgements

This thesis, and all it includes, would not have been possible without the guidance, support and kindness of my supervisor, Dr. Erin Mulvihill. She absolutely took a chance on me, and I could not be more thankful. Entering medical research after working with plants was truly an uphill battle, however, there is no other scientist I can imagine climbing that mountain with. It was such a privilege to learn from an incredible woman in science who instilled confidence in my abilities and showed patience when I had lost all hope. The future is very bright for someone like that who possesses these qualities, alongside an insatiable hunger for scientific discovery. The best is yet to come, and I cannot wait to bear witness to it from wherever I am.

Additionally, my thesis advisory committee members, Dr. Thomas Lagace, Dr. Kyoung-Han Kim and Dr. Mathieu Lavallée-Adam, were instrumental in my growth over the course of my PhD. Their constructive criticism, thoughtful ideas to strengthen my research and overall encouragement were paramount to my success and are exemplified throughout this thesis. I would also like to thank Dr. Katey Rayner for her compassion and kindheartedness. Further, I would like to specifically recognize the expertise, helpfulness and friendship that I was lucky to experience from the UOHI ACVS staff, including Dan de Vette, Caroline St-Denis, Emily Beaudoin, Claire Wolf and Rick Seymour.

I would be remiss to not thank my current and former lab mates and friends who supported me throughout my studies. I have the distinct privilege of calling Nadya Morrow and Andrew Clément my best friends, a title they each live up to. Without them I would have no one to complain to, laugh with, or yap to. I cannot imagine my PhD, or life, without them, and no words can begin to describe how thankful I am for their unwavering friendship. I cannot forget my first best friend, Dr. Adil Rasheed, and his better half, Dr. Sabrina Robichaud. Again, nothing I say or do can fully or effectively add up to a ‘thank you’ that Adil deserves. In both my research and personal life, I would not be where I am today without his support, and for that, I am immeasurably grateful. Sabrina is one of the reasons why I still have some of my sanity intact. Thank you, Sabrina, for your friendship, unconditional support and for allowing me to be a perpetual third wheel in your marriage. Lastly, I would like to thank all my other friends without whom I would be bored to death, less sane and much less successful; Antonio Hanson, Serena Pulente, Cassie Locatelli, Cameron Stotts, Claire Fong-McMaster and Tyler Smith.

Most importantly, I would like to wholeheartedly thank my family. My Babcia and Dziadzi who instilled in me a strong work ethic and emphasized the importance of an education. My Dad who supported me in every way he could; I wish you were here to see the person I have grown to be. My sister, Nicole, who keeps my life eventful, fun and bright, I am lucky to have you as my lifelong best friend. My brother-in-law, Kyle, who can finally stop asking me when I’ll get a real job, I am fortunate to have him on my side and I am so thankful to call him family. My step-in-dad, Dan, who excels as honourary dad, supporting me through school and in life. He is cherished beyond words; I am extraordinarily luck to know and love him. Lastly, my mom, to whom this thesis is dedicated to. No amount of thanks or praise could begin to fully encompass the amount of gratitude I have for her, her support, love and steadiness. She has supported me through my entire life and this achievement could not be possible without her. She is my biggest inspiration, my best friend and the only person I think to call when I need support with a tear-filled conversation. I hope I have made her as proud as she has made me.

Co-authorship Statement

Natasha A. Trzaskalski and Dr. Erin E. Mulvihill confirm that more than 50% of the manuscripts in this thesis were written by Natasha A. Trzaskalski.

Chapter 2

All mouse breeding, colony management and genotyping was performed by Dr. Ilka Lorenzen-Schmidt.

Animal sacrifice at endpoint was performed by Natasha A. Trzaskalski, Dr. Branka Vulesevic, Rick Seymour and Dr. Erin. E. Mulvihill.

Hyperinsulinemic-euglycemic clamps and associated measurements and calculations were conducted by Dr. Julia R.C. Nunes, Conor O'Dwyer and Dr. Morgan D. Fullerton. Accompanying gene expression analysis was performed by Natasha A. Trzaskalski and Antonio A. Hanson.

Portal vein studies were planned and executed by Natasha A. Trzaskalski. PTT and ATT experiments were designed, planned and lead by Natasha A. Trzaskalski, with assistance from Nadya M. Morrow, My-Anh Nguyen, Serena M. Pulente and Andrew C. Clément. Associated molecular assays were performed by Natasha A. Trzaskalski.

Oral glucose tolerance tests in our obese and aged NAFLD mice were conducted by Dr. Branka Vulesevic, Evgenia Fadzeyeva and Dr. Ilka Lorenzen-Schmidt, and GLP-1 assays were performed by Natasha A Trzaskalski. Glycogen content was evaluated by Dr. Branka Vulesevic and Dr. Ilka Lorenzen-Schmidt. Liver histology was completed by Dr. Branka Vulesevic and Dr. Ilka Lorenzen-Schmidt. Associated gene expression analysis was conducted by Natasha A. Trzaskalski, Antonio A. Hanson and Natasha Jeraj. Related plasma and liver cytokine and chemokine protein assays were conducted by Natasha A. Trzaskalski, Dr. Branka Vulesevic, Natasha Jeraj and Cassandra A. A. Locatelli. Lipid analysis was performed by Natasha A Trzaskalski and Nadya M. Morrow.

F4/80+ cells were isolated by Dr. Branka Vulesevic and Natasha Jeraj. Subsequent NanoString mRNA experiment analysis was performed by Natasha A. Trzaskalski and confirmed by Dr. Han Kim, confirmatory immunofluorescence, and analysis, were conducted by Natasha A. Trzaskalski.

Clinical samples were provided by Dr. Angela M. Crawley, Dr. Mary Anne Doyle and Dr. Curtis L. Cooper. Sample analysis was conducted by Dr. Branka Vulesevic, Natasha Jeraj and Nicole Travis.

Pemt$^{-/-}$ mice were provided by Dr. Jelske N. van der Veen and Dr. René L. Jacobs. Associated molecular analyses were conducted by Natasha Jeraj.

Data analysis and data visualization were primarily performed by Natasha A. Trzaskalski, with assistance from Dr. Branka Vulesevic, Natasha Jeraj and Dr. Ilka Lorensen Schmidt.

Chapter 3

All mouse breeding, colony management and genotyping was performed by Dr. Ilka Lorenzen-Schmidt.

Animal sacrifice at endpoint was performed by Natasha A. Trzaskalski, Dr. Branka Vulesevic, Rick Seymour and Dr. Erin. E. Mulvihill.

Echocardiography was performed by Natasha A. Trzaskalski and Rick Seymour. Subsequent analysis was completed by Melissa M. Dann, Dr. Branka Vulesevic and Dr. Ilka Lorenzen-Schmidt.

All NanoString mRNA experiment, analysis and data visualization were conducted by Natasha A. Trzaskalski.

Molecular assays were completed by Dr. Branka Vulesevic, Evgenia Fadzeyeva and Natasha Jeraj. Gene expression analysis was conducted by Natasha A. Trzaskalski and Antonio A. Hanson.

Data analysis and data visualization were primarily performed by Natasha A. Trzaskalski, with assistance from Dr. Branka Vulesevic, Natasha Jeraj and Dr. Ilka Lorensen Schmidt.

Chapter 4

All mouse breeding, colony management and genotyping was performed by Dr. Ilka Lorenzen-Schmidt.

Preliminary study animal sacrifices were performed by Dr. Branka Vulesevic and Natasha Jeraj. Main study animal sacrifices were performed by Natasha A. Trzaskalski.

Echocardiography was performed by Natasha A. Trzaskalski. Subsequent analysis was completed by Natasha A. Trzaskalski and Jessica Hursti.

Plasma DPP4 molecular assays were conducted by Natasha A. Trzaskalski abd Jessica Hursti. Preliminary data molecular assays were completed by Natasha Trzaskalski, Dr. Branka Vulesevic and Natasha Jeraj.

Preliminary study gene expression analyses and chemokine assays were completed by Dr. Branka Vulesevic and Natasha Jeraj.

Data analysis and data visualization were primarily performed by Natasha A. Trzaskalski, with assistance from Jessica Hursti, Dr. Branka Vulesevic and Natasha Jeraj.

Table of Contents

List of Abbreviations

αSMA	α-smooth muscle actin
AAV	Adeno-associated virus
ACC	Acetyl-CoA carboxylase
ACTB	β-actin
ADA	Adenosine deaminase
aDLS	Average diastolic longitudinal strain
aDLSR	Average diastolic longitudinal strain rate
ADP	Adenosine diphosphate
aDRS	Average diastolic radial strain
aDRSR	Average diastolic radial strain rate
ALP	Alkaline phosphatase
ALT	Alanine transaminase
AMP	Adenosine monophosphate
AMPK	Adenosine monophosphate-activated protein
ANKRD1	Ankyrin repeat domain 1
ANP	Atrial natriuretic peptide
ApoC1	Apolipoprotein C1
Asn	Asparagine
AST	Aspartate transaminase
AT	Adipose tissue
ATP	Adenosine triphosphate
AVC	Aortic valve closure
B-mode	Brightness mode
BMDM	Bone marrow-derived macrophage
BNP	Brain natriuretic peptide
BPM	Beats per minute
BW	Body weight
Ca^{2+}	Calcium ion
cAMP	Cyclic adenosine monophosphate
CAV	Caveolin
CETP	Cholesterol ester transfer protein
cGMP	Cyclic guanosine monophosphate
ChREBP	Carbohydrate response element-binding protein
CO	Cardiac output
COL1A1	Collagen type 1, α1
COL3A1	Collagen type 3, α1
CP	Cardiac puncture
CTGF	Connective tissue growth factor
CV	Cardiovascular

CVD	Cardiovascular disease
CVOT	Cardiovascular outcome trial
CXCR4	C-X-C chemokine receptor type 4
d	Diastole
DAG	Diacylglycerol
DAMP	Danger-associated molecular pattern
DNA	Deoxyribonucleic acid
DNL	*De novo* lipogenesis
DPP4	Dipeptidyl peptidase-4
Dpp4$^{-/-}$	Systemic *Dpp4* knockout mouse
Dpp4$^{+/+}$	*Dpp4* wildtype mouse
Dpp4$^{EC-/-}$	Endothelial cell-specific *Dpp4* knockout mouse
Dpp4$^{hep-/-}$	Hepatocyte-specific *Dpp4* knockout mouse
DPP4i	Dipeptidyl peptidase-4 inhibitor
EC	Endothelial cell
ECG	Electrocardiogram
ECM	Extracellular matrix
EDLVM	End diastolic left ventricular mass
EDP	End-diastolic pressure
EPDR1	Ependymin related 1
ER	Endoplasmic reticulum
ESLVM	End systolic left ventricular mass
FA	Fatty acid
$FADH_2$	Flavin adenine dinucleotide
FAO	Fatty acid oxidation
FAP	Fibroblast activation protein
FAT/CD36	Fatty acid translocase
FATP	Fatty acid transfer protein
FDA	Food and Drug Administration
FFA	Free fatty acid
FoxO1	Forkhead box O1
G-CSF	Granulocyte colony-stimulating factor
G6P	Glucose 6-phosphate
gDNA	Genomic deoxyribonucleic acid
GDR	Glucose disposal rate
GFP	Green fluorescent protein
GHBP	Growth hormone binding protein
GIP	Glucose-dependent insulinotropic polypeptide
GIPR	Glucose-dependent insulinotropic polypeptide receptor
GIR	Glucose infusion rate
GLP-1	Glucagon-like peptide-1

GLP-1R	Glucagon-like peptide-1 receptor
GLP-1RA	Glucagon-like peptide-1 receptor agonist
GLP-2	Glucagon-like peptide-2
GLS	Global longitudinal strain
Glu	Glutamic acid
GLUT2	Glucose transporter type 2
GLUT4	Glucose transporter type 4
GM-CSF	Granulocyte-macrophage colony-stimulating factor
GSIS	Glucose stimulated insulin secretion
GSK3β	Glycogen synthase kinase-3 β
H_2O_2	Hydrogen peroxide
HbA1c	Glycated hemoglobin
HCC	Hepatocellular carcinoma
HCV	Hepatitis C virus
HDL	High-density lipoprotein
HF	Heart failure
HFD	High-fat diet
HFHC	High-fat, high cholesterol
HFpEF	Heart failure with preserved ejection fraction
HFrEF	Heart failure with reduced ejection fraction
HGP	Hepatic glucose production
HIV	Human immunodeficiency virus
HMGB1	High mobility group box-1
HOMA-IR	Homeostatic Model Assessment of Insulin Resistance
HR	Heart rate
HSC	Hepatic stellate cell
HW	Heart weight
HYTANE	Hydrophobic Tagging-Assisted N-termini Enrichment
i.p.	Intraperitoneal
i.v.	Intravenous
IFN	Interferon
IGFBP1	Insulin-like growth factor-binding protein 1
IL	Interleukin
INSR	Insulin receptor
IP-10	Interferon gamma-induced protein 10
IR	Insulin resistance
IRS	Insulin receptor substrate
IVRT	Isovolumetric relaxation time
IVS	Interventricular septal thickness
JAK-STAT	Janus kinase-signal transducer and activator of transcription
JNK	c-Jun N-terminal kinase

KC	Kupffer cell
KLK5	Kellikrein-related peptidase 5
LAD	Left anterior descending coronary artery
LD	Lipid droplet
LDL	Low-density lipoprotein
LoxP	Locus of X-over P1
LS	Longitudinal strain
LSR	Longitudinal strain rate
LVEF	Left ventricular ejection fraction
LVID	Left ventricular internal diameter
LVPW	Left ventricular posterior wall thickness
M-CSF	Macrophage colony-stimulating factor
MACE	Major adverse cardiovascular endpoint
MAFLD	Metabolic dysfunction-associated fatty liver disease
MAPK	Mitogen-activated protein kinase
MASH	Metabolic dysfunction-associated steatohepatitis
MASLD	Metabolic dysfunction-associated steatotic liver disease
MCP-1	Monocyte chemoattractant protein-1
METAVIR	Meta-analysis of histological data in viral hepatitis
MI	Myocardial infarction
MIP-1α	Macrophage inflammatory protein-1α
MMP	Matrix metalloproteinase 2 LV
mRNA	Messenger ribonucleic acid
MTTP	Microsomal triglyceride transfer protein
NAALADase	N-acetyl alpha-linked acidic dipeptidase
NADH	Nicotinamide adenine dinucleotide
NAFLD	Non-alcoholic fatty liver disease
Nano-LC-M/MS	Nano-liquid chromatography tandem mass spectrometry
NAPDH	Nicotinamide adenine dinucleotide phosphate
NASH	Non-alcoholic steatohepatitis
NF-κB	Nuclear factor-κB
NO	Nitric oxide
OCT1	Organic cation transporter 1
$ONOO^-$	Peroxynitrite
PE	Peak ejection
PEMT	Phosphatidylethanolamine N-methyltransferase
PI3K	Phosphatidylinositol-3-OH kinase
PIP2	Phosphatidylinositol-4,5-triphosphate
PIP3	Phosphatidylinositol-3,4,5-triphosphate
PKA	Protein kinase A

PKB/AKT	Protein kinase B
PKC	Protein kinase C
PKG	Protein kinase G
PTM	Post-translational modification
PV	Portal vein
PYY	Peptide YY
qRT-PCR	Quantitative real-time reverse-transcription polymerase chain reaction
RANTES	Regulated on activation, normal T-cell expressed and secreted
RNA	Ribonucleic acid
ROS	Reactive oxygen species
RS	Radial strain
RSR	Radial strain rate
s	Systole
SASP	Senescence-associated secretory phenotype
SDF-1	Stromal-derived factor 1
sDPP4	Soluble dipeptidyl peptidase-4
sICAM-1	Soluble intercellular adhesion molecule-1
siRNA	Small interfering ribonucleic acid
SLD	Standard laboratory diet
SMAD	Mothers against decapentaplegic
SREBF1	Sterol regulatory element-binding protein 1
SREBP-1c	Sterol regulatory element-binding protein 1c
STE	Speckle tracking echocardiography
STZ	Streptozotocin
SV	Stroke volume
T2D	Type 2 diabetes
TAC	Trans-aortic constriction
TAILS	Terminal Amine Isotopic Labelling of Substrates
tApoC1	Truncated apolipoprotein C1
TBG	Thyroxine binding globulin
TCA	Tricarboxylic acid
Tek/Tie2	Receptor tyrosine kinase
TG	Triglyceride
TGF-β	Transforming growth factor β
TGFBI	Transforming growth factor β induced
TIMP	Tissue inhibitors of metalloproteinase
TL	Tibia length
TLR	Toll-like receptor
TNFα	Tumour necrosis factor-α

TTP	Time-to-peak
UPR	Unfolded protein response
VEGF	Vascular endothelial growth factor
WT	Wildtype

List of Tables

List of Figures

1. Introduction

1.1 Cardiovascular Disease

Cardiovascular disease (CVD) is the second leading cause of death in Canada accounting for 17.5% of deaths in 2020[1]. In comparison to COVID-19 in 2020, more Canadians died from heart disease or stroke than from complications from the virus itself (67,399 vs. 16,151)[1]. In Canada, approximately 70,000 patients with acute myocardial infarction (MI) are admitted to Canadian hospitals each year[2]. Of these individuals, 5,000 will die and between 10-15% are readmitted[3]. MI is typically preceded by the development of atherosclerosis, a chronic process characterized by the subendothelial accumulation of lipids and a non-resolving inflammatory response[4,5]. Atherosclerotic plaque rupture may result in a thrombus leading to acute occlusion of a coronary artery, the initiating event in MI[6].

This acute injury, or chronic and cumulative stress resulting from metabolic disease (e.g., obesity, hypertension and type 2 diabetes (T2D)), can proceed to heart failure (HF), a chronic and progressive condition that occurs when the heart cannot sufficiently pump enough blood and oxygen to support peripheral tissue and organs[7]. The Heart and Stroke Foundation estimates that approximately 750,000 Canadians are living with HF, making it one of the top reasons for hospital admissions which will cost Canadians more than $2.8 billion dollars a year by 2030[2,8,9]. Risk factors such as age, smoking, a sedentary lifestyle and stress, and comorbidities including diabetes, obesity, hypertension and hypercholesteremia, all contribute to the development and progression of CVD[10,11].

1.1.1 Myocardial Infarction

Upon coronary artery occlusion, downstream cardiac tissue injury is marked by

massive cell death in the infarcted area that initiates an inflammatory response[12]. After this initial inflammation, spatial containment and suppression of the reaction is essential to limit tissue damage and infarct size; healing begins with inflammation suppression[13]. Prolonged inflammation drives adverse remodelling and functional cardiac failure (e.g., reduced left ventricular ejection fraction, LVEF) can occur[14,15].

Within a period of 3-4 days from infarction, in both humans and mice, immune cell infiltration clears damaged and dead cells and extracellular matrix (ECM)[15,16]. This typically occurs between the infarct and unaffected myocardium, termed the border or peri-infarct zone[17], an area comprised of dysfunctional myocardium that is hypocontractile and fibrotic, however, still oxygenated[18]. Angiogenesis occurs within 2 days through the peri-infarct into the infarct zone, and after 7 days, new vessels enlarge and acquire smooth muscle cell support[19]. Cardiomyocyte necrosis leads to endothelial cell activation, acquiring an immunoregulatory and procoagulant phenotype, expressing cell adhesion molecules[20], and promoting immune cell infiltration[16]. Necrosis and ECM fragments deliver the primary inflammatory stimulus by releasing danger-associated molecular patterns (DAMPs)[21,22], including high mobility group box-1 (HMGB1)[23] and fibronectin extra domain A[24]. Once bound to their respective receptor, downstream activation of mitogen-activated protein kinases (MAPKs) and nuclear factor-κB (NF-κB) occurs[25]. The latter drives expression of proinflammatory genes, including tumour necrosis factor-α (TNFα), interleukin-1β (IL-1β), and CXC and CC chemokines[26,27]. These factors recruit leukocytes (neutrophils, monocytes and T-lymphocytes) and stimulate resident macrophage proliferation which further augments the inflammatory response, DAMPs production, efferocytosis,

tissue digestion and proteolysis via the release of proteases and oxidases[16,28,29]. Pivotal studies demonstrated a biphasic functional heterogeneity among monocytes and macrophages after infarct[28,30,31]. After approximately 7 days, post-infarct inflammation resolution is mediated by reparative monocytes and macrophages, with increased expression of anti-inflammatory, profibrotic and angiogenic factors, including transforming growth factor β (TGF-β), vascular endothelial growth factor (VEGF) and IL-10[32]. Neutrophil apoptosis and necrosis occur as the cardiac molecular environment transitions from pro- to anti-inflammatory[16,33,34]. Phagocytosis of neutrophils by macrophages, induces a pro-resolving phenotype, and results in the release of anti-inflammatory and pro-fibrotic cytokines which aid in suppressing inflammation and stimulating tissue repair[35,36]. In the final healing stage, immune and reparative cells are deactivated[16].

Inflammation resolution, cardiac fibroblast population expansion and transformation into synthetic myofibroblasts mark the 'proliferative phase'[37-39]. Further, recent studies suggest that adult cardiomyocytes have a small, limited capacity for proliferation, contrary to earlier reports describing them as postmitotic[40-46]. However, this is not sufficient to restore the cardiomyocyte population, therefore, the remaining cells undergo hypertrophy to adapt to the physical demands of the heart[47,48]. The temporary cardiac matrix, composed of fibrin and fibronectin to prevent acute rupture, is replaced by ECM[49,50]. Initially, normally quiescent cardiac fibroblasts acquire a proinflammatory phenotype and serve as an important source of chemokines and cytokines[51,52]. In this phase however, TGF-β is induced globally after MI and is especially indicated in myofibroblast transdifferentiation and activation[53].

Further, activated myofibroblasts express α-smooth muscle actin (αSMA), allowing scar contraction[38,54]. Normally lowly expressed matricellular proteins are upregulated following MI, including osteopontin[55] and periostin[56,57] which modulate cell function and prevent adverse remodelling, rather than serving a structural role[58]. Eventually, in the 'maturation phase, the ECM becomes cross-linked[16]. Tensile strength of the scar is increased as thick type I collagen replaces thin type-III collagen[59-61]. This matrix becomes devoid of cells as leukocytes undergo apoptosis and inflammation continues to resolve[61]. Myofibroblasts are deactivated, enter a quiescent state and may undergo apoptosis, presumably via inhibitory signals from the clearance of ECM[62]. The mature scar can remain stable without causing functional issues for years, however, fibrosis diffusion further into the viable border zone and remote regions can result in adverse remodeling and subsequent HF[61].

1.1.2 Heart Failure

HF develops after MI due to cardiomyocyte death and scar formation, triggering neurohormonal activation and ventricular remodeling such as wall thinning and mitral valve regurgitation[63]. HF can be stratified into three types; left-sided, right-sided and biventricular, which affect the left, right and both ventricles, respectively[64]. Left-sided or left-ventricular HF can be further subdivided into HF with preserved ejection fraction (HFpEF; diastolic HF), and HF with reduced ejection fraction (HFrEF; systolic HF)[65]. Notably, HFpEF presents with a LVEF ≥50% and HFrEF ≤ 40%, where LVEF is a fraction of the blood volume ejected at systole related to the volume of blood in the ventricle at diastole[66,67]. More recently, international societies like the European Society of Cardiology have proposed HF with mildly reduced EF, where patients

present with a LVEF between 41-49%[7,66,68]. Even though HFrEF and HFpEF share similar risk factors and comorbidities, substantial differences in inflammation, oxidative and nitrosative stress and fibrosis lead to differing cardiac dysfunction[69].

1.1.2.1 Molecular Mechanisms in HFrEF and HFpEF

In HFrEF, inflammation directly results from cardiomyocyte damage and death, contrasting HFpEF, which arises from peripheral metabolic and inflammatory risk factors like obesity and T2D[70]. Cardiomyocyte death in HFrEF leads to cytokine release, activating downstream signaling such as NF-κB , MAPK and interferon (IFN) that upregulate pro-inflammatory cytokines for repair[71,72]. Dying cells release MMPs which degrade ECM[49,73], and infiltrating immune cells, specifically monocytes, produce anti-inflammatory cytokines and growth factors to promote angiogenesis and scar formation by myofibroblast activation[28]. Recruited regulatory T-cells play a protective role by attenuating inflammation and reducing infiltration, however this is not sufficient to prevent damage and adverse remodeling oftentimes[74].

In individuals with HFpEF, clinical peripheral blood analyses indicate increased circulating cytokines, such as IL-1β, IL-6, IL-10, TNFα and C-reactive protein, originating not only from immune cells, but also from inflamed metabolic tissues like adipose tissue (AT) and steatotic hepatocytes[75-78]. Vascular endothelial inflammation (IL-1, IL-6, IL-8, macrophage colony-stimulating factor (M-CSF), granulocyte-macrophage CSF (GM-CSF) and monocyte chemoattractant protein-1 (MCP-1)) and expression of endothelial adhesion molecules vascular cell adhesion molecule 1 and E-selectin lead to monocyte recruitment for transendothelial migration[79-81]. Monocytes undergo differentiation and activation into macrophages, at which point, macrophage-

derived mediators and pro-inflammatory cytokines (connective tissue growth factor (CTGF), fibronectin and TGF-β) promote myofibroblast proliferation and activation from quiescent tissue-resident fibroblasts[82]. ECM and matricellular proteins are produced from continual myofibroblast activation, and collagen crosslinking prevents degradation and increased stiffness, leading to reactive and diffuse fibrosis which is typically in the interstitial and perivascular areas[83-85]. Further, activation of the Janus kinase (JAK)-signal transducer and activator of transcription (STAT) (JAK-STAT) pathway via TGF-β and IL-1 signaling lead to mothers against decapentaplegic homolog 2-4 (SMAD2-4) phosphorylation and increased profibrotic gene expression[75]. Comparatively, replacement fibrosis is a reparative mechanism in HFrEF where granulation tissue, a temporary fibrin matrix, replaces dead cells after ischemia until it is superseded by a collagen-based matrix and a mature scar[16,86]. This fibrosis is essential acutely after MI to prevent ventricular wall rupture and death[86], but may also be present in HFpEF due to micro scars in small pockets of cardiomyocyte death[87].

Endothelial dysfunction occurs in both HFrEF and HFpEF; however, it occurs later in the former and more severely and earlier in the latter[70]. Nonetheless, this leads to imbalanced nitric oxide (NO) bioavailability[70,88]. Nitroso-redox imbalance leads to decreased coronary endothelium-dependent vasodilation, impairing myocardial perfusion and worsening ventricular dysfunction[89]. There is also a cyclical worsening of endothelial function; as NO bioavailability is reduced, dysfunction continues and HFrEF progresses[90]. In both cases, proinflammatory cytokines induce endothelial production of reactive oxygen species (ROS) through activation of nicotinamide

adenine dinucleotide phosphate (NAPDH) oxidases[91,92]. ROS production ultimately leads to the formation of peroxynitrite ($ONOO^-$) and reduces NO bioavailability, both of which lower cyclic guanosine monophosphate (cGMP) production, and subsequently reduce protein kinase G (PKG) activity[80,93]. Decreased PKG increases resting tension of cardiomyocytes and prevents vasorelaxation[94,95], primarily through hypophosphorylation and abundance of the stiffer N2B isoform of titin[96,97]. Further, reduced cGMP and PKG activity result in increased diastolic cytosolic calcium and delayed relaxation, as well as cardiomyocyte hypertrophy, respectively[98-101]. In contrast, in HFrEF, cardiac biopsies indicate more of the flexible N2Ba isoform of titin[102]. Dephosphorylation and aggregation of titin leads to increased passive tension, increasing cardiac stiffness[103], which can be interestingly relieved by MMP2 cleavage[104].

1.1.2.2 Systolic and Diastolic Dysfunction in HFrEF and HFpEF

The pathophysiological differences between HFrEF and HFpEF lead to variances in function, namely in presentation of systolic and diastolic dysfunction. In HFrEF, cardiomyocytes appear thinner and elongated with lower myofibrillar density[80]. The spherical shape of the left ventricle (LV) leads to decreased function, including stroke volume (SV; blood volume pumped out at each contraction), cardiac output (CO; amount of blood pumped out per minute), end-diastolic pressure (EDP; amount of blood in the ventricle when relaxed) and impaired ventricular filling[105]. To facilitate compensation, venous pressure and blood volume are increased[106]. Cardiac preload and afterload, stretching of the heart wall before contraction, and the force required for contraction are increased, leading to wall stress[107]. Collectively, these

abnormalities prevent the heart from pumping enough blood to support the periphery[69].

HFpEF presents with a normal LVEF; however, impaired relaxation of the LV prevents adequate filling and reduces the volume of blood pumped out (SV) to the periphery[108]. Contrasting eccentric remodelling typically observed in HFrEF, concentric remodelling occurs in HFpEF where the LV wall thickens making the lumen smaller[109]. The LV typically relaxes slowly (increased isovolumetric relaxation time; IVRT), with greater resistance and increased EDP[110]. Like in HFrEF, SV and CO are reduced[110,111]. Since LVEF is normal, diagnosis is complicated and testing only begins when symptoms such as fatigue, dyspnea and swelling in the extremities appear[112]. Echocardiography may be used to assess LV structure such as wall thickening. In particular, pulsed-wave and tissue doppler may be used to assess blood and tissue velocity, respectively[113]. Lastly, speckle tracking echocardiography (STE), or strain and strain rate analysis, is used to identify abnormalities in myocardial kinetics and deformation patterns in the radial, longitudinal and circumferential plane[114-116]. STE can be used to identify minute changes otherwise overlooked by standard echocardiography[117,118].

1.2 Metabolic Dysfunction-Associated Steatotic Liver Disease

Non-alcoholic fatty liver disease (NAFLD), is a spectrum of liver diseases ranging from simple steatosis to end-stage cirrhosis and hepatocellular carcinoma (HCC) [119]. It is now the most common chronic liver disease in developed countries[120,121], which currently affects approximately 25-33% of the global population[122-124]. Environmental factors (hypercaloric diet, sedentary lifestyle) in combination with metabolic syndrome, advanced age, dyslipidemia, T2D and obesity

can lead to NAFLD[125]. More recently in 2020, a new term was proposed to describe fatty liver resulting from T2D and obesity, metabolic dysfunction-associated fatty liver disease (MAFLD), diagnosed in individuals who meet two of seven parameters of metabolic dysnfunction[126]. Now, in 2023, metabolic dysfunction-associated steatotic liver disease (MASLD) was proposed and is diagnosed when patients meet one of five cardiovascular (CV) risk factors, such as advanced age, obesity and hyperglycemia[127]. NAFLD was considered an exclusionary acronym which did not consider the cause of the disease, leading to the introduction of inclusionary terms MAFLD and then MASLD, as long as alcohol consumption is less than 20 or 30 grams per day in females and males, respectively[128]. Hereinafter, MASLD will be used throughout this thesis apart from Chapter 2 and previously published work that uses other terms. Without intervention, simple steatosis progresses to non-alcoholic steatohepatitis (NASH) or metabolic dysfunction-associated steatohepatitis (MASH), in an estimated 5-6% of people, and is defined as an irreversible condition that is characterized by fat accumulation, inflammation and fibrosis[129,130]. Without intervention, this condition progresses into irreversible cirrhosis in approximately 20% of individuals, with worsening fibrosis and decompensation[131,132], leading to an increased risk of HCC[133].

The pathogenesis of MASLD involving multiple organ systems often begins with a substrate imbalance. Simple steatosis is defined as excessive lipid accumulation in the liver in more than 5% of hepatocytes, independent of inflammation and fibrosis[125]. MASLD may occur in lean individuals due to genetic disorders[134-136], infectious disorders (i.e., hepatitis C virus (HCV)[137,138], human immunodeficiency virus (HIV)[139]) and with certain drugs[140] (i.e., amiodarone and tamoxifen). Interestingly,

MASLD (previously defined as NAFLD) presents in approximately 55% of individuals living with HCV[141]. In HCV associated MASLD, disease progression and HCC development were driven by inflammation and oxidative stress irrespective of insulin resistance (IR)[142,143]. However, the initiating events of MASLD typically include unresolved obesity and IR[144-148]. In individuals with obesity, AT reaches its storage and expansion capacity, leading to storage of excess lipids in hepatocytes[149,150]. Specifically, increased fatty acid (FA) uptake and export, reduced FA oxidation (FAO), accelerated lipolysis and hepatic *de novo* lipogenesis (DNL) collectively lead to ectopic hepatic lipid accumulation[151]. Insulin plays an important role in free FA (FFA) homeostasis by inhibiting AT lipolysis, via lipoprotein lipase LPL[152,153]. Lipolysis is increased with IR or with decreased insulin sensitivity, typical in metabolic disease, leading to increased circulating FFA, increasing lipid content within the liver[154]. FFA uptake is mediated via plasma membrane proteins such as FA transport proteins (FATPs), caveolins (specifically CAV1) and FA translocase (FAT/CD36), whose expression is significantly increased in individuals with MASLD[155]. Following uptake, FA binding protein 1 facilitates transportation of FAs between organelles and enables its oxidation and incorporation into triglycerides (TGs)[156,157]. FFA may undergo mitochondrial and peroxisomal β-oxidation to generate acetyl-CoA, adenosine triphosphate (ATP) and hydrogen peroxide (H_2O_2)[158-160]. Further, intracellular FAs may also undergo esterification to form TGs, which can play a protective role against lipotoxicity[161] At this point, TGs can be assembled on apolipoprotein B100 and exported into circulation as very low-density lipoproteins or may remain in hepatocytes stored in cytosolic lipid droplets (LDs)[162]. Hepatic LD turnover, or degradation, to form

hepatic FAs may also occur; if these lipids are not incorporated into more complex forms of lipids like TGs or lipoproteins, they lead to lipotoxic species[163,164]. Lipotoxic lipids can elicit organelle dysfunction, cell injury and inflammation when they accumulate in the cytosol of non-AT organs, such as the liver[161,165]. TGs, for example, are inert and do not cause cellular dysfunction, however, accumulation of its toxic intermediates like saturated FAs, glycerophospholipids (i.e., diacylglycerols; DAGs), and sphingolipids (i.e., ceramides) contribute to MASLD pathogenesis[166-170].

The second major source of FAs in the liver is DNL, a process by which lipids are endogenously synthesized, typically from dietary carbohydrates, such as glucose[171]. Conversion of glucose in DNL is highly regulated and dependent on glycolytic enzymes controlled by insulin, ATP and citrate[172]. IR enhances DNL[173], and is regulated post-prandially through insulin and glucose mediated stimulation of lipogenic enzyme promotors and transcription factors sterol regulatory element-binding protein 1c (SREBP-1c) and carbohydrate response element-binding protein (ChREBP)[174]. Glucose is metabolized via glycolysis to produce ATP and pyruvate, or it may be stored as glycogen[175]. The conversion of fructose-6-phosphate, the second metabolite produced in glucose metabolism, to fructose-1-6-biphosphate is tightly regulated by phosphofructokinase which is inhibited by ATP and citrate when energy status is high[176,177]. Pyruvate is converted to acetyl-CoA by the pyruvate dehydrogenase complex, at which point it enters the tricarboxylic acid (TCA) cycle in mitochondria, leading to citrate, then acetyl-CoA by the enzyme ATP citrate lyase[176]. Acetyl Co-A acts as a precursor for lipogenesis, giving rise to hepatic FAs[178,179]. As previously mentioned, excess hepatic FAs resulting from increased synthesis and uptake, decreased export and impaired β-oxidation, leads to the generation of

lipotoxic species[166-169].

Lipotoxicity leads to mitochondrial dysfunction, oxidative stress, ROS production, endoplasmic reticulum (ER) stress, inflammasome activation, and apoptosis[155,180,181]. These processes ultimately result in hepatic inflammation and fibrosis, a key component of simple steatosis progression to MASH[182]. In MASLD, increased mitochondrial FAO and TCA cycle activity constantly supply reduced nicotinamide adenine dinucleotide (NADH) and flavin adenine dinucleotide ($FADH_2$) to the electron transport chain[183,184]. Uncoupling of these processes results in increased ROS production, and concomitantly with decreased mitochondrial ROS disposal, mitochondrial deoxyribonucleic acid (DNA) damage and continued oxidative stress can lead to ER stress due to protein misfolding[185,186]. ER stress is a protective response where the unfolded protein response (UPR) is activated to restore protein homeostasis[187]. The UPR is mediated via ER-resident stress biosensors protein kinase ribonucleic acid (RNA)-like ER kinase, inositol-requiring enzyme 1 and activating transcription factor 6, which are activated after separation from glucose-regulated protein 78[187-189]. Acutely, the UPR serves to alleviate stress, however, chronic activation leads to terminal UPR, leading to apoptosis and inflammation[187,190]. In a bi-directional relationship, calcium ions (Ca^{2+}) leak from the ER which further induces the UPR and apoptosis, however, it also acts on mitochondria, inducing cytochrome *c* release, ROS production and activation of pro-apoptotic factors[191]. Lastly, inflammasome activation occurs in response to DAMPS, such as short chain FAs, which leads to increased expression of inflammatory cytokines, including IL-1β and IL-18, and promotes apoptosis[192,193]. These intrahepatic processes, extrahepatic

AT inflammation (i.e., TNFα, IL-6, adiponectin and leptin) and influence from intestinal barrier dysfunction and gut microbiota imbalance, lead to liver inflammation which drives steatosis progression to MASH[194,195]. Steatotic, damaged and apoptotic hepatocytes release DAMPS, such as HMGB1[196], heat shock proteins, ATP, RNA and DNA, as well as extracellular vesicles which may be filled with lipotoxic FAs and chemokines[197]. These signals are received by pattern recognition receptors on the surfaces of hepatic stellate cells (HSCs), liver-resident macrophages, Kupffer cells (KCs), and to a lesser extent, T-cells (natural killer and regulatory) and neutrophils[197,198]. Signaling from stressed hepatocytes and activated immune cells ultimately leads to activation of HSCs, leading to ECM production that exceed degradation[199,200].

HSCs are normally quiescent and store retinoids, however, liver injury results in transdifferentiation of these cells into collagen-producing myofibroblasts[172,201,202]. Once activated, HSCs lose their retinoid stores and synthesize α-SMA and ECM, including collagens type I, III and IV, as well as hyaluronic acid[203,204]. MMPs are also elevated, which results in increased collagen degradation products[205]. Increased tissue inhibitors of metalloproteinase (TIMPS), namely TIMP1, are secreted by macrophages and fibroblasts, and they function to maintain normal MMP levels[205,206]. MMP/TIMP imbalance shifts towards ECM synthesis and fibrinogenesis, as degradation is reduced[207]. In some cases, if fibrinogenesis is sustained, cirrhosis or permanent scarring of the liver may occur[208]. Collagenous scars encase injured liver parenchymal tissue, and characteristically fibrotic septa connect the portal tracts and the ventral veins[209]. This leads to the disconnection of hepatocytes from the central

vein, creating 'islands' of cells[209]. A hallmark feature of cirrhosis, capillarization of the sinusoids, appears as loss of fenestrae and increased basement membrane matrix deposition on liver sinusoidal endothelial cells[210,211]. These molecular changes lead to intravascular resistance in the portal system and reduced hepatic perfusion[212]. To date, there is only one Food and Drug Administration (FDA) approved drug therapy to treat individuals with NASH/MASH. Resmetriom, commercially known as Rezdriffa may be used to treat individuals with NASH/MASH with moderate to advanced liver fibrosis, concomitantly with diet and exercise intervention. After 1 year, individuals treated with 80 mg or 100 mg of Rezdriffa, experienced a 26-27% or 24-36% improvement in fibrosis and no worsening of NASH/MASH, respectively. This is directly compared to individuals who received placebo, where diet and exercise alone improved liver scarring by 9-13% (MAESTRO-NASH trial, NTC03900429)[213]. Additionally, a number of promising clinical trials are ongoing[214]. These include farnesoid X receptor agonists, pan-peroxisome proliferator-activated receptor agonists, glucagon-like peptide-1 (GLP-1) receptor agonists (GLP-1RA), coagonists (i.e. GLP-1RA/glucose-dependent insulinotropic polypeptide (GIP) receptor agonist (GIPRA)) and triagonists (i.e. GLP-1RA/GIPRA/glucagon), fibroblast growth factor 21 (FGF21) targeting therapeutics, acetyl-CoA carboxylase (ACC) 1 and ACC2 inhibitors, fatty acid synthase inhibitors and diacylglycerol O-acyltransferase 2 inhibitors[215].

1.2.1 Hepatic Glucose Production

Hepatic glucose production (HGP) maintains glucose homeostasis through fasting via gluconeogenesis and glycogenolysis. In the postprandial state, storage and disposal through glycogen synthesis and glycolysis is favoured[216]. Accounting for 90%

of endogenous glucose production[217,218], HGP is indirectly regulated and stimulated by lipolysis, which provides FAs and glycerol[216,219]. FAs undergo β-oxidation to yield mitochondrial acetyl-CoA, which activates pyruvate carboxylase, and this catalyzes pyruvate conversion into oxaloacetate, a gluconeogenic substrate[220]. Glycerol may be phosphorylated to dihydroxyacetone phosphate to become a precursor as well[221,222]. HGP may also use lactate derived from Cori cycling as a substrate[223]. Lactate is converted to pyruvate by lactate dehydrogenase (LDH), at which point pyruvate is processed in the mitochondria to oxaloacetate for gluconeogenesis[224,225]. In the liver, when insulin binds to its receptor it activates protein kinase B (PKB/AKT), which phosphorylates and prevents the transcription of factor Forkhead box O1 (FoxO1) from the nucleus in a dose dependent manner[226]. Without insulin signaling, FoxO1 promotes gluconeogenic gene transcription alongside peroxisome proliferator-activated receptor-γ co-activator 1α[227,228]. In contrast, glucagon stimulates HGP by increasing cyclic adenosine monophosphate (cAMP) to activate protein kinase A (PKA)[229], which increases cytosolic Ca^{2+} levels and activates cAMP-responsive element-binding protein-regulated transcription co-activator 2[230,231]. PKA activation by glucagon also inhibits phosphorylation of glycolytic enzymes to decrease glucose oxidation and inhibits glycogen synthase to suppress glycogen synthesis[229,232]. In contrast, under fed conditions, glucose is converted to glucose 6-phosphate (G6P) and may act as a substrate for glycogen synthesis while also activating glycogen synthase[233] while suppressing glycogenolysis via glycogen phosphorylate inhibition[234]. Further in the fed state, insulin activates AKT to ultimately reduce intracellular cAMP levels, thereby inhibiting PKA to promote glycogen synthesis[235].

Glucose homeostasis is maintained in healthy individuals, but importantly, individuals with metabolic disease, namely MASLD and T2D, have increased HGP by 30%[236]. Amplified lipolysis, such as in the setting of obesity and IR, results in hepatic lipid accumulation as DAGs[237,238]. Intrahepatic lipid accumulation impairs insulin signaling, effectively reducing glycogen synthesis, and allowing FoxO1 dependent transcriptional regulation of gluconeogenic genes[239]. Further, increased lipolysis also yields increased gluconeogenic substrates, FAs and glycerol[240,241]. Hyperglycemia from increased HGP is the main contributor to increased fasting blood glucose in T2D[242-244], and a contributing factor in increased steatosis in MASLD[173].

1.2.2 The Hepatic Portal Vein

Venous blood from the gastrointestinal tract, consisting of the stomach, intestines, pancreas and spleen, is delivered to the liver via the portal venous system[245]. The main blood vessel in this system is the hepatic portal vein, which provides the liver with approximately 75% of the total venous blood[245,246]. Uniquely, the portal vein does not drain into the heart, rather, this blood enters the hepatic sinusoids of the liver[245]. Ultimately, the hepatic portal vein serves to remove toxins and bacteria, absorb nutrients and transport and process peptide hormones[246].

The hepatic portal vein delivers insulin produced by pancreatic β-cells to the liver, at which point the liver extracts and processes approximately 50-60% of the newly secreted insulin[247,248]. The remaining insulin is delivered to extrahepatic tissue through the hepatic veins into arterial circulation, however, any remaining insulin is removed by the liver in subsequent passes[249]. It has been demonstrated that hepatic glucose uptake is the same between oral and direct intraportal infusion, therefore

ruling out the gut as a factor regulating hepatic glucose uptake[250]. In fact, intraportal infusion stimulated glycogen synthesis to a significantly greater extent than peripheral infusion[250]. This signal does not alter systemic glucose clearance[251,252], rather, it appears to reduce extrahepatic glucose uptake with increased hepatic uptake[253]. Further, the hepatic portal vein is exposed to the widest range of glucose concentrations and is largely involved in glucose sensing and subsequent physiological changes[254]. Vagal and spinal afferent nerves sense glucose and relay information to the brain, increasing satiety and satiation, and suppressing food intake cues[255,256]. Importantly, beyond nutrients, the portal vein experiences higher concentrations of gut-derived hormones, namely the incretin hormone GLP-1 and GIP than peripheral tissues[254,257]. GLP-1 and GIP are secreted from enteroendocrine cells (K-cells and L cells, respectively), in the gut postprandially, and are tightly regulated by dipeptidyl peptidase-4 (DPP4) a protease which regulates their bioavailability[258]. These hormones stimulate insulin secretion in a glucose-dependent manner when they interact with their respective receptor in the pancreas, minimizing the risk of hypoglycemia[258]. However, <25% of active GLP-1 leaves the gut, another 40-50% is degraded in the portal vein, allowing only 10-15% entering systemic circulation[259,260]. Important as well is GLP-1 receptor (GLP-1R) expression in the portal vein[261,262], here, intrahepatic peptide infusion stimulates satiety via vagal afferent nerve activity[263,264].

1.3 Type 2 Diabetes Mellitus

Approximately 30% of Canadians currently live with diabetes or prediabetes, and 90% of these cases are T2D[265]. Closely linked to the obesity epidemic, T2D is expanding as a global health and economic problem[266]. Individuals with T2D experience hyperglycemia due to pancreatic β-cell exhaustion, decreased insulin

secretion and systemic IR, and the impaired response of target tissues to circulating insulin[267]. In addition, chronic dysglycemia, dyslipidemia[268], inflammation[269,270], and hypertension[271], lead to microvascular (diabetic retinopathy and nephropathy) and macrovascular (MI and atherosclerosis) complications[272].

1.3.1 Insulin Signaling

Insulin, a peptide hormone released by pancreatic β-cells, is necessary for glucose and lipid homeostasis[273,274]. Typically, insulin binds the insulin receptor (INSR), inducing a conformational change resulting in autophosphorylation of the tyrosine residues[275,276]. This in turn phosphorylates and activates phosphotyrosine-binding proteins, including insulin receptor substrate (IRS) which then recruits phosphatidylinositol-3-OH kinase (PI3K) and catalyzes the production of phosphatidylinositol-3,4,5-triphosphate (PIP3) from phosphatidylinositol-4,5-triphosphate (PIP2) [277,278] . PIP3 recruits the serine/threonine kinase, AKT, to the cell surface, where it is activated via phosphorylation by 3-phosphoinositide-dependent kinase-1 and mechanistic target of rapamycin complex 2[279-282]. From there, downstream phosphorylation and induction of signaling regulates glucose uptake, anti-lipolysis and lipid synthesis[283,284]. Glucose uptake is mediated by a well-characterized glucose transporter, glucose transporter type 4 (GLUT4)[285]. Under insulin stimulation, intracellular GLUT4 storage vesicles (i.e., insulin responsive vesicles) are translocated to the cell surface, after which glucose, converted to G6P, enters the glycolysis pathway[286,287].

1.3.2 Peripheral Tissues in Obesity and Insulin Resistance

β-cell loss is accelerated by overnutrition leading to weight gain and obesity,

which makes these factors a leading cause of T2D[288]. Adipocyte hyperplasia from differentiation of adipose precursors and hypertrophy both contribute to AT expansion[289]. As a result, hypoxia, adipocyte cell death and increased cytokine, chemokine and FFA secretion cause systemic issues[150,290]. Tissue hypertrophy causes microhypoxia even in the earliest stages of AT expansion[291,292]. This increases expression of transcription factor hypoxia-inducible factor-1α, a master regulator of hypoxia and oxygen homeostasis, which induces other hypoxia and inflammation associated genes such as VEGF, IL-6 and leptin[293]. Further, hypertrophic adipocytes secrete inflammatory cytokines, including TNF, which promotes immune cell recruitment and activation, while anti-inflammatory factors, such as adiponectin, are reduced[294,295]. Activated macrophages are necessary in the early stages of obesity for healthy expansion and remodeling of AT, however, continued activation leads to fibrosis with the deposition of ECM further promoting metabolic dysfunction and inflammation[291,296]. Infiltrating macrophages are recruited by apoptotic and necroptotic adipocytes by MCP-1 and arrange themselves around dead cells, forming distinctive crown-like structures which are phenotypically pro-inflammatory[297,298]. These processes, namely AT remodeling and inflammation, ultimately lead to AT dysfunction which leads to AT IR[299].

Macrophages in expanding AT release TNFα, IL-6 and IL-1β, which activate the c-Jun N-terminal kinase (JNK)-inflammatory cascade, effectively inhibiting IRS1 phosphorylation leading to reduced insulin sensitivity and GLUT4 translocation[300]. The anti-lipolytic effect of insulin is also blunted, which is already defective in hypertrophic adipocytes, leading to chronic, elevated FA release and TG

hydrolysis[301]. Further, IR pushes glucose metabolism towards glycogen and lactate production and synthesis[302]. Excessive glycogen leads to adipocyte apoptosis and immune cell recruitment, while lactate release reduces AT lipolysis and GLUT4 abundance and trafficking in skeletal muscle specifically[303,304]. In addition, systemic inflammation, and the release of FFA from AT, contribute to skeletal muscle and liver IR[300].

Skeletal muscle is the main site of glucose disposal, accounting for absorption and metabolism of up to 80% of post-prandial glucose, whose catabolism is necessary for energy for muscle contraction[303]. Ectopic lipid accumulation and inflammatory signals from AT in skeletal muscle leads to incomplete FAO and defective insulin signaling[305], or conversion to ceramides and DAGs, due to activation of Toll-like receptors (TLRs), and subsequently the JNK- NF-κB pathway[306]. Increased DAGs also activates protein kinase C (PKC) θ (PKCθ), which increases phosphorylation of IRS1, hindering insulin signaling, activating the PI3K/AKT pathway leading to decreased glucose transport and glycogen synthesis[307]. Further, excessive FA uptake and increased intracellular FAs in skeletal muscle effectively inhibit hexokinase activity, and as a result, glucose uptake[302].

As previously described, the liver is susceptible to ectopic lipid accumulation and lipotoxicity, namely, the accumulation of DAGs which activates PKCε, thereby blunting insulin signaling[308]. Here, this process also reduces the activity of glycogen synthase and induces HGP through decreased phosphorylation of FoxO, where in its unphosphorylated form, FoxO translocates to the nucleus and enhances transcription of gluconeogenic enzymes phosphoenolpyruvate carboxykinase and G6P[308]. Lastly,

circulating cytokines and adipokines also increase HGP by activating NF-κB and JNK[308].

1.3.3 Islet Hormone Secretion

In response to obesity and IR, the insulin producing β-cells, in the islets of Langerhans in the pancreas, compensate by increasing insulin synthesis and secretion, and by increasing in mass via proliferation and hypertrophy[309]. In homeostatic conditions, ingested carbohydrates are broken down into glucose, which enters the β-cell through GLUT2[310]. Glucose is phosphorylated to G6P, and through glycolysis, pyruvate is generated[311]. In the mitochondria, pyruvate is oxidized to give rise to ATP through the TCA cycle[312]. Increases in the intracellular ATP/adenosine diphosphate (ADP) induce ATP-dependent potassium channel closure, effectively depolarizing the plasma membrane, leading to the influx of Ca^{2+}, ultimately triggering insulin granule exocytosis[313].

In metabolic disease and prediabetes, hyperglycemia and IR lead to increased insulin secretion and hyperinsulinemia to maintain normal glucose levels[314]. Unfortunately, hyperinsulinemia then downregulates the INSR, further increasing compensatory insulin secretion. In the early stages of T2D, individuals experience hyperinsulinemia, but insulin steadily drops as β-cell dysfunction progresses[315]. β-cell function decreases and is lost by 40-50% by the time T2D is diagnosed, with further loss (~5%) each year afterwards[316]. While acute exposure to FFAs increases glucose stimulated insulin secretion (GSIS) following a mixed meal[317], chronic exposure suppresses GSIS, insulin synthesis and ultimately leads to β-cell loss[318]. Further, FFAs activate TLR2 and TLR4 which stimulates the release of cytokines such MCP-

1, macrophage inflammatory protein 1α (MIP-1α) and IL-8 through the NF-κB pathway[319]. Circulating proinflammatory cytokines and those secreted by infiltrating immune cells cause β-cell death due to mitochondrial and ER stress, and ROS production[320]. However, β-cell failure is largely attributed to dedifferentiation and death in response to hyperglycemia[321]. Cells lose identity as β-cell enriched genes are downregulated and normally lowly expressed genes are upregulated[322]. Importantly, the incretin effect, a phenomenon whereby oral glucose elicits a stronger insulin secretory response compared to isoglycemic intravenous glucose, is greatly reduced in individuals with T2D[323]. In individuals with T2D or obesity, GLP-1 secretion and β-cell sensitivity to the incretin hormones is diminished while DPP4 expression and circulating DPP4 are increased[324].

1.3.4 Pharmacological Treatments for T2D

Currently 12 classes of drugs are approved to treat or prevent hyperglycemia in individuals living with T2D[325]. Less commonly used drugs include amylinomimetics, meglitinides, thiazolidinediones, bile acid sequestrants, dopaminergic antagonists and α-glucosidase inhibitors[325]. Instead, according to the most recent guidelines[326] individuals are typically prescribed, biguanides (metformin), sulfonylureas, DPP4 inhibitors (DPP4i's), sodium-glucose cotransporter-2 inhibitors, GLP-1RA's and insulins[325].

The only biguanide derivative currently prescribed is metformin, which is typically the first line most commonly used glucose-lowering therapy[327,328]. The liver highly expresses membrane transporter solute carrier family 22 member 1, necessary for metformin cellular uptake[329]. Importantly, metformin concentration is higher in the

portal vein versus systemic circulation, which may point to why it accumulates in the liver[330]. Further, organic cation transporter 1 (OCT1) which is responsible for metformin uptake, is largely expressed in hepatocytes[331]. Metformin primarily elicits glucose control by effectively inhibiting HGP by up to 75% in individuals with T2D[332]. This is thought to occur through decreased mitochondrial oxygen consumption, specifically through inhibition of mitochondrial respiratory complex I, which elevates AMP thereby inhibiting cAMP synthesis and activating AMP-activated protein kinase (AMPK)[333-335]. AMPK then phosphorylates and increases the activity of the INSR and of IRS2 to increase glucose uptake via translocation of GLUT2 to the membrane, ultimately enhancing insulin-mediated gluconeogenesis suppression[336]. Further, metformin contrasts the action of glucagon by inhibiting gluconeogenic enzymes and stimulating glycolysis. Gluconeogenic substrate uptake, such as alanine and lactate, is also reduced with metformin[337]. Peripherally, metformin improves insulin sensitivity by increasing INSR expression and increases glucose uptake in skeletal muscle via increased activity and translocation of GLUT4 to the plasma membrane[336,338,339]. In addition, metformin has been reported to stimulate expression of the GLP-1R in the pancreas and increase GLP-1 in circulation[340].

DPP4i's, known as gliptins, are used for the treatment of T2D and work by blocking enzymatic activity of DPP4, preventing the degradation and inactivation of the incretin hormones, restoring GSIS, regulating glucagon secretion and glycemic control[341]. While the DPP4i mode of action is consistent among each family of compounds, this class of small molecules is heterogenous in their chemistry and pharmacokinetic properties[342]. Structural heterogeneity results in differences in metabolism, for example, when saxagliptin is metabolized by cytochrome P450 3A4

and 3A5, an active molecule is produced, however the same cannot be said for sitagliptin, linagliptin and vildagliptin[343]. Chemical structure also dictates half-life, with linagliptin being the most efficacious DPP4i due to strength and reversibility of binding[344]. However, all therapies are effective and safe as oral therapies, with virtually no risk of hypoglycemia[345]. Additionally, DPP4i anti-hyperglycemic affects follow a diurnal pattern, where mice treated with sitagliptin during the light phase experienced significantly lower plasma glucose and insulin levels, and improved glucose tolerance, while these parameters were unchanged in the dark phase-treated mice[346].

Interestingly, when used in combination, metformin and DPP4i's demonstrate a numerically additive reduction in mean glycated hemoglobin (HbA1c)[347], presumably in part due to increased GLP-1 action through metformin increasing GLP-1 secretion and DPP4i's maintaining bioactivity[348,349]. Some studies suggest that metformin inhibits DPP4 catalytic activity in humans[350,351] and in mice[352]. While direct inhibition was not substantiated *in vitro*[353] or shown *in vivo*[354], metformin may decrease DPP4 shedding into circulation[348,352].

Additionally, GLP-1RA's, or incretin mimetics, are small peptidic injectable or oral medications which are designed to resist DPP4 cleavage, enabling GLP-1R activation and islet hormone secretion. Endogenous GLP-1 and GLP-1RA's exert both direct and indirect effects, including reducing IR[355], HGP[356-358], hepatic steatosis[359,360], inflammation[361-365], lipoprotein secretion[366,367], and gastric emptying[368,369], while increasing β-cell proliferation[370], skeletal muscle glucose uptake[371], kidney diuresis and natriuresis[372] and white adipose tissue lipolysis[373]. Notably, a meta-analysis of 8

cardiovascular outcome trials (CVOTs) revealed a 14% reduction in the primary outcome of a 3-component major adverse cardiovascular events (MACE; cardiovascular death, nonfatal MI, and nonfatal stroke)[374]. More recently however, GLP-1RA's[375], dual (GLP-1/GIP)[376,377] and tri (GLP-1/GIP/glucagon)[378] agonists have garnered international attention and were named Science's breakthrough of the year in 2023 for significantly reducing body weight and obesity-related diseases[379].

1.3.5 DPP4 Cardiovascular Outcome Trials

Historically, the FDA considered an appreciable decrease in HbA1c a suitable endpoint for anti-diabetic drugs[380]. In a highly publicized meta-analysis, rosiglitazone, an insulin sensitizing and glucose-lowering drug, increased the incidence of ischemic MI by 43% and CV death by 64%[381]. As a result, this increased concerns surrounding safety of drugs for T2D. Thus, pharmaceuticals approved to treat patients with T2D are required to undergo extensive cardiovascular profiling and rigorous safety trials to obtain FDA approval, as of 2008[382].

A number of CVOT of DPP4i's have reported neutral effect, or no significant increase or decrease in MACE[383]. However, the largest CVOT for a DPP4i, the Saxagliptin Assessment of Vascular Outcomes Recorded in Patients with Diabetes Mellitus – Thrombolysis in Myocardial infarction 53 (SAVOR-TIMI 53; NCT01107886) reported elevated risk for hospitalization for HF. Approximately 16,000 patients with T2D with a history of established CVD or multiple risk factors were randomized to receive either saxagliptin or placebo. Saxagliptin neither reduced nor increased the risk of the primary composite endpoint (CV death, MI or ischemic stroke), however, it did significantly increase the risk of hospitalization for HF[384,385]. Another clinical trial, the Examination of Cardiovascular Outcomes with Alogliptin versus Standard of Care

(EXAMINE; NCT00968708[386]) trial, which randomized over 5,300 patients with T2D to receive either alogliptin or placebo, demonstrated an increased number of hospitalization for HF among a subset of patients[387,388]. In contrast, in the Trial Evaluating Cardiovascular Outcomes with Sitagliptin (TECOS; NCT00790205[389]), with 14,671 patients with T2D and prevalent atherosclerotic vascular disease randomized to either sitagliptin or placebo, there was a net neutral CV outcome and no increase in hospitalization for HF[390]. This was substantiated by the OMNEON 018 trial (omarigliptin, MK-3102; NCT01703208[391]), after which a meta-analysis revealed that patients in the TECOS and OMNEON 018 trial were more likely to be treated with metformin versus insulin and thaizolidinediones at randomization, compared to SAVOR-TIMI and EXAMINE[389,392]. Noninferiority of additional DPP4i's was demonstrated in more recent and smaller CVOTs, including The Cardiovascular and Renal Microvascular Outcome Study with Linagliptin (CARMELINA; NTC01897532[393,394]), the Cardiovascular Outcome Trial of Linagliptin Versus Glimepiride in Type 2 Diabetes (CAROLINA; NCT01243424[395]) and the OPTIMUS study (Gemigliptin; NCT02290301[396]) (**Table 6.1**).

1.4 DPP4 Structure, Distribution and Function

DPP4 is a single pass type II transmembrane glycoprotein[397] which belongs to the DPP4 activity and/or structure homolog family[398] along with fibroblast activation protein (FAP)[399], DPP8[400], DPP9[401], DPP-like protein 1 (i.e., DPP6)[402], and DPP-like protein 2 (i.e., DPP10)[403], relating to the *DPP4* gene family (serine clan SC, subfamily 9b). In addition, there are non-related DPP4-like enzymes, including DPP2, attractin and N-acetyl alpha-linked acidic dipeptidases (NAALADases I, NAALADases II and NAALADases L)[404]. At the N-terminal of the membrane-bound isoform, a short domain

(6 residues) extends into the cytoplasm, followed by a hydrophobic transmembrane domain (22 residues) (**Figure 1.1A**) and an extracellular domain comprised of an 8-blade ß-propellor and an α/ß hydrolase domain[398,405,406] (**Figure 1.1B, C**). At the C-terminal, a classic catalytic active site contains the well-conserved serine triad[407] (residues Ser^{630}, His^{740} and Asp^{708}) (**Figure 1.1D**). Substrate recognition is due to the highly conserved glutamic (Glu) acid-rich loop (Glu^{205}/Glu^{206})[408] (**Figure 1.1D**). DPP4 exerts peptidase function by selectively cleaving dipeptides from the N-termini of peptides which possess a proline, alanine or serine at the penultimate amino acid residue[397,409] (**Figure 1.1E**). The DPP4 homodimer represents the majority of its catalytically active form[410]. It may also exist as a monomer, homotetramer, and membrane-bound heterodimer with FAP[411,412].

DPP4 is expressed in many metabolically active tissues, including the pancreas (α-cells[413-415], β-cells[413,416], epithelial cells), intestine (enterocytes[417,418]) kidneys (glomerular podocytes[419], proximal tubules[420]) and liver (hepatocytes, endothelial cells, Kupffer cells), vascular endothelial[418] and immune cells, monocytes, macrophages and lymphocytes, and the circulating form many bodily fluids (blood, urine, bile, seminal fluid and cerebral spinal fluid)[397,421]. DPP4 liberation from the cell surface leads to a circulating soluble form (sDPP4), however the exact sheddase responsible is incompletely understood[407]. Kellikrein-related peptidase 5 (KLK5) is a proposed sheddase found to cleave DPP4 from Th17 cells, particularly in the setting of T2D[422]. Röhrborn *et. al.* treated smooth muscle cells (SMC) with a broad spectrum MMP inhibitor Batimastat (BB-94), a general cysteine protease inhibitor (E64) and serine protease inhibitor 4-(2-aminoethyl) benzenesulfonyl fluoride hydrochloride

(AEBSF) to reveal reduced soluble DPP4 release. After probing further, it was concluded that inhibiting MMP2 and silencing MMP1 and MMP14 via small interfering RNA (siRNA) showed a 20-30% decrease in DPP4 shedding[423]. In contrast, MMP9 inhibition in adipocytes resulted in a 25% decrease in DPP4 shedding. However, these findings are not supported with *in vivo* evidence and in both studies, incomplete DPP4 release (~50%) suggests it may not be regulated by a single sheddase.

The extracellular domain contains a heavily glycosylated region (aa 49-289) which undergoes post-translational modifications (PTMs) via glycosylation at 9 asparagine (Asn) resides[398] (**Figure 1.1A**). Fan *et. al.* converted Asn residues to Glu using site-directed mutagenesis in stable transfected Chinese hamster ovary cells[424]. Interestingly, enzymatic activity, cell-surface expression and dimer formation were eliminated with mutation at the sixth N-glycosylation site (Asn^{319})[424]. In addition, this mutation resulted in incorrect folding and retention in the ER, reduced intracellular trafficking to the cell membrane, significantly increased its degradation and prevented dimerization[424]. Interestingly, all three mutations (Asn^{83}, Asn^{319} and Asn^{686}) lead to reduced protein stability, effectively decreasing DPP4 half-life[424]. Further, there are two potential, yet controversial, O-glycosylation sites that were shown to be important for apical targetting[425-427]. Similarly, reduced terminal sialylation decreased DPP4 apical targetting[428], however, increased modification reduces DPP4 enzymatic activity[429], which can be rescued with desialylation with *Vibrio cholera* neurominidase[430]. DPP4 sialylation increases significantly with age as detected in peripheral blood mononuclear cells of healthy elderly individuals, namely T-cell associated DPP4[431]. Hypersialylation also occurs in HIV-positive individuals[431]. Most recently, DPP4 activity was found to be reduced in patients after elective cardiac

surgery with the use of cardiopulmonary bypass, revealed to be due to DPP4 oxidation by H_2O_2[432]. Low post-operative DPP4 activity was associated with worse patient outcomes while in the intensive care unit[432]. DPP4 oxidation and reduced activity correlated with surgery-induced myocardial ischemia severity, and importantly, prior MI and reduced LVEF (<30%) significantly reduced intra-operative DPP4 activity[432]. In this same domain is a highly conserved cysteine-rich region (9 of 12 cysteines, aa 290-510) which acts as a binding site, resulting in non-catalytic DPP4 action such as signaling and binding[433].

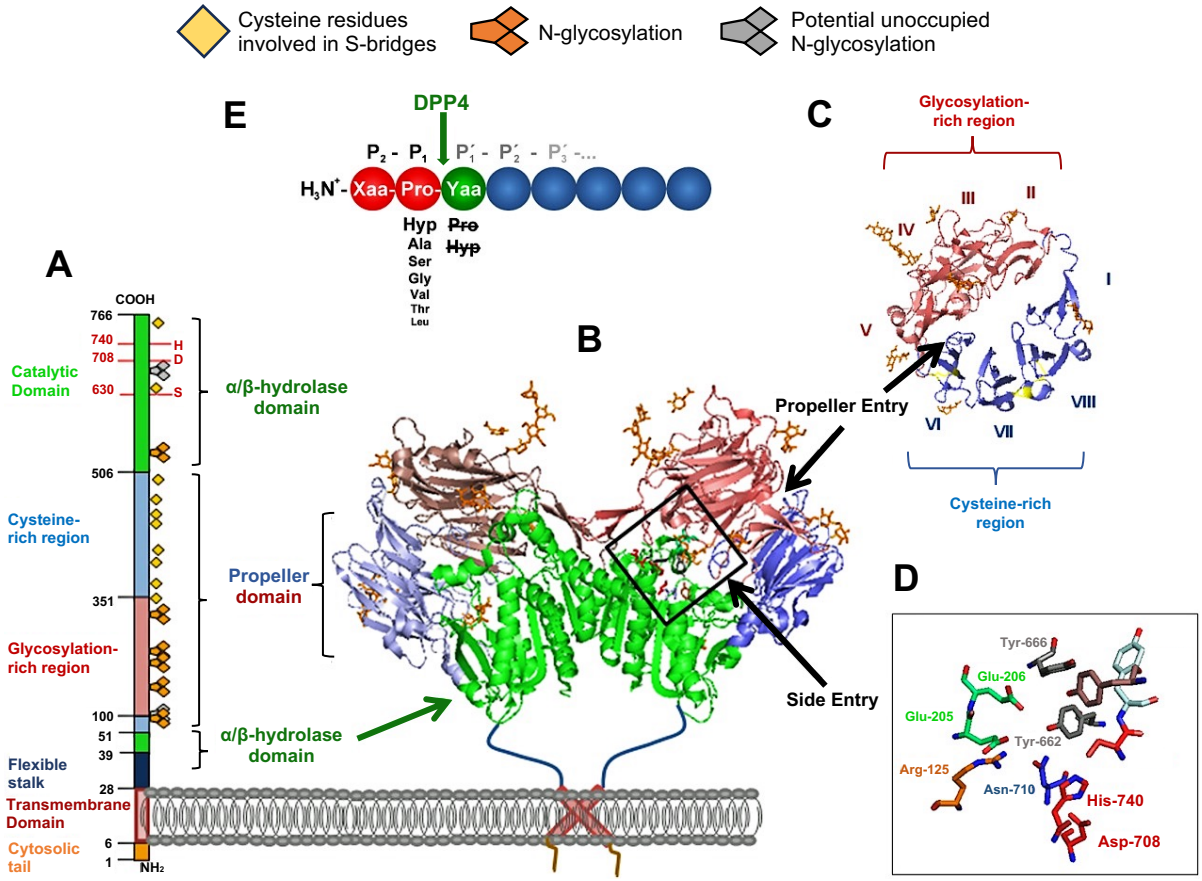

Figure 1.1: Primary and quaternary structure of human dipeptidyl peptidase-4 (DPP4). Primary structure of DPP4 subunit, consisting of an intracellular tail (aa 1–6), transmembrane region (aa 7–28), flexible stalk (aa 29–39), glycosylated region (aa 101–350), cysteine-rich region (aa 55–100, 351–497), and catalytic region (aa 506–766). Red numbers and letters indicate the catalytic triad. (**B**) quaternary structure of homodimeric human recombinant DPP4 as determined by Weihofen et al[406], showing the α/β-hydrolase domain (aa 39–51 and 506–766) in green and propeller domain (aa 55–497) with the glycosylation-rich subdomain (red) and the cystein-rich subdomain (blue). (**C**) Propeller domain viewed from the top, illustrating the eight propeller blades designated with roman numbers and two subdomains. (**D**) Active site zoomed in, depicting the residues involved in catalysis, catalytic triad Ser630, Asp708, His740 are shown in red, Tyr547 responsible for oxyanion hole in brown, Tyr662 and Tyr666 forming the hydrophobic pocket in grey, Arg125 and Asn710, contributing to an electrostatic sink in orange and blue, respectively, and Glu205 and Glu206 ensuring N-terminal anchoring in pale green. (**E**) Substrate specificity of DPP4. Xaa and Yaa indicate any amino acid. Decreasing font of amino acid at P1 position represents declining rate of hydrolysis. Amino acids crossed out must not occupy P1′. Arrow indicates site of cleavage. S–S bridges are illustrated in yellow and carbohydrates in orange. Structures were drawn with PyMOLTM 2008 DeLano Scientific LLC, using Protein Data Base: 1W1I.

Reproduced from Klemann C. *et. al.*[405], modified with the addition of a legend. Creative Commons CC BY-NC 4.0

1.4.1 DPP4 Enzymatic Action

Beyond the incretin hormones, DPP4 targets other substrates including neuropeptides[341] and chemokines[434]. Most of these have been identified as pharmacologic substrates, where high concentrations used *in vitro* or *in vivo* reveal cleavage by DPP4. These proteins include, but are not limited to, eotaxin[435], HMGB1[436], MIP-1α[437], interferon gamma-induced protein 10 (IP-10)[438] and regulated on activation, normal T-cell expressed and secreted (RANTES)[439]. In addition, several substrates have been validated *in vivo*, as physiologic substrates, namely GLP-1[440], GLP-2[441], GIP[442], stromal-derived factor 1 (SDF-1), granulocyte colony-stimulating factor (G-CSF) and peptide YY (PYY)[443]. DPP4 is elevated in patients with T2D[444,445] and enzymatic activity positively correlates with hyperglycemia in this population[444]. Further, hepatic protein expression is increased in patients with MASLD[446] and HCV[447] and remodelling and inflammation in CVD[397], collectively suggesting increased substrate inactivation in these diseases, which may be contributing to disease progression.

The best characterized DPP4 substrates are the incretin hormones, GLP-1 and GIP[440,442]. Secreted from the gut as GLP-1 [7-37], GLP-1[7-36]NH_2 and GIP[1-42], they activate their respective G protein-coupled receptors on β-cells to potentiate GSIS[444]. However, they have very short half-lives: 2-5 and 5-7 minutes respectively, due to cleavage and inactivation by DPP4 resulting in GLP-1[9-37], GLP-1[9–36]NH_2 and GIP[3-42][440,448]. DPP4 was confirmed as the primary enzyme regulating the bioactivity of GLP-1 and GIP in both mice and humans with systemic DPP4 genetic elimination, where glucose excursion was reduced and the active, insulinotropic form

of GLP-1 was increased in circulation[449].

Prevention of DPP4 mediated degradation of SDF-1, a peptide hormone produced by immune and hematopoietic cells in response to cardiac vessel damage and ischemia, has demonstrated cardioprotection[450]. Specifically, uncleaved, intact SDF-1 stimulates recruitment of bone marrow-derived progenitor cells to the myocardium in response to cardiac damage[450]. This process results in increased angiogenesis, and improved survival of cardiomyocytes. Clinically, this paradigm has been tested in the SITAgliptin plus GRanulocyte-colony-stimulating factor in patients suffering from Acute Myocardial Infarction (SITAGRAMI; NCT00650143) study[451,452]. Angina patients, with substantial documented damage to the myocardium, underwent a successful percutaneous coronary intervention[452]. The patients were exogenously given G-CSF for 5 days to stimulate egress of C-X-C chemokine receptor type 4 (CXCR4; an alpha-chemokine receptor specific for SDF-1) positive progenitor cells from bone marrow in combination with the DPP4i sitagliptin for 28 days to stabilize G-CSF and SDF-1 levels. No significant differences in mortality or cardiac function were observed in the small 68 patient population, but there were intriguing trends to reduce cardiac events and death from any cause suggesting this paradigm of inhibiting DPP4 and infusing DPP4 substrates may have merit for improving cardiac function post-MI[451,453].

RANTES[1-68], involved in leukocyte recruitment to sites of inflammation, is cleaved to RANTES[3-68], at which point it is unable to increase cytosolic calcium levels or induce *in vitro* human monocyte chemotaxis[454]. In addition, following radiation or chemotherapy, DPP4 genetic ablation or inhibition enhanced hematopoiesis via preserved GM-CSF function[434]. Typically, DPP4 cleavage

inactivates proteins, however MIP-1α[1-70] cleavage results in a more active form, MIP-1α[3-70], improving monocyte chemotactic activity and inflammatory properties via C-C chemokine receptor type 1 in human THP-1 cells[437].

1.4.2 DPP4 Non-Enzymatic Action

In addition to its catalytic activity, DPP4 serves as a binding partner for numerous peptides[341,398,455]. DPP4 can associate with adenosine deaminase (ADA)[406,456], CD45[457], CAV1[458-460], streptokinase, plasminogen, collagen and fibronectin[461]. Compared to its enzymatic action, non-enzymatic action of DPP4 is not as well defined, however actions that are not impacted with a catalytic inhibitor highlight its multifunctional role in inflammation and fibrosis.

ADA degrades adenosine and deoxyinosine which inhibits the function of lymphocytes[462]. When interacting with DPP4, the complex might potentiate inflammation in obesity after T-cell activation. Interestingly, this is inhibited by interrupting protein/protein interactions with exogenous soluble DPP4, but not by targeting DPP4 activity with inhibitors[463]. Moreover, patients with T2D have been documented to have elevated ADA activity[464]. Beyond inflammation, ADA has also been shown to positively correlate with fasting plasma glucose and HbA1c. DPP4i's did not affect ADA activity despite glycemic control[465], suggesting the effects of ADA/DPP4 interactions are independent of DPP4 enzymatic activity.

CAV1 is present on antigen presenting cells, and when it binds to T-cell DPP4, upregulation of CD68 initiates a signaling cascade[466]. This interaction effectively suppresses TLR4-mediated inflammation in murine and human macrophages[467]. Notably, increased inflammation in bone marrow-derived macrophages (BMDMs)

treated with recombinant factor Xa, an inflammatory trigger, and recombinant DPP4 was significantly reduced in BMDMs from *Cav1*$^{-/-}$ mice, illustrated by decreased *Il6* and *Mcp-1* messenger RNA (mRNA) expression[468]. Interestingly, in AT, CAV1 modulates downstream signaling, including AKT, in the insulin transduction pathway, suggesting an influential role for DPP4 in AT insulin sensitivity[469,470].

Importantly, DPP4 can also bind ECM components collagen and fibronectin. DPP4 preferentially binds to the collagen type 1, α1 (COL1A1) and COL3A1 chain[471], however, the function of this interaction is contested. It has been reported to promote cell migration, act as a collagen receptor for CD4+ T cell activation and in cell adhesion. Further, DPP4 bound to surface fibronectin on hepatocytes isolated from rats in an *in vitro* nitrocellular binding assay[472]. This was interestingly amplified with DPP4 inhibition, which accelerated the initial fibronectin binding to hepatocytes identified by kinetic studies, illustrating a unique relationship between enzymatic inhibition and non-enzymatic binding of DPP4 to fibronectin[472].

1.5 Pathogenic Role of DPP4 in Cardiometabolic Disease

1.5.1 DPP4 in MASLD

Metabolic dysregulation in both obesity[473-475] and aging[473,476] increases circulating DPP4, and in particular, patients with MASLD have increased hepatic *DPP4* mRNA expression[446]. In addition, small clinical studies suggest that DPP4i's decrease blood glucose by targeting hepatic glucose production[477]. Therefore, these drugs have been investigated as a therapy for the management of MASLD alongside its established glucoregulatory role. Several studies show that DPP4i's improve steatosis, hepatocyte ballooning, decrease alanine transaminase (ALT) levels and

overall disease progression[478-481]. Several pre-clinical studies in mice robustly support these positive findings. DPP4i's prevented the progression of MASLD to HCC by suppressing DNA replication[482]. In another study, DPP4i in melanocortin 4 receptor–deficient mice decreased inflammation, fibrosis and carcinogenesis, most likely through greater GLP-1-mediated suppression of proinflammatory and profibrotic phenotypes in macrophages[483]. Further, 8 weeks of linagliptin treatment in male diabetic *db/db* mice reduced steatosis, and lead to more heterogenous hepatocytes with preserved cell structure independent of glucose regulation, compared to controls[484]. These promising results were further recapitulated in streptozotocin (STZ)-induced diabetic mice where 12 weeks of consuming a sitagliptin-supplemented diet attenuated liver injury and oxidative stress, reduced liver fibrosis and apoptosis, and inhibited the NF-κB pathway improving inflammation compared to controls[485]. In addition, in an obese, diabetic leptin deficient mouse model, *ob/ob*, 4 weeks of sitagliptin treatment by gavage attenuated aberrant lipid metabolism, hepatic steatosis and IR compared to the saline-treated mice. Further, inflammation was decreased through regulation of pro-inflammatory and pro-resolving macrophage polarization and NF-κB inhibition[486].

Locally, through hepatocyte-targeted siRNA, Ghorpade *et. al*.[468] demonstrated that silencing hepatocyte DPP4 suppressed AT inflammation and IR in obese mice. Consistent with these findings, Varin *et. al.*[473] showed that genetic elimination of hepatocyte-derived DPP4 decreased inflammation, but had no effect on glucose tolerance. In contrast, Baumeier *et. al.*[487] overexpressed hepatic DPP4 which worsened NAFLD progression and IR. This effect was linked to reduced levels of

active GLP-1 in the vena cava compared to portal vein, suggesting that inactivation by hepatocyte-derived DPP4 was the cause. Lastly, in the context of fatty liver disease, Gorgens *et. al.*[488] revealed that, compared to systemic DPP4 inhibition with linagliptin, hepatocyte-specific *Dpp4* knockout (*Dpp4*$^{hep-/-}$) mice experienced reduced hepatic steatosis with no change in glucose metabolism in *db/db* mice.

Liver-resident Kupffer cells (KC) initiate inflammation and help recruit blood-derived monocytes; both differentiate into proinflammatory macrophages and further promote NAFLD progression[489]. Interestingly, serum DPP4 is a proposed systemic surrogate marker of severe impairments in the KC population imposed by clinical and subclinical liver conditions as these levels increase, regardless of liver damage[490]. However, the interaction of DPP4 with ADA and KC's in NAFLD progression[463] remains to be investigated.

1.5.2 DPP4 in CVD

1.5.2.1 Heart Failure, Diastolic Dysfunction and Adverse Remodelling

Interestingly, several preclinical studies have illustrated cardioprotection with DPP4 inhibition. Wildtype (WT) C57BL6/J mice fed a high fructose Western diet supplemented with DPP4i MK-0626 for 16 weeks became obese, insulin resistant and experienced cardiomegaly and diastolic dysfunction measured using high-resolution cine-cardiac MRI. However, myocardial oxidant stress and fibrosis was attenuated with MK-0626 treatment, which led to rescued diastolic function[491]. These results are supported by another study in Dahl salt-sensitive rats, which experience HFpEF after being fed salt. Nine weeks of DPP4i vildagliptin treatment decreased left ventricular end-diastolic pressure and the expression of collagen genes[492]. Another study in WT mice revealed that MK-0626 treatment decreased COL3A1 (thin) type fibres and lead

to an overall decrease in the amount of collagen fibres with a concomitant increase in collagen quality. These results were also observed in whole body *Dpp4* knockout mice[493]. More recently, DPP4i evogliptin treatment in *db/db* mice rescued systolic and diastolic function compared to controls. Evogliptin also alleviated the presentation of disordered cardiomyocytes and reduced the heart weight to tibia length ratio. These improvements appeared to be driven in part by decreased fibrosis, myocardial injury, and interestingly, cardiac lipotoxicity[494].

Notably, Shigeta *et. al.*[495] revealed increased *Dpp4* expression in the hearts of diabetic rats. When *Dpp4* was systemically genetically eliminated, these rats experienced decreased diastolic stiffness, and improved vascularity compared to their WT counterparts, namely through the MMP2/TIMP2 axis which is reversed with DPP4 inhibition. Further, HFD-fed, STZ-injected mice subjected to experimental trans-aortic constriction (TAC) surgery to induce pressure overload hypertrophy treated with DPP4i's had elevated expression of fibrosis and hypertrophy genes and inflammation-related genes which collectively resulted in cardiac hypertrophy and decreased cardiac function[496]. However, euglycemic systemic *Dpp4* knockout (*Dpp4*$^{-/-}$) mice with HF had preserved cardiac function and reduced fibrosis, inflammation, and hypertrophy, suggesting complete genetic ablation of DPP4 is cardioprotective in a pressure-overload model[496].

1.5.2.2 Myocardial Infarction

Inflammatory stimuli increase GLP-1 secretion[497], which was recapitulated in mice after left anterior descending coronary artery (LAD)-ligation[498]. On a molecular level, GLP-1 dependent improvements in LV contractility were attributable to favourable rescuing of non-infarcted tissue. Linagliptin treatment increased AMPK

activity acutely after LAD-ligation, and decreased cardiac AKT-phosphorylation, thereby reducing GLUT4 expression and increasing FAT/CD36 expression[498]. Further, linagliptin treatment also increased mitochondrial respiratory control ratio in isolated mitochondria due to increased maximal ADP-induced respiration[498]. After permanent LAD-ligation, normoglycemic *Dpp4*$^{-/-}$ mice exhibited a 20% increase in survival compared to *Dpp4* WT (*Dpp4*$^{+/+}$) mice, found to be due to increased expression of cardioprotective genes pAKT, phosphorylated glycogen synthase kinase-3 β (GSK3β) and atrial natriuretic peptide (ANP)[499]. In this same study after LAD-ligation, sitagliptin treated *Dpp4*$^{+/+}$ mice with STZ-induced diabetes had improved cumulative survival, and similarly ANP and heme oxygenase (HO-1) expression was increased[499]. In a comparable study, C57BL/6 STZ-injected mice treated with sitagliptin had significantly improved survival and cardiac function after LAD-ligation, presumably due to reduced infarct size and myocardial fibrosis[500]. Molecularly, 7 days post-MI the number of autophagosomes adjacent to infarcted tissue was markedly increased in diabetic mice treated with sitagliptin[500]. Further, protein levels of inflammatory factors IL-1β, IL-6 and TNF-α were significantly decreased in treated mice, as was NF-κB in myocardial cells[500]. Lastly, in normoglycemic mice, after LAD-ligation treated with vildagliptin, infarct size, fibrosis and myocardial necrosis was significantly decreased, which in turn increased survival and cardiac function[501]. Increased cardiac SDF-1 and CXCR4 expression was observed, partly due to stem cell recruitment of CD34+ cells, which led to increased neovascularization and angiogenesis with decreased apoptosis and cell death[501].

1.6 MASLD and CVD Mouse Models

Multiple mouse models are used throughout Chapters 2-4 to model human disease and investigate how DPP4 is involved in pathogenesis. The sequencing of the entire mouse genome has enabled the development of several genetic models of CVD, both MI and HF, and MASLD, including MASH and HCC[502]. However, these models fail to completely mimic the complexity of human disease as they do not account for interactions between genetics, environment, and lifestyle. Despite these limitations, these models allow the study of hereditary conditions. In Chapter 1 for example, we use a phosphatidylethanolamine N-methyltransferase (*Pemt*) knockout mouse which lacks the PEMT enzyme necessary for conversion of phosphatidylethanolamine to phosphatidylcholine[503], similar to a V175M polymorphism in humans[504], leading to the development of NAFLD independent of systemic metabolic disease and weight gain, to study DPP4 perturbations. Chemically induced models exist for all aforementioned diseases, including isoproterenol to induce MI[505] and carbon tetrachloride administration to mimic MASH and HCC[506]. Similar to genetic techniques, these substances are useful to artificially incite disease and at times mimic histopathological traits, however they again fail to consider metabolic disturbances, namely obesity, which drive pathogenesis. The mouse models used in subsequent chapters rely on diet induction (**Table 6.2**). MASLD and MASH present when mice are chronically fed a high-fat, high-cholesterol (HFHC) diet[507]. HFD-fed mice display prominent features of MASLD, including obesity and IR, and closely follow human histopathological and pathogenesis[507]. The addition of dietary cholesterol triggers hepatic inflammation and fibrosis, resulting in a MASH phenotype[508]. However, these studies require longer experimental timelines, variation

in diets and genotype susceptibility (e.g., BALB/c mice tolerate diet, C57BL/6 mice are susceptible to the effects[508])[509,510]. In terms of heart failure, HFHC-induced cardiac dysfunction and structural damage have been reported in some studies[511-514] while others have reported resistance or inadequate damage to mimic heart failure[515,516]. Nonetheless, HFHC-feeding can lead to heart failure preceded by metabolic disturbances such as changes in cardiac metabolism, glucose intolerance, inflammation, and fibrosis[511-514]. Spontaneous ischemia to induce MI is possible in some genetic models (e.g*.,* apolipoprotein E knockout (*apoE*$^{-/-}$) mice crossed with mice deficient in scavenger receptor class V type I), however, this is uncontrolled[517-519]. Therefore, surgical methods are oftentimes employed; in Chapter 4, LAD-ligation is used. The LAD artery is the largest coronary artery which extends from the base to the apex of the heart[520]. In this model, the LAD is ligated permanently, preventing blood from oxygenating a portion of the myocardium, leading to an infarction[521-523]. This model results in significant apoptosis and a large scar[522,523], especially when compared to an ischemia-reperfusion model where the LAD is only temporarily ligated before blood flow is restored[524,525]. The latter results in a smaller scar, however there is a risk of reperfusion injury and a smaller necrotic wave of damage[526]. Permanent ligation infarcts are typically used to assess injury and wound healing and are usually more accurate and consistent making it a leading procedure to study MI[521,527]. However, this procedure does have limitations, including surgical difficulty, post-operative mortality due to arrythmias, bleeding and cardiac rupture, and does not necessarily model clinical situations perfectly as only 15-30% of people do not experience successful reperfusion[528-530]. Additionally, considering most of these diseases occur in middle-aged or elderly individuals, it is essential to incorporate this

additional factor by using aged mice. In the studies presented in this thesis, we use mice aged 25 weeks to 1 year, which is equivalent to 30-42.5 years of age in humans, or mature adult to middle-aged[531].

1.6.1 Genetic Elimination of DPP4

In subsequent chapters, several genetic mouse models are used to induce DPP4 depletion, including a whole-body knockout (*Dpp4*$^{-/-}$), a hepatocyte-specific knockout (*Dpp4*$^{hep-/-}$), as well as an endothelial- and hematopoietic-specific knockout (*Dpp4*$^{EC-/-}$). *Dpp4*$^{hep-/-}$ mice are generated using a cre/lox system induced with a tissue-specific adeno-associated virus (AAV). Locus of X-over P1 (loxP) sites are introduced into the introns that flank exon 22 of the *Dpp4* gene to generate *Dpp4*$^{flox/flox}$ mice[532]. Subsequently, control mice are injected with an AAV-green fluorescent protein (GFP), to simulate injection and gene expression without gene excision to generate *Dpp4*^{GFP} mice[473]. *Dpp4*$^{hep-/-}$ mice are injected with an AAV serotype 8[473], meaning it has tropism to transduce hepatocytes efficiently without significant off-target impacts[533]. Cre expression is driven by a promoter, thyroxin-binding globulin (TBG) protein, that additionally helps with hepatocyte targeting, without affecting Kupffer cells and endothelial cells[473,534].

In contrast, *Dpp4*$^{EC-/-}$ mice were generated by crossing *Dpp4*$^{flox/flox}$ mice with transgenic mice expressing cre recombinase directed by an endothelial-specific receptor tyrosine kinase (*Tek* or *Tie2*) promoter[532]. Offspring homozygous for the loxP flanked allele with no cre transgene and those with cre transgene without loxP flanked alleles were used as control mice[532]. Experimental mice were homozygous for the loxP flanked allele and possessed a cre transgene[532].

1.7 Scope of Thesis, Hypotheses and Aims

Approximately 1 in 5 Canadians are living with metabolic syndrome, increasing their risk of developing debilitating diseases like MASLD, HF and acute MI[535]. This statistic is increasing as the population ages (1 in 10 aged 18-39 versus 4 in 10 aged 60-79)[535]. Currently, aggressive lifestyle changes (i.e. exercise, healthy eating, smoking cessation) are first prescribed prior to pharmaceuticals. Despite scientific and clinical advancements, individuals are succumbing to these chronic diseases at an alarming rate. Therefore, it is of importance to expand our knowledge of these diseases at a molecular level, particularly processes involving DPP4, and leverage the findings to increase quality of life.

The studies in this thesis employ a diet-induced *in vivo* model of obesity and metabolic disease in aged mice to explore the pathophysiological implications of DPP4 in MASLD and CVD. Using systemic (*Dpp4*$^{-/-}$) and tissue-specific knockout models (*Dpp4*$^{hep-/-}$ and *Dpp4*$^{EC-/-}$ mice), DPP4 was assessed as a moderator of HGP, hepatic steatosis, fibrosis and inflammation. Further, the involvement of DPP4 in HCV associated MASLD and in a lean mouse model of MASLD was investigated, to probe infectious and obesity-independent disease models. Diastolic dysfunction and molecular cardiac remodeling and inflammation were also examined in the absence of hepatocyte-derived DPP4. Here we investigated how a hepatokine, DPP4, can affect disease progression in peripheral tissue. Lastly, the cardioprotective effects of metformin and DPP4i's in obese mice following experimental MI (LAD-ligation) was considered in *Dpp4*$^{-/-}$, *Dpp4*$^{hep-/-}$ and *Dpp4*$^{EC-/-}$ mice to illuminate pharmaceutical mechanisms and the multifaceted origin-dependent function of DPP4.

Chapters 2, 3 and 4 address the following hypotheses:

Chapter 2: Reducing glucoregulatory endothelial cell-derived and proinflammatory hepatocyte-derived DPP4 will reduce HGP and prevent the progression of MASLD in old, obese mice.

Chapter 3: Reducing proinflammatory hepatocyte-derived DPP4 will prevent cardiac diastolic dysfunction and adverse remodeling in old, obese male mice.

Chapter 4: Reducing circulating endothelial cell- and immune cell-derived DPP4 will reduce inflammation and metabolic disease related CVD progression, independent of catalytic activity.

We will address these hypotheses by completing the following aims:

Chapter 2: Determine if dysglycemia and liver disease progression can be prevented by genetic elimination of endothelial cell-derived or hepatocyte-derived DPP4.

Chapter 3: Determine if age and HFHC diet-induced diastolic dysfunction can be prevented by genetic elimination of hepatocyte-derived DPP4

Chapter 4: Determine the mechanism by which metformin, DPP4 inhibition and combination therapy affect DPP4 activity, GLP-1 secretion and bioactivity, inflammation, and remodeling to maintain cardiac function after myocardial infarction.

1.8 References

1. Heart and Stroke Month. Statistics Canada. https://www.statcan.gc.ca/o1/en/plus/353-heart-and-stroke-month. Published 2023. Accessed October 16 2023.
2. Information CIfH. *Hospital stays in Canda.*
3. Ko DT, Khera R, Lau G, et al. Readmission and Mortality After Hospitalization for Myocardial Infarction and Heart Failure. *J Am Coll Cardiol.* 2020;75(7):736-746.
4. Williams KJ, Tabas I. The response-to-retention hypothesis of early atherogenesis. *Arterioscler Thromb Vasc Biol.* 1995;15(5):551-561.
5. Chien S. Mechanotransduction and endothelial cell homeostasis: the wisdom of the cell. *Am J Physiol Heart Circ Physiol.* 2007;292(3):H1209-1224.
6. Salari N, Morddarvanjoghi F, Abdolmaleki A, et al. The global prevalence of myocardial infarction: a systematic review and meta-analysis. *BMC Cardiovasc Disord.* 2023;23(1):206.
7. Ponikowski P, Voors AA, Anker SD, et al. 2016 ESC Guidelines for the diagnosis and treatment of acute and chronic heart failure: The Task Force for the diagnosis and treatment of acute and chronic heart failure of the European Society of Cardiology (ESC)Developed with the special contribution of the Heart Failure Association (HFA) of the ESC. *Eur Heart J.* 2016;37(27):2129-2200.
8. Tran DT, Ohinmaa A, Thanh NX, et al. The current and future financial burden of hospital admissions for heart failure in Canada: a cost analysis. *CMAJ Open.* 2016;4(3):E365-E370.
9. Foundation HaS. Falling Short: How Canada is failing people with heart failure – and how we can change that. https://heartstrokeprod.azureedge.net/-/media/pdf-files/canada/2022-heart-month/hs-heart-failure-report-2022-final. Accessed December 5, 2023.
10. Yusuf S, Hawken S, Ounpuu S, et al. Effect of potentially modifiable risk factors associated with myocardial infarction in 52 countries (the INTERHEART study): case-control study. *Lancet.* 2004;364(9438):937-952.
11. Anand SS, Islam S, Rosengren A, et al. Risk factors for myocardial infarction in women and men: insights from the INTERHEART study. *Eur Heart J.* 2008;29(7):932-940.
12. Reimer KA, Jennings RB, Tatum AH. Pathobiology of acute myocardial ischemia: metabolic, functional and ultrastructural studies. *Am J Cardiol.* 1983;52(2):72A-81A.
13. Huang S, Frangogiannis NG. Anti-inflammatory therapies in myocardial infarction: failures, hopes and challenges. *Br J Pharmacol.* 2018;175(9):1377-1400.
14. Halade GV, Lee DH. Inflammation and resolution signaling in cardiac repair and heart failure. *EBioMedicine.* 2022;79:103992.
15. Frangogiannis NG. Regulation of the inflammatory response in cardiac repair. *Circ Res.* 2012;110(1):159-173.

16. Prabhu SD, Frangogiannis NG. The Biological Basis for Cardiac Repair After Myocardial Infarction: From Inflammation to Fibrosis. *Circ Res.* 2016;119(1):91-112.
17. Janse MJ, Cinca J, Morena H, et al. The "border zone" in myocardial ischemia. An electrophysiological, metabolic, and histochemical correlation in the pig heart. *Circ Res.* 1979;44(4):576-588.
18. Palojoki E, Saraste A, Eriksson A, et al. Cardiomyocyte apoptosis and ventricular remodeling after myocardial infarction in rats. *Am J Physiol Heart Circ Physiol.* 2001;280(6):H2726-2731.
19. Dube KN, Thomas TM, Munshaw S, Rohling M, Riley PR, Smart N. Recapitulation of developmental mechanisms to revascularize the ischemic heart. *JCI Insight.* 2017;2(22).
20. Liao JK. Linking endothelial dysfunction with endothelial cell activation. *J Clin Invest.* 2013;123(2):540-541.
21. Zhang W, Lavine KJ, Epelman S, et al. Necrotic myocardial cells release damage-associated molecular patterns that provoke fibroblast activation in vitro and trigger myocardial inflammation and fibrosis in vivo. *J Am Heart Assoc.* 2015;4(6):e001993.
22. Zhang Q, Wang L, Wang S, et al. Signaling pathways and targeted therapy for myocardial infarction. *Signal Transduct Target Ther.* 2022;7(1):78.
23. Loukili N, Rosenblatt-Velin N, Li J, et al. Peroxynitrite induces HMGB1 release by cardiac cells in vitro and HMGB1 upregulation in the infarcted myocardium in vivo. *Cardiovasc Res.* 2011;89(3):586-594.
24. Arslan F, Smeets MB, Riem Vis PW, et al. Lack of fibronectin-EDA promotes survival and prevents adverse remodeling and heart function deterioration after myocardial infarction. *Circ Res.* 2011;108(5):582-592.
25. Lugrin J, Parapanov R, Rosenblatt-Velin N, et al. Cutting edge: IL-1alpha is a crucial danger signal triggering acute myocardial inflammation during myocardial infarction. *J Immunol.* 2015;194(2):499-503.
26. Gordon JW, Shaw JA, Kirshenbaum LA. Multiple facets of NF-kappaB in the heart: to be or not to NF-kappaB. *Circ Res.* 2011;108(9):1122-1132.
27. Chen LF, Greene WC. Shaping the nuclear action of NF-kappaB. *Nat Rev Mol Cell Biol.* 2004;5(5):392-401.
28. Swirski FK, Nahrendorf M, Etzrodt M, et al. Identification of splenic reservoir monocytes and their deployment to inflammatory sites. *Science.* 2009;325(5940):612-616.
29. Horckmans M, Ring L, Duchene J, et al. Neutrophils orchestrate post-myocardial infarction healing by polarizing macrophages towards a reparative phenotype. *Eur Heart J.* 2017;38(3):187-197.
30. Nahrendorf M, Pittet MJ, Swirski FK. Monocytes: protagonists of infarct inflammation and repair after myocardial infarction. *Circulation.* 2010;121(22):2437-2445.
31. Nahrendorf M, Swirski FK, Aikawa E, et al. The healing myocardium sequentially mobilizes two monocyte subsets with divergent and complementary functions. *J Exp Med.* 2007;204(12):3037-3047.

32. Leuschner F, Rauch PJ, Ueno T, et al. Rapid monocyte kinetics in acute myocardial infarction are sustained by extramedullary monocytopoiesis. *J Exp Med.* 2012;209(1):123-137.
33. Kolaczkowska E, Kubes P. Neutrophil recruitment and function in health and inflammation. *Nat Rev Immunol.* 2013;13(3):159-175.
34. Mantovani A, Cassatella MA, Costantini C, Jaillon S. Neutrophils in the activation and regulation of innate and adaptive immunity. *Nat Rev Immunol.* 2011;11(8):519-531.
35. Serhan CN, Chiang N, Van Dyke TE. Resolving inflammation: dual anti-inflammatory and pro-resolution lipid mediators. *Nat Rev Immunol.* 2008;8(5):349-361.
36. Soehnlein O, Lindbom L. Phagocyte partnership during the onset and resolution of inflammation. *Nat Rev Immunol.* 2010;10(6):427-439.
37. Willems IE, Havenith MG, De Mey JG, Daemen MJ. The alpha-smooth muscle actin-positive cells in healing human myocardial scars. *Am J Pathol.* 1994;145(4):868-875.
38. Frangogiannis NG, Michael LH, Entman ML. Myofibroblasts in reperfused myocardial infarcts express the embryonic form of smooth muscle myosin heavy chain (SMemb). *Cardiovasc Res.* 2000;48(1):89-100.
39. Turner NA, Porter KE. Function and fate of myofibroblasts after myocardial infarction. *Fibrogenesis Tissue Repair.* 2013;6(1):5.
40. Porrello ER, Mahmoud AI, Simpson E, et al. Transient regenerative potential of the neonatal mouse heart. *Science.* 2011;331(6020):1078-1080.
41. Bergmann O, Bhardwaj RD, Bernard S, et al. Evidence for cardiomyocyte renewal in humans. *Science.* 2009;324(5923):98-102.
42. Linzbach AJ. Heart failure from the point of view of quantitative anatomy. *Am J Cardiol.* 1960;5:370-382.
43. Quaini F, Cigola E, Lagrasta C, et al. End-stage cardiac failure in humans is coupled with the induction of proliferating cell nuclear antigen and nuclear mitotic division in ventricular myocytes. *Circ Res.* 1994;75(6):1050-1063.
44. Kajstura J, Leri A, Finato N, Di Loreto C, Beltrami CA, Anversa P. Myocyte proliferation in end-stage cardiac failure in humans. *Proc Natl Acad Sci U S A.* 1998;95(15):8801-8805.
45. Kajstura J, Zhang X, Reiss K, et al. Myocyte cellular hyperplasia and myocyte cellular hypertrophy contribute to chronic ventricular remodeling in coronary artery narrowing-induced cardiomyopathy in rats. *Circ Res.* 1994;74(3):383-400.
46. Beltrami AP, Urbanek K, Kajstura J, et al. Evidence that human cardiac myocytes divide after myocardial infarction. *N Engl J Med.* 2001;344(23):1750-1757.
47. Hill JA, Olson EN. Cardiac plasticity. *N Engl J Med.* 2008;358(13):1370-1380.
48. Sutton MG, Sharpe N. Left ventricular remodeling after myocardial infarction: pathophysiology and therapy. *Circulation.* 2000;101(25):2981-2988.
49. Frangogiannis NG. The Extracellular Matrix in Ischemic and Nonischemic Heart Failure. *Circ Res.* 2019;125(1):117-146.

50. Dobaczewski M, Gonzalez-Quesada C, Frangogiannis NG. The extracellular matrix as a modulator of the inflammatory and reparative response following myocardial infarction. *J Mol Cell Cardiol.* 2010;48(3):504-511.
51. Liu B, Wang B, Zhang X, Lock R, Nash T, Vunjak-Novakovic G. Cell type-specific microRNA therapies for myocardial infarction. *Sci Transl Med.* 2021;13(580).
52. Souders CA, Bowers SL, Baudino TA. Cardiac fibroblast: the renaissance cell. *Circ Res.* 2009;105(12):1164-1176.
53. Bujak M, Ren G, Kweon HJ, et al. Essential role of Smad3 in infarct healing and in the pathogenesis of cardiac remodeling. *Circulation.* 2007;116(19):2127-2138.
54. Shinde AV, Humeres C, Frangogiannis NG. The role of alpha-smooth muscle actin in fibroblast-mediated matrix contraction and remodeling. *Biochim Biophys Acta Mol Basis Dis.* 2017;1863(1):298-309.
55. Trueblood NA, Xie Z, Communal C, et al. Exaggerated left ventricular dilation and reduced collagen deposition after myocardial infarction in mice lacking osteopontin. *Circ Res.* 2001;88(10):1080-1087.
56. Oka T, Xu J, Kaiser RA, et al. Genetic manipulation of periostin expression reveals a role in cardiac hypertrophy and ventricular remodeling. *Circ Res.* 2007;101(3):313-321.
57. Shimazaki M, Nakamura K, Kii I, et al. Periostin is essential for cardiac healing after acute myocardial infarction. *J Exp Med.* 2008;205(2):295-303.
58. Frangogiannis NG. Matricellular proteins in cardiac adaptation and disease. *Physiol Rev.* 2012;92(2):635-688.
59. Rusu M, Hilse K, Schuh A, et al. Biomechanical assessment of remote and postinfarction scar remodeling following myocardial infarction. *Sci Rep.* 2019;9(1):16744.
60. Holmes JW, Borg TK, Covell JW. Structure and mechanics of healing myocardial infarcts. *Annu Rev Biomed Eng.* 2005;7:223-253.
61. Dittrich A, Lauridsen H. Myocardial infarction and the immune response - Scarring or regeneration? A comparative look at mammals and popular regenerating animal models. *Journal of Immunology and Regenerative Medicine.* 2019;4.
62. Shinde AV, Frangogiannis NG. Fibroblasts in myocardial infarction: a role in inflammation and repair. *J Mol Cell Cardiol.* 2014;70:74-82.
63. Jenca D, Melenovsky V, Stehlik J, et al. Heart failure after myocardial infarction: incidence and predictors. *ESC Heart Fail.* 2021;8(1):222-237.
64. Friedberg MK, Redington AN. Right versus left ventricular failure: differences, similarities, and interactions. *Circulation.* 2014;129(9):1033-1044.
65. Types of Heart Failure. https://www.heart.org/en/health-topics/heart-failure/what-is-heart-failure/types-of-heart-failure. Updated March 23, 2023. Accessed February 2, 2024.
66. Savarese G, Stolfo D, Sinagra G, Lund LH. Heart failure with mid-range or mildly reduced ejection fraction. *Nat Rev Cardiol.* 2022;19(2):100-116.
67. Vedin O, Lam CSP, Koh AS, et al. Significance of Ischemic Heart Disease in Patients With Heart Failure and Preserved, Midrange, and Reduced Ejection Fraction: A Nationwide Cohort Study. *Circ Heart Fail.* 2017;10(6).

68. Soufi MK, Almahmoud MF, Kadri AN, et al. Heart Failure With Stable Mildly-reduced Ejection Fraction: Prognosis and Predictors of Outcomes. *Curr Probl Cardiol.* 2023;48(5):101631.
69. Simmonds SJ, Cuijpers I, Heymans S, Jones EAV. Cellular and Molecular Differences between HFpEF and HFrEF: A Step Ahead in an Improved Pathological Understanding. *Cells.* 2020;9(1).
70. Paulus WJ, Tschope C. A novel paradigm for heart failure with preserved ejection fraction: comorbidities drive myocardial dysfunction and remodeling through coronary microvascular endothelial inflammation. *J Am Coll Cardiol.* 2013;62(4):263-271.
71. Chen GY, Nunez G. Sterile inflammation: sensing and reacting to damage. *Nat Rev Immunol.* 2010;10(12):826-837.
72. Bezbradica JS, Coll RC, Schroder K. Sterile signals generate weaker and delayed macrophage NLRP3 inflammasome responses relative to microbial signals. *Cell Mol Immunol.* 2017;14(1):118-126.
73. Spinale FG, Zile MR. Integrating the myocardial matrix into heart failure recognition and management. *Circ Res.* 2013;113(6):725-738.
74. Tang TT, Yuan J, Zhu ZF, et al. Regulatory T cells ameliorate cardiac remodeling after myocardial infarction. *Basic Res Cardiol.* 2012;107(1):232.
75. Mishra S, Kass DA. Cellular and molecular pathobiology of heart failure with preserved ejection fraction. *Nat Rev Cardiol.* 2021;18(6):400-423.
76. Collier P, Watson CJ, Voon V, et al. Can emerging biomarkers of myocardial remodelling identify asymptomatic hypertensive patients at risk for diastolic dysfunction and diastolic heart failure? *Eur J Heart Fail.* 2011;13(10):1087-1095.
77. Kalogeropoulos A, Georgiopoulou V, Psaty BM, et al. Inflammatory markers and incident heart failure risk in older adults: the Health ABC (Health, Aging, and Body Composition) study. *J Am Coll Cardiol.* 2010;55(19):2129-2137.
78. DuBrock HM, AbouEzzeddine OF, Redfield MM. High-sensitivity C-reactive protein in heart failure with preserved ejection fraction. *PLoS One.* 2018;13(8):e0201836.
79. Westermann D, Lindner D, Kasner M, et al. Cardiac inflammation contributes to changes in the extracellular matrix in patients with heart failure and normal ejection fraction. *Circ Heart Fail.* 2011;4(1):44-52.
80. van Heerebeek L, Borbely A, Niessen HW, et al. Myocardial structure and function differ in systolic and diastolic heart failure. *Circulation.* 2006;113(16):1966-1973.
81. Franssen C, Chen S, Unger A, et al. Myocardial Microvascular Inflammatory Endothelial Activation in Heart Failure With Preserved Ejection Fraction. *JACC Heart Fail.* 2016;4(4):312-324.
82. Fu X, Khalil H, Kanisicak O, et al. Specialized fibroblast differentiated states underlie scar formation in the infarcted mouse heart. *J Clin Invest.* 2018;128(5):2127-2143.
83. Humeres C, Frangogiannis NG. Fibroblasts in the Infarcted, Remodeling, and Failing Heart. *JACC Basic Transl Sci.* 2019;4(3):449-467.
84. Eschalier R, Rossignol P, Kearney-Schwartz A, et al. Features of cardiac remodeling, associated with blood pressure and fibrosis biomarkers, are

frequent in subjects with abdominal obesity. *Hypertension.* 2014;63(4):740-746.
85. Sweeney M, Corden B, Cook SA. Targeting cardiac fibrosis in heart failure with preserved ejection fraction: mirage or miracle? *EMBO Mol Med.* 2020;12(10):e10865.
86. van Amerongen MJ, Harmsen MC, van Rooijen N, Petersen AH, van Luyn MJ. Macrophage depletion impairs wound healing and increases left ventricular remodeling after myocardial injury in mice. *Am J Pathol.* 2007;170(3):818-829.
87. Bomb R, Heckle MR, Sun Y, et al. Myofibroblast secretome and its auto-/paracrine signaling. *Expert Rev Cardiovasc Ther.* 2016;14(5):591-598.
88. Alem MM. Endothelial Dysfunction in Chronic Heart Failure: Assessment, Findings, Significance, and Potential Therapeutic Targets. *Int J Mol Sci.* 2019;20(13).
89. Hare JM. Nitroso-redox balance in the cardiovascular system. *N Engl J Med.* 2004;351(20):2112-2114.
90. Karantalis V, Schulman IH, Hare JM. Nitroso-redox imbalance affects cardiac structure and function. *J Am Coll Cardiol.* 2013;61(9):933-935.
91. Frey RS, Ushio-Fukai M, Malik AB. NADPH oxidase-dependent signaling in endothelial cells: role in physiology and pathophysiology. *Antioxid Redox Signal.* 2009;11(4):791-810.
92. Premer C, Kanelidis AJ, Hare JM, Schulman IH. Rethinking Endothelial Dysfunction as a Crucial Target in Fighting Heart Failure. *Mayo Clin Proc Innov Qual Outcomes.* 2019;3(1):1-13.
93. Schulz E, Jansen T, Wenzel P, Daiber A, Munzel T. Nitric oxide, tetrahydrobiopterin, oxidative stress, and endothelial dysfunction in hypertension. *Antioxid Redox Signal.* 2008;10(6):1115-1126.
94. Greene SJ, Gheorghiade M, Borlaug BA, et al. The cGMP signaling pathway as a therapeutic target in heart failure with preserved ejection fraction. *J Am Heart Assoc.* 2013;2(6):e000536.
95. Brutsaert DL. Cardiac endothelial-myocardial signaling: its role in cardiac growth, contractile performance, and rhythmicity. *Physiol Rev.* 2003;83(1):59-115.
96. Borbely A, Falcao-Pires I, van Heerebeek L, et al. Hypophosphorylation of the Stiff N2B titin isoform raises cardiomyocyte resting tension in failing human myocardium. *Circ Res.* 2009;104(6):780-786.
97. Hamdani N, Franssen C, Lourenco A, et al. Myocardial titin hypophosphorylation importantly contributes to heart failure with preserved ejection fraction in a rat metabolic risk model. *Circ Heart Fail.* 2013;6(6):1239-1249.
98. Mollace R, Scarano F, Bava I, et al. Modulation of the nitric oxide/cGMP pathway in cardiac contraction and relaxation: Potential role in heart failure treatment. *Pharmacol Res.* 2023;196:106931.
99. Tsai EJ, Kass DA. Cyclic GMP signaling in cardiovascular pathophysiology and therapeutics. *Pharmacol Ther.* 2009;122(3):216-238.
100. Takimoto E, Champion HC, Li M, et al. Chronic inhibition of cyclic GMP phosphodiesterase 5A prevents and reverses cardiac hypertrophy. *Nat Med.* 2005;11(2):214-222.

101. Koitabashi N, Aiba T, Hesketh GG, et al. Cyclic GMP/PKG-dependent inhibition of TRPC6 channel activity and expression negatively regulates cardiomyocyte NFAT activation Novel mechanism of cardiac stress modulation by PDE5 inhibition. *J Mol Cell Cardiol.* 2010;48(4):713-724.
102. Nagueh SF, Shah G, Wu Y, et al. Altered titin expression, myocardial stiffness, and left ventricular function in patients with dilated cardiomyopathy. *Circulation.* 2004;110(2):155-162.
103. Franssen C, Kole J, Musters R, Hamdani N, Paulus WJ. alpha-B Crystallin Reverses High Diastolic Stiffness of Failing Human Cardiomyocytes. *Circ Heart Fail.* 2017;10(3):e003626.
104. Ali MA, Cho WJ, Hudson B, Kassiri Z, Granzier H, Schulz R. Titin is a target of matrix metalloproteinase-2: implications in myocardial ischemia/reperfusion injury. *Circulation.* 2010;122(20):2039-2047.
105. Ponikowski P, Voors AA, Anker SD, et al. 2016 ESC Guidelines for the diagnosis and treatment of acute and chronic heart failure: The Task Force for the diagnosis and treatment of acute and chronic heart failure of the European Society of Cardiology (ESC). Developed with the special contribution of the Heart Failure Association (HFA) of the ESC. *Eur J Heart Fail.* 2016;18(8):891-975.
106. Hsu S, Fang JC, Borlaug BA. Hemodynamics for the Heart Failure Clinician: A State-of-the-Art Review. *J Card Fail.* 2022;28(1):133-148.
107. Schultheiss HP, Fairweather D, Caforio ALP, et al. Dilated cardiomyopathy. *Nat Rev Dis Primers.* 2019;5(1):32.
108. Borlaug BA. The pathophysiology of heart failure with preserved ejection fraction. *Nat Rev Cardiol.* 2014;11(9):507-515.
109. Nauta JF, Hummel YM, Tromp J, et al. Concentric vs. eccentric remodelling in heart failure with reduced ejection fraction: clinical characteristics, pathophysiology and response to treatment. *Eur J Heart Fail.* 2020;22(7):1147-1155.
110. Ogilvie LM, Edgett BA, Huber JS, et al. Hemodynamic assessment of diastolic function for experimental models. *Am J Physiol Heart Circ Physiol.* 2020;318(5):H1139-H1158.
111. Borlaug BA, Olson TP, Lam CS, et al. Global cardiovascular reserve dysfunction in heart failure with preserved ejection fraction. *J Am Coll Cardiol.* 2010;56(11):845-854.
112. Solomon SD, Rizkala AR, Lefkowitz MP, et al. Baseline Characteristics of Patients With Heart Failure and Preserved Ejection Fraction in the PARAGON-HF Trial. *Circ Heart Fail.* 2018;11(7):e004962.
113. Chengode S. Left ventricular global systolic function assessment by echocardiography. *Ann Card Anaesth.* 2016;19(Supplement):S26-S34.
114. Abduch MC, Alencar AM, Mathias W, Jr., Vieira ML. Cardiac mechanics evaluated by speckle tracking echocardiography. *Arq Bras Cardiol.* 2014;102(4):403-412.
115. Voigt JU, Pedrizzetti G, Lysyansky P, et al. Definitions for a common standard for 2D speckle tracking echocardiography: consensus document of the EACVI/ASE/Industry Task Force to standardize deformation imaging. *Eur Heart J Cardiovasc Imaging.* 2015;16(1):1-11.

116. Dandel M, Lehmkuhl H, Knosalla C, Suramelashvili N, Hetzer R. Strain and strain rate imaging by echocardiography - basic concepts and clinical applicability. *Curr Cardiol Rev.* 2009;5(2):133-148.
117. Whelton PK, Carey RM, Aronow WS, et al. 2017 ACC/AHA/AAPA/ABC/ACPM/AGS/APhA/ASH/ASPC/NMA/PCNA Guideline for the Prevention, Detection, Evaluation, and Management of High Blood Pressure in Adults: Executive Summary: A Report of the American College of Cardiology/American Heart Association Task Force on Clinical Practice Guidelines. *Circulation.* 2018;138(17):e426-e483.
118. van den Dorpel MMP, Heinonen I, Snelder SM, et al. Early detection of left ventricular diastolic dysfunction using conventional and speckle tracking echocardiography in a large animal model of metabolic dysfunction. *Int J Cardiovasc Imaging.* 2018;34(5):743-749.
119. Benedict M, Zhang X. Non-alcoholic fatty liver disease: An expanded review. *World J Hepatol.* 2017;9(16):715-732.
120. Targher G, Byrne CD. Clinical Review: Nonalcoholic fatty liver disease: a novel cardiometabolic risk factor for type 2 diabetes and its complications. *J Clin Endocrinol Metab.* 2013;98(2):483-495.
121. Dharmalingam M, Yamasandhi PG. Nonalcoholic Fatty Liver Disease and Type 2 Diabetes Mellitus. *Indian J Endocrinol Metab.* 2018;22(3):421-428.
122. Cotter TG, Rinella M. Nonalcoholic Fatty Liver Disease 2020: The State of the Disease. *Gastroenterology.* 2020;158(7):1851-1864.
123. Riazi K, Azhari H, Charette JH, et al. The prevalence and incidence of NAFLD worldwide: a systematic review and meta-analysis. *Lancet Gastroenterol Hepatol.* 2022;7(9):851-861.
124. Younossi ZM, Golabi P, Paik JM, Henry A, Van Dongen C, Henry L. The global epidemiology of nonalcoholic fatty liver disease (NAFLD) and nonalcoholic steatohepatitis (NASH): a systematic review. *Hepatology.* 2023;77(4):1335-1347.
125. Anstee QM, Reeves HL, Kotsiliti E, Govaere O, Heikenwalder M. From NASH to HCC: current concepts and future challenges. *Nat Rev Gastroenterol Hepatol.* 2019;16(7):411-428.
126. Eslam M, Newsome PN, Sarin SK, et al. A new definition for metabolic dysfunction-associated fatty liver disease: An international expert consensus statement. *J Hepatol.* 2020;73(1):202-209.
127. Rinella ME, Lazarus JV, Ratziu V, et al. A multisociety Delphi consensus statement on new fatty liver disease nomenclature. *Hepatology.* 2023;78(6):1966-1986.
128. Rinella ME, Lazarus JV, Ratziu V, et al. A multisociety Delphi consensus statement on new fatty liver disease nomenclature. *J Hepatol.* 2023;79(6):1542-1556.
129. Diehl AM, Day C. Cause, Pathogenesis, and Treatment of Nonalcoholic Steatohepatitis. *N Engl J Med.* 2017;377(21):2063-2072.
130. Wong VW, Ekstedt M, Wong GL, Hagstrom H. Changing epidemiology, global trends and implications for outcomes of NAFLD. *J Hepatol.* 2023;79(3):842-852.

131. Singh S, Allen AM, Wang Z, Prokop LJ, Murad MH, Loomba R. Fibrosis progression in nonalcoholic fatty liver vs nonalcoholic steatohepatitis: a systematic review and meta-analysis of paired-biopsy studies. *Clin Gastroenterol Hepatol.* 2015;13(4):643-654 e641-649; quiz e639-640.
132. Loomba R, Adams LA. The 20% Rule of NASH Progression: The Natural History of Advanced Fibrosis and Cirrhosis Caused by NASH. *Hepatology.* 2019;70(6):1885-1888.
133. Fattovich G, Stroffolini T, Zagni I, Donato F. Hepatocellular carcinoma in cirrhosis: incidence and risk factors. *Gastroenterology.* 2004;127(5 Suppl 1):S35-50.
134. Struben VM, Hespenheide EE, Caldwell SH. Nonalcoholic steatohepatitis and cryptogenic cirrhosis within kindreds. *Am J Med.* 2000;108(1):9-13.
135. Eslam M, George J. Genetic and epigenetic mechanisms of NASH. *Hepatol Int.* 2016;10(3):394-406.
136. Kneeman JM, Misdraji J, Corey KE. Secondary causes of nonalcoholic fatty liver disease. *Therap Adv Gastroenterol.* 2012;5(3):199-207.
137. Petruzziello A, Marigliano S, Loquercio G, Cozzolino A, Cacciapuoti C. Global epidemiology of hepatitis C virus infection: An up-date of the distribution and circulation of hepatitis C virus genotypes. *World J Gastroenterol.* 2016;22(34):7824-7840.
138. Patel A, Harrison SA. Hepatitis C virus infection and nonalcoholic steatohepatitis. *Gastroenterol Hepatol (N Y).* 2012;8(5):305-312.
139. van Welzen BJ, Mudrikova T, El Idrissi A, Hoepelman AIM, Arends JE. A Review of Non-Alcoholic Fatty Liver Disease in HIV-Infected Patients: The Next Big Thing? *Infect Dis Ther.* 2019;8(1):33-50.
140. Grieco A, Forgione A, Miele L, et al. Fatty liver and drugs. *Eur Rev Med Pharmacol Sci.* 2005;9(5):261-263.
141. Adinolfi LE, Rinaldi L, Guerrera B, et al. NAFLD and NASH in HCV Infection: Prevalence and Significance in Hepatic and Extrahepatic Manifestations. *Int J Mol Sci.* 2016;17(6).
142. Vidali M, Tripodi MF, Ivaldi A, et al. Interplay between oxidative stress and hepatic steatosis in the progression of chronic hepatitis C. *J Hepatol.* 2008;48(3):399-406.
143. Adinolfi LE, Zampino R, Restivo L, et al. Chronic hepatitis C virus infection and atherosclerosis: clinical impact and mechanisms. *World J Gastroenterol.* 2014;20(13):3410-3417.
144. Fabbrini E, Sullivan S, Klein S. Obesity and nonalcoholic fatty liver disease: biochemical, metabolic, and clinical implications. *Hepatology.* 2010;51(2):679-689.
145. Sarafidis PA, Nilsson PM. The metabolic syndrome: a glance at its history. *J Hypertens.* 2006;24(4):621-626.
146. Choudhury J, Sanyal AJ. Insulin resistance and the pathogenesis of nonalcoholic fatty liver disease. *Clin Liver Dis.* 2004;8(3):575-594, ix.
147. Manco M. Insulin Resistance and NAFLD: A Dangerous Liaison beyond the Genetics. *Children (Basel).* 2017;4(8).

148. van der Poorten D, George J. Disease-specific mechanisms of fibrosis: hepatitis C virus and nonalcoholic steatohepatitis. *Clin Liver Dis.* 2008;12(4):805-824, ix.
149. Spalding KL, Bernard S, Naslund E, et al. Impact of fat mass and distribution on lipid turnover in human adipose tissue. *Nat Commun.* 2017;8:15253.
150. Sun K, Kusminski CM, Scherer PE. Adipose tissue remodeling and obesity. *J Clin Invest.* 2011;121(6):2094-2101.
151. Ipsen DH, Lykkesfeldt J, Tveden-Nyborg P. Molecular mechanisms of hepatic lipid accumulation in non-alcoholic fatty liver disease. *Cell Mol Life Sci.* 2018;75(18):3313-3327.
152. Froesch ER. The physiology and pharmacology of adipose tissue lipolysis: its inhibition and implications for the treatment of diabetes. *Diabetologia.* 1967;3(6):475-487.
153. Yang A, Mottillo EP. Adipocyte lipolysis: from molecular mechanisms of regulation to disease and therapeutics. *Biochem J.* 2020;477(5):985-1008.
154. Lomonaco R, Ortiz-Lopez C, Orsak B, et al. Effect of adipose tissue insulin resistance on metabolic parameters and liver histology in obese patients with nonalcoholic fatty liver disease. *Hepatology.* 2012;55(5):1389-1397.
155. Rada P, Gonzalez-Rodriguez A, Garcia-Monzon C, Valverde AM. Understanding lipotoxicity in NAFLD pathogenesis: is CD36 a key driver? *Cell Death Dis.* 2020;11(9):802.
156. Bordewick U, Heese M, Borchers T, Robenek H, Spener F. Compartmentation of hepatic fatty-acid-binding protein in liver cells and its effect on microsomal phosphatidic acid biosynthesis. *Biol Chem Hoppe Seyler.* 1989;370(3):229-238.
157. Wang G, Bonkovsky HL, de Lemos A, Burczynski FJ. Recent insights into the biological functions of liver fatty acid binding protein 1. *J Lipid Res.* 2015;56(12):2238-2247.
158. Sanyal AJ, Campbell-Sargent C, Mirshahi F, et al. Nonalcoholic steatohepatitis: association of insulin resistance and mitochondrial abnormalities. *Gastroenterology.* 2001;120(5):1183-1192.
159. Pessayre D, Fromenty B. NASH: a mitochondrial disease. *J Hepatol.* 2005;42(6):928-940.
160. Del Rio LA, Lopez-Huertas E. ROS Generation in Peroxisomes and its Role in Cell Signaling. *Plant Cell Physiol.* 2016;57(7):1364-1376.
161. Yamaguchi K, Yang L, McCall S, et al. Inhibiting triglyceride synthesis improves hepatic steatosis but exacerbates liver damage and fibrosis in obese mice with nonalcoholic steatohepatitis. *Hepatology.* 2007;45(6):1366-1374.
162. Alves-Bezerra M, Cohen DE. Triglyceride Metabolism in the Liver. *Compr Physiol.* 2017;8(1):1-8.
163. Mashek DG. Hepatic lipid droplets: A balancing act between energy storage and metabolic dysfunction in NAFLD. *Mol Metab.* 2021;50:101115.
164. Friedman SL, Neuschwander-Tetri BA, Rinella M, Sanyal AJ. Mechanisms of NAFLD development and therapeutic strategies. *Nat Med.* 2018;24(7):908-922.

165. Musso G, Saba F, Cassader M, Gambino R. Lipidomics in pathogenesis, progression and treatment of nonalcoholic steatohepatitis (NASH): Recent advances. *Prog Lipid Res.* 2023;91:101238.
166. Neuschwander-Tetri BA. Hepatic lipotoxicity and the pathogenesis of nonalcoholic steatohepatitis: the central role of nontriglyceride fatty acid metabolites. *Hepatology.* 2010;52(2):774-788.
167. Wree A, Broderick L, Canbay A, Hoffman HM, Feldstein AE. From NAFLD to NASH to cirrhosis-new insights into disease mechanisms. *Nat Rev Gastroenterol Hepatol.* 2013;10(11):627-636.
168. Han MS, Park SY, Shinzawa K, et al. Lysophosphatidylcholine as a death effector in the lipoapoptosis of hepatocytes. *J Lipid Res.* 2008;49(1):84-97.
169. Luukkonen PK, Zhou Y, Sadevirta S, et al. Hepatic ceramides dissociate steatosis and insulin resistance in patients with non-alcoholic fatty liver disease. *J Hepatol.* 2016;64(5):1167-1175.
170. Chiappini F, Coilly A, Kadar H, et al. Metabolism dysregulation induces a specific lipid signature of nonalcoholic steatohepatitis in patients. *Sci Rep.* 2017;7:46658.
171. Donnelly KL, Smith CI, Schwarzenberg SJ, Jessurun J, Boldt MD, Parks EJ. Sources of fatty acids stored in liver and secreted via lipoproteins in patients with nonalcoholic fatty liver disease. *J Clin Invest.* 2005;115(5):1343-1351.
172. Friedman SL. Molecular regulation of hepatic fibrosis, an integrated cellular response to tissue injury. *The Journal of biological chemistry.* 2000;275(4):2247-2250.
173. Smith GI, Shankaran M, Yoshino M, et al. Insulin resistance drives hepatic de novo lipogenesis in nonalcoholic fatty liver disease. *J Clin Invest.* 2020;130(3):1453-1460.
174. Benhamed F, Denechaud PD, Lemoine M, et al. The lipogenic transcription factor ChREBP dissociates hepatic steatosis from insulin resistance in mice and humans. *J Clin Invest.* 2012;122(6):2176-2194.
175. Agius L. Glucokinase and molecular aspects of liver glycogen metabolism. *Biochem J.* 2008;414(1):1-18.
176. Han HS, Kang G, Kim JS, Choi BH, Koo SH. Regulation of glucose metabolism from a liver-centric perspective. *Exp Mol Med.* 2016;48(3):e218.
177. Pilkis SJ, Claus TH. Hepatic gluconeogenesis/glycolysis: regulation and structure/function relationships of substrate cycle enzymes. *Annu Rev Nutr.* 1991;11:465-515.
178. Machado MV, Diehl AM. Pathogenesis of Nonalcoholic Steatohepatitis. *Gastroenterology.* 2016;150(8):1769-1777.
179. Kawano Y, Cohen DE. Mechanisms of hepatic triglyceride accumulation in non-alcoholic fatty liver disease. *J Gastroenterol.* 2013;48(4):434-441.
180. Szabo G, Petrasek J. Inflammasome activation and function in liver disease. *Nat Rev Gastroenterol Hepatol.* 2015;12(7):387-400.
181. Puri P, Mirshahi F, Cheung O, et al. Activation and dysregulation of the unfolded protein response in nonalcoholic fatty liver disease. *Gastroenterology.* 2008;134(2):568-576.
182. Huby T, Gautier EL. Immune cell-mediated features of non-alcoholic steatohepatitis. *Nat Rev Immunol.* 2022;22(7):429-443.

183. Eaton S, Bartlett K, Pourfarzam M. Mammalian mitochondrial beta-oxidation. *Biochem J.* 1996;320 (Pt 2)(Pt 2):345-357.
184. Begriche K, Massart J, Robin MA, Bonnet F, Fromenty B. Mitochondrial adaptations and dysfunctions in nonalcoholic fatty liver disease. *Hepatology.* 2013;58(4):1497-1507.
185. Gao D, Wei C, Chen L, Huang J, Yang S, Diehl AM. Oxidative DNA damage and DNA repair enzyme expression are inversely related in murine models of fatty liver disease. *Am J Physiol Gastrointest Liver Physiol.* 2004;287(5):G1070-1077.
186. Schonfeld P, Wojtczak L. Fatty acids as modulators of the cellular production of reactive oxygen species. *Free Radic Biol Med.* 2008;45(3):231-241.
187. Hetz C, Chevet E, Harding HP. Targeting the unfolded protein response in disease. *Nat Rev Drug Discov.* 2013;12(9):703-719.
188. Lebeaupin C, Vallee D, Hazari Y, Hetz C, Chevet E, Bailly-Maitre B. Endoplasmic reticulum stress signalling and the pathogenesis of non-alcoholic fatty liver disease. *J Hepatol.* 2018;69(4):927-947.
189. Chen Z, Tian R, She Z, Cai J, Li H. Role of oxidative stress in the pathogenesis of nonalcoholic fatty liver disease. *Free Radic Biol Med.* 2020;152:116-141.
190. Hetz C, Chevet E, Oakes SA. Proteostasis control by the unfolded protein response. *Nat Cell Biol.* 2015;17(7):829-838.
191. Magee N, Zou A, Zhang Y. Pathogenesis of Nonalcoholic Steatohepatitis: Interactions between Liver Parenchymal and Nonparenchymal Cells. *Biomed Res Int.* 2016;2016:5170402.
192. Mridha AR, Wree A, Robertson AAB, et al. NLRP3 inflammasome blockade reduces liver inflammation and fibrosis in experimental NASH in mice. *J Hepatol.* 2017;66(5):1037-1046.
193. Csak T, Ganz M, Pespisa J, Kodys K, Dolganiuc A, Szabo G. Fatty acid and endotoxin activate inflammasomes in mouse hepatocytes that release danger signals to stimulate immune cells. *Hepatology.* 2011;54(1):133-144.
194. Wang H, Mehal W, Nagy LE, Rotman Y. Immunological mechanisms and therapeutic targets of fatty liver diseases. *Cell Mol Immunol.* 2021;18(1):73-91.
195. Gong T, Liu L, Jiang W, Zhou R. DAMP-sensing receptors in sterile inflammation and inflammatory diseases. *Nat Rev Immunol.* 2020;20(2):95-112.
196. Gan LT, Van Rooyen DM, Koina ME, McCuskey RS, Teoh NC, Farrell GC. Hepatocyte free cholesterol lipotoxicity results from JNK1-mediated mitochondrial injury and is HMGB1 and TLR4-dependent. *J Hepatol.* 2014;61(6):1376-1384.
197. Schuster S, Cabrera D, Arrese M, Feldstein AE. Triggering and resolution of inflammation in NASH. *Nat Rev Gastroenterol Hepatol.* 2018;15(6):349-364.
198. Arrese M, Cabrera D, Kalergis AM, Feldstein AE. Innate Immunity and Inflammation in NAFLD/NASH. *Dig Dis Sci.* 2016;61(5):1294-1303.
199. Mederacke I, Hsu CC, Troeger JS, et al. Fate tracing reveals hepatic stellate cells as dominant contributors to liver fibrosis independent of its aetiology. *Nat Commun.* 2013;4:2823.

200. Pellicoro A, Ramachandran P, Iredale JP, Fallowfield JA. Liver fibrosis and repair: immune regulation of wound healing in a solid organ. *Nat Rev Immunol.* 2014;14(3):181-194.
201. Jiang JX, Torok NJ. Liver Injury and the Activation of the Hepatic Myofibroblasts. *Curr Pathobiol Rep.* 2013;1(3):215-223.
202. Aguilar RP, Genta S, Oliveros L, Anzulovich A, Gimenez MS, Sanchez SS. Vitamin A deficiency injures liver parenchyma and alters the expression of hepatic extracellular matrix. *J Appl Toxicol.* 2009;29(3):214-222.
203. Perepelyuk M, Terajima M, Wang AY, et al. Hepatic stellate cells and portal fibroblasts are the major cellular sources of collagens and lysyl oxidases in normal liver and early after injury. *Am J Physiol Gastrointest Liver Physiol.* 2013;304(6):G605-614.
204. Rojkind M, Giambrone MA, Biempica L. Collagen types in normal and cirrhotic liver. *Gastroenterology.* 1979;76(4):710-719.
205. Bonnans C, Chou J, Werb Z. Remodelling the extracellular matrix in development and disease. *Nat Rev Mol Cell Biol.* 2014;15(12):786-801.
206. Roeb E, Purucker E, Breuer B, et al. TIMP expression in toxic and cholestatic liver injury in rat. *J Hepatol.* 1997;27(3):535-544.
207. Yoshiji H, Kuriyama S, Miyamoto Y, et al. Tissue inhibitor of metalloproteinases-1 promotes liver fibrosis development in a transgenic mouse model. *Hepatology.* 2000;32(6):1248-1254.
208. Lee UE, Friedman SL. Mechanisms of hepatic fibrogenesis. *Best Pract Res Clin Gastroenterol.* 2011;25(2):195-206.
209. Schuppan D, Afdhal NH. Liver cirrhosis. *Lancet.* 2008;371(9615):838-851.
210. Fukuda Y, Nagura H, Imoto M, Koyama Y. Immunohistochemical studies on structural changes of the hepatic lobules in chronic liver diseases. *Am J Gastroenterol.* 1986;81(12):1149-1155.
211. Ruan B, Duan JL, Xu H, et al. Capillarized Liver Sinusoidal Endothelial Cells Undergo Partial Endothelial-Mesenchymal Transition to Actively Deposit Sinusoidal ECM in Liver Fibrosis. *Front Cell Dev Biol.* 2021;9:671081.
212. Iwakiri Y, Groszmann RJ. The hyperdynamic circulation of chronic liver diseases: from the patient to the molecule. *Hepatology.* 2006;43(2 Suppl 1):S121-131.
213. Harrison SA, Bedossa P, Guy CD, et al. A Phase 3, Randomized, Controlled Trial of Resmetirom in NASH with Liver Fibrosis. *N Engl J Med.* 2024;390(6):497-509.
214. Attia SL, Softic S, Mouzaki M. Evolving Role for Pharmacotherapy in NAFLD/NASH. *Clin Transl Sci.* 2021;14(1):11-19.
215. Harrison SA, Loomba R, Dubourg J, Ratziu V, Noureddin M. Clinical Trial Landscape in NASH. *Clin Gastroenterol Hepatol.* 2023;21(8):2001-2014.
216. Petersen MC, Vatner DF, Shulman GI. Regulation of hepatic glucose metabolism in health and disease. *Nat Rev Endocrinol.* 2017;13(10):572-587.
217. Ekberg K, Landau BR, Wajngot A, et al. Contributions by kidney and liver to glucose production in the postabsorptive state and after 60 h of fasting. *Diabetes.* 1999;48(2):292-298.
218. Moore MC, Coate KC, Winnick JJ, An Z, Cherrington AD. Regulation of hepatic glucose uptake and storage in vivo. *Adv Nutr.* 2012;3(3):286-294.

219. Levine R, Fritz IB. The relation of insulin to liver metabolism. *Diabetes.* 1956;5(3):209-219; discussion, 219-222.
220. Cappel DA, Deja S, Duarte JAG, et al. Pyruvate-Carboxylase-Mediated Anaplerosis Promotes Antioxidant Capacity by Sustaining TCA Cycle and Redox Metabolism in Liver. *Cell Metab.* 2019;29(6):1291-1305 e1298.
221. LaMoia TE, Shulman GI. Cellular and Molecular Mechanisms of Metformin Action. *Endocr Rev.* 2021;42(1):77-96.
222. Wapnir RA, Stiel L. Regulation of gluconeogenesis by glycerol and its phosphorylated derivatives. *Biochem Med.* 1985;33(2):141-148.
223. Katz J, Tayek JA. Gluconeogenesis and the Cori cycle in 12-, 20-, and 40-h-fasted humans. *Am J Physiol.* 1998;275(3):E537-542.
224. Skilleter DN, Kun E. The oxidation of L-lactate by liver mitochondria. *Arch Biochem Biophys.* 1972;152(1):92-104.
225. Kline ES, Brandt RB, Laux JE, et al. Localization of L-lactate dehydrogenase in mitochondria. *Arch Biochem Biophys.* 1986;246(2):673-680.
226. Cherrington AD, Edgerton D, Sindelar DK. The direct and indirect effects of insulin on hepatic glucose production in vivo. *Diabetologia.* 1998;41(9):987-996.
227. Puigserver P, Rhee J, Donovan J, et al. Insulin-regulated hepatic gluconeogenesis through FOXO1-PGC-1alpha interaction. *Nature.* 2003;423(6939):550-555.
228. Yoon JC, Puigserver P, Chen G, et al. Control of hepatic gluconeogenesis through the transcriptional coactivator PGC-1. *Nature.* 2001;413(6852):131-138.
229. Exton JH, Park CR. Control of gluconeogenesis in liver. II. Effects of glucagon, catecholamines, and adenosine 3',5'-monophosphate on gluconeogenesis in the perfused rat liver. *The Journal of biological chemistry.* 1968;243(16):4189-4196.
230. Wang Y, Inoue H, Ravnskjaer K, et al. Targeted disruption of the CREB coactivator Crtc2 increases insulin sensitivity. *Proc Natl Acad Sci U S A.* 2010;107(7):3087-3092.
231. He L, Sabet A, Djedjos S, et al. Metformin and insulin suppress hepatic gluconeogenesis through phosphorylation of CREB binding protein. *Cell.* 2009;137(4):635-646.
232. Blair JB, Cimbala MA, Foster JL, Morgan RA. Hepatic pyruvate kinase. Regulation by glucagon, cyclic adenosine 3'-5'-monophosphate, and insulin in the perfused rat liver. *The Journal of biological chemistry.* 1976;251(12):3756-3762.
233. von Wilamowitz-Moellendorff A, Hunter RW, Garcia-Rocha M, et al. Glucose-6-phosphate-mediated activation of liver glycogen synthase plays a key role in hepatic glycogen synthesis. *Diabetes.* 2013;62(12):4070-4082.
234. Aiston S, Andersen B, Agius L. Glucose 6-phosphate regulates hepatic glycogenolysis through inactivation of phosphorylase. *Diabetes.* 2003;52(6):1333-1339.
235. Nakae J, Kitamura T, Silver DL, Accili D. The forkhead transcription factor Foxo1 (Fkhr) confers insulin sensitivity onto glucose-6-phosphatase expression. *J Clin Invest.* 2001;108(9):1359-1367.

236. Brown MS, Goldstein JL. Selective versus total insulin resistance: a pathogenic paradox. *Cell Metab.* 2008;7(2):95-96.
237. Morino K, Petersen KF, Shulman GI. Molecular mechanisms of insulin resistance in humans and their potential links with mitochondrial dysfunction. *Diabetes.* 2006;55 Suppl 2(Suppl 2):S9-S15.
238. Perry RJ, Samuel VT, Petersen KF, Shulman GI. The role of hepatic lipids in hepatic insulin resistance and type 2 diabetes. *Nature.* 2014;510(7503):84-91.
239. Petersen KF, Laurent D, Rothman DL, Cline GW, Shulman GI. Mechanism by which glucose and insulin inhibit net hepatic glycogenolysis in humans. *J Clin Invest.* 1998;101(6):1203-1209.
240. Young SG, Zechner R. Biochemistry and pathophysiology of intravascular and intracellular lipolysis. *Genes Dev.* 2013;27(5):459-484.
241. Nurjhan N, Consoli A, Gerich J. Increased lipolysis and its consequences on gluconeogenesis in non-insulin-dependent diabetes mellitus. *J Clin Invest.* 1992;89(1):169-175.
242. Magnusson I, Rothman DL, Katz LD, Shulman RG, Shulman GI. Increased rate of gluconeogenesis in type II diabetes mellitus. A 13C nuclear magnetic resonance study. *J Clin Invest.* 1992;90(4):1323-1327.
243. Wajngot A, Chandramouli V, Schumann WC, et al. Quantitative contributions of gluconeogenesis to glucose production during fasting in type 2 diabetes mellitus. *Metabolism.* 2001;50(1):47-52.
244. Kunert O, Stingl H, Rosian E, et al. Measurement of fractional whole-body gluconeogenesis in humans from blood samples using 2H nuclear magnetic resonance spectroscopy. *Diabetes.* 2003;52(10):2475-2482.
245. Carneiro C, Brito J, Bilreiro C, et al. All about portal vein: a pictorial display to anatomy, variants and physiopathology. *Insights Imaging.* 2019;10(1):38.
246. Kalra A, Yetiskul E, Wehrle CJ, Tuma F. Physiology, Liver. In: *StatPearls.* Treasure Island (FL) ineligible companies. Disclosure: Ekrem Yetiskul declares no relevant financial relationships with ineligible companies. Disclosure: Chase Wehrle declares no relevant financial relationships with ineligible companies. Disclosure: Faiz Tuma declares no relevant financial relationships with ineligible companies.2023.
247. Ferrannini E, Wahren J, Faber OK, Felig P, Binder C, DeFronzo RA. Splanchnic and renal metabolism of insulin in human subjects: a dose-response study. *Am J Physiol.* 1983;244(6):E517-527.
248. Madison LL, Uger RH, Rencz K. The physiologic significance of secretion of insulin into portal circulation: II. Effect of rate of administration of glucagon-free insulin on magnitude of peripheral and hepatic actions. *Metabolism.* 1960;9:97-108.
249. Koh HE, Cao C, Mittendorfer B. Insulin Clearance in Obesity and Type 2 Diabetes. *Int J Mol Sci.* 2022;23(2).
250. Myers SR, Biggers DW, Neal DW, Cherrington AD. Intraportal glucose delivery enhances the effects of hepatic glucose load on net hepatic glucose uptake in vivo. *J Clin Invest.* 1991;88(1):158-167.
251. Vella A, Shah P, Basu R, et al. Effect of enteral vs. parenteral glucose delivery on initial splanchnic glucose uptake in nondiabetic humans. *Am J Physiol Endocrinol Metab.* 2002;283(2):E259-266.

252. Pagliassotti MJ, Holste LC, Moore MC, Neal DW, Cherrington AD. Comparison of the time courses of insulin and the portal signal on hepatic glucose and glycogen metabolism in the conscious dog. *J Clin Invest.* 1996;97(1):81-91.
253. Galassetti P, Shiota M, Zinker BA, Wasserman DH, Cherrington AD. A negative arterial-portal venous glucose gradient decreases skeletal muscle glucose uptake. *Am J Physiol.* 1998;275(1):E101-111.
254. Bacharach SZ, Tordoff MG, Alhadeff AL. Glucose Sensing in the Hepatic Portal Vein and Its Role in Food Intake and Reward. *Cell Mol Gastroenterol Hepatol.* 2023;16(2):189-199.
255. Russek M. Demonstration of the influence of an hepatic glucosensitive mechanism on food-intake. *Physiol Behav.* 1970;5(10):1207-1209.
256. Baird JP, Grill HJ, Kaplan JM. Effect of hepatic glucose infusion on glucose intake and licking microstructure in deprived and nondeprived rats. *Am J Physiol.* 1999;277(4):R1136-1143.
257. Hjollund KR, Deacon CF, Holst JJ. Dipeptidyl peptidase-4 inhibition increases portal concentrations of intact glucagon-like peptide-1 (GLP-1) to a greater extent than peripheral concentrations in anaesthetised pigs. *Diabetologia.* 2011;54(8):2206-2208.
258. Drucker DJ, Nauck MA. The incretin system: glucagon-like peptide-1 receptor agonists and dipeptidyl peptidase-4 inhibitors in type 2 diabetes. *Lancet.* 2006;368(9548):1696-1705.
259. Deacon CF, Pridal L, Klarskov L, Olesen M, Holst JJ. Glucagon-like peptide 1 undergoes differential tissue-specific metabolism in the anesthetized pig. *Am J Physiol.* 1996;271(3 Pt 1):E458-464.
260. Holst JJ. The physiology of glucagon-like peptide 1. *Physiol Rev.* 2007;87(4):1409-1439.
261. Aulinger BA, Perabo M, Seeley RJ, Parhofer KG, D'Alessio DA. Rapid hepatic metabolism blunts the endocrine action of portally infused GLP-1 in male rats. *Am J Physiol Endocrinol Metab.* 2020;318(2):E189-E197.
262. Andersen DB, Grunddal KV, Pedersen J, et al. Using a Reporter Mouse to Map Known and Novel Sites of GLP-1 Receptor Expression in Peripheral Tissues of Male Mice. *Endocrinology.* 2021;162(3).
263. Ruttimann EB, Arnold M, Hillebrand JJ, Geary N, Langhans W. Intrameal hepatic portal and intraperitoneal infusions of glucagon-like peptide-1 reduce spontaneous meal size in the rat via different mechanisms. *Endocrinology.* 2009;150(3):1174-1181.
264. Burcelin R, Da Costa A, Drucker D, Thorens B. Glucose competence of the hepatoportal vein sensor requires the presence of an activated glucagon-like peptide-1 receptor. *Diabetes.* 2001;50(8):1720-1728.
265. Ottawa DC. Diabetes in Canada: Backgrounder. 2020.
266. DeFronzo RA, Ferrannini E, Groop L, et al. Type 2 diabetes mellitus. *Nat Rev Dis Primers.* 2015;1:15019.
267. Grundy SM. Metabolic syndrome update. *Trends Cardiovasc Med.* 2016;26(4):364-373.
268. Schofield JD, Liu Y, Rao-Balakrishna P, Malik RA, Soran H. Diabetes dyslipidemia. *Diabetes Therapy.* 2016;7(2):203-219.

269. Donath MY, Shoelson SE. Type 2 diabetes as an inflammatory disease. *Nature Reviews Immunology.* 2011;11(2):98.
270. Pollack RM, Donath MY, LeRoith D, Leibowitz G. Anti-inflammatory agents in the treatment of diabetes and its vascular complications. *Diabetes Care.* 2016;39(Supplement 2):S244-S252.
271. Association AD. Treatment of hypertension in adults with diabetes. *Clinical Diabetes.* 2003;21(3):122-127.
272. Fowler MJ. Microvascular and macrovascular complications of diabetes. *Clinical diabetes.* 2008;26(2):77-82.
273. Bliss M. Banting's, Best's, and Collip's accounts of the discovery of insulin. *Bull Hist Med.* 1982;56(4):554-568.
274. Banting FG, Best CH. Pancreatic extracts. 1922. *J Lab Clin Med.* 1990;115(2):254-272.
275. Herrera R, Rosen OM. Autophosphorylation of the insulin receptor in vitro. Designation of phosphorylation sites and correlation with receptor kinase activation. *The Journal of biological chemistry.* 1986;261(26):11980-11985.
276. Baron V, Kaliman P, Gautier N, Van Obberghen E. The insulin receptor activation process involves localized conformational changes. *The Journal of biological chemistry.* 1992;267(32):23290-23294.
277. White MF, Kahn CR. The insulin signaling system. *The Journal of biological chemistry.* 1994;269(1):1-4.
278. Ruderman NB, Kapeller R, White MF, Cantley LC. Activation of phosphatidylinositol 3-kinase by insulin. *Proc Natl Acad Sci U S A.* 1990;87(4):1411-1415.
279. Levina A, Fleming KD, Burke JE, Leonard TA. Activation of the essential kinase PDK1 by phosphoinositide-driven trans-autophosphorylation. *Nat Commun.* 2022;13(1):1874.
280. Alessi DR, James SR, Downes CP, et al. Characterization of a 3-phosphoinositide-dependent protein kinase which phosphorylates and activates protein kinase Balpha. *Curr Biol.* 1997;7(4):261-269.
281. Stokoe D, Stephens LR, Copeland T, et al. Dual role of phosphatidylinositol-3,4,5-trisphosphate in the activation of protein kinase B. *Science.* 1997;277(5325):567-570.
282. Sarbassov DD, Guertin DA, Ali SM, Sabatini DM. Phosphorylation and regulation of Akt/PKB by the rictor-mTOR complex. *Science.* 2005;307(5712):1098-1101.
283. McGarry JD. Banting lecture 2001: dysregulation of fatty acid metabolism in the etiology of type 2 diabetes. *Diabetes.* 2002;51(1):7-18.
284. Santoro A, McGraw TE, Kahn BB. Insulin action in adipocytes, adipose remodeling, and systemic effects. *Cell Metab.* 2021;33(4):748-757.
285. James DE, Brown R, Navarro J, Pilch PF. Insulin-regulatable tissues express a unique insulin-sensitive glucose transport protein. *Nature.* 1988;333(6169):183-185.
286. Bryant NJ, Govers R, James DE. Regulated transport of the glucose transporter GLUT4. *Nat Rev Mol Cell Biol.* 2002;3(4):267-277.
287. Leto D, Saltiel AR. Regulation of glucose transport by insulin: traffic control of GLUT4. *Nat Rev Mol Cell Biol.* 2012;13(6):383-396.

288. Zimmet P, Alberti KG, Shaw J. Global and societal implications of the diabetes epidemic. *Nature.* 2001;414(6865):782-787.
289. Hirsch J, Han PW. Cellularity of rat adipose tissue: effects of growth, starvation, and obesity. *J Lipid Res.* 1969;10(1):77-82.
290. Kusminski CM, Scherer PE. Mitochondrial dysfunction in white adipose tissue. *Trends Endocrinol Metab.* 2012;23(9):435-443.
291. Sun K, Tordjman J, Clement K, Scherer PE. Fibrosis and adipose tissue dysfunction. *Cell Metab.* 2013;18(4):470-477.
292. Trayhurn P, Wood IS. Adipokines: inflammation and the pleiotropic role of white adipose tissue. *Br J Nutr.* 2004;92(3):347-355.
293. Rasouli N. Adipose tissue hypoxia and insulin resistance. *J Investig Med.* 2016;64(4):830-832.
294. Carobbio S, Pellegrinelli V, Vidal-Puig A. Adipose Tissue Function and Expandability as Determinants of Lipotoxicity and the Metabolic Syndrome. *Adv Exp Med Biol.* 2017;960:161-196.
295. Caer C, Rouault C, Le Roy T, et al. Immune cell-derived cytokines contribute to obesity-related inflammation, fibrogenesis and metabolic deregulation in human adipose tissue. *Sci Rep.* 2017;7(1):3000.
296. Wernstedt Asterholm I, Tao C, Morley TS, et al. Adipocyte inflammation is essential for healthy adipose tissue expansion and remodeling. *Cell Metab.* 2014;20(1):103-118.
297. Cinti S, Mitchell G, Barbatelli G, et al. Adipocyte death defines macrophage localization and function in adipose tissue of obese mice and humans. *J Lipid Res.* 2005;46(11):2347-2355.
298. Murano I, Barbatelli G, Parisani V, et al. Dead adipocytes, detected as crown-like structures, are prevalent in visceral fat depots of genetically obese mice. *J Lipid Res.* 2008;49(7):1562-1568.
299. Hildebrandt X, Ibrahim M, Peltzer N. Cell death and inflammation during obesity: "Know my methods, WAT(son)". *Cell Death Differ.* 2023;30(2):279-292.
300. Ruze R, Liu T, Zou X, et al. Obesity and type 2 diabetes mellitus: connections in epidemiology, pathogenesis, and treatments. *Front Endocrinol (Lausanne).* 2023;14:1161521.
301. Iizuka K, Bruick RK, Liang G, Horton JD, Uyeda K. Deficiency of carbohydrate response element-binding protein (ChREBP) reduces lipogenesis as well as glycolysis. *Proc Natl Acad Sci U S A.* 2004;101(19):7281-7286.
302. Shulman GI. Ectopic fat in insulin resistance, dyslipidemia, and cardiometabolic disease. *N Engl J Med.* 2014;371(23):2237-2238.
303. Chadt A, Al-Hasani H. Glucose transporters in adipose tissue, liver, and skeletal muscle in metabolic health and disease. *Pflugers Arch.* 2020;472(9):1273-1298.
304. Ceperuelo-Mallafre V, Ejarque M, Serena C, et al. Adipose tissue glycogen accumulation is associated with obesity-linked inflammation in humans. *Mol Metab.* 2016;5(1):5-18.
305. Koves TR, Ussher JR, Noland RC, et al. Mitochondrial overload and incomplete fatty acid oxidation contribute to skeletal muscle insulin resistance. *Cell Metab.* 2008;7(1):45-56.

306. Samuel VT, Petersen KF, Shulman GI. Lipid-induced insulin resistance: unravelling the mechanism. *Lancet.* 2010;375(9733):2267-2277.
307. Lowell BB, Shulman GI. Mitochondrial dysfunction and type 2 diabetes. *Science.* 2005;307(5708):384-387.
308. Samuel VT, Liu ZX, Qu X, et al. Mechanism of hepatic insulin resistance in non-alcoholic fatty liver disease. *The Journal of biological chemistry.* 2004;279(31):32345-32353.
309. Tarabra E, Pelengaris S, Khan M. A simple matter of life and death-the trials of postnatal Beta-cell mass regulation. *Int J Endocrinol.* 2012;2012:516718.
310. Roder PV, Wu B, Liu Y, Han W. Pancreatic regulation of glucose homeostasis. *Exp Mol Med.* 2016;48(3):e219.
311. Matschinsky FM, Wilson DF. The Central Role of Glucokinase in Glucose Homeostasis: A Perspective 50 Years After Demonstrating the Presence of the Enzyme in Islets of Langerhans. *Front Physiol.* 2019;10:148.
312. Martinez-Reyes I, Chandel NS. Mitochondrial TCA cycle metabolites control physiology and disease. *Nat Commun.* 2020;11(1):102.
313. Hoang Do O, Thorn P. Insulin secretion from beta cells within intact islets: location matters. *Clin Exp Pharmacol Physiol.* 2015;42(4):406-414.
314. Fonseca VA. Defining and characterizing the progression of type 2 diabetes. *Diabetes Care.* 2009;32 Suppl 2(Suppl 2):S151-156.
315. Wysham C, Shubrook J. Beta-cell failure in type 2 diabetes: mechanisms, markers, and clinical implications. *Postgrad Med.* 2020;132(8):676-686.
316. U.K. prospective diabetes study 16. Overview of 6 years' therapy of type II diabetes: a progressive disease. U.K. Prospective Diabetes Study Group. *Diabetes.* 1995;44(11):1249-1258.
317. Ashcroft FM, Rorsman P. Diabetes mellitus and the beta cell: the last ten years. *Cell.* 2012;148(6):1160-1171.
318. Yaney GC, Corkey BE. Fatty acid metabolism and insulin secretion in pancreatic beta cells. *Diabetologia.* 2003;46(10):1297-1312.
319. Dasu MR, Jialal I. Free fatty acids in the presence of high glucose amplify monocyte inflammation via Toll-like receptors. *Am J Physiol Endocrinol Metab.* 2011;300(1):E145-154.
320. Kulkarni A, Muralidharan C, May SC, Tersey SA, Mirmira RG. Inside the beta Cell: Molecular Stress Response Pathways in Diabetes Pathogenesis. *Endocrinology.* 2022;164(1).
321. Bensellam M, Laybutt DR, Jonas JC. The molecular mechanisms of pancreatic beta-cell glucotoxicity: recent findings and future research directions. *Mol Cell Endocrinol.* 2012;364(1-2):1-27.
322. Talchai C, Xuan S, Lin HV, Sussel L, Accili D. Pancreatic beta cell dedifferentiation as a mechanism of diabetic beta cell failure. *Cell.* 2012;150(6):1223-1234.
323. Creutzfeldt W. The incretin concept today. *Diabetologia.* 1979;16(2):75-85.
324. Nauck MA, Heimesaat MM, Orskov C, Holst JJ, Ebert R, Creutzfeldt W. Preserved incretin activity of glucagon-like peptide 1 [7-36 amide] but not of synthetic human gastric inhibitory polypeptide in patients with type-2 diabetes mellitus. *J Clin Invest.* 1993;91(1):301-307.

325. Taylor SI, Yazdi ZS, Beitelshees AL. Pharmacological treatment of hyperglycemia in type 2 diabetes. *J Clin Invest.* 2021;131(2).
326. Diabetes Canada Clinical Practice Guidelines Expert C, Lipscombe L, Butalia S, et al. Pharmacologic Glycemic Management of Type 2 Diabetes in Adults: 2020 Update. *Can J Diabetes.* 2020;44(7):575-591.
327. DeFronzo RA, Goodman AM. Efficacy of metformin in patients with non-insulin-dependent diabetes mellitus. The Multicenter Metformin Study Group. *N Engl J Med.* 1995;333(9):541-549.
328. Baker C, Retzik-Stahr C, Singh V, Plomondon R, Anderson V, Rasouli N. Should metformin remain the first-line therapy for treatment of type 2 diabetes? *Ther Adv Endocrinol Metab.* 2021;12:2042018820980225.
329. Shitara Y, Nakamichi N, Norioka M, Shima H, Kato Y, Horie T. Role of organic cation/carnitine transporter 1 in uptake of phenformin and inhibitory effect on complex I respiration in mitochondria. *Toxicol Sci.* 2013;132(1):32-42.
330. Nies AT, Koepsell H, Damme K, Schwab M. Organic cation transporters (OCTs, MATEs), in vitro and in vivo evidence for the importance in drug therapy. *Handb Exp Pharmacol.* 2011(201):105-167.
331. Shu Y, Sheardown SA, Brown C, et al. Effect of genetic variation in the organic cation transporter 1 (OCT1) on metformin action. *J Clin Invest.* 2007;117(5):1422-1431.
332. Stumvoll M, Nurjhan N, Perriello G, Dailey G, Gerich JE. Metabolic effects of metformin in non-insulin-dependent diabetes mellitus. *N Engl J Med.* 1995;333(9):550-554.
333. El-Mir MY, Nogueira V, Fontaine E, Averet N, Rigoulet M, Leverve X. Dimethylbiguanide inhibits cell respiration via an indirect effect targeted on the respiratory chain complex I. *The Journal of biological chemistry.* 2000;275(1):223-228.
334. Miller RA, Birnbaum MJ. An energetic tale of AMPK-independent effects of metformin. *J Clin Invest.* 2010;120(7):2267-2270.
335. Zhou G, Myers R, Li Y, et al. Role of AMP-activated protein kinase in mechanism of metformin action. *J Clin Invest.* 2001;108(8):1167-1174.
336. Gunton JE, Delhanty PJ, Takahashi S, Baxter RC. Metformin rapidly increases insulin receptor activation in human liver and signals preferentially through insulin-receptor substrate-2. *J Clin Endocrinol Metab.* 2003;88(3):1323-1332.
337. Lutz TA, Estermann A, Haag S, Scharrer E. Depolarization of the liver cell membrane by metformin. *Biochim Biophys Acta.* 2001;1513(2):176-184.
338. Fischer Y, Thomas J, Rosen P, Kammermeier H. Action of metformin on glucose transport and glucose transporter GLUT1 and GLUT4 in heart muscle cells from healthy and diabetic rats. *Endocrinology.* 1995;136(2):412-420.
339. Fantus IG, Brosseau R. Mechanism of action of metformin: insulin receptor and postreceptor effects in vitro and in vivo. *J Clin Endocrinol Metab.* 1986;63(4):898-905.
340. Goldstein BJ, Feinglos MN, Lunceford JK, Johnson J, Williams-Herman DE, Sitagliptin 036 Study G. Effect of initial combination therapy with sitagliptin, a dipeptidyl peptidase-4 inhibitor, and metformin on glycemic control in patients with type 2 diabetes. *Diabetes Care.* 2007;30(8):1979-1987.

341. Mulvihill EE, Drucker DJ. Pharmacology, physiology, and mechanisms of action of dipeptidyl peptidase-4 inhibitors. *Endocrine reviews.* 2014;35(6):992-1019.
342. Saini K, Sharma S, Khan Y. DPP-4 inhibitors for treating T2DM - hype or hope? an analysis based on the current literature. *Front Mol Biosci.* 2023;10:1130625.
343. Gerich J. DPP-4 inhibitors: what may be the clinical differentiators? *Diabetes Res Clin Pract.* 2010;90(2):131-140.
344. Ligueros-Saylan M, Foley JE, Schweizer A, Couturier A, Kothny W. An assessment of adverse effects of vildagliptin versus comparators on the liver, the pancreas, the immune system, the skin and in patients with impaired renal function from a large pooled database of Phase II and III clinical trials. *Diabetes Obes Metab.* 2010;12(6):495-509.
345. Farngren J, Persson M, Schweizer A, Foley JE, Ahren B. Vildagliptin reduces glucagon during hyperglycemia and sustains glucagon counterregulation during hypoglycemia in type 1 diabetes. *J Clin Endocrinol Metab.* 2012;97(10):3799-3806.
346. Yoshioka H, Hirose Y, Ohishi R, et al. Diurnal Variation of Sitagliptin-Induced Pharmacological Effects in C57BL/6J Mice. *Biol Pharm Bull.* 2019;42(9):1562-1568.
347. Inzucchi SE, Maggs DG, Spollett GR, et al. Efficacy and metabolic effects of metformin and troglitazone in type II diabetes mellitus. *N Engl J Med.* 1998;338(13):867-872.
348. Migoya EM, Bergeron R, Miller JL, et al. Dipeptidyl peptidase-4 inhibitors administered in combination with metformin result in an additive increase in the plasma concentration of active GLP-1. *Clin Pharmacol Ther.* 2010;88(6):801-808.
349. Green BD, Irwin N, Duffy NA, Gault VA, O'Harte F P, Flatt PR. Inhibition of dipeptidyl peptidase-IV activity by metformin enhances the antidiabetic effects of glucagon-like peptide-1. *Eur J Pharmacol.* 2006;547(1-3):192-199.
350. Mannucci E, Ognibene A, Cremasco F, et al. Effect of metformin on glucagon-like peptide 1 (GLP-1) and leptin levels in obese nondiabetic subjects. *Diabetes Care.* 2001;24(3):489-494.
351. Cuthbertson J, Patterson S, O'Harte FP, Bell PM. Investigation of the effect of oral metformin on dipeptidylpeptidase-4 (DPP-4) activity in Type 2 diabetes. *Diabet Med.* 2009;26(6):649-654.
352. Lenhard JM, Croom DK, Minnick DT. Reduced serum dipeptidyl peptidase-IV after metformin and pioglitazone treatments. *Biochem Biophys Res Commun.* 2004;324(1):92-97.
353. Hinke SA, Kuhn-Wache K, Hoffmann T, Pederson RA, McIntosh CH, Demuth HU. Metformin effects on dipeptidylpeptidase IV degradation of glucagon-like peptide-1. *Biochem Biophys Res Commun.* 2002;291(5):1302-1308.
354. Yasuda N, Inoue T, Nagakura T, et al. Enhanced secretion of glucagon-like peptide 1 by biguanide compounds. *Biochem Biophys Res Commun.* 2002;298(5):779-784.
355. Mashayekhi M, Nian H, Mayfield D, et al. Weight Loss-Independent Effect of Liraglutide on Insulin Sensitivity in Individuals With Obesity and Prediabetes. *Diabetes.* 2024;73(1):38-50.

356. Larsson H, Holst JJ, Ahren B. Glucagon-like peptide-1 reduces hepatic glucose production indirectly through insulin and glucagon in humans. *Acta Physiol Scand.* 1997;160(4):413-422.
357. Jun LS, Millican RL, Hawkins ED, et al. Absence of glucagon and insulin action reveals a role for the GLP-1 receptor in endogenous glucose production. *Diabetes.* 2015;64(3):819-827.
358. Tomas E, Stanojevic V, Habener JF. GLP-1-derived nonapeptide GLP-1(28-36)amide targets to mitochondria and suppresses glucose production and oxidative stress in isolated mouse hepatocytes. *Regul Pept.* 2011;167(2-3):177-184.
359. Ding X, Saxena NK, Lin S, Gupta NA, Anania FA. Exendin-4, a glucagon-like protein-1 (GLP-1) receptor agonist, reverses hepatic steatosis in ob/ob mice. *Hepatology.* 2006;43(1):173-181.
360. Gupta NA, Mells J, Dunham RM, et al. Glucagon-like peptide-1 receptor is present on human hepatocytes and has a direct role in decreasing hepatic steatosis in vitro by modulating elements of the insulin signaling pathway. *Hepatology.* 2010;51(5):1584-1592.
361. Wong CK, McLean BA, Baggio LL, et al. Central glucagon-like peptide 1 receptor activation inhibits Toll-like receptor agonist-induced inflammation. *Cell Metab.* 2024;36(1):130-143 e135.
362. Balogh DB, Wagner LJ, Fekete A. An Overview of the Cardioprotective Effects of Novel Antidiabetic Classes: Focus on Inflammation, Oxidative Stress, and Fibrosis. *Int J Mol Sci.* 2023;24(9).
363. Iwai T, Ito S, Tanimitsu K, Udagawa S, Oka J. Glucagon-like peptide-1 inhibits LPS-induced IL-1beta production in cultured rat astrocytes. *Neurosci Res.* 2006;55(4):352-360.
364. Wang XC, Gusdon AM, Liu H, Qu S. Effects of glucagon-like peptide-1 receptor agonists on non-alcoholic fatty liver disease and inflammation. *World J Gastroenterol.* 2014;20(40):14821-14830.
365. Vittone F, Liberman A, Vasic D, et al. Sitagliptin reduces plaque macrophage content and stabilises arteriosclerotic lesions in Apoe (-/-) mice. *Diabetologia.* 2012;55(8):2267-2275.
366. Hsieh J, Longuet C, Baker CL, et al. The glucagon-like peptide 1 receptor is essential for postprandial lipoprotein synthesis and secretion in hamsters and mice. *Diabetologia.* 2010;53(3):552-561.
367. Farr S, Taher J, Adeli K. Glucagon-like peptide-1 as a key regulator of lipid and lipoprotein metabolism in fasting and postprandial states. *Cardiovasc Hematol Disord Drug Targets.* 2014;14(2):126-136.
368. Schirra J, Katschinski M, Weidmann C, et al. Gastric emptying and release of incretin hormones after glucose ingestion in humans. *J Clin Invest.* 1996;97(1):92-103.
369. Schirra J, Kuwert P, Wank U, et al. Differential effects of subcutaneous GLP-1 on gastric emptying, antroduodenal motility, and pancreatic function in men. *Proc Assoc Am Physicians.* 1997;109(1):84-97.
370. Blandino-Rosano M, Perez-Arana G, Mellado-Gil JM, Segundo C, Aguilar-Diosdado M. Anti-proliferative effect of pro-inflammatory cytokines in cultured beta cells is associated with extracellular signal-regulated kinase 1/2 pathway

inhibition: protective role of glucagon-like peptide -1. *J Mol Endocrinol.* 2008;41(1):35-44.
371. Abdulla H, Phillips B, Wilkinson D, et al. Effects of GLP-1 Infusion Upon Whole-body Glucose Uptake and Skeletal Muscle Perfusion During Fed-state in Older Men. *J Clin Endocrinol Metab.* 2023;108(4):971-978.
372. Yu JH, Park SY, Lee DY, Kim NH, Seo JA. GLP-1 receptor agonists in diabetic kidney disease: current evidence and future directions. *Kidney Res Clin Pract.* 2022;41(2):136-149.
373. Villanueva-Penacarrillo ML, Marquez L, Gonzalez N, Diaz-Miguel M, Valverde I. Effect of GLP-1 on lipid metabolism in human adipocytes. *Horm Metab Res.* 2001;33(2):73-77.
374. Marx N, Husain M, Lehrke M, Verma S, Sattar N. GLP-1 Receptor Agonists for the Reduction of Atherosclerotic Cardiovascular Risk in Patients With Type 2 Diabetes. *Circulation.* 2022;146(24):1882-1894.
375. Wilding JPH, Batterham RL, Calanna S, et al. Once-Weekly Semaglutide in Adults with Overweight or Obesity. *N Engl J Med.* 2021;384(11):989-1002.
376. Garvey WT, Frias JP, Jastreboff AM, et al. Tirzepatide once weekly for the treatment of obesity in people with type 2 diabetes (SURMOUNT-2): a double-blind, randomised, multicentre, placebo-controlled, phase 3 trial. *Lancet.* 2023;402(10402):613-626.
377. Jastreboff AM, Aronne LJ, Ahmad NN, et al. Tirzepatide Once Weekly for the Treatment of Obesity. *N Engl J Med.* 2022;387(3):205-216.
378. Jastreboff AM, Kaplan LM, Frias JP, et al. Triple-Hormone-Receptor Agonist Retatrutide for Obesity - A Phase 2 Trial. *N Engl J Med.* 2023;389(6):514-526.
379. Beckwith W. Science's 2023 Breakthrough: GLP-1 Agonists Show Promise Against Obesity-Associated Disease. 2023. https://www.aaas.org/news/sciences-2023-breakthrough-glp-1-agonists-show-promise-against-obesity-associated-disease.
380. Hiatt WR, Kaul S, Smith RJ. The cardiovascular safety of diabetes drugs--insights from the rosiglitazone experience. *N Engl J Med.* 2013;369(14):1285-1287.
381. Nissen SE, Wolski K. Effect of rosiglitazone on the risk of myocardial infarction and death from cardiovascular causes. *N Engl J Med.* 2007;356(24):2457-2471.
382. U.S. Food and Drug Administration Meeting of the Endocrinologic and Metabolic Drugs Advisory Committee. https://www.federalregister.gov/documents/2008/05/22/E8-11449/endocrinologic-and-metabolic-drugs-advisory-committee-notice-of-meeting. Accessed November 3 2023.
383. Cefalu WT, Kaul S, Gerstein HC, et al. Cardiovascular outcomes trials in type 2 diabetes: where do we go from here? Reflections from a diabetes care editors' expert forum. *Diabetes care.* 2018;41(1):14-31.
384. Scirica BM, Braunwald E, Raz I, et al. Heart failure, saxagliptin, and diabetes mellitus: observations from the SAVOR-TIMI 53 randomized trial. *Circulation.* 2014;130(18):1579-1588.
385. Udell JA, Bhatt DL, Braunwald E, et al. Saxagliptin and cardiovascular outcomes in patients with type 2 diabetes and moderate or severe renal

impairment: observations from the SAVOR-TIMI 53 Trial. *Diabetes care.* 2015;38(4):696-705.
386. White WB, Cannon CP, Heller SR, et al. Alogliptin after acute coronary syndrome in patients with type 2 diabetes. *N Engl J Med.* 2013;369(14):1327-1335.
387. White WB, Cannon CP, Heller SR, et al. Alogliptin after acute coronary syndrome in patients with type 2 diabetes. *New England Journal of Medicine.* 2013;369(14):1327-1335.
388. White WB, Bakris GL, Bergenstal RM, et al. EXamination of cArdiovascular outcoMes with alogliptIN versus standard of carE in patients with type 2 diabetes mellitus and acute coronary syndrome (EXAMINE): a cardiovascular safety study of the dipeptidyl peptidase 4 inhibitor alogliptin in patients with type 2 diabetes with acute coronary syndrome. *Am Heart J.* 2011;162(4):620-626 e621.
389. Green JB, Bethel MA, Armstrong PW, et al. Effect of Sitagliptin on Cardiovascular Outcomes in Type 2 Diabetes. *N Engl J Med.* 2015;373(3):232-242.
390. Scirica BM, Im K, Murphy SA, et al. Re-adjudication of the Trial Evaluating Cardiovascular Outcomes with Sitagliptin (TECOS) with study-level meta-analysis of hospitalization for heart failure from cardiovascular outcomes trials with dipeptidyl peptidase-4 (DPP-4) inhibitors. *Clin Cardiol.* 2022;45(7):794-801.
391. Gantz I, Chen M, Suryawanshi S, et al. A randomized, placebo-controlled study of the cardiovascular safety of the once-weekly DPP-4 inhibitor omarigliptin in patients with type 2 diabetes mellitus. *Cardiovasc Diabetol.* 2017;16(1):112.
392. Packer M. Worsening Heart Failure During the Use of DPP-4 Inhibitors: Pathophysiological Mechanisms, Clinical Risks, and Potential Influence of Concomitant Antidiabetic Medications. *JACC Heart Fail.* 2018;6(6):445-451.
393. McGuire DK, Alexander JH, Johansen OE, et al. Linagliptin Effects on Heart Failure and Related Outcomes in Individuals With Type 2 Diabetes Mellitus at High Cardiovascular and Renal Risk in CARMELINA. *Circulation.* 2019;139(3):351-361.
394. Rosenstock J, Perkovic V, Alexander JH, et al. Rationale, design, and baseline characteristics of the CArdiovascular safety and Renal Microvascular outcomE study with LINAgliptin (CARMELINA((R))): a randomized, double-blind, placebo-controlled clinical trial in patients with type 2 diabetes and high cardio-renal risk. *Cardiovasc Diabetol.* 2018;17(1):39.
395. Rosenstock J, Kahn SE, Johansen OE, et al. Effect of Linagliptin vs Glimepiride on Major Adverse Cardiovascular Outcomes in Patients With Type 2 Diabetes: The CAROLINA Randomized Clinical Trial. *JAMA.* 2019;322(12):1155-1166.
396. Kim EH, Kim SS, Kim DJ, et al. A prospective cohort study on effects of gemigliptin on cardiovascular outcomes in patients with type 2 diabetes (OPTIMUS study). *Sci Rep.* 2020;10(1):19033.
397. Zhong J, Maiseyeu A, Davis SN, Rajagopalan S. DPP4 in cardiometabolic disease: recent insights from the laboratory and clinical trials of DPP4 inhibition. *Circulation research.* 2015;116(8):1491-1504.

398. Lambeir A-M, Durinx C, Scharpé S, De Meester I. Dipeptidyl-peptidase IV from bench to bedside: an update on structural properties, functions, and clinical aspects of the enzyme DPP IV. *Critical reviews in clinical laboratory sciences.* 2003;40(3):209-294.
399. Scanlan MJ, Raj BK, Calvo B, et al. Molecular cloning of fibroblast activation protein alpha, a member of the serine protease family selectively expressed in stromal fibroblasts of epithelial cancers. *Proc Natl Acad Sci U S A.* 1994;91(12):5657-5661.
400. Abbott CA, Yu DM, Woollatt E, Sutherland GR, McCaughan GW, Gorrell MD. Cloning, expression and chromosomal localization of a novel human dipeptidyl peptidase (DPP) IV homolog, DPP8. *Eur J Biochem.* 2000;267(20):6140-6150.
401. Olsen C, Wagtmann N. Identification and characterization of human DPP9, a novel homologue of dipeptidyl peptidase IV. *Gene.* 2002;299(1-2):185-193.
402. Wada K, Yokotani N, Hunter C, Doi K, Wenthold RJ, Shimasaki S. Differential expression of two distinct forms of mRNA encoding members of a dipeptidyl aminopeptidase family. *Proc Natl Acad Sci U S A.* 1992;89(1):197-201.
403. Qi SY, Riviere PJ, Trojnar J, Junien JL, Akinsanya KO. Cloning and characterization of dipeptidyl peptidase 10, a new member of an emerging subgroup of serine proteases. *Biochem J.* 2003;373(Pt 1):179-189.
404. Sedo A, Malik R. Dipeptidyl peptidase IV-like molecules: homologous proteins or homologous activities? *Biochim Biophys Acta.* 2001;1550(2):107-116.
405. Klemann C, Wagner L, Stephan M, von Horsten S. Cut to the chase: a review of CD26/dipeptidyl peptidase-4's (DPP4) entanglement in the immune system. *Clin Exp Immunol.* 2016;185(1):1-21.
406. Weihofen WA, Liu J, Reutter W, Saenger W, Fan H. Crystal structure of CD26/dipeptidyl-peptidase IV in complex with adenosine deaminase reveals a highly amphiphilic interface. *J Biol Chem.* 2004;279(41):43330-43335.
407. Mulvihill EE. Dipeptidyl peptidase inhibitor therapy in type 2 diabetes: control of the incretin axis and regulation of postprandial glucose and lipid metabolism. *Peptides.* 2018;100:158-164.
408. Aertgeerts K, Ye S, Tennant MG, et al. Crystal structure of human dipeptidyl peptidase IV in complex with a decapeptide reveals details on substrate specificity and tetrahedral intermediate formation. *Protein Sci.* 2004;13(2):412-421.
409. Ogata S, Misumi Y, Ikehara Y. Primary structure of rat liver dipeptidyl peptidase IV deduced from its cDNA and identification of the NH2-terminal signal sequence as the membrane-anchoring domain. *Journal of Biological Chemistry.* 1989;264(6):3596-3601.
410. Mulvihill EE, Drucker DJ. Pharmacology, Physiology and Mechanisms of Action of Dipeptidyl Peptidase-4 Inhibitors. *Endocr Rev.* 2014:er20141035.
411. Gorrell MD. Dipeptidyl peptidase IV and related enzymes in cell biology and liver disorders. *Clin Sci (Lond).* 2005;108(4):277-292.
412. Wagner L, Klemann C, Stephan M, von Horsten S. Unravelling the immunological roles of dipeptidyl peptidase 4 (DPP4) activity and/or structure homologue (DASH) proteins. *Clin Exp Immunol.* 2016;184(3):265-283.
413. Omar BA, Liehua L, Yamada Y, Seino Y, Marchetti P, Ahren B. Dipeptidyl peptidase 4 (DPP-4) is expressed in mouse and human islets and its activity is

decreased in human islets from individuals with type 2 diabetes. *Diabetologia.* 2014;57(9):1876-1883.
414. Segerstolpe A, Palasantza A, Eliasson P, et al. Single-Cell Transcriptome Profiling of Human Pancreatic Islets in Health and Type 2 Diabetes. *Cell Metab.* 2016;24(4):593-607.
415. Blodgett DM, Nowosielska A, Afik S, et al. Novel Observations From Next-Generation RNA Sequencing of Highly Purified Human Adult and Fetal Islet Cell Subsets. *Diabetes.* 2015;64(9):3172-3181.
416. Bugliani M, Syed F, Paula FMM, et al. DPP-4 is expressed in human pancreatic beta cells and its direct inhibition improves beta cell function and survival in type 2 diabetes. *Mol Cell Endocrinol.* 2018;473:186-193.
417. Gorvel JP, Ferrero A, Chambraud L, Rigal A, Bonicel J, Maroux S. Expression of sucrase-isomaltase and dipeptidylpeptidase IV in human small intestine and colon. *Gastroenterology.* 1991;101(3):618-625.
418. Hansen L, Deacon CF, Orskov C, Holst JJ. Glucagon-like peptide-1-(7-36)amide is transformed to glucagon-like peptide-1-(9-36)amide by dipeptidyl peptidase IV in the capillaries supplying the L cells of the porcine intestine. *Endocrinology.* 1999;140(11):5356-5363.
419. Kettmann U, Humbel B, Holzhausen HJ. Ultrastructural localization of dipeptidylpeptidase IV in the glomerulum of the rat kidney. *Acta Histochem.* 1992;92(2):225-227.
420. Hartel S, Gossrau R, Hanski C, Reutter W. Dipeptidyl peptidase (DPP) IV in rat organs. Comparison of immunohistochemistry and activity histochemistry. *Histochemistry.* 1988;89(2):151-161.
421. Richardson WJ, Clarke SA, Quinn TA, Holmes JW. Physiological implications of myocardial scar structure. *Comprehensive Physiology.* 2011;5(4):1877-1909.
422. Nargis T, Kumar K, Ghosh AR, et al. KLK5 induces shedding of DPP4 from circulatory Th17 cells in type 2 diabetes. *Mol Metab.* 2017;6(11):1529-1539.
423. Rohrborn D, Eckel J, Sell H. Shedding of dipeptidyl peptidase 4 is mediated by metalloproteases and up-regulated by hypoxia in human adipocytes and smooth muscle cells. *FEBS Lett.* 2014;588(21):3870-3877.
424. Fan H, Meng W, Kilian C, Grams S, Reutter W. Domain-specific N-glycosylation of the membrane glycoprotein dipeptidylpeptidase IV (CD26) influences its subcellular trafficking, biological stability, enzyme activity and protein folding. *Eur J Biochem.* 1997;246(1):243-251.
425. Hansen JE, Lund O, Tolstrup N, Gooley AA, Williams KL, Brunak S. NetOglyc: prediction of mucin type O-glycosylation sites based on sequence context and surface accessibility. *Glycoconj J.* 1998;15(2):115-130.
426. Naim HY, Joberty G, Alfalah M, Jacob R. Temporal association of the N- and O-linked glycosylation events and their implication in the polarized sorting of intestinal brush border sucrase-isomaltase, aminopeptidase N, and dipeptidyl peptidase IV. *The Journal of biological chemistry.* 1999;274(25):17961-17967.
427. Matter K, McDowell W, Schwartz RT, Hauri HP. Asynchronous transport to the cell surface of intestinal brush border hydrolases is not due to differential trimming of N-linked oligosaccharides. *The Journal of biological chemistry.* 1989;264(22):13131-13139.

428. Delacour D, Gouyer V, Leteurtre E, et al. 1-benzyl-2-acetamido-2-deoxy-alpha-D-galactopyranoside blocks the apical biosynthetic pathway in polarized HT-29 cells. *The Journal of biological chemistry.* 2003;278(39):37799-37809.
429. Schmauser B, Kilian C, Reutter W, Tauber R. Sialoforms of dipeptidylpeptidase IV from rat kidney and liver. *Glycobiology.* 1999;9(12):1295-1305.
430. Cuchacovich M, Gatica H, Pizzo SV, Gonzalez-Gronow M. Characterization of human serum dipeptidyl peptidase IV (CD26) and analysis of its autoantibodies in patients with rheumatoid arthritis and other autoimmune diseases. *Clin Exp Rheumatol.* 2001;19(6):673-680.
431. Smith RE, Talhouk JW, Brown EE, Edgar SE. The significance of hypersialylation of dipeptidyl peptidase IV (CD26) in the inhibition of its activity by Tat and other cationic peptides. CD26: a subverted adhesion molecule for HIV peptide binding. *AIDS Res Hum Retroviruses.* 1998;14(10):851-868.
432. Noels H, Theelen W, Sternkopf M, et al. Reduced post-operative DPP4 activity associated with worse patient outcome after cardiac surgery. *Sci Rep.* 2018;8(1):11820.
433. Engel M, Hoffmann T, Wagner L, et al. The crystal structure of dipeptidyl peptidase IV (CD26) reveals its functional regulation and enzymatic mechanism. *Proc Natl Acad Sci U S A.* 2003;100(9):5063-5068.
434. Broxmeyer HE, Hoggatt J, O'Leary HA, et al. Dipeptidylpeptidase 4 negatively regulates colony-stimulating factor activity and stress hematopoiesis. *Nat Med.* 2012;18(12):1786-1796.
435. Struyf S, Proost P, Schols D, et al. CD26/dipeptidyl-peptidase IV down-regulates the eosinophil chemotactic potency, but not the anti-HIV activity of human eotaxin by affecting its interaction with CC chemokine receptor 3. *J Immunol.* 1999;162(8):4903-4909.
436. Marchetti C, Di Carlo A, Facchiano F, et al. High mobility group box 1 is a novel substrate of dipeptidyl peptidase-IV. *Diabetologia.* 2012;55(1):236-244.
437. Proost P, Menten P, Struyf S, Schutyser E, De Meester I, Van Damme J. Cleavage by CD26/dipeptidyl peptidase IV converts the chemokine LD78beta into a most efficient monocyte attractant and CCR1 agonist. *Blood.* 2000;96(5):1674-1680.
438. Proost P, Struyf S, Schols D, et al. Truncation of macrophage-derived chemokine by CD26/ dipeptidyl-peptidase IV beyond its predicted cleavage site affects chemotactic activity and CC chemokine receptor 4 interaction. *The Journal of biological chemistry.* 1999;274(7):3988-3993.
439. Oravecz T, Pall M, Roderiquez G, et al. Regulation of the receptor specificity and function of the chemokine RANTES (regulated on activation, normal T cell expressed and secreted) by dipeptidyl peptidase IV (CD26)-mediated cleavage. *J Exp Med.* 1997;186(11):1865-1872.
440. Deacon CF, Johnsen AH, Holst JJ. Degradation of glucagon-like peptide-1 by human plasma in vitro yields an N-terminally truncated peptide that is a major endogenous metabolite in vivo. *J Clin Endocrinol Metab.* 1995;80(3):952-957.
441. Brubaker PL, Crivici A, Izzo A, Ehrlich P, Tsai CH, Drucker DJ. Circulating and tissue forms of the intestinal growth factor, glucagon-like peptide-2. *Endocrinology.* 1997;138(11):4837-4843.

442. Deacon CF, Nauck MA, Meier J, Hucking K, Holst JJ. Degradation of endogenous and exogenous gastric inhibitory polypeptide in healthy and in type 2 diabetic subjects as revealed using a new assay for the intact peptide. *J Clin Endocrinol Metab.* 2000;85(10):3575-3581.
443. Zhong J, Maiseyeu A, Davis SN, Rajagopalan S. DPP4 in cardiometabolic disease: recent insights from the laboratory and clinical trials of DPP4 inhibition. *Circ Res.* 2015;116(8):1491-1504.
444. Mannucci E, Pala L, Ciani S, et al. Hyperglycaemia increases dipeptidyl peptidase IV activity in diabetes mellitus. *Diabetologia.* 2005;48(6):1168-1172.
445. Ryskjaer J, Deacon CF, Carr RD, et al. Plasma dipeptidyl peptidase-IV activity in patients with type-2 diabetes mellitus correlates positively with HbAlc levels, but is not acutely affected by food intake. *Eur J Endocrinol.* 2006;155(3):485-493.
446. Miyazaki M, Kato M, Tanaka K, et al. Increased hepatic expression of dipeptidyl peptidase-4 in non-alcoholic fatty liver disease and its association with insulin resistance and glucose metabolism. *Mol Med Rep.* 2012;5(3):729-733.
447. Itou M, Kawaguchi T, Taniguchi E, et al. Altered expression of glucagon-like peptide-1 and dipeptidyl peptidase IV in patients with HCV-related glucose intolerance. *J Gastroenterol Hepatol.* 2008;23(2):244-251.
448. Deacon CF, Plamboeck A, Rosenkilde MM, de Heer J, Holst JJ. GIP-(3-42) does not antagonize insulinotropic effects of GIP at physiological concentrations. *Am J Physiol Endocrinol Metab.* 2006;291(3):E468-475.
449. Marguet D, Baggio L, Kobayashi T, et al. Enhanced insulin secretion and improved glucose tolerance in mice lacking CD26. *Proc Natl Acad Sci U S A.* 2000;97(12):6874-6879.
450. Penn M, Pastore J, Miller T, Aras R. SDF-1 in myocardial repair. *Gene therapy.* 2012;19(6):583.
451. Theiss HD, Gross L, Vallaster M, et al. Antidiabetic gliptins in combination with G-CSF enhances myocardial function and survival after acute myocardial infarction. *International journal of cardiology.* 2013;168(4):3359-3369.
452. Brenner C, Adrion C, Grabmaier U, et al. Sitagliptin plus granulocyte colony-stimulating factor in patients suffering from acute myocardial infarction: A double-blind, randomized placebo-controlled trial of efficacy and safety (SITAGRAMI trial). *Int J Cardiol.* 2016;205:23-30.
453. Röhrborn D, Wronkowitz N, Eckel J. DPP4 in diabetes. *Frontiers in immunology.* 2015;6:386.
454. Mentlein R. Dipeptidyl-peptidase IV (CD26)--role in the inactivation of regulatory peptides. *Regul Pept.* 1999;85(1):9-24.
455. Cordero OJ, Salgado FJ, Nogueira M. On the origin of serum CD26 and its altered concentration in cancer patients. *Cancer Immunol Immunother.* 2009;58(11):1723-1747.
456. Kameoka J, Tanaka T, Nojima Y, Schlossman SF, Morimoto C. Direct association of adenosine deaminase with a T cell activation antigen, CD26. *Science.* 1993;261(5120):466-469.
457. Ishii T, Ohnuma K, Murakami A, et al. CD26-mediated signaling for T cell activation occurs in lipid rafts through its association with CD45RO. *Proc Natl Acad Sci U S A.* 2001;98(21):12138-12143.

458. Ohnuma K, Inoue H, Uchiyama M, et al. T-cell activation via CD26 and caveolin-1 in rheumatoid synovium. *Mod Rheumatol.* 2006;16(1):3-13.
459. Ohnuma K, Uchiyama M, Yamochi T, et al. Caveolin-1 triggers T-cell activation via CD26 in association with CARMA1. *J Biol Chem.* 2007;282(13):10117-10131.
460. Ohnuma K, Uchiyama M, Hatano R, et al. Blockade of CD26-mediated T cell costimulation with soluble caveolin-1-Ig fusion protein induces anergy in CD4+T cells. *Biochem Biophys Res Commun.* 2009;386(2):327-332.
461. Lambeir AM, Durinx C, Scharpe S, De Meester I. Dipeptidyl-peptidase IV from bench to bedside: an update on structural properties, functions, and clinical aspects of the enzyme DPP IV. *Crit Rev Clin Lab Sci.* 2003;40(3):209-294.
462. Busek P, Malik R, Sedo A. Dipeptidyl peptidase IV activity and/or structure homologues (DASH) and their substrates in cancer. *Int J Biochem Cell Biol.* 2004;36(3):408-421.
463. Zhong J, Rao X, Deiuliis J, et al. A potential role for dendritic cell/macrophage-expressing DPP4 in obesity-induced visceral inflammation. *Diabetes.* 2013;62(1):149-157.
464. Belle LP, Bitencourt PE, De Bona KS, Moresco RN, Moretto MB. Association between HbA1c and dipeptidyl peptidase IV activity in type 2 diabetes mellitus. *Clin Chim Acta.* 2012;413(11-12):1020-1021.
465. Lee JG, Kang DG, Yu JR, et al. Changes in Adenosine Deaminase Activity in Patients with Type 2 Diabetes Mellitus and Effect of DPP-4 Inhibitor Treatment on ADA Activity. *Diabetes Metab J.* 2011;35(2):149-158.
466. Ohnuma K, Yamochi T, Uchiyama M, et al. CD26 up-regulates expression of CD86 on antigen-presenting cells by means of caveolin-1. *Proc Natl Acad Sci U S A.* 2004;101(39):14186-14191.
467. Hiromura M, Nohtomi K, Mori Y, et al. Caveolin-1, a binding protein of CD26, is essential for the anti-inflammatory effects of dipeptidyl peptidase-4 inhibitors on human and mouse macrophages. *Biochem Biophys Res Commun.* 2018;495(1):223-229.
468. Ghorpade DS, Ozcan L, Zheng Z, et al. Hepatocyte-secreted DPP4 in obesity promotes adipose inflammation and insulin resistance. *Nature.* 2018;555(7698):673-677.
469. Cohen AW, Combs TP, Scherer PE, Lisanti MP. Role of caveolin and caveolae in insulin signaling and diabetes. *Am J Physiol Endocrinol Metab.* 2003;285(6):E1151-1160.
470. Deacon CF. Physiology and Pharmacology of DPP-4 in Glucose Homeostasis and the Treatment of Type 2 Diabetes. *Front Endocrinol (Lausanne).* 2019;10:80.
471. Loster K, Zeilinger K, Schuppan D, Reutter W. The cysteine-rich region of dipeptidyl peptidase IV (CD 26) is the collagen-binding site. *Biochem Biophys Res Commun.* 1995;217(1):341-348.
472. Piazza GA, Callanan HM, Mowery J, Hixson DC. Evidence for a role of dipeptidyl peptidase IV in fibronectin-mediated interactions of hepatocytes with extracellular matrix. *Biochem J.* 1989;262(1):327-334.

473. Varin EM, Mulvihill EE, Beaudry JL, et al. Circulating Levels of Soluble Dipeptidyl Peptidase-4 Are Dissociated from Inflammation and Induced by Enzymatic DPP4 Inhibition. *Cell Metab.* 2019;29(2):320-334 e325.
474. Lamers D, Famulla S, Wronkowitz N, et al. Dipeptidyl peptidase 4 is a novel adipokine potentially linking obesity to the metabolic syndrome. *Diabetes.* 2011;60(7):1917-1925.
475. Sell H, Bluher M, Kloting N, et al. Adipose dipeptidyl peptidase-4 and obesity: correlation with insulin resistance and depot-specific release from adipose tissue in vivo and in vitro. *Diabetes Care.* 2013;36(12):4083-4090.
476. Kim KM, Noh JH, Bodogai M, et al. Identification of senescent cell surface targetable protein DPP4. *Genes Dev.* 2017;31(15):1529-1534.
477. Balas B, Baig MR, Watson C, et al. The dipeptidyl peptidase IV inhibitor vildagliptin suppresses endogenous glucose production and enhances islet function after single-dose administration in type 2 diabetic patients. *J Clin Endocrinol Metab.* 2007;92(4):1249-1255.
478. Alam S, Ghosh J, Mustafa G, Kamal M, Ahmad N. Effect of sitagliptin on hepatic histological activity and fibrosis of nonalcoholic steatohepatitis patients: a 1-year randomized control trial. *Hepat Med.* 2018;10:23-31.
479. Yilmaz Y, Yonal O, Deyneli O, Celikel CA, Kalayci C, Duman DG. Effects of sitagliptin in diabetic patients with nonalcoholic steatohepatitis. *Acta Gastroenterol Belg.* 2012;75(2):240-244.
480. Mashitani T, Noguchi R, Okura Y, et al. Efficacy of alogliptin in preventing non-alcoholic fatty liver disease progression in patients with type 2 diabetes. *Biomed Rep.* 2016;4(2):183-187.
481. Macauley M, Hollingsworth KG, Smith FE, et al. Effect of vildagliptin on hepatic steatosis. *J Clin Endocrinol Metab.* 2015;100(4):1578-1585.
482. Kawaguchi T, Nakano D, Koga H, Torimura T. Effects of a DPP4 Inhibitor on Progression of NASH-related HCC and the p62/ Keap1/Nrf2-Pentose Phosphate Pathway in a Mouse Model. *Liver Cancer.* 2019;8(5):359-372.
483. Kawakubo M, Tanaka M, Ochi K, et al. Dipeptidyl peptidase-4 inhibition prevents nonalcoholic steatohepatitis–associated liver fibrosis and tumor development in mice independently of its anti-diabetic effects. *Scientific Reports.* 2020;10(1):983.
484. Michurina SV, Ishenko IJ, Klimontov VV, et al. Linagliptin alleviates fatty liver disease in diabetic db/db mice. *World J Diabetes.* 2016;7(19):534-546.
485. Wang X, Ke J, Zhu YJ, et al. Dipeptidyl peptidase-4 (DPP4) inhibitor sitagliptin alleviates liver inflammation of diabetic mice by acting as a ROS scavenger and inhibiting the NFkappaB pathway. *Cell Death Discov.* 2021;7(1):236.
486. Zheng W, Zhou J, Song S, et al. Dipeptidyl-Peptidase 4 Inhibitor Sitagliptin Ameliorates Hepatic Insulin Resistance by Modulating Inflammation and Autophagy in ob/ob Mice. *Int J Endocrinol.* 2018;2018:8309723.
487. Baumeier C, Schluter L, Saussenthaler S, et al. Elevated hepatic DPP4 activity promotes insulin resistance and non-alcoholic fatty liver disease. *Mol Metab.* 2017;6(10):1254-1263.
488. Gorgens SW, Jahn-Hofmann K, Bangari D, et al. A siRNA mediated hepatic dpp4 knockdown affects lipid, but not glucose metabolism in diabetic mice. *PLoS One.* 2019;14(12):e0225835.

489. Cha JY, Kim DH, Chun KH. The role of hepatic macrophages in nonalcoholic fatty liver disease and nonalcoholic steatohepatitis. *Lab Anim Res.* 2018;34(4):133-139.
490. Duarte N, Coelho I, Holovanchuk D, Ines Almeida J, Penha-Goncalves C, Paula Macedo M. Dipeptidyl Peptidase-4 Is a Pro-Recovery Mediator During Acute Hepatotoxic Damage and Mirrors Severe Shifts in Kupffer Cells. *Hepatol Commun.* 2018;2(9):1080-1094.
491. Bostick B, Habibi J, Ma L, et al. Dipeptidyl peptidase inhibition prevents diastolic dysfunction and reduces myocardial fibrosis in a mouse model of Western diet induced obesity. *Metabolism.* 2014;63(8):1000-1011.
492. Nakajima Y, Ito S, Asakura M, et al. A dipeptidyl peptidase-IV inhibitor improves diastolic dysfunction in Dahl salt-sensitive rats. *J Mol Cell Cardiol.* 2019;129:257-265.
493. Hirose M, Takano H, Hasegawa H, et al. The effects of dipeptidyl peptidase-4 on cardiac fibrosis in pressure overload-induced heart failure. *J Pharmacol Sci.* 2017;135(4):164-173.
494. Pham TK, Nguyen THT, Yi JM, et al. Evogliptin, a DPP-4 inhibitor, prevents diabetic cardiomyopathy by alleviating cardiac lipotoxicity in db/db mice. *Exp Mol Med.* 2023;55(4):767-778.
495. Shigeta T, Aoyama M, Bando YK, et al. Dipeptidyl peptidase-4 modulates left ventricular dysfunction in chronic heart failure via angiogenesis-dependent and -independent actions. *Circulation.* 2012;126(15):1838-1851.
496. Mulvihill EE, Varin EM, Ussher JR, et al. Inhibition of Dipeptidyl Peptidase-4 Impairs Ventricular Function and Promotes Cardiac Fibrosis in High Fat-Fed Diabetic Mice. *Diabetes.* 2016;65(3):742-754.
497. Kahles F, Meyer C, Mollmann J, et al. GLP-1 secretion is increased by inflammatory stimuli in an IL-6-dependent manner, leading to hyperinsulinemia and blood glucose lowering. *Diabetes.* 2014;63(10):3221-3229.
498. Diebold S, Moellmann J, Kahles F, et al. Myocardial infarction is sufficient to increase GLP-1 secretion, leading to improved left ventricular contractility and mitochondrial respiratory capacity. *Diabetes Obes Metab.* 2018;20(12):2911-2918.
499. Sauve M, Ban K, Momen MA, et al. Genetic deletion or pharmacological inhibition of dipeptidyl peptidase-4 improves cardiovascular outcomes after myocardial infarction in mice. *Diabetes.* 2010;59(4):1063-1073.
500. Gu Y, Ma CT, Gu HL, Shi L, Tian XT, Xu WQ. Sitagliptin improves cardiac function after myocardial infarction through activation of autophagy in streptozotocin-induced diabetic mice. *Eur Rev Med Pharmacol Sci.* 2018;22(24):8973-8983.
501. Li M, Wang Z, Xia H, Yu L, Hu Z. Vildagliptin and G-CSF Improved Angiogenesis and Survival after Acute Myocardial Infarction. *Arch Med Res.* 2019;50(3):133-141.
502. Mouse Genome Sequencing C, Waterston RH, Lindblad-Toh K, et al. Initial sequencing and comparative analysis of the mouse genome. *Nature.* 2002;420(6915):520-562.

503. Walkey CJ, Donohue LR, Bronson R, Agellon LB, Vance DE. Disruption of the murine gene encoding phosphatidylethanolamine N-methyltransferase. *Proc Natl Acad Sci U S A.* 1997;94(24):12880-12885.
504. Song J, da Costa KA, Fischer LM, et al. Polymorphism of the PEMT gene and susceptibility to nonalcoholic fatty liver disease (NAFLD). *FASEB J.* 2005;19(10):1266-1271.
505. Zbinden G, Bagdon RE. Isoproterenol-Induced Heart Necrosis, an Experimental Model for the Study of Angina Pectoris and Myocardial Infarct. *Rev Can Biol.* 1963;22:257-263.
506. Tsuchida T, Lee YA, Fujiwara N, et al. A simple diet- and chemical-induced murine NASH model with rapid progression of steatohepatitis, fibrosis and liver cancer. *J Hepatol.* 2018;69(2):385-395.
507. Lau JK, Zhang X, Yu J. Animal models of non-alcoholic fatty liver disease: current perspectives and recent advances. *J Pathol.* 2017;241(1):36-44.
508. Savard C, Tartaglione EV, Kuver R, et al. Synergistic interaction of dietary cholesterol and dietary fat in inducing experimental steatohepatitis. *Hepatology.* 2013;57(1):81-92.
509. Lai M, Chandrasekera PC, Barnard ND. You are what you eat, or are you? The challenges of translating high-fat-fed rodents to human obesity and diabetes. *Nutr Diabetes.* 2014;4(9):e135.
510. Montgomery MK, Hallahan NL, Brown SH, et al. Mouse strain-dependent variation in obesity and glucose homeostasis in response to high-fat feeding. *Diabetologia.* 2013;56(5):1129-1139.
511. Bostick B, Habibi J, DeMarco VG, et al. Mineralocorticoid receptor blockade prevents Western diet-induced diastolic dysfunction in female mice. *Am J Physiol Heart Circ Physiol.* 2015;308(9):H1126-1135.
512. Chiang SH, Harrington WW, Luo G, et al. Genetic Ablation of CD38 Protects against Western Diet-Induced Exercise Intolerance and Metabolic Inflexibility. *PLoS One.* 2015;10(8):e0134927.
513. Tadinada SM, Weatherford ET, Collins GV, et al. Functional resilience of C57BL/6J mouse heart to dietary fat overload. *Am J Physiol Heart Circ Physiol.* 2021;321(5):H850-H864.
514. Maurya SK, Carley AN, Maurya CK, Lewandowski ED. Western Diet Causes Heart Failure With Reduced Ejection Fraction and Metabolic Shifts After Diastolic Dysfunction and Novel Cardiac Lipid Derangements. *JACC Basic Transl Sci.* 2023;8(4):422-435.
515. Brainard RE, Watson LJ, Demartino AM, et al. High fat feeding in mice is insufficient to induce cardiac dysfunction and does not exacerbate heart failure. *PLoS One.* 2013;8(12):e83174.
516. Liu H, Huang Y, Zhao Y, et al. Inflammatory Macrophage Interleukin-1beta Mediates High-Fat Diet-Induced Heart Failure With Preserved Ejection Fraction. *JACC Basic Transl Sci.* 2023;8(2):174-185.
517. Trigatti B, Rayburn H, Vinals M, et al. Influence of the high density lipoprotein receptor SR-BI on reproductive and cardiovascular pathophysiology. *Proc Natl Acad Sci U S A.* 1999;96(16):9322-9327.

518. Yesilaltay A, Daniels K, Pal R, Krieger M, Kocher O. Loss of PDZK1 causes coronary artery occlusion and myocardial infarction in Paigen diet-fed apolipoprotein E deficient mice. *PLoS One.* 2009;4(12):e8103.
519. Zaragoza C, Gomez-Guerrero C, Martin-Ventura JL, et al. Animal models of cardiovascular diseases. *J Biomed Biotechnol.* 2011;2011:497841.
520. Rehman I, Kerndt CC, Rehman A. Anatomy, Thorax, Heart Left Anterior Descending (LAD) Artery. In: *StatPearls.* Treasure Island (FL) ineligible companies. Disclosure: Connor Kerndt declares no relevant financial relationships with ineligible companies. Disclosure: Afzal Rehman declares no relevant financial relationships with ineligible companies.2023.
521. De Villiers C, Riley PR. Mouse models of myocardial infarction: comparing permanent ligation and ischaemia-reperfusion. *Dis Model Mech.* 2020;13(11).
522. Johns TN, Olson BJ. Experimental myocardial infarction. I. A method of coronary occlusion in small animals. *Ann Surg.* 1954;140(5):675-682.
523. Zolotareva AG, Kogan ME. Production of experimental occlusive myocardial infarction in mice. *Cor Vasa.* 1978;20(4):308-314.
524. Bolli R, Patel BS, Jeroudi MO, Lai EK, McCay PB. Demonstration of free radical generation in "stunned" myocardium of intact dogs with the use of the spin trap alpha-phenyl N-tert-butyl nitrone. *J Clin Invest.* 1988;82(2):476-485.
525. Gao E, Lei YH, Shang X, et al. A novel and efficient model of coronary artery ligation and myocardial infarction in the mouse. *Circ Res.* 2010;107(12):1445-1453.
526. De Celle T, Cleutjens JP, Blankesteijn WM, Debets JJ, Smits JF, Janssen BJ. Long-term structural and functional consequences of cardiac ischaemia-reperfusion injury in vivo in mice. *Exp Physiol.* 2004;89(5):605-615.
527. Virag JA, Lust RM. Coronary artery ligation and intramyocardial injection in a murine model of infarction. *J Vis Exp.* 2011(52).
528. Cohen M, Boiangiu C, Abidi M. Therapy for ST-segment elevation myocardial infarction patients who present late or are ineligible for reperfusion therapy. *J Am Coll Cardiol.* 2010;55(18):1895-1906.
529. Martin TP, MacDonald EA, Elbassioni AAM, et al. Preclinical models of myocardial infarction: from mechanism to translation. *Br J Pharmacol.* 2022;179(5):770-791.
530. Reichert K, Colantuono B, McCormack I, Rodrigues F, Pavlov V, Abid MR. Murine Left Anterior Descending (LAD) Coronary Artery Ligation: An Improved and Simplified Model for Myocardial Infarction. *J Vis Exp.* 2017(122).
531. Hagan C. When are mice considered old? 2017. https://www.jax.org/news-and-insights/jax-blog/2017/november/when-are-mice-considered-old.
532. Mulvihill EE, Varin EM, Gladanac B, et al. Cellular Sites and Mechanisms Linking Reduction of Dipeptidyl Peptidase-4 Activity to Control of Incretin Hormone Action and Glucose Homeostasis. *Cell Metab.* 2017;25(1):152-165.
533. Gao GP, Alvira MR, Wang L, Calcedo R, Johnston J, Wilson JM. Novel adeno-associated viruses from rhesus monkeys as vectors for human gene therapy. *Proc Natl Acad Sci U S A.* 2002;99(18):11854-11859.
534. Yan Z, Yan H, Ou H. Human thyroxine binding globulin (TBG) promoter directs efficient and sustaining transgene expression in liver-specific pattern. *Gene.* 2012;506(2):289-294.

535. Riediger ND, Clara I. Prevalence of metabolic syndrome in the Canadian adult population. *CMAJ.* 2011;183(15):E1127-1134.

2 Hepatocyte-derived DPP4 regulates portal GLP-1 bioactivity, modulates glucose production, and when absent influences NAFLD progression

Authors: **Natasha A. Trzaskalski***, Branka Vulesevic*, My-Anh Nguyen, Natasha Jeraj, Evgenia Fadzeyeva, Nadya M. Morrow, Cassandra A.A. Locatelli, Nicole Travis, Antonio A. Hanson, Julia R.C. Nunes, Conor O'Dwyer, Jelske N. van der Veen, Ilka Lorenzen-Schmidt, Rick Seymour, Serena M. Pulente, Andrew C. Clément, Angela M. Crawley, René L. Jacobs, Mary-Anne Doyle, Curtis L. Cooper, Kyoung-Han Kim, Morgan D. Fullerton, and Erin E. Mulvihill

*Authors contributed equally

Published: JCI Insight
Trzaskalski, N. A., Vulesevic, B., Nguyen, M. A., Jeraj, N., Fadzeyeva, E., Morrow, N. M., ... & Mulvihill, E. E. (2023). Hepatocyte-derived DPP4 regulates portal GLP-1 bioactivity, modulates glucose production, and when absent influences NAFLD progression. *JCI insight*, *8*(2).

2.1 Author Contributions

Conceptualization: MAD, MDF, EEM Methodology: KHK, MDF, EEM; Formal Analysis: NAT; Investigation: NAT, BV, MAN, NJ, EF, NMM, CAAL, NT, AAH, JRCN, CO, JNV, ILS, RS, SMP, ACC, AMC, RLJ, MAD, CLC, KHK, MDF EEM; Resources: MDF, EEM; Writing – Original Draft: NAT, BV, EEM; Writing – Review and Editing: all authors; Supervision: KHK, MDF, EEM, RJ; Project Administration: EEM; Funding

Acquisition: EEM. Order of co-first authors was decided between the two authors and the corresponding author.

2.2 Abstract

Elevated circulating dipeptidyl peptidase-4 (DPP4) is a biomarker for liver disease, but its involvement in gluconeogenesis and metabolic associated fatty liver disease progression remains unclear. Here, we identified that DPP4 in hepatocytes but not TEK receptor tyrosine kinase–positive endothelial cells regulates the local bioactivity of incretin hormones and gluconeogenesis. However, the complete absence of DPP4 (*Dpp4*$^{-/-}$) in aged mice with metabolic syndrome accelerates liver fibrosis without altering dyslipidemia and steatosis. Analysis of transcripts from the livers of *Dpp4*$^{-/-}$ mice displayed enrichment for inflammasome, p53, and senescence programs compared with littermate controls. High-fat, high-cholesterol feeding decreased *Dpp4* expression in F4/80+ cells, with only minor changes in immune signaling. Moreover, in a lean mouse model of severe non-alcoholic fatty liver disease, phosphatidylethanolamine N-methyltransferase mice, we observed a 4-fold increase in circulating DPP4, in contrast with previous findings connecting DPP4 release and obesity. Last, we evaluated DPP4 levels in patients with hepatitis C infection with dysglycemia (Homeostatic Model Assessment of Insulin Resistance > 2) who underwent direct antiviral treatment (with/without ribavirin). DPP4 protein levels decreased with viral clearance; DPP4 activity levels were reduced at long-term follow-up in ribavirin-treated patients; but metabolic factors did not improve. These data suggest elevations in DPP4 during hepatitis C infection are not primarily regulated by metabolic disturbances.

2.3 Introduction

Type 2 diabetes (T2D) is a metabolic disease characterized by the development of hyperglycemia. Dysregulated islet hormone secretion and an inability to overcome peripheral insulin resistance are central components[1,2]. Given the increased appreciation of the reciprocal nature of dyslipidemia, obesity, dysglycemia and liver disease, including nonalcoholic fatty liver disease (NAFLD) and traditional risk factors, a new classification of metabolic (dysfunction) associated fatty liver disease (MAFLD) has emerged[3].

The secretion of incretin hormones from enteroendocrine cells in the gut epithelium, including glucagon-like peptide-1 (GLP-1) and glucose-dependent insulinotropic polypeptide (GIP), potentiates postprandial insulin secretion, a phenomenon known as the incretin effect. GLP-1 and GIP are central in coordinating nutrient intake, nutrient disposal, and satiety[4-6]. In patients with T2D, there is a defect in the incretin-mediated potentiation of insulin secretion[7]. Additionally, individuals with NAFLD exhibit an impaired incretin effect independent of diabetes, displaying fasting hyperglucagonemia[8] and increased hepatic gluconeogenesis[9].

The bioactivity and action of endogenous incretin hormones are limited through proteolytic cleavage and inactivation by the serine protease dipeptidyl peptidase-4 (DPP4) and renal elimination[10,11]. Enzymatically active DPP4 is present in both membrane-bound and circulating forms[12]. Plasma DPP4 levels are elevated in several settings associated with metabolic dysfunction, such as obesity[13,14]; chronic liver disease, including NAFLD and hepatitis C infection (HCV)[12,15,16]; as well as type 1 diabetes[17] and T2D[18,19]. Increased DPP4 expression in the liver positively correlates with the degree of steatosis and NAFLD[20,21]. Studies in mice using several tissue-

specific targeting strategies have confirmed that the elevation of circulating DPP4 in obesity is liver derived[22-24], suggesting that DPP4 produced in the liver may primarily contribute to the progression of NAFLD[25]. Systemic inhibition of DPP4 decreases blood glucose by reducing hepatic glucose production (HGP) in patients with T2D[26]. Given the success of incretin-based drugs in treating both diabetes and obesity, and their potential for treating NAFLD, further dissection of the regulation of hepatic metabolic pathways by DPP4 is warranted[27-33]. Here, we evaluated the role of hepatic DPP4 on incretin bioactivity within the portal vein (PV), hepatic glucose metabolism, and chronic liver disease progression in mice. We additionally examined circulating DPP4 levels and the mRNA abundances of sheddases in a mouse model of severe metabolic liver disease without obesity, phosphatidylethanolamine N-methyltransferase (*Pemt*$^{-/-}$) mice. We also evaluated circulating DPP4 levels and substrates in a patient population undergoing treatment for HCV.

2.4 Materials and Methods

2.4.1 Animals

All studies were performed according to protocols approved by the University of Ottawa Animal Care Committee and in accordance with guidelines of the Canadian Council on Animal Care. Male mice were housed under a 12-hour light/12-hour dark cycle and maintained on SLD (Harlan Teklad) or HFHC diet (TD.88137, Envigo-Teklad Custom Diets). Whole-body *Dpp4*$^{-/-}$ mice, on a C57BL/6 background, have been described[34,35]. To generate *Dpp4*$^{hep-/-}$ mice, *Dpp4*$^{fl/fl}$ adult mice, provided by Merck Research Laboratories[34], were i.v. injected with 1.5×10^{11} genome copies per mouse of AAV8.TBG.pi.egfp.wpre.bgh (AAV-GFP; control virus, 105535-AAV8, *Dpp4*^{GFP}) or AAV8.TBG.PI.CRE.rBG (AAV-Cre; 107787-AAV8, *Dpp4*$^{hep-/-}$) prior to the

onset of HFHC diet feeding. Both AAV constructs were obtained from the University of Pennsylvania Vector Core Lab as a gift from James M. Wilson (Perelman School of Medicine, University of Pennsylvania, Philadelphia, Pennsylvania, USA). B6.Cg-Tg(Tek-cre) 1Ywa/J mice were obtained from The Jackson Laboratory (Strain 008863, RRID: IMSR_JAX:008863) and bred with *Dpp4*$^{fl/fl}$ to generate *Dpp4*$^{EC-/-}$ mice. Experiments in *Pemt*$^{+/+}$ and *Pemt*$^{-/-}$ mice, provided by LKS Centre for Health Research Innovation[36], were approved by the University of Alberta's Institutional Animal Care Committee. Mice were fed an HFHC diet (F3282; Bio-Serv) for 3 weeks and fasted for 12 hours before sacrifice and tissue collection. Hyperinsulinemic-euglycemic clamps were performed in 12-week-old *Dpp4*$^{+/+}$, *Dpp4*$^{-/-}$, *Dpp4*$^{fl/fl}$, and *Dpp4*$^{hep-/-}$ mice subjected to 12–16 weeks of HFHC diet. Experiments were performed in 18- to 20-week-old mice after 5 weeks of HFHC diet to validate our HGP results. Last, to assess NAFLD progression, experiments were performed in 16- to 28-week-old mice fed an HFHC diet for 24 weeks, with sacrifice and tissue collection at 40–52 weeks. Eight mice died prematurely (1 *Dpp4*$^{hep-/-}$, 2 *Dpp4*^{GFP}, 1 *Dpp4*$^{-/-}$, and 4 WT mice), and 1 *Dpp4*^{GFP} mouse was omitted from analysis due to the presence of a very enlarged spleen. Aged, HFHC-fed *Dpp4*$^{hep-/-}$ and *Dpp4*^{GFP} mice were assessed for portal hormone concentrations (n = 2), with averages presented in Supplemental Table 1. Mice were genotyped from genomic DNA (gDNA) isolated from tail samples, and DNA recombination was confirmed in gDNA isolated from the liver. After DNA extraction and amplification, the PCR product was loaded on 1% agarose gels (UltraPure Agarose, Invitrogen, Thermo Fisher Scientific), then separated for 30 minutes at 150V (Owl Easycast B2 Separating System), and the bands were visualized under a blue light transilluminator (UVP GelDoc-It2 Imager).

2.4.2 Hyperinsulinemic-euglycemic clamp

Hyperinsulinemic-euglycemic clamps were performed as previously described[37]. Briefly, a catheter was surgically placed into the right jugular vein, and mice were allowed to recover for 5 days. All mice regained their presurgical weights following surgery. The catheter was made accessible through an adaptor port implanted in the dorsal subscapular region. On the day of the clamp, mice were fasted for 5 hours and then infused with d-[3-3H]-glucose (PerkinElmer) for 1 hour to evaluate basal glucose disposal. Human insulin (10 mU/kg/min, NovoRapid, Novo Nordisk) infusate containing d-[3-3H]-glucose was then administered, and blood glucose levels were titrated with 50% dextrose to achieve and maintain euglycemia. Mice were not physically restrained and were free to move around their cage, with blood samples taken via the tail vein. Basal and clamped rates of glucose disposal and HGP were calculated as described[37]. All tissues were rapidly dissected, snap-frozen in liquid nitrogen, and stored at −80°C for later analyses.

2.4.3 PV and CP cannulation

Mice were given an oral bolus of glucose (2 g/kg) and subsequently anesthetized with 4% isoflurane. Once fully unconscious, the abdomen was disinfected, and the mouse was placed on a heated surgical platform. A sagittal incision was made through the skin and fascia of the lower abdomen. A lateral transverse incision was made through the muscular layer to expose the abdominal contents. The PV was gently exposed by moving the intestines laterally toward the left body wall. Once exposed, the PV was cannulated with a 20-gauge butterfly needle 15 minutes after the glucose bolus, and the needle was withdrawn to collect blood. Approximately 1 minute later, the beating heart was exposed by cutting through the

diaphragm and thorax. An 18-gauge needle was used to collect blood from the right ventricle. Blood was aliquoted into 2 EDTA-coated capillary microvette tubes, one with 10% TED (5,000 KIU/mL Trasylol, 1.2 mg/mL EDTA, and 0.1 nmol/L Diprotin A) (vol/vol) and one without. Plasma was isolated after centrifugation (13,523*g*, 10 minutes, 4°C) and stored at −80°C for later analyses.

2.4.4 Pyruvate, arginine, and glucose tolerance tests

After a 16-hour fast, mice were intraperitoneally injected with either saline or exendin-9-39 (24 nmol/kg body weight[38]; Bachem), 15 minutes prior to injection, with 2 g/kg body weight pyruvate in sterile 0.9% saline. After a 4-hour fast, mice were intraperitoneally injected with 2 g/kg body weight arginine in sterile 0.9% saline. For glucose tolerance tests, mice were fasted for 5 hours and given glucose in PBS (2 g/kg body weight) in sterile 0.9% saline. Blood for glucose measurements (Glucometer, MediCure Canada) was obtained from the tail vein before pyruvate injection and at 15, 30, 45, 60, and 90 minutes after pyruvate injection, or before arginine injection and at 15 and 30 minutes after arginine injection.

2.4.5 Blood and tissue collection

All blood samples were collected in EDTA-coated capillary microvette tubes, and plasma was isolated after centrifugation (13,523*g*, 10 minutes, 4°C). During metabolic tolerance tests, blood was taken via tail vein. For terminal studies, mice were sacrificed by CO_2 inhalation, and blood was obtained by CP. For measurement of plasma active GLP-1 (Meso Scale Diagnostics) and active GIP (Crystal Chem), blood was mixed with 10% TED (vol/vol) and plasma stored at −80°C until further analysis. Plasma insulin (Alpco Diagnostics) and glucagon (Crystal Chem) levels were determined as per manufacturer's instructions. Analysis for plasma ALT, AST, alkaline

phosphatase, TG, cholesterol, LDL, and HDL was performed by the Pathology core at The Centre for Phenogenomics. The Beckman Coulter AU480 clinical chemistry analyzer was used in combination with appropriate reagents (ALT, AST, TG, cholesterol, LDL, and HDL), calibrators (Beckman Coulter Lyophilized Chemistry Calibrator levels 1 and 2), and quality control materials (Bio-Rad Liquid Assayed Multiqual levels 1 and 3). DPP4 activity was assessed using fluorometric assay (substrate: 10 mM H-Gly-Pro-AMC HBr, Bachem catalog I-1225; standard: AMC, Bachem catalog Q-1025). DPP4 protein level was measured using DPPIV/CD26 DuoSet ELISA kit (DY954; R&D Systems, Bio-Techne) following the manufacturer's instructions.

2.4.6 Picrosirius red and Oil Red O staining

Liver tissue was fixed in 4% paraformaldehyde (PFA) and routinely processed for paraffin-embedding and cross-sectioned to obtain 5 µm–thick sections. The slides were incubated with a 0.1% Picrosirius red solution and mounted with Permount Mounting Medium (Thermo Fisher Scientific). Collagen accumulation was determined by the number of red-stained pixels using ImageJ (NIH). Accumulation of fat droplets in the liver was visualized using Lipid (Oil Red O) Staining Kit as per manufacturer protocol (BioVision). A pathologist assessed the Picrosirius red sections and provided a METAVIR score following a protocol blinded to genotype.

2.4.7 Immunofluorescence staining

Liver tissue was fixed in 4% PFA and routinely processed for paraffin-embedding and cross-sectioned to obtain 5 µm–thick sections. Sections were dewaxed with toluene, then rehydrated with graded washes of ethanol, ending with water. Antigen retrieval was performed using sodium citrate buffer (0.1 M, pH 6, with

0.05% Tween-20) in a microwave, then washed with de-ionized water and PBS on a shaker. Sections were blocked with 10% donkey serum (catalog D9663 MilliporeSigma) for 30 minutes at room temperature. Antibodies against MARCO (Abcam, clone EPR22944-66, catalog ab259264, 1:200), F4/80 (Invitrogen, Thermo Fisher Scientific, clone CI:A3-1, catalog MA1-91124, 1:250), and CLEC4F (R&D Systems, Bio-Techne, catalog AF2784, 1:200) were incubated overnight at 4°C. Slides were washed with PBS-Tween, then incubated with secondary antibodies donkey anti-rabbit IgG (H+L) highly cross-absorbed Alexa Fluor Plus 647 (A32795, 1:500), donkey anti-rat IgG (H+L) highly cross-absorbed Alexa Fluor Plus 647 (A48272, 1:500), and donkey anti-goat IgG (H+L) cross-absorbed Alexa Fluor 555 (A-21432, 1:500) for 45 minutes at room temperature. Slides were washed and nuclei were stained using DAPI (Thermo Fisher Scientific 62248, 1:2,000) for 5 minutes at room temperature, washed, and mounted (Abcam, ab104135). Images were obtained on a Zeiss AxioImager Z1 epifluorescence micro- scope with 20× or 63× oil immersion objective and analyzed using Zeiss ZEN Blue microscopy software.

2.4.8 Liver TG and cholesterol content

Total liver lipids were extracted using a modified Folch method[39]. For SLD- and HFHC-fed mice, a 100 mg or 50 mg piece of liver tissue was homogenized in 4 mL chloroform/ methanol (2:1, v/v) and processed as described previously[40]. Lipids were quantified using Infinity Cholesterol or Triglyceride reagent (both Thermo Fisher Scientific) at 540 nm.

2.4.9 Hepatic F4/80$^+$ cell isolation

Fresh mouse livers were enzymatically digested using the components of a liver dissociation kit (kit 130-105-807, Miltenyi Biotec), and the gentleMACS

Dissociators were used for the mechanical dissociation steps as previously described[41]. Hepatic F4/80$^+$ cells were isolated from dissociated liver samples with Anti-F4/80 MicroBeads UltraPure (mouse, Miltenyi Biotec) as per manufacturer's protocol and flash-frozen in liquid nitrogen before being stored at –80°C for mRNA extraction.

2.4.10 RNA isolation, cDNA, and qRT-PCR

Frozen liver and isolated hepatic F4/80$^+$ cells were homogenized with Tri Reagent (MilliporeSigma) using a TissueLyser II system (QIAGEN), and total RNA was extracted using manufacturer's protocol. Reverse transcription was performed with the Applied Biosystems (Thermo Fisher Scientific) High-Capacity cDNA Reverse Transcription Kit. cDNA was subsequently used to assess mRNA expression by qRT-PCR (QuantStudio 5 System, Thermo Fisher Scientific) with TaqMan Fast Advanced Master Mix (Thermo Fisher Scientific, 4444557) and TaqMan Gene Expression Assays (Thermo Fisher Scientific). The specific gene expression assays used are listed (**Supplemental Table 1**). Quantification of transcript levels was performed by the standard curve method, and expression levels for each gene were normalized to *Actb* (β-actin).

2.4.11 NanoString mRNA analysis

NanoString Technologies nCounter Mouse Immunology Panel (catalog XT-CSO-MIM1-12) was used where 100 ng RNA was incubated with reporter and capture probes, consisting of 547 immunology-related mouse genes and 14 internal reference controls, for 16 hours at 65°C. Following hybridization, unbound probes were removed. According to the manufacturer's instructions, assays were performed and

quantified on the nCounter system, sample preparation station, and digital analyzer (NanoString Technologies).

Raw gene expression data were analyzed using NanoString's software, nSolver v4.0.70, with the Advanced Analysis Module v2.0.115 with background subtraction. Genes with counts below a threshold of 20 were excluded from subsequent analysis. Data normalization was performed on background-subtracted samples using internal positive controls and selected housekeeping genes. Housekeeping genes were selected based on those that were consistent in all analyses across genotypes and diets: *Sdha*, *Eef1g*, *Gapdh*, *Hprt*, *Polr2a*, *Rpl19*, *Oaz1*, *Tbp*, and *Tubb5* for liver tissue and *Rpl19*, *Ppia*, *Oaz1*, *Eef1g*, *Sdha*, *Pol2a*, *Gusb*, *Tubb5*, *Gapdh*, and *Hprt* for F4/80$^+$ cells. Differential gene expression analyses were performed using nSolver, which applies several multivariate linear regression models to identify significant genes (mixture negative binomial, simplified negative binomial, or log-linear model). Raw mRNA counts were $\log_2$-transformed, and significance was determined using 2-tailed *t* test. Statistically significant differentially expressed genes were identified as those with a $P < 0.05$. Ratios of $\log_2$-normalized transcript count data were generated for SLD *Dpp4*$^{-/-}$ mice versus baseline SLD WT mice, HFHC-fed *Dpp4*$^{-/-}$ mice versus baseline HFHC-fed WT mice, and HFHC-fed *Dpp4*$^{hep-/-}$ mice versus baseline HFHC-fed *Dpp4*^{GFP} mice. The NanoString data have been deposited in NCBI's Gene Expression Omnibus (GEO) and are accessible through GEO Series accession number GSE218767.

Pathway scores generated from nSolver Advanced Analysis were standardized by *Z*-scaling. ClustVis[42] was used to perform supervised hierarchical clustering

analysis and principal component analysis of $\log_2$-transformed transcript count data and *Z*-scaled pathway scores.

2.4.12 Human studies

Participants were recruited between July 2015 and April 2016 from The Ottawa Hospital Viral Hepatitis Program (Ottawa, Canada). All participants were 18 years or older, planned to initiate HCV antiviral treatment, and provided signed informed consent documents to participate in a single-center, open-label study (ClinicalTrials.gov Identifier: NCT02734173), which was approved by The Ottawa Health Science Network Research Ethics Board (REB 2015-0305). Three groups of patients were examined for this study: noncirrhotic genotype 1a–infected participants receiving standard therapy plus ribavirin, noncirrhotic genotype 1b–infected participants receiving standard therapy, and compensated cirrhotic genotype 1a– or 1b–infected participants dosed with standard therapy plus ribavirin; all had a HOMA-IR ≥ 2[43]. Patients were treated for 12 weeks with ribavirin and direct-acting antivirals, after which they achieved sustained virologic response, and they were followed up for an additional 36 weeks. Inclusion and exclusion criteria, as well as methods for treatment, have been described[43]. Plasma measurements were conducted by Laboratory Services at The Ottawa Hospital, as standard clinical procedure. Additional blood samples were treated with 1% Triton X-100 and 0.3% tributyl phosphate and incubated at 37°C for 1 hour to destroy any virus. The concentrations of circulating factors in treated plasma were quantified using multiplexing immunobead assays analyzed using Meso Scale Diagnostics as described above. Plasma DPP4 concentration was quantified using the R-PLEX Human DPPIV Antibody Set (Meso Scale Diagnostics, catalog F21YC)[44]. To remove the variance in

trait values attributed to sex and age differences for results described in Figure 7, a linear regression model compared the retrieved residuals (adjusted trait values) using the unpaired *t* test function available in R (version 4.0.5). Data are expressed as mean ± SD, and $P < 0.05$ was considered statistically significant.

2.4.13 Statistics

All data were plotted and statistical analyses were performed using GraphPad Prism (version 8.4.3). Data are expressed as mean ± SEM; human data are expressed as mean ± SD. Statistical differences between groups were evaluated by 2-way ANOVA with Tukey's multiple-comparison post hoc test when analyzing time course data. All other differences were evaluated by a 2-tailed unpaired *t* test with Welch's correction. $P < 0.05$ was considered statistically significant.

2.4.14 Study approval

Animals were cared for in accordance with the Canadian *Guide to the Care and Use of Laboratory Animals* (Canadian Council on Animal Care, 2020). Experimental procedures were approved under AUP#2909 and AUP#2029 by the University of Ottawa Animal Care and Veterinary Service (Ottawa, Ontario, Canada). Experiments in $Pemt^{+/+}$ and $Pemt^{-/-}$ were approved by the University of Alberta's Institutional Animal Care Committee (Edmonton, Alberta, Canada).

All participants were 18 years or older, planned to initiate HCV antiviral treatment, and provided written informed consent to participate in a single-center, open-label study (ClinicalTrials.gov Identifier: NCT02734173), which was approved by The Ottawa Health Science Network Research Ethics Board (REB 2015-0305, Ottawa, Ontario, Canada).

2.5 Results

2.5.1 Reduced HGP in high-fat, high-cholesterol–fed *Dpp4*$^{-/-}$ mice is due to loss of hepatocyte-derived DPP4

In patients with T2D, DPP4 inhibitors contribute to glucose homeostasis by decreasing hepatic gluconeogenesis[26,45]. To validate this effect in mice, we performed hyperinsulinemic-euglycemic clamps in *Dpp4*$^{+/+}$ (wild- type, WT) and *Dpp4*$^{-/-}$ (global *Dpp4* deletion) mice fed a high-fat, high-cholesterol (HFHC) diet for 12 weeks. Glucose infusion rates (GIRs, **Figure 2.1A**) and glucose disposal rates (GDRs, **Figure 2.1B**) were indistinguishable between *Dpp4*$^{-/-}$ mice and their WT littermate controls. Although basal levels of HGP were unchanged, insulin-stimulated HGP was significantly lower in HFHC-fed *Dpp4*$^{-/-}$ (**Figure 2.1C),** resulting in a significantly greater suppression of HGP by insulin in *Dpp4*$^{-/-}$ mice (**Figure 2.1D**). Body weight and fasting glucose levels were unchanged (**Supplemental Figure 2.1, A** and **B**). Although the mRNA abundance of hepatic *Gck*, the enzyme that phosphorylates glucose to produce glucose-6-phosphate, was significantly upregulated in *Dpp4*$^{-/-}$ mice compared with livers of control mice (**Figure 2.1E**), transcript levels of the gluconeogenic enzymes, *Pck* and *G6p*, were unchanged (**Figure 1E**). mRNA levels of hepatic *Gsk3β*, a protein kinase that phosphorylates and inhibits glycogen synthase, were also elevated in *Dpp4*$^{-/-}$ mice compared with *Dpp4*$^{+/+}$ (**Figure 1E**). Hepatic mRNA expression of *Pygl*, *Gcgr*, *Igf1*, and *Igf1r* was indistinguishable between *Dpp4*$^{-/-}$ and *Dpp4*$^{+/+}$ mice (**Figure 2.1E** and **F**).

To determine if the reduction in HGP in *Dpp4*$^{-/-}$ mice was mediated through the actions of hepatocyte-derived DPP4, we then measured HGP in HFHC-fed, hepatocyte-specific Dpp4-knockout mice (*Dpp4*$^{hep-/-}$). Similar to *Dpp4*$^{-/-}$ mice, HFHC-

fed control mice (*Dpp4*^{GFP}) and *Dpp4*$^{hep-/-}$ mice did not differ in GIR (**Figure 2.1G**) or GDR (**Figure 2.1H**) or in body weight or fasting glucose (**Supplemental Figure 2.1, C** and **D**). In addition, as seen in *Dpp4*$^{-/-}$ mice, basal levels of HGP were unchanged, and *Dpp4*$^{hep-/-}$ mice showed lower HGP under clamp conditions and greater insulin suppression of HGP (**Figure 2.1, I** and **J**). Akin to *Dpp4*$^{-/-}$ mice, mRNA expression of hepatic glucose utilization or gluconeogenic enzymes was unchanged except *Gck*, which trended (P = 0.09) upward in *Dpp4*$^{hep-/-}$ mice (**Figure 2.1K**). The gene expression of *Gcgr*, *Igf1*, and *Igf1r* was comparable between genotypes (**Figure 2.1L**).

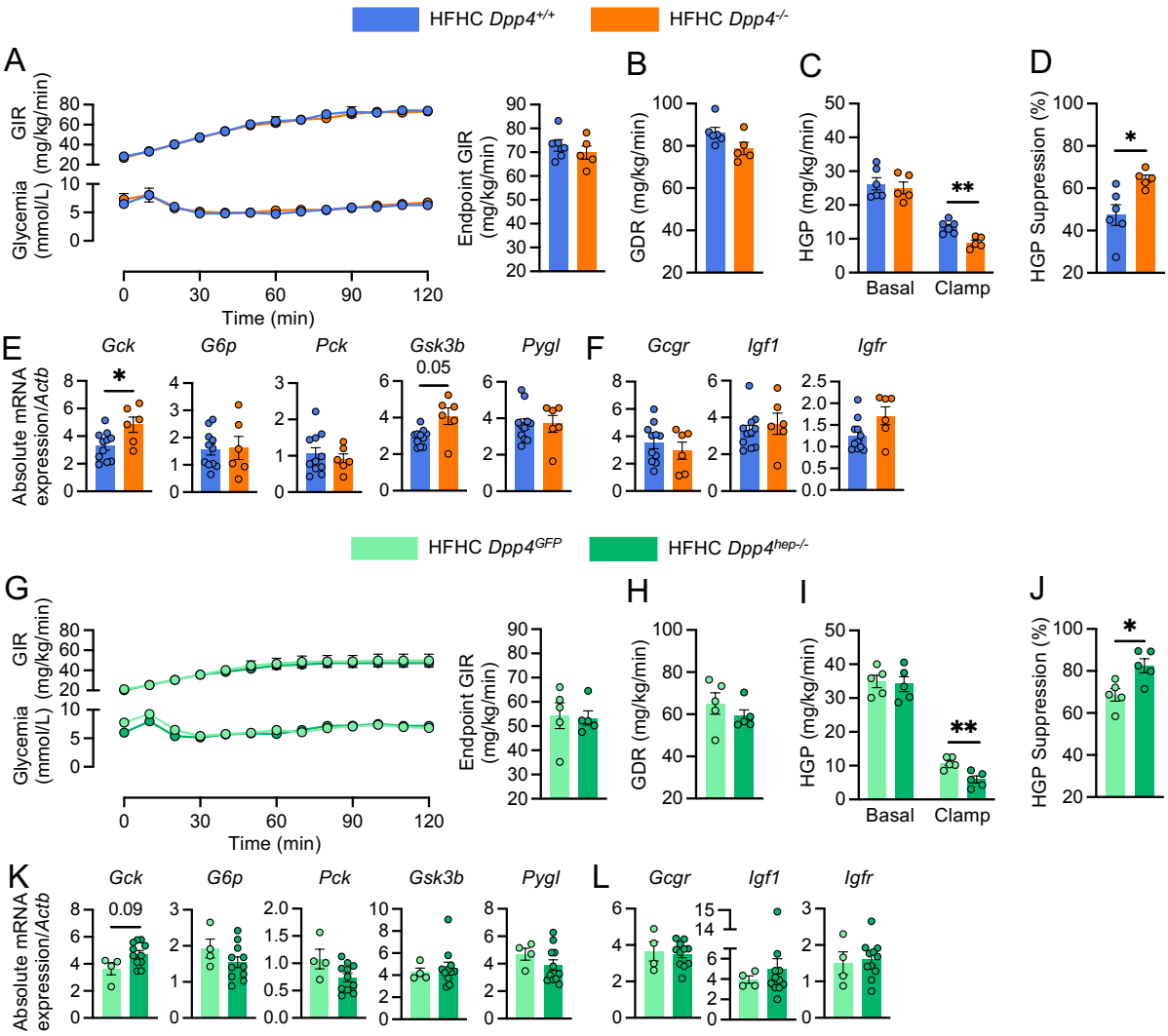

Figure 2.1: HGP is decreased in HFHC-fed *Dpp4*$^{-/-}$ and hepatocyte-specific *Dpp4*-knockout mice. Time-course of glucose infusion rates and plasma glucose, and endpoint GIR during hyperinsulinemic-euglycemic clamp of *Dpp4*$^{+/+}$ (n=6) and *Dpp4*$^{-/-}$ (n=5) mice. (**B**) Glucose disposal rate (GDR), (**C**) basal and clamp hepatic glucose production (HGP) and (**D**) percent of HGP suppression under clamp conditions. Hepatic mRNA abundance (relative to *Actb*) for genes associated with (**E**) hepatic gluconeogenesis (*Gck*, *G6p*, *Pck*, *Gsk3β* and *Pygl*) (**F**) insulin signaling (*Gcgr*, *Igf* and *Igf1r*) in *Dpp4*$^{+/+}$ (n=11) and *Dpp4*$^{-/-}$ (n=7) mice (**G**) Time-course of plasma glucose and glucose infusion rates, and endpoint GIR during hyperinsulinemic-euglycemic clamp of *Dpp4*^{GFP} (n=4) and *Dpp4*$^{hep-/-}$ (n=5) mice. (**H**) GDR (**I**) basal and clamp HGP and (**J**) percent of HGP suppression under clamp conditions. Hepatic mRNA abundance (relative to *Actb*) for genes associated with (**K**) hepatic gluconeogenesis (*Gck*, *G6p*, *Pck*, *Gsk3β* and *Pygl*) and (**L**) insulin signaling (*Gcgr*, *Igf* and *Igf1r*) in *Dpp4*^{GFP} (n=4) and *Dpp4*$^{hep-/-}$ (n=11) mice. Data are presented as the mean ± SEM. Time-course data is analyzed by two-way ANOVA with Tukey's multiple comparisons post hoc test, remaining data analyzed by unpaired students t-test with Welch's correction, ns P<0.05, *P=0.01-0.05, **P=0.001-0.01.

2.5.2 Deletion of *Dpp4* in hepatocytes lowers portal DPP4 activity and increases portal concentrations of bioactive GLP-1 and GIP

We evaluated glucose excursion after intraperitoneal injection of pyruvate to further evaluate the cell-specific roles of DPP4 in regulating HGP. Consistent with our previous work[22], $Dpp4^{hep-/-}$ mice had significantly reduced *Dpp4* mRNA expression in whole liver extracts (**Supplemental Figure 2.2A**); fasted DPP4 activity in plasma was decreased 50% in 20-week-old $Dpp4^{GFP}$ and $Dpp4^{hep-/-}$ mice fed an HFHC diet for 4 weeks (**Supplemental Figure 2.2B**); but DPP4 plasma concentration was unchanged (**Supplemental Figure 2.2C**).

Accordant with the clamp data, $Dpp4^{hep-/-}$ mice had significantly reduced glucose excursion AUC after injection of pyruvate compared with littermate $Dpp4^{GFP}$ controls (**Figure 2.2A**). Next, we examined whether reduced HGP in $Dpp4^{hep-/-}$ mice is mediated by DPP4's action on GLP-1 receptor (GLP-1R) signaling. The decrease in plasma glucose following pyruvate injection was abrogated with the administration of exendin-9-39, a compound that blocks signaling through the GLP-1R[46], 15 minutes before injection of pyruvate (**Figure 2.2B**). $Dpp4^{hep-/-}$ mice showed no change compared to $Dpp4^{GFP}$ in an arginine tolerance test, indicating that islet responsivity to acute depolarization was normal (**Supplemental Figure 2.2D**). In addition, in response to arginine, mice lacking hepatocyte *Dpp4* did not demonstrate any differences in blood glucose, active GLP-1, insulin, or glucagon (**Supplemental Figure 2.2E–G**). GLP-1 has been reported to circulate through the portal circulation and the lymphatics to enter systemic circulation at the thoracic duct[47,48]. To evaluate how DPP4 in hepatocytes may influence the bioactivity of incretin hormones at each of these sites (i.e., portal or systemic concentration), we administered oral glucose to

Dpp4$^{hep-/-}$ and control mice and sampled PV blood via cannulation followed by systemic blood 15 minutes later by cardiac puncture (CP). DPP4 activity but not protein level within the PV was significantly reduced in *Dpp4*$^{hep-/-}$ mice compared with *Dpp4*^{GFP} mice (**Figure 2.2, C** and **D**). In addition, active GLP-1 and active GIP levels were elevated approximately 4-fold in the local portal circulation in *Dpp4*$^{hep-/-}$ mice compared with *Dpp4*^{GFP} mice (**Figure 2.2E** and **F**). On the other hand, no significant differences in active GLP-1 and GIP were noted in plasma isolated immediately in the same mice by CP (**Figure 2.2, E** and **F**). Despite the increase in circulating incretin, plasma insulin and glucagon levels were unchanged in local hepatic and systemic circulations (**Figure 2.2, G** and **H**).

To investigate the role of DPP4 in hepatocytes versus other sites that contribute to circulating DPP4, including TEK receptor tyrosine kinase–positive (Tie2+) endothelial cells (ECs) and immune cells, we used *Dpp4*$^{EC-/-}$ mice. Previously, we have reported that deletion of *Dpp4* from the Tie2+ ECs (*Dpp4*$^{EC-/-}$) of high-fat–fed mice results in increased systemic concentrations of GLP-1 and improved glucose excursion but does not affect HGP[34]. As expected, in contrast to *Dpp4*$^{hep-/-}$, *Dpp4*$^{EC-/-}$ mice had no decrease in hepatic *Dpp4* mRNA expression (**Supplemental Figure 2.2H**), and, consistent with previous reports[34], systemic fasting plasma DPP4 activity and DPP4 protein levels (**Supplemental Figure 2.2, I** and **J**) were significantly decreased in *Dpp4*$^{EC-/-}$ mice compared with controls. Furthermore, a pyruvate tolerance test showed no change in HGP in HFHC-fed *Dpp4*$^{EC+/+}$ and *Dpp4*$^{EC-/-}$ mice previously administered saline or exendin-9-39 (**Figure 2.2, I** and **J**), consistent with our previous hyperglycemic-euglycemic clamp analyses[34].

To directly determine how DPP4 in these different tissue settings governs incretin bioactivity and HGP, we measured the portal concentrations of DPP4 and incretins and also examined pyruvate tolerance in HFHC-fed *Dpp4*$^{EC+/+}$ and *Dpp4*$^{EC-/-}$ mice. Although portal DPP4 activity was unchanged (**Figure 2.2K**), DPP4 protein levels in the PV were significantly decreased in *Dpp4*$^{EC-/-}$ mice (**Figure 2.2L**). Furthermore, levels of active GLP-1 and active GIP were unchanged in the portal circulation in *Dpp4*$^{EC-/-}$ mice, but systemic concentrations of incretins were increased 2.5-fold (GLP-1) or trended 2-fold higher (GIP) in samples isolated by CP (**Figure 2.2M** and **N**). Levels of insulin and glucagon at either sampling site (**Figure 2.2O** and **P**) were unaltered. Together, these results suggest that the reduction in HGP observed in HFHC-fed *Dpp4*$^{-/-}$ mice is driven by the loss of *Dpp4* in hepatocytes and not Tie2+ EC populations. Furthermore, this improved suppression of HGP is associated with elevated incretin concentrations within the PV, not the systemic circulation.

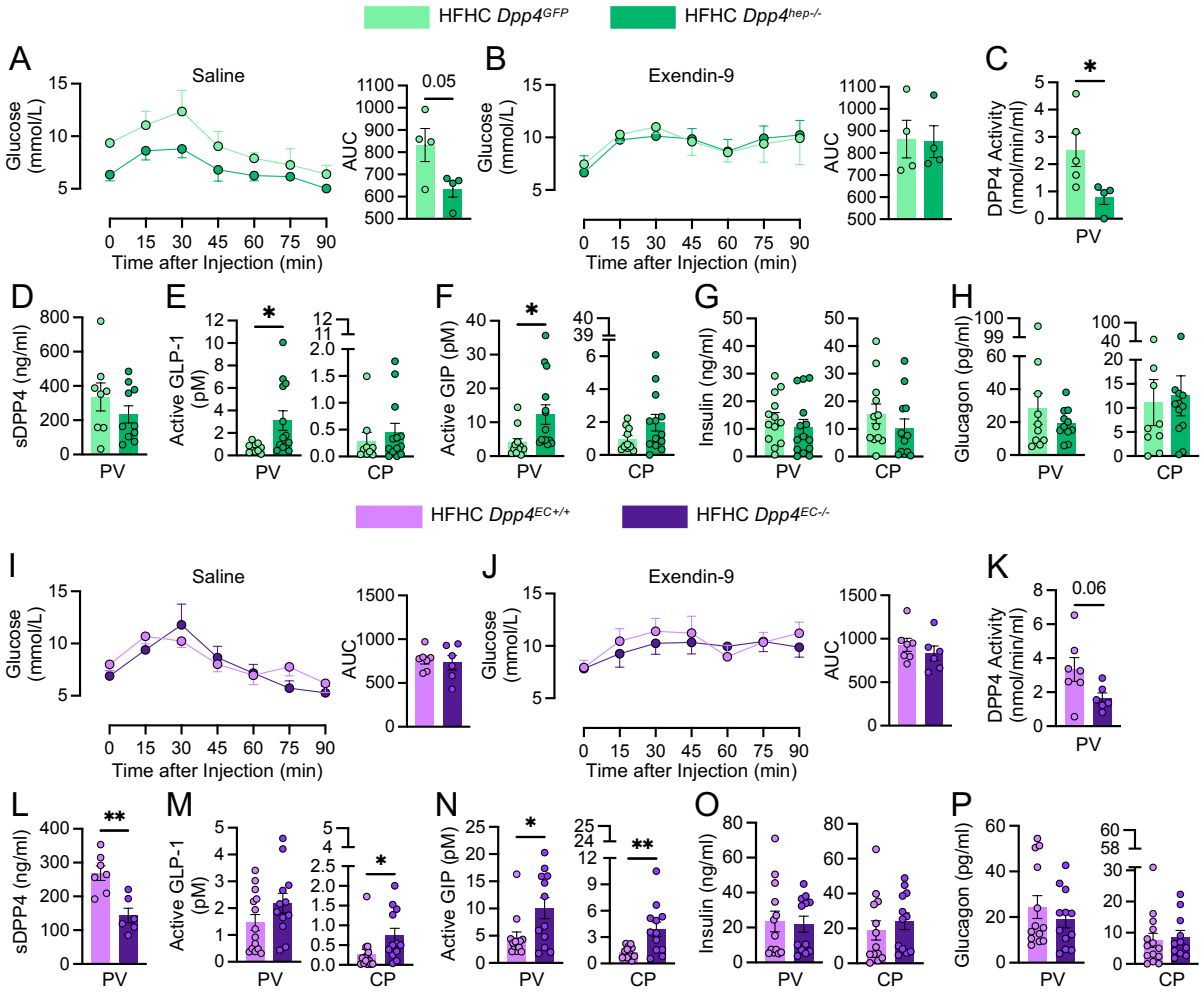

Figure 2.2: Hepatic glucose production is decreased in *Dpp4*$^{hep-/-}$ but not *Dpp4*$^{EC-/-}$ via GLP-1 and GIP dependent pathways. Blood glucose prior to and during a pyruvate tolerance test (PTT) following (**A**) saline or (**B**) Exendin-9-39 i.p. injection and resulting area under the curve (AUC) in *Dpp4*^{GFP} (n=4) and *Dpp4*$^{hep-/-}$ (n=4) mice. (**C**) DPP4 activity, (**D**) concentration, (**E**) active GLP-1, (**F**) active GIP, (**G**) insulin and (**H**) glucagon from the portal vein (PV) and cardiac puncture (CP) 15 minutes after glucose bolus in *Dpp4*^{GFP} (n=4-12) and *Dpp4*$^{hep-/-}$ (n=4-11) mice. Blood glucose prior to and during a pyruvate tolerance test (PTT) following (**I**) saline or (**J**) Exendin-9-39 i.p. injection and resulting area under the curve (AUC) in *Dpp4*$^{EC+/+}$ (n=7) and *Dpp4*$^{EC-/-}$ (n=6) mice. (**K**) DPP4 activity, (**L**) concentration, (**M**) active GLP-1, (**N**) active GIP, (**O**) insulin and (**P**) glucagon from the portal vein (PV) and cardiac puncture (CP) 15 minutes after glucose bolus in *Dpp4*$^{EC+/+}$ (n=7-13) and *Dpp4*$^{EC-/-}$ (n=6-11) mice. Data are presented as the means ± SEM. Time-course data is analyzed by two-way ANOVA with Tukey's multiple comparisons post hoc test, remaining data analyzed by unpaired students t-test with Welch's correction, ns P<0.05, *P=0.01-0.05, **P=0.001-0.01.

2.5.3 Dyslipidemia and liver steatosis are unaffected by the genetic elimination of *Dpp4* in aged, HFHC-fed mice

Insulin resistance, de novo lipogenesis, and dysregulated blood glucose are key hallmarks in the progression of NAFLD as part of the multiple-hit hypothesis[49]. To determine whether the reduction in HGP observed following the deletion of *Dpp4* from the whole animal or liver only can prevent NAFLD progression, we fed aged 6-month-old mice either a standard laboratory diet (SLD) or an HFHC diet for 24 weeks. In a small subset of aged mice (n = 2/group), we performed similar PV cannulations and CPs and observed trends consistent with those shown in Figure 2 (**Supplemental Table 2.2**). Analysis of *Dpp4* mRNA in whole liver extracts revealed elimination in all expected genotypes (**Figure 2.3A**). DPP4 activity in plasma and liver was absent from *Dpp4*$^{-/-}$ on SLD and HFHC diet and reduced by 60% and 75% in *Dpp4*$^{hep-/-}$ mice compared with controls (**Figure 2.3B** and **C**). Agreeing with our previous results[22], deletion of hepatocyte Dpp4 led to sustained reductions in plasma and hepatic DPP4 activities, with little change in circulating DPP4 protein levels (**Figure 2.3D**). Deletion of hepatocyte-specific DPP4 in these aged mice did not affect glucose tolerance as only whole-body deletion of DPP4 increased systemic active GLP-1 and led to reduced blood glucose excursion during oral glucose tolerance test (**Supplemental Figure 2.3A** and **B**), consistent with previous work[22,23]. Glycogen concentrations were unchanged in all settings (**Supplemental Figure 2.3C**). In both SLD-fed and HFHC-fed *Dpp4*$^{-/-}$ mice, lack of *Dpp4* did not affect HDL, LDL, or total cholesterol levels in plasma (**Figure 2.3E–G**). However, fasting plasma triglycerides were significantly reduced in *Dpp4*$^{-/-}$ mice (**Figure 2.3H**). Biochemical measurement and histochemical analysis with Oil Red O staining in livers revealed no differences in neutral lipid

concentrations between genotypes (**Figure 2.3I–M**). Hepatic gene expression analysis also revealed that sterol regulatory element–binding transcription factor 1 (*Srebf1*) mRNA expression was significantly upregulated in HFHC-fed *Dpp4*$^{-/-}$ mice but unchanged in SLD-fed mice and HFHC-fed *Dpp4*$^{hep-/-}$ mice, compared with controls (**Figure 2.3N**). Microsomal triglyceride transfer protein (*Mttp*) mRNA expression was significantly decreased in SLD-fed *Dpp4*$^{-/-}$ mice compared with controls but unchanged in all genotypes under HFHC feeding (**Figure 2.3O**). In contrast, hepatic Forkhead box protein O1 (*FoxO1*) expression was unchanged between all genotypes under both diets (**Figure 2.3P**). Taken together, these data suggest that hepatic lipid accumulation is largely unaffected by whole-body or hepatocyte-specific elimination of *Dpp4* gene in aged, SLD- or HFHC-fed mice.

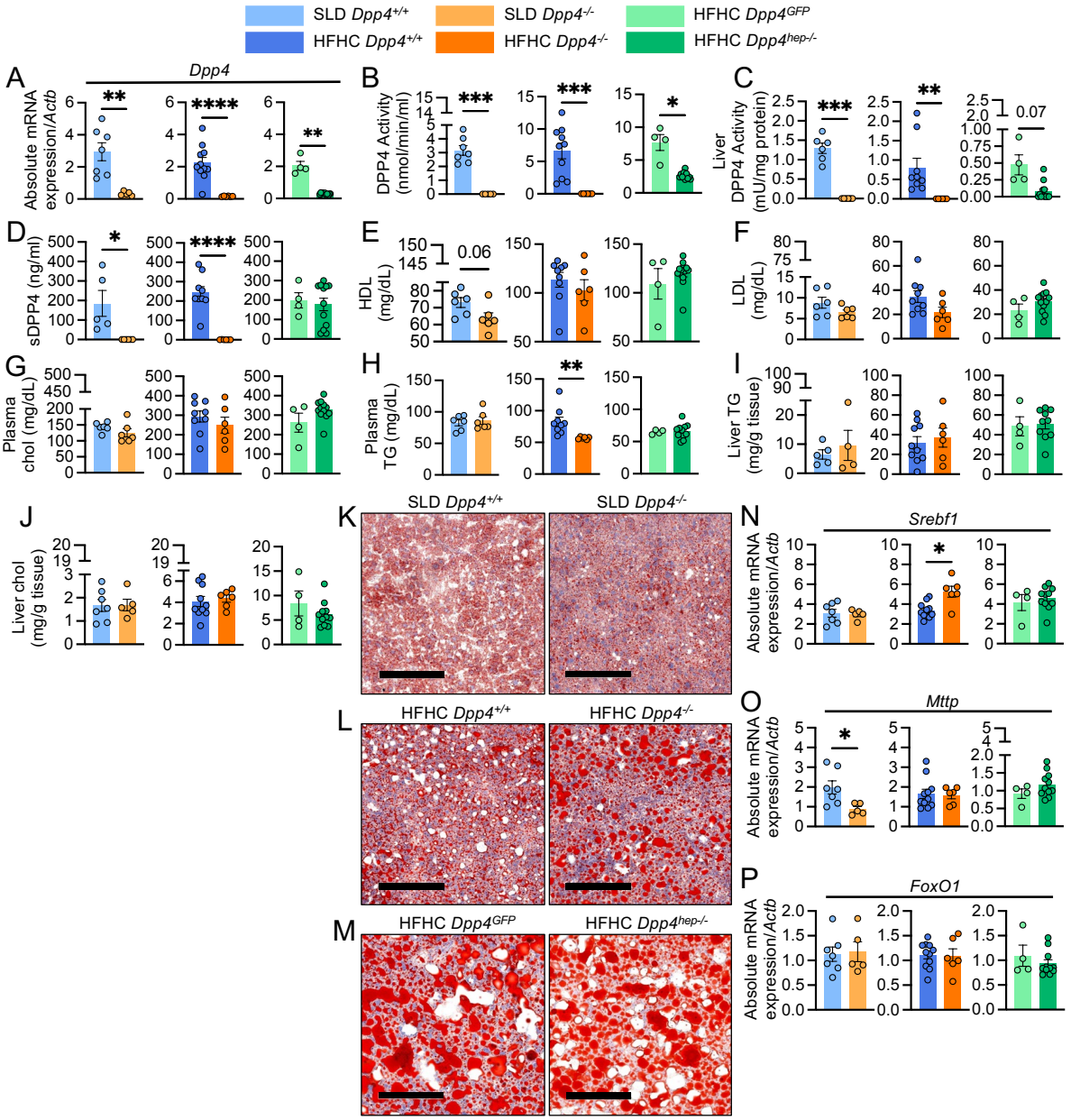

Figure 2.3: Plasma and liver lipid profiles remain largely unchanged between genotypes. (**A**) Hepatic *Dpp4* mRNA abundance (relative to *Actb*) (**B**) Plasma DPP4 activity. (**C**) Liver DPP4 activity. (**D**) Plasma DPP4 protein. (**E**) Plasma high-density lipoprotein (HDL), (**F**) low-density lipoprotein (LDL), (**G**) plasma cholesterol (chol), (**H**) plasma triglycerides (TG), (**I**) liver TG mass and (**J**) total cholesterol mass. Representative images of liver stained with Oil Red O in (**K**) SLD-fed *Dpp4*$^{+/+}$ (n=5-7) and *Dpp4*$^{-/-}$ (n=4-6) mice, (**L**) HFHC-fed *Dpp4*$^{+/+}$ (n=9-11) and *Dpp4*$^{-/-}$ (n=6) mice and (**M**) HFHC-fed *Dpp4*^{GFP} (n=4) and *Dpp4*$^{hep-/-}$ (n=10-11) mice (scale bar = 200μm). Hepatic mRNA abundance (relative to *Actb*) of (**N**) *Srebf1*, (**O**) *Mttp* and (**P**) *FoxO1*. Data are presented as the means ± SEM, analyzed by unpaired students t-test with Welch's correction, ns P <0.05, * P =0.01-0.05, ** P =0.001-0.01, *** P =0.0001-0.001 and ****P<0.0001.

2.5.4 Systemic, not hepatic, loss of *Dpp4* in aged mice increases hepatic fibrosis

Soluble, circulating DPP4 has been shown to be a marker of liver fibrosis[50]. Thus, we examined if systemic and hepatic loss of *Dpp4* in mice affected liver fibrosis. Liver damage markers, such as alanine aminotransferase (ALT), aspartate transaminase (AST), and alkaline phosphatase, were not significantly different between all groups and their respective controls (**Figure 2.4, A–C**). Liver size normalized to tibia length was also unchanged (data not shown). To our surprise, mRNA levels of fibrosis markers, including *Col1a1, Col3a1, Mmp2, Mmp11, Des*, and *Ddr2*, were elevated in HFHC-fed *Dpp4*$^{-/-}$ mouse livers (**Figure 2.4, D–I**), suggesting worsening fibrosis in the *Dpp4*$^{-/-}$ mice. However, this elevated gene expression was not observed in *Dpp4*$^{hep-/-}$ mouse livers. No changes of expression were noted in fibrosis and hepatic stellate cell activation factors, *Mmp9, Gfap* and *Vim*, between any of the genotypes (**Supplemental Figure 2.4, A–C**) while both *Lrat* and *Pcdh7* were significantly reduced in SLD-fed *Dpp4*$^{-/-}$ mice compared with controls (**Supplemental Figure 2.4, D** and **E**). Consistent with gene expression, visualization of collagen with Picrosirius red staining revealed that HFHC-fed *Dpp4*$^{-/-}$ mice had elevated fibrotic area in the liver, whereas it was relatively unchanged in *Dpp4*^{GFP} and *Dpp4*$^{hep-/-}$ mice (**Figure 2.4, J–M**). Supporting increased fibrosis, blinded meta-analysis of histological data in viral hepatitis (METAVIR) histopathological scoring of liver samples revealed a shift of 33% in *Dpp4*$^{-/-}$ mice to level 4 relative to littermate controls, while no *Dpp4*$^{hep-/-}$ mice were scored in this range (**Figure 2.4N**). Overall, these data suggest that systemic, not hepatic, loss of Dpp4 increases liver fibrosis.

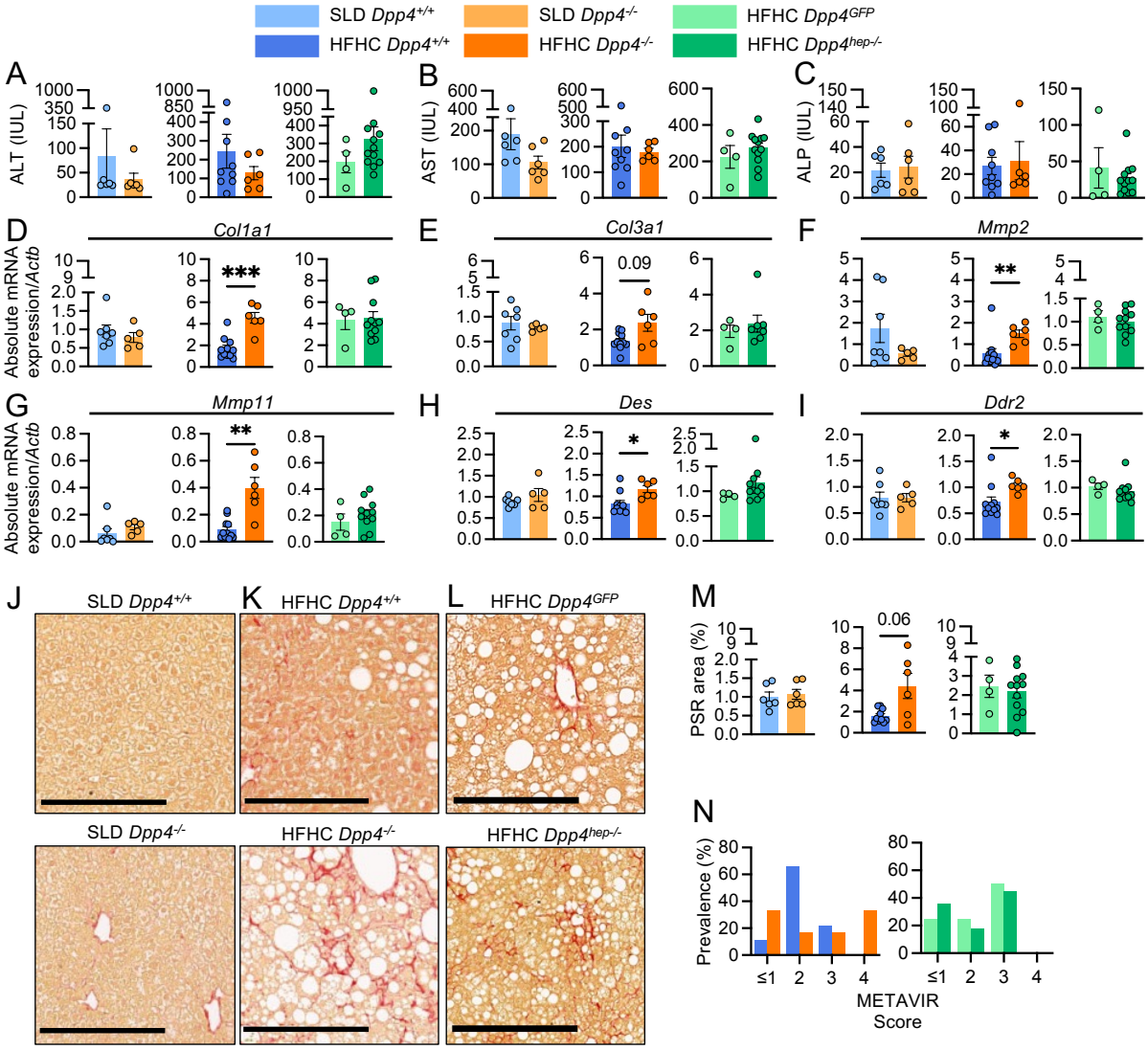

Figure 2.4: Fibrosis-related genes are up-regulated in HFHC-fed *Dpp4*$^{-/-}$ but not *Dpp4*$^{hep-/-}$ mice. (**A**) Alanine aminotransferase (ALT), (**B**) aspartate transaminase (AST) and (**C**) alkaline phosphatase (ALP). Liver mRNA abundance (relative to *Actb*) of (**D**) *Col1a1*, (**E**) *Col3a1*, (**F**) *Mmp2*, (**G**) *Mmp11*, (**H**) *Des* and (**I**) *Ddr2*. Representative images of liver stained with Picrosirius Red and quantitation of red-stained pixels in (**J**) SLD-fed *Dpp4*$^{+/+}$ (n=6-7) and *Dpp4*$^{-/-}$ (n=5-6) mice, (**K**) HFHC-fed *Dpp4*$^{+/+}$ (n=9-11) and *Dpp4*$^{-/-}$ (n=6) mice and (**L**) HFHC-fed *Dpp4*^{GFP} (n=4) and *Dpp4*$^{hep-/-}$ (n=11-12) mice (scale bar = 250um) and (**M**) quantitation of red-stained pixels. (**N**) Liver METAVIR score prevalence. Data are presented as the means ± SEM, analyzed by unpaired students t-test with Welch's correction, ns P<0.05, * P=0.01-0.05, ** P=0.001-0.01, *** P=0.0001-0.001.

2.5.5 Global, but not hepatic, loss of DPP4 increases expression of genes associated with adaptive immunity, inflammasome, and senescence-associated genes and pathways

To gain molecular insights into the inflammatory responses in the liver mediated by loss of *Dpp4*, we conducted NanoString mRNA analysis on liver tissue using an immunology panel of over 500 immune-related genes. All $Dpp4^{hep-/-}$ mice were confirmed by quantitative real-time PCR (qRT-PCR) with primers specific for the recombined *Dpp4* flox sites (**Figure 2.3A**), given the location of the flox deletion site toward the C-terminal end of the *Dpp4* transcript and modest reduction in gene expression detected by NanoString probes (**Supplemental Figure 2.5A**). Supervised hierarchical clustering analysis of differentially expressed genes in $Dpp4^{-/-}$ mice revealed a distinct cluster of genes that were upregulated in SLD- and HFHC-fed $Dpp4^{-/-}$ mice compared with $Dpp4^{+/+}$ and $Dpp4^{GFP}$ versus $Dpp4^{hep-/-}$ (**Supplemental Figure 2.5B** and **C**). We identified differentially expressed genes that were distinct and overlapping among SLD-fed $Dpp4^{-/-}$, HFHC-fed $Dpp4^{-/-}$, and HFHC-fed $Dpp4^{hep-/-}$ livers (**Supplemental Figure 2.5D**). Pathway analysis in each comparison was performed, showing that only cytokine signaling in SLD-fed $Dpp4^{-/-}$ mice was significantly upregulated compared with $Dpp4^{+/+}$ mice (**Figure 2.5A**). Notably, 18 pathways, including adaptive and innate immune pathways, inflammasome, Toll-like receptor signaling, oxidative stress, and TGF-β signaling, were all significantly upregulated in HFHC-fed $Dpp4^{-/-}$ compared with $Dpp4^{+/+}$ mice (**Figure 2.5B**). Consistent with no difference in liver fibrosis (**Figure 2.4H**), all pathways were indistinguishable between HFHC-fed $Dpp4^{GFP}$ and $Dpp4^{hep-/-}$ mouse livers (**Figure 2.5C**), suggesting that hepatocyte DPP4 was not influencing the immunological

response. We validated these results by immunostaining for the top differentially expressed transcript, Marco, in mice fed the HFHC diet. Consistent with the NanoString analysis, Marco staining was significantly reduced in the HFHC-fed *Dpp4*$^{-/-}$ mouse livers compared with controls (**Supplemental Figure 2.6A–G**). Additionally, Marco expression in *Dpp4*^{GFP} mice exhibited a spread of high- and low-expressing livers, which was recapitulated with immunostaining (**Supplemental Figure 2.6C, D, F,** and **G**). When we probed gene expression within the inflammasome pathway, whose activation is a contributing factor in the initial progression of NAFLD[51], we found that all genes (*App, Bcl2, Nfkb1, Nfkb2*, and *Rela*) were significantly upregulated in HFHC-fed *Dpp4*$^{-/-}$ mice (**Figure 2.5D**). In contrast, only *App* and *Rela* were significantly upregulated in SLD-fed *Dpp4*$^{-/-}$ mice compared with controls, and *Rela* was significantly downregulated in *Dpp4*$^{hep-/-}$ mice (**Figure 2.5D**). Similarly, 19 of 28 NF-κB signaling pathway genes were significantly upregulated in HFHC-fed *Dpp4*$^{-/-}$ mice, whereas many genes were unchanged, or downregulated, in SLD-fed *Dpp4*$^{-/-}$ mice and HFHC- fed *Dpp4*$^{hep-/-}$ mice, compared with respective controls (**Figure 2.5E**). To further complement this analysis, we analyzed mRNA expression of known chemokine substrates of DPP4 in whole liver extracts. Consistent with its role in NAFLD progression[52], *Ip-10* (*Cxcl10*) gene expression was significantly upregulated in HFHC-fed *Dpp4*$^{-/-}$ mice compared with controls but unchanged in SLD-fed mice and HFHC-fed *Dpp4*$^{hep-/-}$ mice compared with controls (**Figure 2.5F**). Expression of the gene regulated on activation, T cell expressed, and secreted (*RANTES*; *Ccl5*), which is associated with severe liver fibrosis[53], was also significantly upregulated in HFHC-fed *Dpp4*$^{-/-}$ mice (**Figure 2.5G**), whereas no changes in *Mcp-1* (*Ccl2*) or *Eotaxin* (*Ccl11*) gene expression were noted

(**Figure 2.5, H** and **I**). In contrast, gene expression of *Ip-10, RANTES, Mcp-1*, and *Eotaxin* were unchanged between HFHC-fed *Dpp4*^{GFP} and *Dpp4*$^{hep-/-}$ mice (**Figure 2.5, F–I**).

Cellular senescence has been identified to be involved in the transition from liver steatosis to a more severe phenotype involving hepatocyte ballooning and elevated fibrosis[54]. DPP4 has been identified on the surface of senescent cells, preferentially sensitizing them to cytotoxicity by NK cells[55]. Therefore, we were prompted to evaluate gene expression of senescence-associated secretory phenotype (SASP) factors[56] in our models. Our liver NanoString analysis identified increased expression of *Trp53* in both SLD-fed and HFHC-fed, aged *Dpp4*$^{-/-}$ compared with their respective controls (**Figure 2.5J** and **K**), which was unchanged in *Dpp4*$^{hep-/-}$ mice compared with *Dpp4*^{GFP} mice (**Figure 2.5L**). We additionally measured genes associated with p53 signaling[57,58]. The mRNA level of *Ankrd1* was increased in SLD- and HFHC-fed *Dpp4*$^{-/-}$, but unchanged in *Dpp4*$^{hep-/-}$, compared with controls (**Figure 2.5M**). *Cdkn1a* expression was unchanged across both diets, and all genotypes (**Figure 2.5N**), while *Cdkn2a* was significantly decreased in HFHC-fed *Dpp4*$^{-/-}$ mice only (**Figure 2.5O**). When we analyzed protein levels of chemokine and cytokine SASPs, 8 weeks after starting the diet, CXCL1 levels were significantly increased in SLD-fed *Dpp4*$^{-/-}$ mice (**Supplemental Figure 2.7A**), while IL-6 was significantly increased in HFHC-fed *Dpp4*$^{-/-}$ mice (**Supplemental Figure 2.7B**). Other plasma cytokines, including IL-1β, IFN-γ, IL-10, and IL-2, were unchanged (**Supplemental Figure 2.7, C–H**). However, in HFHC-fed mice, IL-4 was significantly decreased in *Dpp4*$^{-/-}$ mice compared with controls (**Supplemental Figure 2.7I**), while it was increased in *Dpp4*$^{hep-/-}$ as was IL-5 at both 8 weeks and endpoint

(**Supplemental Figure 2.7I** and **G**). Few other significant changes were noted in plasma or within liver tissue at endpoint (**Supplemental Figure 2.7J–Y**).

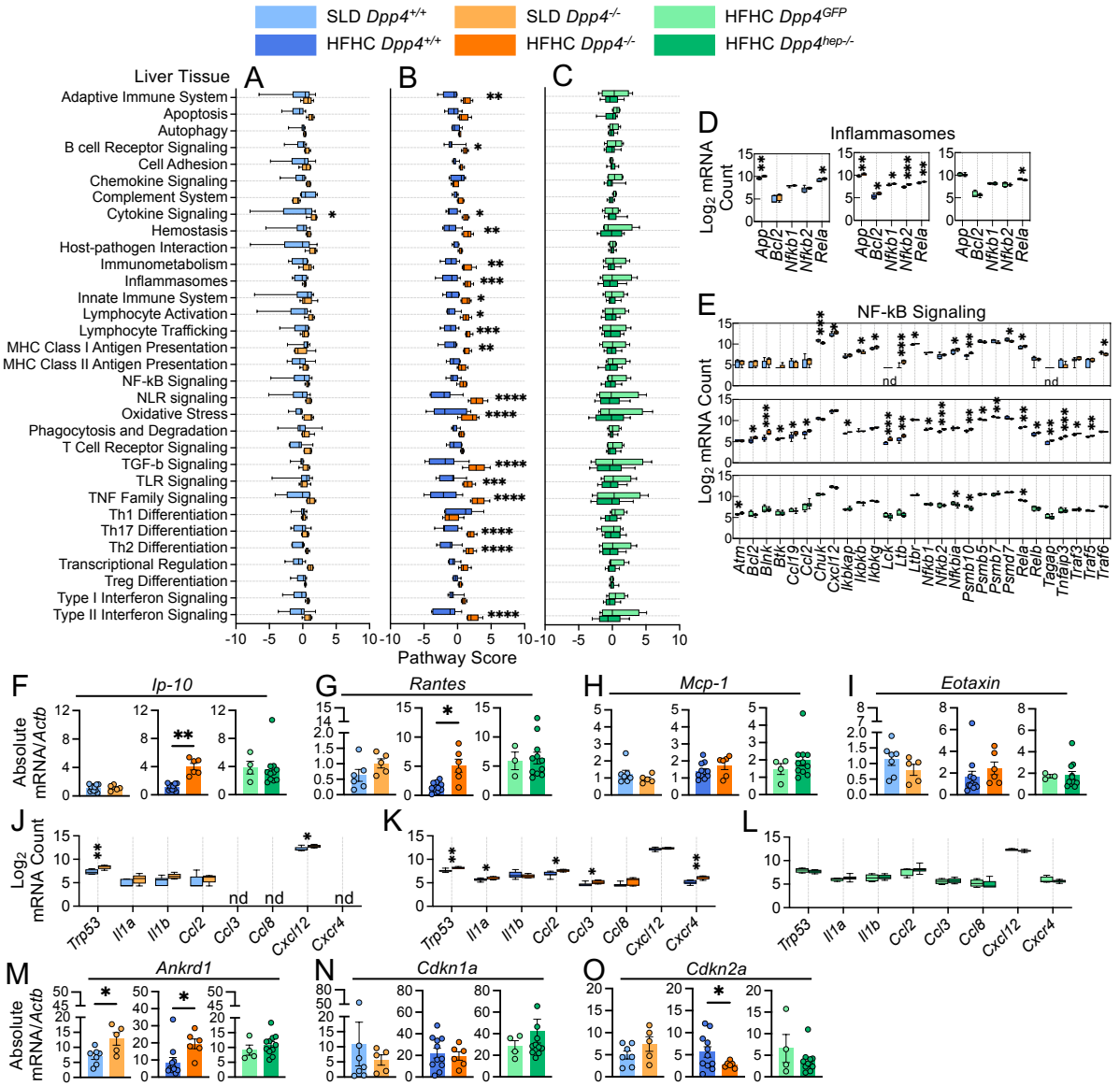

Figure 2.5: In whole liver tissue, immune-related genes and pathways are up-regulated in HFHC-fed *Dpp4*$^{-/-}$ mice, but unchanged in *Dpp4*$^{hep-/-}$ mice. Pathway scores of immunological pathways in liver tissue of (**A**) SLD-fed *Dpp4*$^{+/+}$ (n=7) and *Dpp4*$^{-/-}$ (n=5) mice, (**B**) HFHC-fed *Dpp4*$^{+/+}$ (n=11) and *Dpp4*$^{-/-}$ (n=6) mice and (**C**) HFHC-fed *Dpp4*^{GFP} (n=4) and *Dpp4*$^{hep-/-}$ (n=11) mice. Log_2 normalized mRNA counts of genes associated with (**D**) inflammasome pathways and (**E**) NF-kB signaling pathways. Liver mRNA abundance (relative to *Actb*) of known DPP4 substrates and chemokines/cytokines of (**F**) *Ip-10*, (**G**) *Rantes*, (**H**) *Mcp-1* and (**I**) *Eotaxin* in liver tissue. Log_2 normalized mRNA counts of senescence associated signaling phenotype (SASPs) genes in liver tissue of (**J**) SLD-fed *Dpp4*$^{+/+}$ and *Dpp4*$^{-/-}$ mice, (**K**) HFHC-fed *Dpp4*$^{+/+}$ and *Dpp4*$^{-/-}$ mice and (**L**) HFHC-fed *Dpp4*^{GFP} and *Dpp4*$^{hep-/-}$ mice. Liver mRNA abundance (relative to *Actb*) of SASP genes (**M**) *Ankrd1*, (**N**) *Cdkn1a* and (**O**) *Cdkn2a*. Box and whisker plots: box extends from the 25th to 75th percentiles, the whiskers go down to the smallest value and up to the largest. Data are presented as the means ± SEM, analyzed by unpaired students t-test with Welch's correction, ns p<0.05, * *P*=0.01-0.05, ** *P*=0.001-0.01, *** *P*=0.0001-0.001 and **** *P*<0.0001. nd = not detected.

2.5.6 Immune-related genes are upregulated in F4/80$^+$ cells of SLD-fed *Dpp4*$^{-/-}$ mice, but HFHC feeding reduces DPP4 expression in F4/80$^+$ cells

Roles of both liver-resident macrophages and recruited monocyte-derived macrophages in NAFLD progression[59] and liver fibrosis[60] have been established. Additionally, DPP4 is known to be upregulated when macrophages are polarized with proinflammatory stimuli and implicated in macrophage polarization and activation to mediate inflammation[61]. We therefore probed if liver-resident macrophages were critical in driving the increased inflammation in livers of mice with global *Dpp4* deletion. We isolated F4/80$^+$ cells from the liver and conducted NanoString mRNA analysis using the same immunology panel described above. Surprisingly, a large cluster of immune-related genes were upregulated in F4/80$^+$ cells of SLD-fed *Dpp4*$^{-/-}$ mice compared with controls. However, these same genes were not differentially expressed in HFHC-fed *Dpp4*$^{-/-}$ mice (**Supplemental Figure 2.8A** and **C**) whereas in HFHC-fed *Dpp4*$^{hep-/-}$ mice, 2 distinct clusters were revealed to be significantly altered compared with controls (**Supplemental Figure 2.8B** and **C**). Pathway analysis revealed significant increases in NF-κB signaling, adaptive and innate immune system, and cytokine signaling (**Figure 2.6A**) in SLD-fed *Dpp4*$^{-/-}$ mice compared with controls. However, no pathways were significantly altered in HFHC-fed *Dpp4*$^{-/-}$ (**Figure 2.6B**) and *Dpp4*$^{hep-/-}$ mice (**Figure 2.6C**). In the isolated F4/80$^+$ cells, unexpectedly, Dpp4 was downregulated in HFHC-fed *Dpp4*$^{+/+}$ mice compared with SLD-fed *Dpp4*$^{+/+}$ mice. Its expression was unchanged between HFHC-fed *Dpp4*^{GFP} and *Dpp4*$^{hep-/-}$ mice, verifying deletion was restricted to hepatocytes (**Figure 2.6D**). To further understand potential differences in F4/80$^+$ cells' composition within the liver, we assessed differences in the abundance of transcripts associated with

characterized populations. We found *Adgre1* was upregulated in HFHC-fed *Dpp4*$^{-/-}$ mice (**Figure 2.6E**), and *Ccr2* trended toward increase in HFHC-fed *Dpp4*$^{-/-}$ mice compared with controls. These markers remained unchanged in SLD-fed *Dpp4*$^{-/-}$ and *Dpp4*$^{hep-/-}$ mice versus their respective controls (**Figure 2.6F**). However, no differences in F4/80 immunostaining were noted (**Supplemental Figure 2.9A–E**) between the HFHC-fed groups. Additionally, no changes were observed in macrophage polarization and population markers, *Itgax* (**Figure 2.6G**), *Mrc1* (**Figure 2.6H**), *Cd163* (**Figure 2.6I**), *Arg1* (**Figure 2.6J**), and *Clec4f* (CLC4F) (**Figure 2.6K**), between genotypes and their respective controls. Consistent with these results, CLEC4F immunostaining revealed no differences between HFHC-fed groups (**Supplemental Figure 2.9A–D** and **F**). *Trp53* was upregulated in SLD-fed *Dpp4*$^{-/-}$ and downregulated in HFHC-fed *Dpp4*$^{hep-/-}$, while *Cxcr4* was upregulated in both (**Figure 2.6L**). SLD-fed *Dpp4*$^{-/-}$ mice had significant changes in many components of the NF-κB signaling pathway, but few of these patterns were observed in HFHC-fed *Dpp4*$^{-/-}$ or *Dpp4*$^{hep-/-}$ mice (**Figure 2.6M**). These data reveal an unexpected, complex relationship between DPP4 and liver-resident F4/80^{+} cells' immunological profiles associated with diet composition.

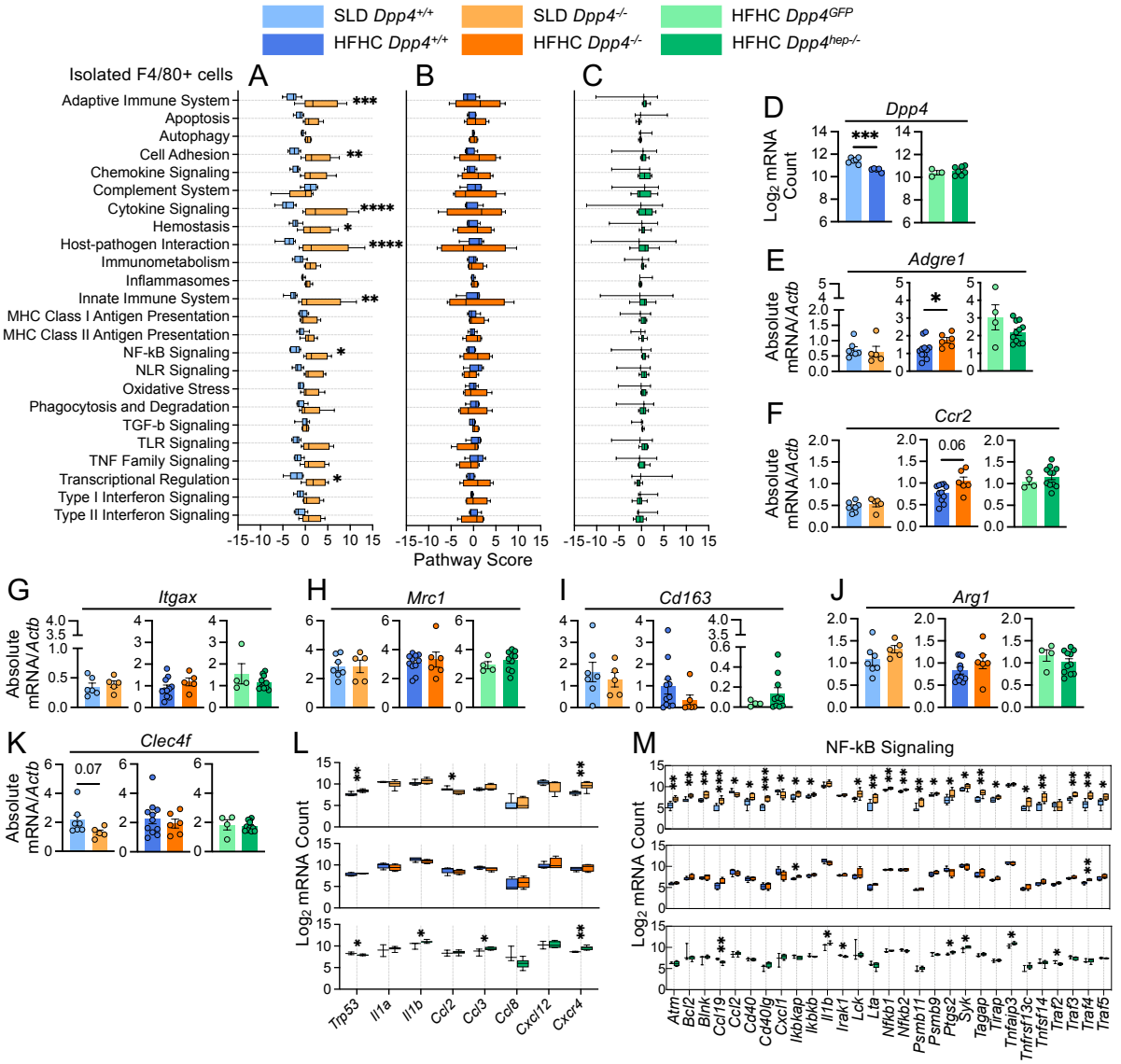

Figure 2.6: In hepatic F4/80+ cells, immune related genes and pathways are up-regulated in SLD-fed *Dpp4*$^{-/-}$ mice, but unchanged in HFHC-fed *Dpp4*$^{-/-}$ and *Dpp4*$^{hep-/-}$ mice. Pathway scores of immunological pathways in F4/80^{+} cells isolated from liver tissue of (**A**) SLD-fed *Dpp4*$^{+/+}$ (n=6) and *Dpp4*$^{-/-}$ (n=6) mice, (**B**) HFHC-fed *Dpp4*$^{+/+}$ (n=5) and *Dpp4*$^{-/-}$ (n=4) mice and (**C**) HFHC-fed *Dpp4*^{GFP} (n=3) and *Dpp4*$^{hep-/-}$ (n=7) mice. (**D**) Log_2 normalized mRNA count of *Dpp4* in F4/80^{+} cells isolated from liver. Liver mRNA abundance (relative to *Actb*) of (**E**) *Adgre1* and (**F**) *Ccr2*. Liver mRNA abundance (relative to Actb) of (**G**) *Itgax*, (**H**) Mrc1, (**I**) *Cd163*, (**J**) *Arg1* and (**K**) *Clec4f*. (**L**) Log_2 normalized mRNA counts of senescence associated signaling proteins (SASPs) in F4/80^{+} cells. Log_2 normalized mRNA counts of genes associated with (**M**) NF-kB signaling pathway in F4/80+ cells in SLD-fed *Dpp4*$^{+/+}$ (n=7) and *Dpp4*$^{-/-}$ (n=5) mice, HFHC-fed *Dpp4*$^{+/+}$ (n=11) and *Dpp4*$^{-/-}$ (n=5-6) mice and HFHC-fed *Dpp4*^{GFP} (n=4) and *Dpp4*$^{hep-/-}$ (n=11) mice. Box and whisker plots: box extends from the 25th to 75th percentiles, the whiskers go down to the smallest value and up to the largest. Data are presented as the means ± SEM, analyzed by unpaired students t-test with Welch's correction, ns P<0.05, *P=0.01-0.05, **P=0.001-0.01, ***P=0.0001-0.001 and ****P<0.0001. nd = not detected.

2.5.7 Liver-specific insults affect circulating DPP4 protein concentrations

Given its strong correlation with adipose tissue accumulation and obesity in both humans and mice, soluble, circulating DPP4 was initially characterized as an adipokine[13,22]. Recent studies with adipocyte-specific targeting of DPP4 have determined that although adipocytes shed a small amount of DPP4[22,62], hepatocytes account for the significant elevation in DPP4 observed in high-fat diet feeding and metabolic dysregulation[22,24]. Further, liver DPP4 expression is elevated in NAFLD[20,21]. Comprehensive studies in cultured hepatocytes have determined that a combination of leptin and palmitic acid stimulates a 6-fold increase in *Dpp4* mRNA expression[63]. To test the necessity of adiposity and peripheral insulin resistance in vivo for elevated enzymatically active, circulating DPP4, we assessed plasma DPP4 activity in HFHC-fed *Pemt*$^{-/-}$ mice, which are a lean model of hepatomegaly and hepatic steatosis due to disruption in de novo synthesis of choline[64] (**Supplemental Figure 2.10A**). *Pemt*$^{-/-}$ mice do not develop obesity with high-fat feeding, retain insulin sensitivity, and have lower leptin concentrations compared with littermate controls[64,65]. Notably, systemic DPP4 activity was increased 4-fold relative to controls (**Supplemental Figure 2.10B**), suggesting dysregulation of hepatic lipid pathways is related to increased DPP4 activity, independent of the development of obesity. Unexpectedly, *Dpp4* mRNA level in the liver was unchanged (**Supplemental Figure 2.10C**). However, mRNA expression of candidate sheddases was significantly increased, including *Mmp9, Mmp2*, and *Adamst*, but not *Adam17* (**Supplemental Figure 2.10D–G**).

In addition to steatosis, other liver-specific insults associated with elevated circulating DPP4 include HCV[66]. Chronic HCV's association with metabolic disease has been established[67]. We have recently shown that in patients with HCV treated

with paritaprevir/ritonavir/ombitasvir/dasabuvir (PrOD), with or without ribavirin, fasting glucose, insulin, and Homeostatic Model Assessment of Insulin Resistance (HOMA-IR) are unchanged during treatment and follow-up after treatment[43]. We now sought to investigate whether elevated DPP4 levels are reversed following successful therapy for viral clearance in patients with metabolic dysfunction (HOMA-IR > 2) that persists through the treatment and follow-up period. Plasma AST (**Figure 2.7A**) and ALT (**Figure 2.7B**) significantly decreased in all treatment groups and were maintained at decreased levels during follow-up. Not surprisingly, given the lack of change in metabolic disease parameters, high variability and no significant changes were observed in C-reactive protein concentrations (**Figure 2.7C**). Consistent with other studies utilizing IFN-α treatment[68,69], DPP4 concentration in plasma significantly decreased within all PrOD regimens from baseline to 12 weeks posttreatment (**Figure 2.7D**). In comparison, DPP4 activity substantially decreased with ribavirin treatment from baseline to follow-up in ribavirin-treated patients (**Figure 2.7E**). A similar trend to DPP4 protein was observed with known DPP4 substrates IP-10 (**Figure 2.7F**) and macrophage inflammatory protein 1α (MIP-1α) (**Figure 2.7G**). However, Eotaxin, another substrate, was unaffected (**Figure 2.7H**). Soluble intracellular adhesion molecule 1 (sICAM-1) was significantly decreased with treatment (**Figure 2.7I**). Taken together, DPP4 concentration and activity decrease with HCV treatment and viral clearance. However, this occurs independently of changes in metabolic parameters.

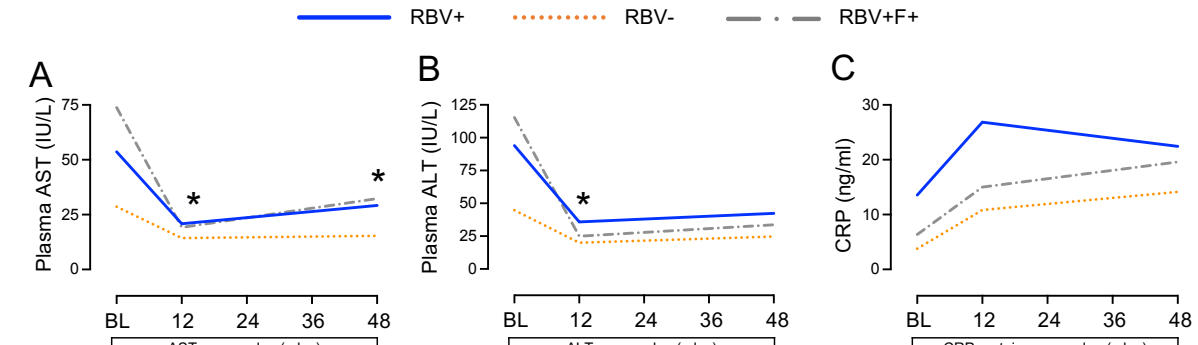

A

	AST mean value (sdev)		
	Baseline	12 weeks	Follow-up
RBV+	53.667 (23.261)	20.83 * (6.080)	29.200 * (6.080)
RBV-	28.600 (8.414)	14.22 * (3.326)	15.333 * (3.326)
RBV+F4+	73.833 (55.550)	19.17 * (8.376)	34.800 * (8.376)

B

	ALT mean value (sdev)		
	Baseline	12 weeks	Follow-up
RBV+	94.000 (50.904)	35.83 * (23.404)	42.400 * (27.555)
RBV-	44.833 (15.943)	20.00 * (7.4297)	24.667 * (23.088)
RBV+F4+	115.333 (102.886)	25.00 * (6.9282)	34.400 * (21.870)

C

	CRP protein mean value (sdev)		
	Baseline	12 weeks	Follow-up
RBV+	13.550 (18.215)	26.860 (21.128)	22.43 (22.040)
RBV-	3.777 (1.925)	10.846 (12.672)	14.13 (10.906)
RBV+F4+	28.296 (49.052)	15.005 (17.196)	19.60 (21.443)

D

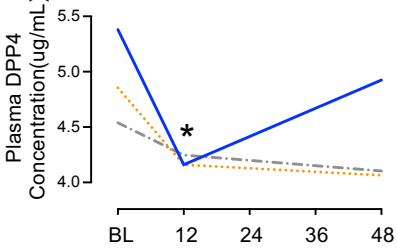

	DPP4 protein mean value (sdev)		
	Baseline	12 weeks	Follow-up
RBV+	5.380 (1.027)	4.16 * (0.4976)	4.924 (0.953)
RBV-	4.855 (0.660)	4.16 * (0.5946)	4.065 (0.702)
RBV+F4+	4.539 (1.022)	4.25 * (1.1474)	4.104 (1.283)

E

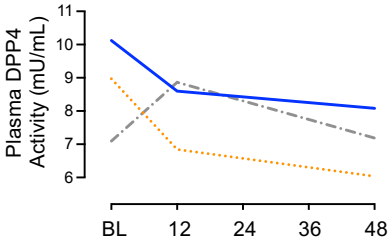

	DPP4 activity mean value (sdev)		
	Baseline	12 weeks	Follow-up
RBV+	10.123 (2.276)	8.60 (3.914)	8.081 * (1.575)
RBV-	8.972 (2.296)	6.84 (1.452)	6.038 * (2.289)
RBV+F4+	7.093 (3.335)	8.87 (3.576)	7.188 * (3.034)

F

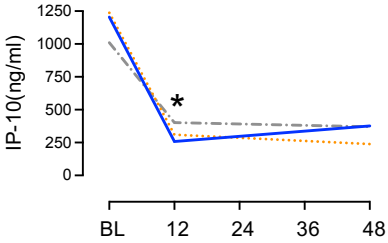

	IP-10 protein mean value (sdev)		
	Baseline	12 weeks	Follow-up
RBV+	1205.019 (701.776)	257.562 * (60.544)	377.05 * (84.759)
RBV-	1237.252 (884.371)	309.800 * (223.539)	239.17 * (72.995)
RBV+F4+	1009.808 (475.208)	401.674 * (156.096)	370.56 * (179.440)

G

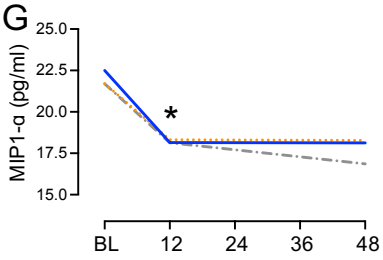

	MIP-1α protein mean value (sdev)		
	Baseline	12 weeks	Follow-up
RBV+	22.503 (4.062)	18.149 * (2.868)	18.12 * (3.1046)
RBV-	21.709 (4.174)	18.326 * (3.371)	18.28 * (2.6961)
RBV+F4+	21.697 (6.137)	18.137 * (4.217)	16.86 * (3.1647)

H

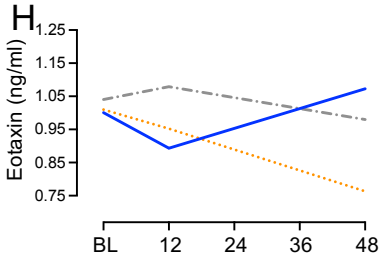

	Eotaxin protein mean value (sdev)		
	Baseline	12 weeks	Follow-up
RBV+	1.001 (0.290)	0.89 (0.249)	1.073 (0.245)
RBV-	1.010 (0.632)	0.95 (0.356)	0.763 (0.281)
RBV+F4+	1.040 (0.512)	1.08 (0.654)	0.980 (0.406)

I

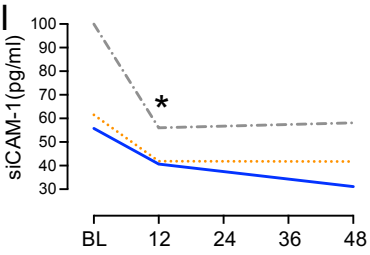

	sICAM protein mean value (sdev)		
	Baseline	12 weeks	Follow-up
RBV+	55.752 (27.148)	40.64 * (16.2)	31.091 * (23.102)
RBV-	61.515 (29.577)	41.85 * (8.91)	41.756 * (21.574)
RBV+F4+	99.948 (36.668)	56.06 * (19.6)	58.096 * (31.060)

Figure 2.7: Independent of metabolic parameters, DPP4 concentration and activity decrease with HCV clearance and viral treatment. Changes in plasma (**A**) AST, (**B**) ALT, (**C**) CRP levels, (**D**) DPP4 concentration, (**E**) DPP4 activity and changes in plasma cytokines and chemokines that are known substrates of DPP4, including (**F**) IP-10, (**G**) MIP1-a, (**H**) Eotaxin and (**I**) siCAM in patients (n=5-6) with HOMA-IR >2 treated for HCV infection. Time points: BL = baseline, week 12 = end of treatment; follow up = 24 to 48 weeks after treatment. Groups: RBV+ = hepatitis C (HCV) treatment containing ribavirin in participants without cirrhosis, RBV− = ribavirin free HCV treatment in participants without cirrhosis, RBV+FIB+ = HCV treatment containing ribavirin in participants with cirrhosis. To remove the variance in trait values attributed to sex and age differences, a linear regression model compared the retrieved residuals (adjusted trait values) using unpaired t-test. Data are presented as the mean ± SD and $P<0.05$ was considered statistically significant.

2.6 Discussion

Potentiation of GLP-1 action through receptor agonists has demonstrated efficacy in treating metabolic disease[70,71]; however, our knowledge of the effects of DPP4 elimination to potentiate endogenous GLP-1 action within the context of chronic liver disease progression is limited. The present data demonstrate that eliminating hepatocyte DPP4 in HFHC-fed mice decreased DPP4 activity and increased intact incretins in the portal circulation and reduced HGP. These data are also consistent with patients in which DPP4 inhibitors (DPP4i's) decrease HGP and are associated with reductions in glucagon[26,45]. In contrast, in HFHC-fed *Dpp4*$^{EC-/-}$, we report increased levels of active GLP-1 in the systemic circulation and no effect on HGP as assessed by hyperinsulinemic-euglycemic clamp[34].

Studies in mice have also demonstrated that intact GLP-1R signaling within the portal circulation is integral to glucose sensing[72]. This is interesting given that postprandial GLP-1 levels measured in the lymph are 5–6 times higher relative to sampling performed in portal plasma[47]. Consistent with our data identifying different regulation of incretin bioactivity and modulation of glucose metabolism with DPP4 in hepatocytes versus Tie2+ cells, recent reports have determined that elevated levels of active portal GLP-1 are disconnected from the classic definition of the incretin effect as increased portal circulation of GLP-1 does not potentiate nutrient-stimulated insulin secretion[73,74]. In studies performed in rats, samples taken 20 minutes following a high-fat diet meal showed elevated GLP-1 in the lymph collected from the mesenteric lymph duct rather than the PV, while no difference was observed after a low-fat meal[75]. Circulating DPP4 activity is lower in lymph than in plasma[47,75]. However, lymphatic ECs have been reported to express DPP4, and modulation of levels with siRNA

affects migration and function[76]. Therefore, our current study is consistent with a model where, during HFHC diet–induced metabolic dysregulation, the deletion of *Dpp4* within Tie2+ cells increases the abundance of GLP-1 delivered to the systemic circulation, enabling the incretin effect, and improves oral glucose tolerance but does not affect HGP. This is in contrast to *Dpp4* in hepatocytes, which when deleted in HFHC-fed mice, increases GLP-1 bioactivity within the portal circulation and improves insulin-mediated suppression of HGP. Our data align with results from *Hif1α*$^{hep-/-}$ mice, demonstrating that elevation in DPP4 through activation of hepatocyte HIF-1α reduces active GLP-1 in the portal circulation[63]. Additionally, Baumeier *et. al.*[25] demonstrated that hepatic *Dpp4* overexpression results in decreased active, glucose-stimulated GLP-1 in the vena cava after liver passage. Recent studies have documented that GLP-1R engagement in the portal circulation is reduced under high-fat diet–feeding conditions[77], suggesting together with our data that multiple mechanisms converge to control GLP-1 action in the hepatic portal circulation, which may contribute to glucose dysregulation in mice upon high-fat feeding.

Elevated concentrations of plasma DPP4 are associated with liver disease severity and fibrosis[78]. Consistent with this, hepatocyte-specific overexpression of DPP4 in mice results in increased hepatic steatosis, liver enzymes, and markers of inflammation[25]. In the current study, we report DPP4 was elevated 4-fold in *Pemt*$^{-/-}$ mice, which have both hepatomegaly and non-alcoholic steatohepatitis[64], demonstrating that in addition to obesity, liver-specific insults can induce the release of DPP4. Surprisingly, however, complete genetic elimination of *Dpp4* or hepatocyte-specific elimination in aged mice resulted in no changes in liver enzymes and the degree of steatosis. Consistent with our results, using liver-specific knockdown of

DPP4 via therapeutic siRNA, in obese and diabetic *db/db* mice, no effect on liver enzymes or glucose tolerance is observed[23]. Both Varin *et. al.* and Ghorpade *et. al.* reported modest impact on the liver with long-term targeting strategies[22,24], suggesting that acute treatments targeting DPP4 more readily influence mouse lipid metabolism than long-term deletion of DPP4, which may be prone to metabolic adaptation.

In mice, DPP4i's decrease liver fibrosis[79,80]; however, this was not recapitulated by genetically eliminating *Dpp4* as Picrosirius red staining revealed a trend toward increased fibrosis, and expression of *Col1a1* and *Col3a1* was increased in $Dpp4^{-/-}$ mice. Chronic liver inflammation and immune reactions often precede fibrosis[81]; therefore, we assessed mRNA expression of immune-related genes. Under HFHC-fed conditions, livers of $Dpp4^{-/-}$ mice but not $Dpp4^{hep-/-}$ mice exhibited upregulation of transcripts associated with the inflammasome and markers of NF-κB signaling, pathways characterized to be activated in NAFLD[82,83]. This was surprising given that DPP4is have been reported to suppress NF-κB activation[84,85]. These results support important differences obtained by enzymatic inhibition versus complete deletion of the DPP4 protein.

Cellular senescence has been proposed as a key factor in NAFLD progression[86]. Further, DPP4 has been identified as a surface protein that is enriched in senescent cells[55], and modulation of DPP4 in presenescent WI-38 cells[55] or in vascular endothelial cells[87] reduces markers of senescence. Additionally, senescence induced by glucocorticoid treatment, known to increase DPP4 transcriptionally[88], can be modulated by inhibition of DPP4 activity[89]. In our study, lifelong deletion of DPP4 in aged mice led to upregulation of *Trp53*, a component of the senescent machinery[90]. Additionally, the expression of *Ankrd1*, *Il1a*, *Ccl2*, and *Ccl3* was increased in HFHC-

fed *Dpp4*$^{-/-}$ mice. A molecular link between p53 and DPP4 has been established in which p53 antagonizes ferroptosis by blocking DPP4 activity[91]. However, the mechanistic link between DPP4, p53, cellular senescence, and liver fibrosis could not be deduced from this study and warrants further investigation.

Elevated DPP4 is also observed in other chronic liver diseases, such as HCV, in addition to NAFLD[15]. Consistent with data from patients who received IFN treatment[68], plasma DPP4 concentrations, liver enzymes, and cytokine levels were reduced after resolution of infection with direct-acting antiviral therapy with or without ribavirin. DPP4 activity varied between treatment groups at baseline but overall remained decreased from baseline at follow-up in all. Additionally, plasma AST, ALT, IP-10, MIP-1α, and sICAM-1 all decreased with treatment. However, these changes were not associated with changes in glucose regulation[43].

We acknowledge several shortcomings to our study, including that the effects of exendin-9-39 cannot exclude the potential for signaling of glucagon through the GLP-1R[92-95], in addition to active GLP-1[96]. Additionally, while mice remained unrestrained during the hyperinsulinemic-euglycemic clamps, they were sampled by the tail vein, which may contribute differential physiological responses to stress across genotypes. In addition, many of our inferences are dependent on transcript levels rather than direct protein quantitation due to the availability and reliability of relevant antibodies.

In summary, we have identified hepatocyte-derived *Dpp4* as a key factor in regulating the bioactivity of GLP-1 in the PV and extended these findings to demonstrate that its elimination results in a reduction in HGP. However, despite the elevation in GLP-1 and improvements in hepatic insulin sensitivity, we demonstrate a

disconnect as markers of lipid metabolism, fibrosis, and inflammation were unchanged or worsened in mice.

2.7 Acknowledgements

We would like to thank Majid Nikpay for statistical support; Xiaoling Zhao and the Stewart Whitman Core Histopathology Laboratory for sample preparation, sectioning, and staining; and The Centre for Phenogenomics for plasma analysis. EEM is the guarantor of this work and, as such, had full access to all the data in the study and takes responsibility for the integrity of the data and the accuracy of the data analysis. The Canadian Institutes of Health Research (CIHR) and Diabetes Canada supported this work (ARJ-162628, Project Grant 156136 and New Investigator award to EEM and Project Grant 148634 and New Investigator award 141981 to MDF). NAT is supported by a University of Ottawa Heart Institute endowment scholarship. BV was supported by a CIHR postdoctoral fellowship. CAAL is supported by an Ontario Graduate Scholarship. SMP and AMC are each supported by a CIHR Master's Award. The graphical abstract was generated with BioRender (publication license: ET24NGTPGG).

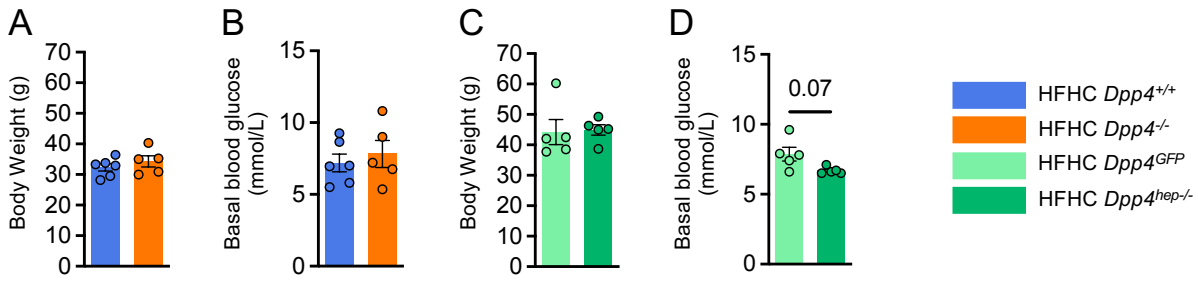

Supplemental Figure 2.1: Body weight and blood glucose of mice used for hyperinsulinemic-euglycemic clamp experiments. Body weight and basal blood glucose in (**A-B**) HFHC-fed *Dpp4*$^{+/+}$ and *Dpp4*$^{-/-}$, and (**C-D**) *Dpp4*^{GFP} and *Dpp4*$^{hep-/-}$ mice, respectively, used for hyperinsulinemic-euglycemic clamp experiments. Data are presented as the means ± SEM, analyzed by unpaired students t-test with Welch's correction, ns P>0.05.

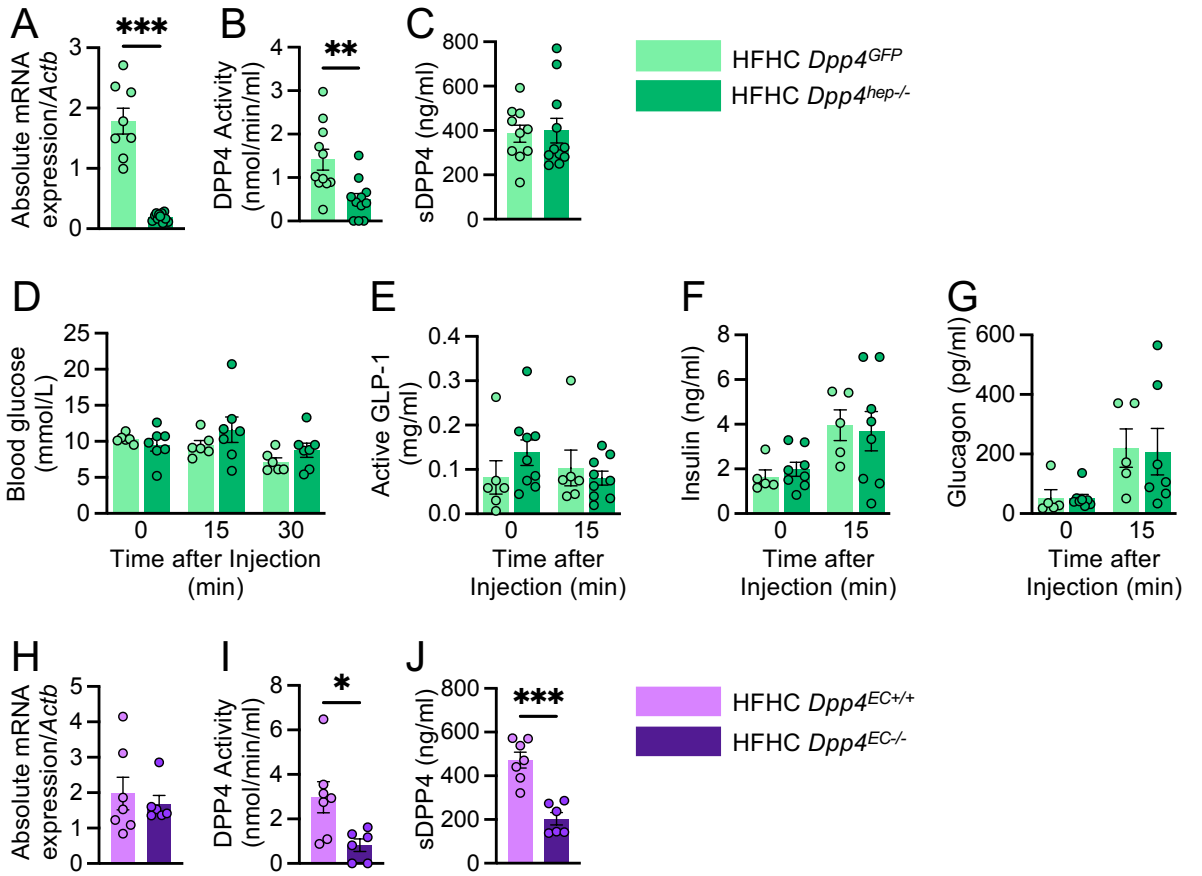

Supplemental Figure 2.2: Biochemical analyses of blood collected during arginine tolerance test. (**A**) *Dpp4* mRNA abundance in the liver (relative to *Actb*), (**B**) fasting plasma DPP4 activity, and (**C**) plasma DPP4 protein in $Dpp4^{GFP}$ and $Dpp4^{hep-/-}$ mice. (**D**) Blood glucose, (**E**) active GLP-1, (**F**) insulin and (**G**) glucagon during an arginine tolerance test at baseline, 15- and 30-minutes after intraperitoneal injection in $Dpp4^{GFP}$ and $Dpp4^{hep-/-}$ mice fed a HFHC diet for 4 weeks. (**H**) *Dpp4* mRNA abundance in the liver (relative to *Actb*), (**I**) fasting plasma DPP4 activity and (**J**) plasma DPP4 protein in $Dpp4^{EC+/+}$ mice and $Dpp4^{EC-/-}$ mice. Data are presented as the means ± SEM, analyzed by unpaired students t-test with Welch's correction, ns $P<0.05$, *P=0.01-0.05, **P=0.001-0.01, ***P=0.0001-0.001.

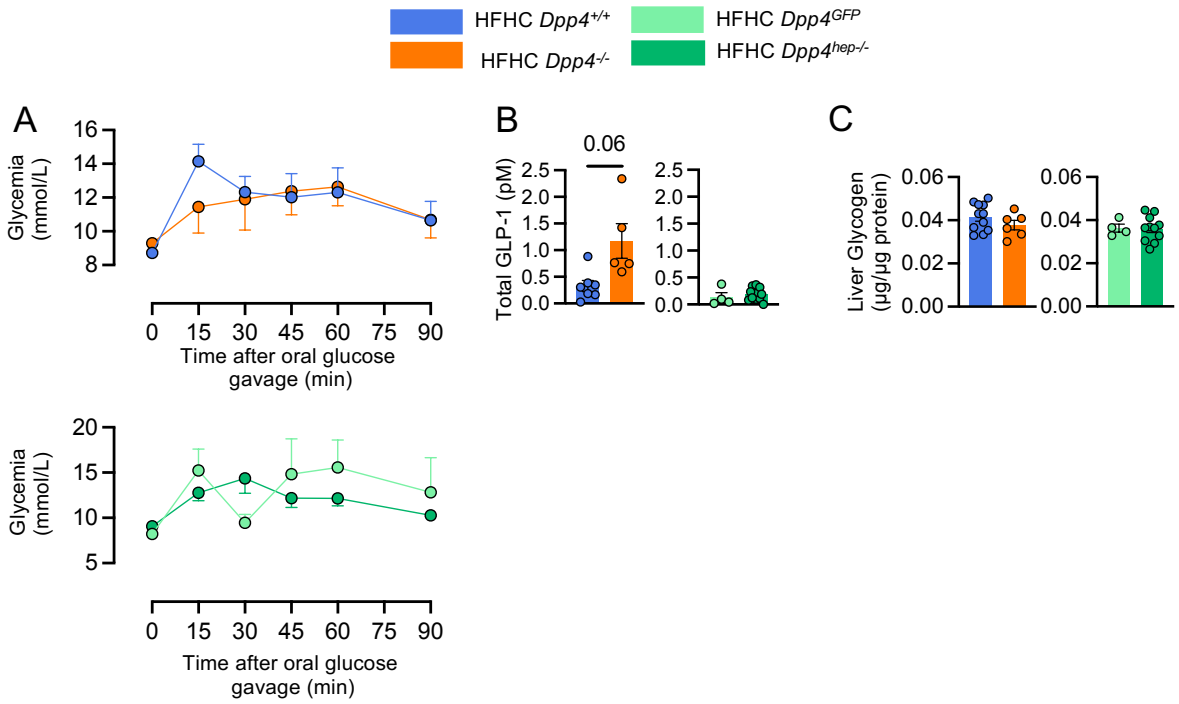

Supplemental Figure 2.3: OGTT, post-glucose total GLP-1 and liver glycogen.(**A**) Oral glucose tolerance test in HFHC-fed *Dpp4*$^{+/+}$ and *Dpp4*$^{-/-}$ mice and HFHC-fed *Dpp4*^{GFP} and *Dpp4*$^{hep-/-}$ mice. (**B**) Total GLP-1 15-minutes post-oral glucose gavage in HFHC-fed *Dpp4*$^{+/+}$ and *Dpp4*$^{-/-}$ mice and HFHC-fed *Dpp4*^{GFP} and *Dpp4*$^{hep-/-}$ mice. (**C**) Liver glycogen content in HFHC-fed mice after 24 weeks. Data are presented as the means ± SEM. Time-course data is analyzed by two-way ANOVA with Tukey's multiple comparisons post hoc test, remaining data analyzed by unpaired students t-test with Welch's correction, ns $P<0.05$.

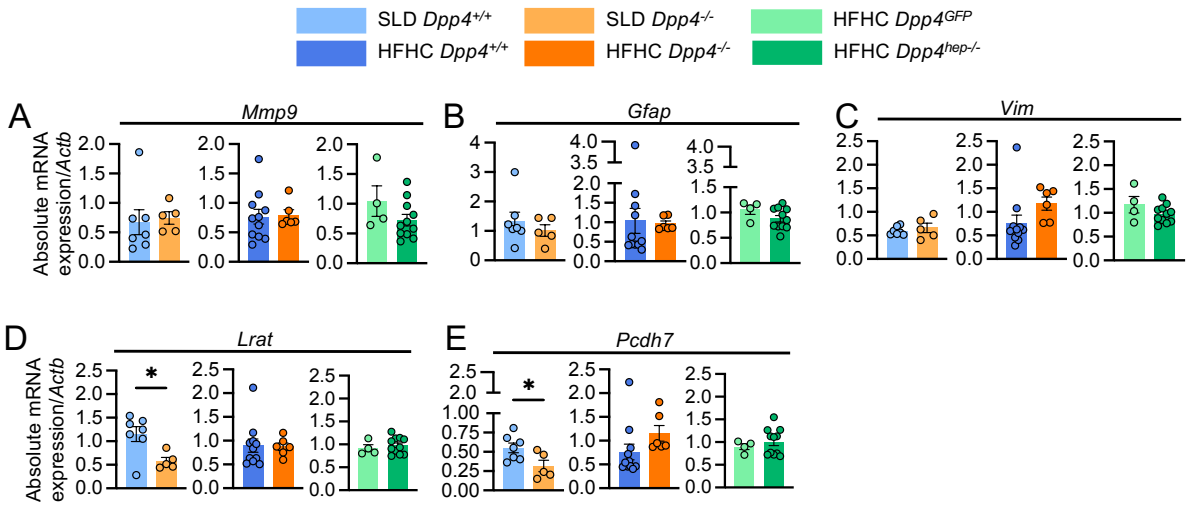

Supplemental Figure 2.4: Liver mRNA abundance. Liver mRNA abundance (relative to *Actb*) for (**A**) *Mmp9*, (**B**) *Gfap*, (**C**) *Vim*, (**D**) *Lrat* and (**E**) Pcdh7. Data are presented as the means ± SEM, analyzed by unpaired students t-test with Welch's correction, ns $P<0.05$, *$P=0.01$-0.05.

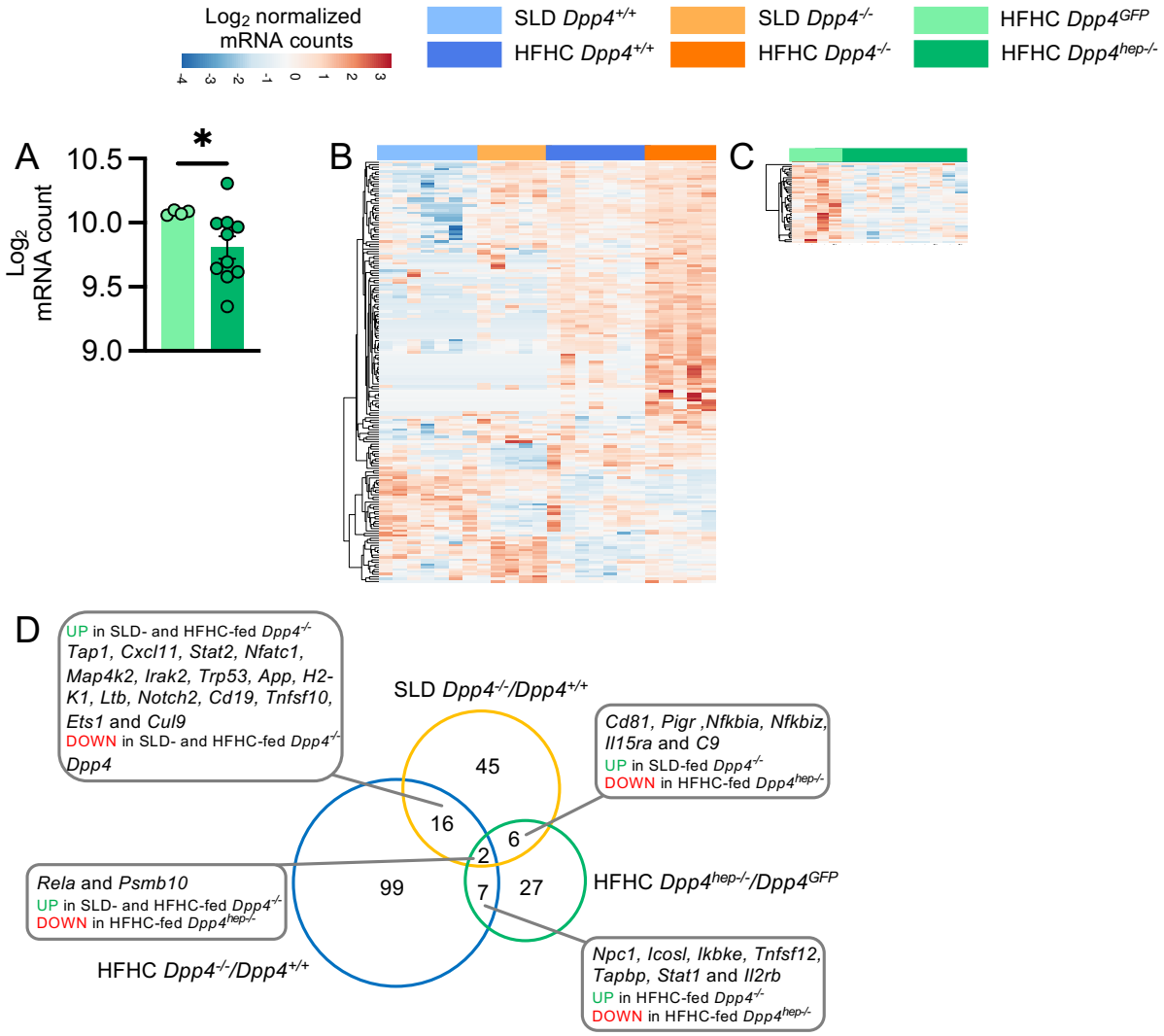

Supplemental Figure 2.5: NanoString analysis of liver tissue. (**A**) Log_2 mRNA count of *Dpp4* in liver tissue. Supervised hierarchical cluster analysis of significantly differentially expressed genes in liver tissue from (**B**) SLD- and HFHC-fed *Dpp4*$^{+/+}$ and *Dpp4*$^{-/-}$ mice, and (**C**) *Dpp4*^{GFP} and *Dpp4*$^{hep-/-}$ mice, using the correlation distance method with average linkage, coloured by the log_2 normalized mRNA count. (**D**) Venn diagram depicting number of genes identified as significantly differentially expressed in each comparison and overlap. Data are presented as the means ± SEM, analyzed by unpaired students t-test with Welch's correction, ns P>0.05 and *P=0.01-0.05.

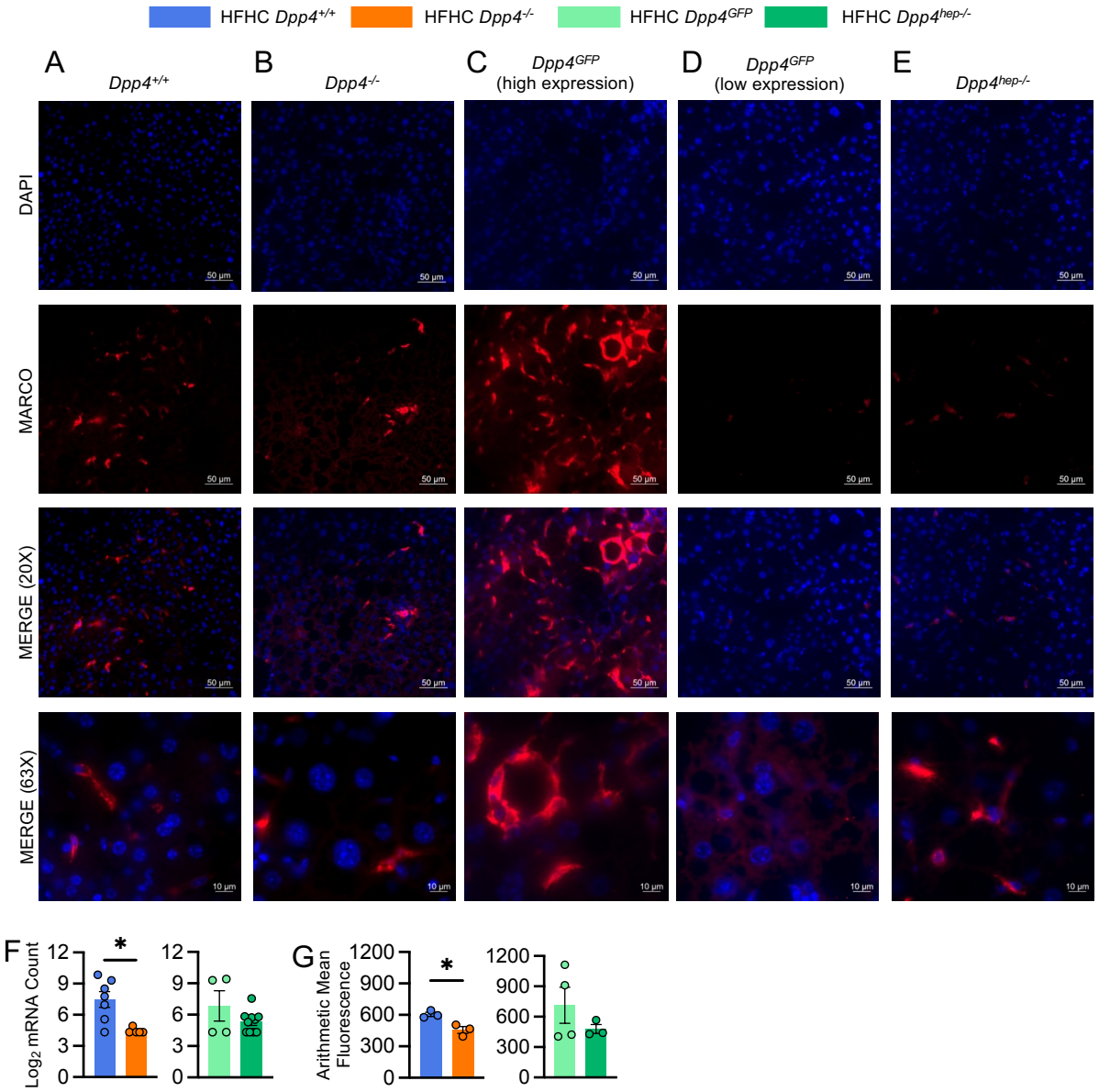

Supplemental Figure 2.6: Liver MARCO immunofluorescence microscopy. Representative immunofluorescent images of MARCO in liver at 20X and 63X magnification for (**A**) HFHC-fed *Dpp4*$^{+/+}$, (**B**) HFHC-fed *Dpp4*$^{-/-}$, (**C**) HFHC-fed *Dpp4*^{GFP} (high expression sample), (**D**) HFHC-fed *Dpp4*^{GFP} (low expression sample) and (**E**) *Dpp4*$^{hep-/-}$ mice (scale bar at 20X = 50um, scale bar at 63X = 10um; 6 regions of interest, n=3-4). (**F**) NanoString $\log_2$ mRNA count for *Marco* (n=4-11). (**G**) Arithmetic mean fluorescence of MARCO. Data are presented as the means ± SEM, analyzed by unpaired students t-test with Welch's correction, ns P>0.05, *P=0.01-0.05.

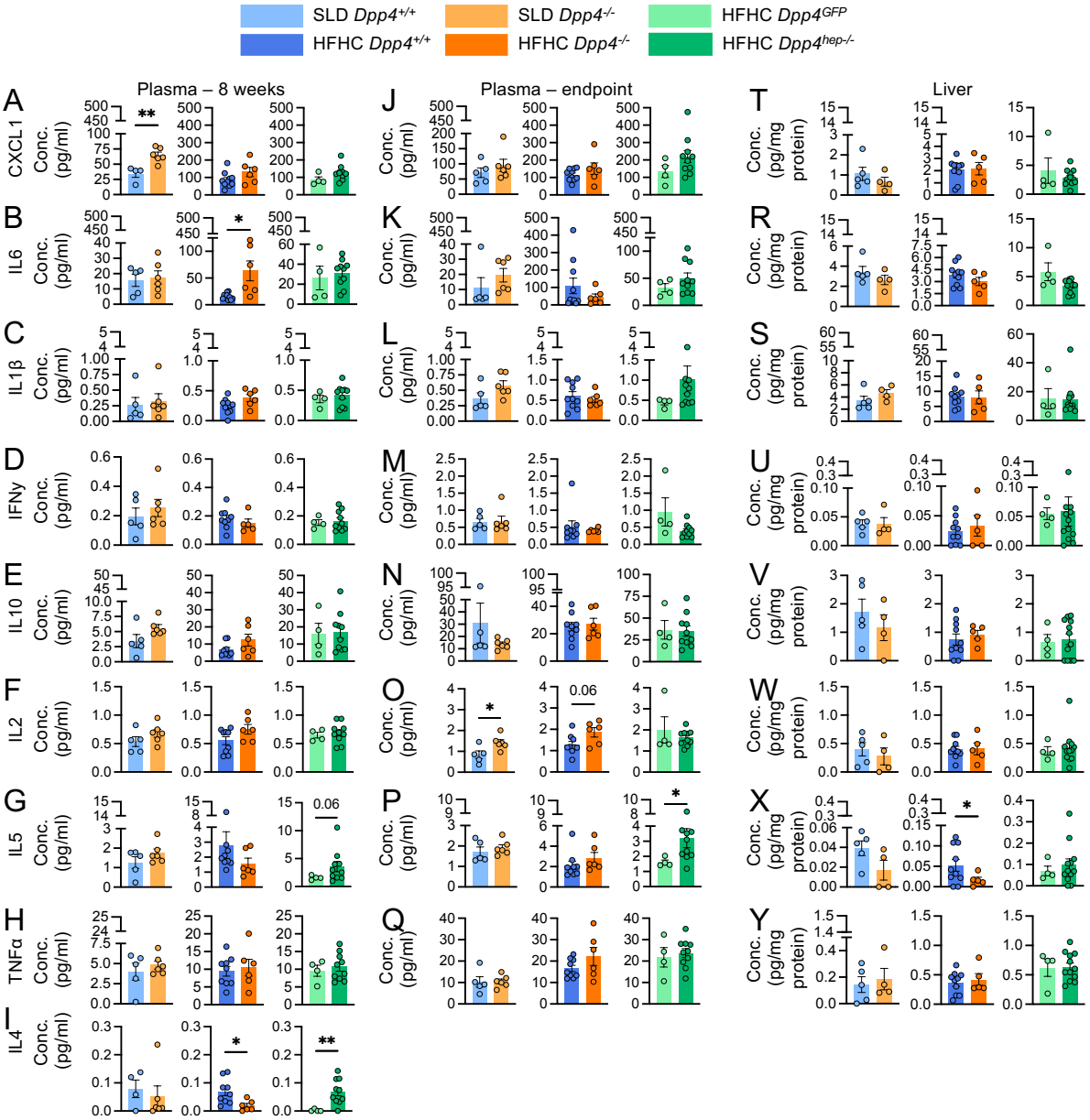

Supplemental Figure 2.7: Plasma concentrations of chemokines and cytokines. Plasma concentration of chemokines in cytokines at (**A-I**) 8 weeks in plasma, (**J-Q**) endpoint in plasma and (**R-Y**) in liver tissue homogenates. Data are presented as the mean ± SEM, analyzed by unpaired students t-test with Welch's correction, **P*=0.01-0.05, ***P*=0.001-0.01.

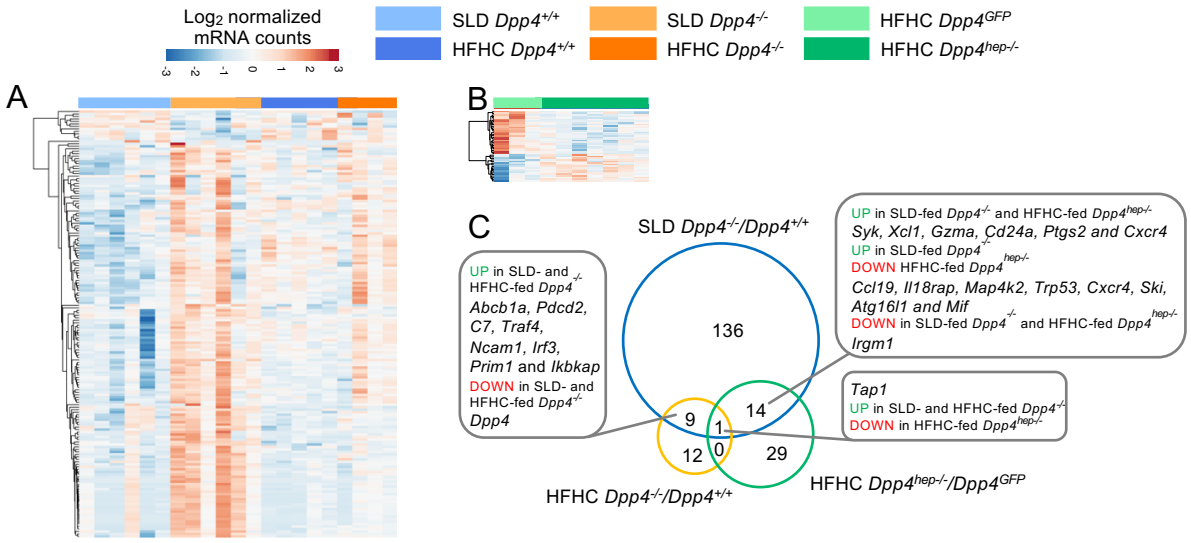

Supplemental Figure 2.8: NanoString analysis of F4/80$^+$ cells isolated from liver tissue. Supervised hierarchical cluster analysis of significantly differentially expressed genes in F4/80$^+$ cells isolated from liver tissue from (**A**) SLD- and HFHC-fed *Dpp4*$^{+/+}$ and *Dpp4*$^{-/-}$ mice, and (**B**) *Dpp4*^{GFP} and *Dpp4*$^{hep-/-}$ mice, using the correlation distance method with average linkage, coloured by the $\log_2$ normalized mRNA count. (**C**) Venn diagram depicting number of genes identified as significantly differentially expressed in each comparison and overlap.

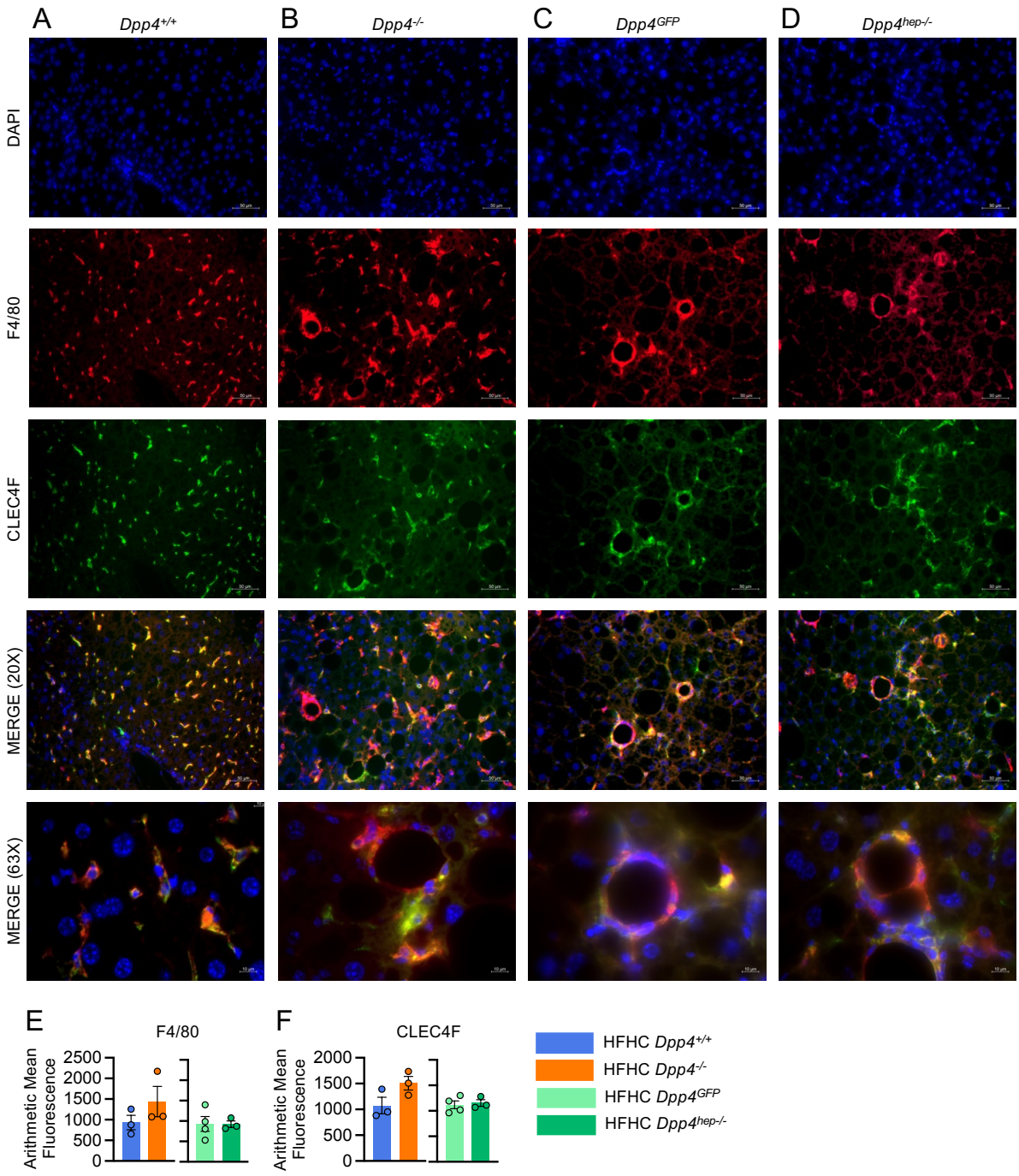

Supplemental Figure 2.9: Liver immunofluorescence images of F4/80 and CLEC4F. Representative immunofluorescent images of F4/80 and CLEC4F in liver at 20X and 63X magnification for (**A**) HFHC-fed *Dpp4*$^{+/+}$, (**B**) HFHC-fed *Dpp4*$^{-/-}$, (**C**) HFHC-fed *Dpp4*^{GFP} and (**D**) *Dpp4*$^{hep-/-}$ mice (scale bar at 20X = 50um, scale bar at 63X = 10um; 6 regions of interest, n=3-4). Arithmetic mean fluorescence of (**E**) F4/80 and (**F**) CLEC4F. Data are presented as the means ± SEM, analyzed by unpaired students t-test with Welch's correction, ns P>0.05.

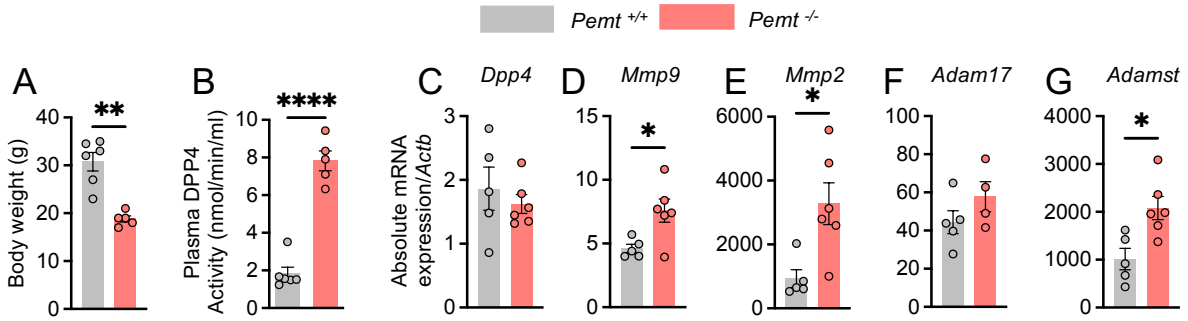

Supplemental Figure 2.10: Body weight, DPP4 activity and sheddase mRNA abundance in *Pemt*$^{-/-}$ mice. (**A**) Body weight, (**B**) plasma DPP4 activity. Liver mRNA abundance of (**C**) *Dpp4*, (**D**) *Mmp9*, (**E**) *Mmp2*, (**F**) *Adam17* and (**G**) *Adamst* in *Pemt*$^{+/+}$ or *Pemt*$^{-/-}$ mice. Data are presented as the means ± SEM, analyzed by unpaired students t-test with Welch's correction, ns $P>0.05$, *P=0.01-0.05, **P=0.001-0.01, ***P=0.0001-0.001 and ****$P<0.0001$.

Supplemental Table 2.1: List of qRT-PCR primers.

Oligonucleotides	Source	Identifier
A disintegrin and metallopeptidase domain 17 (*Adam17*)	Applied Biosystems	Mm01231069_m1
A disintegrin-like and metallopeptidase (reprolysin type) with thrombospondin type 1 motif, 1 (*Adamts1*)	Applied Biosystems	Mm01344169_m1
Adhesion G protein-coupled receptor E1 (*Adgre1*)	Applied Biosystems	Mm00802529_m1
Ankyrin repeat domain 1 (cardiac muscle) (*Ankrd1*)	Applied Biosystems	Mm00496512_m1
Arginase, liver (*Arg1*)	Applied Biosystems	Mm00475988_m1
C-type lectin domain family 4, member f (*Clec4f*)	Applied Biosystems	Mm00443934_m1
CD163 antigen (*Cd163*)	Applied Biosystems	Mm00474091_m1
Chemokine (C-C motif) ligand 11 (*Ccl11*, *Eotaxin*)	Applied Biosystems	Mm00441238_m1
Chemokine (C-C motif) ligand 2 (*Ccl2*, *Mcp-1*)	Applied Biosystems	Mm00441242_m1
Chemokine (C-C motif) ligand 5 (*Ccl5*, *Rantes*)	Applied Biosystems	Mm01302427_m1
Chemokine (C-C motif) receptor 2 (*Ccr2*)	Applied Biosystems	Mm04207877_m1
Chemokine (C-X-C motif) ligand 10 (*Cxcl10*, *Ip-10*)	Applied Biosystems	Mm00445235_m1
Collagen, type I, alpha 1 (*Col1a1*)	Applied Biosystems	Mm01302043_g1
Collagen, type III, alpha 1 (*Col3a1*)	Applied Biosystems	Mm00802331_m1
Cyclin-dependent kinase inhibitor 1A (P21) (*Cdkn1a*)	Applied Biosystems	Mm00432448_m1
Cyclin-dependent kinase inhibitor 2A (*Cdkn2a*)	Applied Biosystems	Mm00494449_m1
Dipeptidyl peptidase-4 (*Dpp4*)	Applied Biosystems	Mm00494548_m1
Forkhead box O1 (*FoxO1*)	Applied Biosystems	Mm00490671_m1
Glucagon receptor (*Gcgr*)	Applied Biosystems	Mm00433550_g1
Glucokinase (*Gck*)	Applied Biosystems	Mm00439129_m1
Glucose-6-phosphatase, catalytic (*G6pc*)	Applied Biosystems	Mm00839363_m1
Glycogen synthase kinase 3 beta (*Gsk3b*)	Applied Biosystems	Mm00444911_m1
Insulin-like growth factor 1 (*Igf1*)	Applied Biosystems	Mm01233960_m1
Insulin-like growth factor I receptor (*Igf1r*)	Applied Biosystems	Mm00802831_m1
Integrin alpha X (*Itgax*)	Applied Biosystems	Mm00498707_m1
Liver glycogen phosphorylase (*Pygl*)	Applied Biosystems	Mm01289790_m1
Mannose receptor, C type 1 (*Mrc1*)	Applied Biosystems	Mm01329359_m1
Matrix metallopeptidase 2 (*Mmp2*)	Applied Biosystems	Mm00439498_m1
Matrix metallopeptidase 9 (*Mmp9*)	Applied Biosystems	Mm01240562_g1
Microsomal triglyceride transfer protein (*Mttp*)	Applied Biosystems	Mm00435015_m1
Phosphoenolpyruvate carboxykinase 1, cytosolic (*Pck1*)	Applied Biosystems	Mm01247058_m1
Sterol regulatory element binding transcription factor 1 (*Srebf1*)	Applied Biosystems	Mm01138344_m1

Supplemental Table 2.2: DPP4 plasma parameters, *Dpp4* liver mRNA expression and CP and PV analyses in aged, HFHC-fed mice.

	***Dpp4*^{GFP}**	***Dpp4*$^{hep-/-}$**
Fasting plasma DPP4 activity (nmol/min/ml)	0.86	0.38
Fasting plasma DPP4 concentration (ng/ml)	250.50	370.50
Absolute *Dpp4* mRNA Expression/*Actb*	1.24	0.17
PV plasma DPP4 concentration (ng/ml)	159.50	185.50
PV plasma active GLP-1 (mg/ml)	1.29	4.55
CP plasma active GLP-1 (mg/ml)	0.18	0.53
PV plasma active GIP (pM)	6.33	27.17
CP plasma active GIP (pM)	1.50	5.17
PV plasma insulin (ng/ml)	5.37	3.47
CP plasma insulin (ng/ml)	2.31	2.77
PV plasma glucagon (pg/ml)	86.54	32.63
CP plasma glucagon (pg/ml)	10.20	12.15

2.8 References

1. Haedersdal S, Lund A, Knop FK, Vilsboll T. The Role of Glucagon in the Pathophysiology and Treatment of Type 2 Diabetes. *Mayo Clin Proc.* 2018;93(2):217-239.
2. Petersen MC, Shulman GI. Mechanisms of Insulin Action and Insulin Resistance. *Physiol Rev.* 2018;98(4):2133-2223.
3. Eslam M, Sanyal AJ, George J, International Consensus P. MAFLD: A Consensus-Driven Proposed Nomenclature for Metabolic Associated Fatty Liver Disease. *Gastroenterology.* 2020;158(7):1999-2014 e1991.
4. McLean BA, Wong CK, Campbell JE, Hodson DJ, Trapp S, Drucker DJ. Revisiting the Complexity of GLP-1 Action from Sites of Synthesis to Receptor Activation. *Endocr Rev.* 2021;42(2):101-132.
5. El K, Campbell JE. The role of GIP in alpha-cells and glucagon secretion. *Peptides.* 2020;125:170213.
6. El K, Gray SM, Capozzi ME, et al. GIP mediates the incretin effect and glucose tolerance by dual actions on alpha cells and beta cells. *Sci Adv.* 2021;7(11).
7. Nauck M, Stockmann F, Ebert R, Creutzfeldt W. Reduced incretin effect in type 2 (non-insulin-dependent) diabetes. *Diabetologia.* 1986;29:46-52.
8. Junker AE, Gluud L, Holst JJ, Knop FK, Vilsboll T. Diabetic and nondiabetic patients with nonalcoholic fatty liver disease have an impaired incretin effect and fasting hyperglucagonaemia. *J Intern Med.* 2016;279(5):485-493.
9. Sunny NE, Parks EJ, Browning JD, Burgess SC. Excessive hepatic mitochondrial TCA cycle and gluconeogenesis in humans with nonalcoholic fatty liver disease. *Cell Metab.* 2011;14(6):804-810.
10. Deacon CF. Dipeptidyl peptidase 4 inhibitors in the treatment of type 2 diabetes mellitus. *Nat Rev Endocrinol.* 2020;16(11):642-653.
11. Mulvihill EE. Dipeptidyl peptidase inhibitor therapy in type 2 diabetes: Control of the incretin axis and regulation of postprandial glucose and lipid metabolism. *Peptides.* 2018;100:158-164.
12. Mulvihill EE, Drucker DJ. Pharmacology, Physiology and Mechanisms of Action of Dipeptidyl Peptidase-4 Inhibitors. *Endocr Rev.* 2014:er20141035.
13. Lamers D, Famulla S, Wronkowitz N, et al. Dipeptidyl peptidase 4 is a novel adipokine potentially linking obesity to the metabolic syndrome. *Diabetes.* 2011;60(7):1917-1925.
14. Sarkar J, Nargis T, Tantia O, Ghosh S, Chakrabarti P. Increased Plasma Dipeptidyl Peptidase-4 (DPP4) Activity Is an Obesity-Independent Parameter for Glycemic Deregulation in Type 2 Diabetes Patients. *Front Endocrinol (Lausanne).* 2019;10:505.
15. Grungreiff K, Hebell T, Gutensohn K, Reinhold A, Reinhold D. Plasma concentrations of zinc, copper, interleukin-6 and interferon-gamma, and plasma dipeptidyl peptidase IV activity in chronic hepatitis C. *Mol Med Rep.* 2009;2(1):63-68.
16. Itou M, Kawaguchi T, Taniguchi E, et al. Altered expression of glucagon-like peptide-1 and dipeptidyl peptidase IV in patients with HCV-related glucose intolerance. *J Gastroenterol Hepatol.* 2008;23(2):244-251.

17. Varga T, Somogyi A, Barna G, et al. Higher serum DPP-4 enzyme activity and decreased lymphocyte CD26 expression in type 1 diabetes. *Pathol Oncol Res.* 2011;17(4):925-930.
18. Mannucci E, Pala L, Ciani S, et al. Hyperglycaemia increases dipeptidyl peptidase IV activity in diabetes mellitus. *Diabetologia.* 2005;48(6):1168-1172.
19. Ryskjaer J, Deacon CF, Carr RD, et al. Plasma dipeptidyl peptidase-IV activity in patients with type-2 diabetes mellitus correlates positively with HbAlc levels, but is not acutely affected by food intake. *Eur J Endocrinol.* 2006;155(3):485-493.
20. Miyazaki M, Kato M, Tanaka K, et al. Increased hepatic expression of dipeptidyl peptidase-4 in non-alcoholic fatty liver disease and its association with insulin resistance and glucose metabolism. *Mol Med Rep.* 2012;5(3):729-733.
21. Baumeier C, Saussenthaler S, Kammel A, et al. Hepatic DPP4 DNA Methylation Associates With Fatty Liver. *Diabetes.* 2017;66(1):25-35.
22. Varin EM, Mulvihill EE, Beaudry JL, et al. Circulating Levels of Soluble Dipeptidyl Peptidase-4 Are Dissociated from Inflammation and Induced by Enzymatic DPP4 Inhibition. *Cell Metab.* 2019;29(2):320-334 e325.
23. Gorgens SW, Jahn-Hofmann K, Bangari D, et al. A siRNA mediated hepatic dpp4 knockdown affects lipid, but not glucose metabolism in diabetic mice. *PLoS One.* 2019;14(12):e0225835.
24. Ghorpade DS, Ozcan L, Zheng Z, et al. Hepatocyte-secreted DPP4 in obesity promotes adipose inflammation and insulin resistance. *Nature.* 2018;555(7698):673-677.
25. Baumeier C, Schluter L, Saussenthaler S, et al. Elevated hepatic DPP4 activity promotes insulin resistance and non-alcoholic fatty liver disease. *Mol Metab.* 2017;6(10):1254-1263.
26. Balas B, Baig MR, Watson C, et al. The dipeptidyl peptidase IV inhibitor vildagliptin suppresses endogenous glucose production and enhances islet function after single-dose administration in type 2 diabetic patients. *J Clin Endocrinol Metab.* 2007;92(4):1249-1255.
27. Carris NW, Dietrich EA. Semaglutide for Weight Loss. *Ann Pharmacother.* 2021:10600280211027204.
28. Da BL, Satapathy SK. Semaglutide or Placebo for Nonalcoholic Steatohepatitis. *N Engl J Med.* 2021;385(2):e6.
29. Meier JJ. Efficacy of Semaglutide in a Subcutaneous and an Oral Formulation. *Front Endocrinol (Lausanne).* 2021;12:645617.
30. Slawson DC. Once-Weekly Semaglutide Is an Effective Adjunct for Weight Loss in Adults without Diabetes Who Are Overweight or Obese. *Am Fam Physician.* 2021;104(1):96-97.
31. Srivastava G, Kumar RB. Once-Weekly Semaglutide in Adults with Overweight or Obesity. *N Engl J Med.* 2021;385(1):e4.
32. Frias JP, Bastyr EJ, 3rd, Vignati L, et al. The Sustained Effects of a Dual GIP/GLP-1 Receptor Agonist, NNC0090-2746, in Patients with Type 2 Diabetes. *Cell Metab.* 2017;26(2):343-352 e342.
33. Jall S, Sachs S, Clemmensen C, et al. Monomeric GLP-1/GIP/glucagon triagonism corrects obesity, hepatosteatosis, and dyslipidemia in female mice. *Mol Metab.* 2017;6(5):440-446.

34. Mulvihill EE, Varin EM, Gladanac B, et al. Cellular Sites and Mechanisms Linking Reduction of Dipeptidyl Peptidase-4 Activity to Control of Incretin Hormone Action and Glucose Homeostasis. *Cell Metab.* 2017;25(1):152-165.
35. Marguet D, Baggio L, Kobayashi T, et al. Enhanced insulin secretion and improved glucose tolerance in mice lacking CD26. *Proc Natl Acad Sci U S A.* 2000;97(12):6874-6879.
36. Walkey CJ, Donohue LR, Bronson R, Agellon LB, Vance DE. Disruption of the murine gene encoding phosphatidylethanolamine N-methyltransferase. *Proc Natl Acad Sci U S A.* 1997;94(24):12880-12885.
37. Fullerton MD, Galic S, Marcinko K, et al. Single phosphorylation sites in Acc1 and Acc2 regulate lipid homeostasis and the insulin-sensitizing effects of metformin. *Nat Med.* 2013;19(12):1649-1654.
38. Chambers AP, Sorrell JE, Haller A, et al. The Role of Pancreatic Preproglucagon in Glucose Homeostasis in Mice. *Cell Metab.* 2017;25(4):927-934 e923.
39. Folch J, Lees M, Sloane Stanley GH. A simple method for the isolation and purification of total lipides from animal tissues. *The Journal of biological chemistry.* 1957;226(1):497-509.
40. Patel R, Patel M, Tsai R, et al. LXRbeta is required for glucocorticoid-induced hyperglycemia and hepatosteatosis in mice. *J Clin Invest.* 2011;121(1):431-441.
41. Rao X, Zhao S, Braunstein Z, et al. Oxidized LDL upregulates macrophage DPP4 expression via TLR4/TRIF/CD36 pathways. *EBioMedicine.* 2019;41:50-61.
42. Metsalu T, Vilo J. ClustVis: a web tool for visualizing clustering of multivariate data using Principal Component Analysis and heatmap. *Nucleic Acids Res.* 2015;43(W1):W566-570.
43. Doyle MA, Galanakis C, Mulvihill E, Crawley A, Cooper CL. Hepatitis C Direct Acting Antivirals and Ribavirin Modify Lipid but not Glucose Parameters. *Cells.* 2019;8(3).
44. Baggio LL, Varin EM, Koehler JA, et al. Plasma levels of DPP4 activity and sDPP4 are dissociated from inflammation in mice and humans. *Nat Commun.* 2020;11(1):3766.
45. Muscelli E, Casolaro A, Gastaldelli A, et al. Mechanisms for the antihyperglycemic effect of sitagliptin in patients with type 2 diabetes. *J Clin Endocrinol Metab.* 2012;97(8):2818-2826.
46. Serre V, Dolci W, Schaerer E, et al. Exendin-(9-39) is an inverse agonist of the murine glucagon-like peptide-1 receptor: implications for basal intracellular cyclic adenosine 3',5'-monophosphate levels and beta-cell glucose competence. *Endocrinology.* 1998;139(11):4448-4454.
47. D'Alessio D, Lu W, Sun W, et al. Fasting and postprandial concentrations of GLP-1 in intestinal lymph and portal plasma: evidence for selective release of GLP-1 in the lymph system. *Am J Physiol Regul Integr Comp Physiol.* 2007;293(6):R2163-2169.
48. Qin X, Shen H, Liu M, et al. GLP-1 reduces intestinal lymph flow, triglyceride absorption, and apolipoprotein production in rats. *Am J Physiol Gastrointest Liver Physiol.* 2005;288(5):G943-949.

49. Buzzetti E, Pinzani M, Tsochatzis EA. The multiple-hit pathogenesis of non-alcoholic fatty liver disease (NAFLD). *Metabolism.* 2016;65(8):1038-1048.
50. Williams KH, Vieira De Ribeiro AJ, Prakoso E, et al. Circulating dipeptidyl peptidase-4 activity correlates with measures of hepatocyte apoptosis and fibrosis in non-alcoholic fatty liver disease in type 2 diabetes mellitus and obesity: A dual cohort cross-sectional study. *J Diabetes.* 2015;7(6):809-819.
51. Wree A, Eguchi A, McGeough MD, et al. NLRP3 inflammasome activation results in hepatocyte pyroptosis, liver inflammation, and fibrosis in mice. *Hepatology.* 2014;59(3):898-910.
52. Wada N, Takaki A, Ikeda F, et al. Serum-inducible protein (IP)-10 is a disease progression-related marker for non-alcoholic fatty liver disease. *Hepatol Int.* 2017;11(1):115-124.
53. Berres ML, Koenen RR, Rueland A, et al. Antagonism of the chemokine Ccl5 ameliorates experimental liver fibrosis in mice. *J Clin Invest.* 2010;120(11):4129-4140.
54. Papatheodoridi AM, Chrysavgis L, Koutsilieris M, Chatzigeorgiou A. The Role of Senescence in the Development of Nonalcoholic Fatty Liver Disease and Progression to Nonalcoholic Steatohepatitis. *Hepatology.* 2020;71(1):363-374.
55. Kim KM, Noh JH, Bodogai M, et al. Identification of senescent cell surface targetable protein DPP4. *Genes Dev.* 2017;31(15):1529-1534.
56. Lopes-Paciencia S, Saint-Germain E, Rowell MC, Ruiz AF, Kalegari P, Ferbeyre G. The senescence-associated secretory phenotype and its regulation. *Cytokine.* 2019;117:15-22.
57. Medeiros Tavares Marques JC, Cornelio DA, Nogueira Silbiger V, Ducati Luchessi A, de Souza S, Batistuzzo de Medeiros SR. Identification of new genes associated to senescent and tumorigenic phenotypes in mesenchymal stem cells. *Sci Rep.* 2017;7(1):17837.
58. el-Deiry WS, Tokino T, Velculescu VE, et al. WAF1, a potential mediator of p53 tumor suppression. *Cell.* 1993;75(4):817-825.
59. Kazankov K, Jorgensen SMD, Thomsen KL, et al. The role of macrophages in nonalcoholic fatty liver disease and nonalcoholic steatohepatitis. *Nat Rev Gastroenterol Hepatol.* 2019;16(3):145-159.
60. Weiskirchen R, Weiskirchen S, Tacke F. Organ and tissue fibrosis: Molecular signals, cellular mechanisms and translational implications. *Mol Aspects Med.* 2019;65:2-15.
61. Zhong J, Rao X, Deiuliis J, et al. A potential role for dendritic cell/macrophage-expressing DPP4 in obesity-induced visceral inflammation. *Diabetes.* 2013;62(1):149-157.
62. Romacho T, Sell H, Indrakusuma I, et al. DPP4 deletion in adipose tissue improves hepatic insulin sensitivity in diet-induced obesity. *Am J Physiol Endocrinol Metab.* 2020;318(5):E590-E599.
63. Lee YS, Riopel M, Cabrales P, Bandyopadhyay GK. Hepatocyte-specific HIF-1alpha ablation improves obesity-induced glucose intolerance by reducing first-pass GLP-1 degradation. *Sci Adv.* 2019;5(7):eaaw4176.
64. Jacobs RL, Zhao Y, Koonen DP, et al. Impaired de novo choline synthesis explains why phosphatidylethanolamine N-methyltransferase-deficient mice

are protected from diet-induced obesity. *The Journal of biological chemistry.* 2010;285(29):22403-22413.
65. Gao X, van der Veen JN, Hermansson M, et al. Decreased lipogenesis in white adipose tissue contributes to the resistance to high fat diet-induced obesity in phosphatidylethanolamine N-methyltransferase-deficient mice. *Biochim Biophys Acta.* 2015;1851(2):152-162.
66. Itou M, Kawaguchi T, Taniguchi E, Sata M. Dipeptidyl peptidase-4: a key player in chronic liver disease. *World J Gastroenterol.* 2013;19(15):2298-2306.
67. Chang ML. Metabolic alterations and hepatitis C: From bench to bedside. *World J Gastroenterol.* 2016;22(4):1461-1476.
68. Maes M, Bonaccorso S, Marino V, et al. Treatment with interferon-alpha (IFN alpha) of hepatitis C patients induces lower serum dipeptidyl peptidase IV activity, which is related to IFN alpha-induced depressive and anxiety symptoms and immune activation. *Mol Psychiatry.* 2001;6(4):475-480.
69. Meissner EG, Decalf J, Casrouge A, et al. Dynamic Changes of Post-Translationally Modified Forms of CXCL10 and Soluble DPP4 in HCV Subjects Receiving Interferon-Free Therapy. *PLoS One.* 2015;10(7):e0133236.
70. Baggio LL, Drucker DJ. Glucagon-like peptide-1 receptor co-agonists for treating metabolic disease. *Mol Metab.* 2021;46:101090.
71. Drucker DJ. Mechanisms of Action and Therapeutic Application of Glucagon-like Peptide-1. *Cell Metab.* 2018;27(4):740-756.
72. Burcelin R, Da Costa A, Drucker D, Thorens B. Glucose competence of the hepatoportal vein sensor requires the presence of an activated glucagon-like peptide-1 receptor. *Diabetes.* 2001;50(8):1720-1728.
73. Aulinger BA, Perabo M, Seeley RJ, Parhofer KG, D'Alessio DA. Rapid hepatic metabolism blunts the endocrine action of portally infused GLP-1 in male rats. *Am J Physiol Endocrinol Metab.* 2020;318(2):E189-E197.
74. Trzaskalski NA, Fadzeyeva E, Mulvihill EE. Dipeptidyl Peptidase-4 at the Interface Between Inflammation and Metabolism. *Clin Med Insights Endocrinol Diabetes.* 2020;13:1179551420912972.
75. Jejelava N, Kaufman S, Krieger JP, Terra MM, Langhans W, Arnold M. Intestinal lymph as a readout of meal-induced GLP-1 release in an unrestrained rat model. *Am J Physiol Regul Integr Comp Physiol.* 2018;314(5):R724-R733.
76. Shin JW, Jurisic G, Detmar M. Lymphatic-specific expression of dipeptidyl peptidase IV and its dual role in lymphatic endothelial function. *Exp Cell Res.* 2008;314(16):3048-3056.
77. Malbert CH, Chauvin A, Horowitz M, Jones KL. Glucose Sensing Mediated by Portal Glucagon-Like Peptide 1 Receptor Is Markedly Impaired in Insulin-Resistant Obese Animals. *Diabetes.* 2021;70(1):99-110.
78. Barchetta I, Ceccarelli V, Cimini FA, et al. Circulating dipeptidyl peptidase-4 is independently associated with the presence and severity of NAFLD/NASH in individuals with and without obesity and metabolic disease. *J Endocrinol Invest.* 2021;44(5):979-988.
79. Kawakubo M, Tanaka M, Ochi K, et al. Dipeptidyl peptidase-4 inhibition prevents nonalcoholic steatohepatitis–associated liver fibrosis and tumor

development in mice independently of its anti-diabetic effects. *Scientific Reports.* 2020;10(1):983.
80. Kaji K, Yoshiji H, Ikenaka Y, et al. Dipeptidyl peptidase-4 inhibitor attenuates hepatic fibrosis via suppression of activated hepatic stellate cell in rats. *J Gastroenterol.* 2014;49(3):481-491.
81. Koyama Y, Brenner DA. Liver inflammation and fibrosis. *J Clin Invest.* 2017;127(1):55-64.
82. Guo Y, Zhang X, Zhao Z, et al. NF- kappa B/HDAC1/SREBP1c pathway mediates the inflammation signal in progression of hepatic steatosis. *Acta Pharm Sin B.* 2020;10(5):825-836.
83. Dela Pena A, Leclercq I, Field J, George J, Jones B, Farrell G. NF-kappaB activation, rather than TNF, mediates hepatic inflammation in a murine dietary model of steatohepatitis. *Gastroenterology.* 2005;129(5):1663-1674.
84. Zeng Y, Li C, Guan M, et al. The DPP-4 inhibitor sitagliptin attenuates the progress of atherosclerosis in apolipoprotein-E-knockout mice via AMPK- and MAPK-dependent mechanisms. *Cardiovasc Diabetol.* 2014;13:32.
85. Shinjo T, Nakatsu Y, Iwashita M, et al. DPP-IV inhibitor anagliptin exerts anti-inflammatory effects on macrophages, adipocytes, and mouse livers by suppressing NF-kappaB activation. *Am J Physiol Endocrinol Metab.* 2015;309(3):E214-223.
86. Meijnikman AS, Herrema H, Scheithauer TPM, Kroon J, Nieuwdorp M, Groen AK. Evaluating causality of cellular senescence in non-alcoholic fatty liver disease. *JHEP Rep.* 2021;3(4):100301.
87. Chen Z, Yu J, Fu M, et al. Dipeptidyl peptidase-4 inhibition improves endothelial senescence by activating AMPK/SIRT1/Nrf2 signaling pathway. *Biochem Pharmacol.* 2020;177:113951.
88. Diaz-Jimenez D, Petrillo MG, Busada JT, Hermoso MA, Cidlowski JA. Glucocorticoids mobilize macrophages by transcriptionally up-regulating the exopeptidase DPP4. *The Journal of biological chemistry.* 2020;295(10):3213-3227.
89. Wang T, Yang L, Liang Z, et al. Targeting cellular senescence prevents glucocorticoid-induced bone loss through modulation of the DPP4-GLP-1 axis. *Signal Transduct Target Ther.* 2021;6(1):143.
90. Rufini A, Tucci P, Celardo I, Melino G. Senescence and aging: the critical roles of p53. *Oncogene.* 2013;32(43):5129-5143.
91. Xie Y, Zhu S, Song X, et al. The Tumor Suppressor p53 Limits Ferroptosis by Blocking DPP4 Activity. *Cell Rep.* 2017;20(7):1692-1704.
92. Svendsen B, Larsen O, Gabe MBN, et al. Insulin Secretion Depends on Intra-islet Glucagon Signaling. *Cell Rep.* 2018;25(5):1127-1134 e1122.
93. Capozzi ME, Svendsen B, Encisco SE, et al. beta Cell tone is defined by proglucagon peptides through cAMP signaling. *JCI Insight.* 2019;4(5).
94. Zhu L, Dattaroy D, Pham J, et al. Intra-islet glucagon signaling is critical for maintaining glucose homeostasis. *JCI Insight.* 2019;5.
95. Song Y, Koehler JA, Baggio LL, Powers AC, Sandoval DA, Drucker DJ. Gut-Proglucagon-Derived Peptides Are Essential for Regulating Glucose Homeostasis in Mice. *Cell Metab.* 2019;30(5):976-986 e973.

96. Chepurny OG, Matsoukas MT, Liapakis G, et al. Nonconventional glucagon and GLP-1 receptor agonist and antagonist interplay at the GLP-1 receptor revealed in high-throughput FRET assays for cAMP. *The Journal of biological chemistry.* 2019;294(10):3514-3531.

3 Elimination of hepatocyte-derived DPP4 downregulates cardiac immune- and collagen-related genes but does not alter cardiac function in aged mice

Authors: **Natasha A. Trzaskalski**, Melissa M. Dann, Antonio Hanson, Branka Vulesevic, Evgenia Fadzeyeva, Natasha Jeraj, Ilka Lorenzen-Schmidt, Rick Seymour & Erin E. Mulvihill

3.1 Author Contributions

Conceptualization: EEM; Methodology: EEM; Formal Analysis: NAT, MMD, BV; Investigation: NAT, MMD, AH, BV, EF, NJ, ILS, RS, EEM; Resources: EEM; Writing – Original Draft: NAT, BV, EEM; Writing – Review and Editing: all authors; Supervision: EEM; Project Administration: EEM; Funding Acquisition: EEM.

3.2 Abstract

Background: In Canada, 20% of the population is living with metabolic syndrome, effectively increasing their risk of MASLD and cardiovascular disease. The relationship between MASLD and cardiovascular disease is well characterized, however, the underlying mechanism is incompletely understood. Interestingly, hepatocyte specific genetic elimination or silencing via siRNA of DPP4 prevents liver fibrosis and adipose tissue inflammation. DPP4 elimination from the liver has both hepatic and extra-hepatic implications, however, how this affects the heart remains to be investigated. This study will evaluate how diastolic function and molecular signatures of HF, like inflammation and fibrosis, are affected by hepatocyte-specific genetic elimination of *Dpp4*.

Methods: *Dpp4*$^{+/+}$, *Dpp4*$^{-/-}$ and *Dpp4*$^{flox/flox}$ mice injected with an AAV to selectively eliminate DPP4 from hepatocytes (*Dpp4*$^{hep-/-}$), and respective controls (*Dpp4*^{GFP}), were aged and fed a HFHC diet for 24 weeks. Mice underwent 2D echocardiography as well as pulsed-wave and tissue doppler echocardiography. Further, speckle-tracking strain analysis was conducted to detect diastolic dysfunction. Differential mRNA analysis using the NanoString platform and qRT-PCR were conducted using ventricular tissue to assess immunological pathway expression, and hypertrophy, modeling-related, senescence and metabolism gene expression.

Results: Immunological pathway analysis of ventricular tissue revealed downregulation of 12 immune-related pathways in *Dpp4*$^{hep-/-}$ mice, including apoptosis and chemokine and cytokine signaling, however, this was not observed in *Dpp4*$^{-/-}$ mice. Further, fibrosis and ECM modeling-related genes, *Col1a1*, *Col3a1*, *Ctgf* and *Myh7*, were significantly upregulated in *Dpp4*$^{-/-}$ mice, but unchanged in *Dpp4*$^{hep-/-}$

mice, compared to controls. Interestingly, cardiac hypertrophy and systolic and diastolic function evaluated with echocardiography were unchanged.

Conclusions: Immune-related pathways are downregulated in *Dpp4*$^{hep-/-}$ mice, while fibrosis genes are significantly upregulated in *Dpp4*$^{-/-}$ mice, compared to respective controls. Despite these molecular changes, cardiac hypertrophy, systolic and diastolic function were unchanged with systemic and organ specific loss of *Dpp4*.

New and Noteworthy: We demonstrated that hepatocyte-specific *Dpp4* genetic elimination protected mice with significant decreases in the mRNA expression of inflammation genes involved in immune-related pathways, like *Ccl11* (*eotaxin-1*), *Cxcl10* (*Ip-10*) and *Tnf,* as well as collagen genes in myocardial tissue, suggesting a better prognosis irrespective of function. Interestingly, these molecular changes did not improve cardiac dysfunction between genotypes and their controls, evaluated via systolic and diastolic measurements. These findings suggest that reducing hepatocyte-derived DPP4 is sufficient to alter molecular perturbations in the heart resulting from age and HFHC feeding.

3.3 Introduction

Currently, 1 in 5 Canadians are living with metabolic syndrome; a cluster of risk factors which increase the risk of cardiovascular disease (CVD) and type 2 diabetes (T2D) in adults[1]. Metabolic dysfunction-associated steatotic liver disease (MASLD) is the most recent acronym introduced to appropriately describe hepatic lipid accumulation with at least one of five cardiovascular risk factors, including obesity, hyperglycemia and hypertriglyceridemia[2]. Interestingly, MASLD appears to have extrahepatic consequences which can contribute to CVD progression[3,4]. In fact, CVD is the leading cause of death in individuals with fatty liver disease (40-45%)[5]. These individuals are also predisposed to atherogenic dyslipidemia that contributes to increasing the risk of atherosclerosis and the development of unstable plaques[6]. Interestingly, growing evidence suggests that MASLD, independent of well-established cardiovascular risk factors, can still contribute significantly to CVD[7], and may be linked to the release of proinflammatory and profibrogenic factors and mediators[8-11]. Currently there is only one FDA approved drug for the later stages of MASLD[12], metabolic dysfunction-associated steatohepatitis (MASH), but unfortunately, there are no pharmacological agents approved for early intervention. However, agents used to regulate dysglycemia in diabetes have recently become of interest, mainly since insulin resistance precedes, and is essential to, hepatocellular lipid accumulation[13,14].

The liver, adipose tissue, and skeletal muscle, secrete proteins, respectively called hepatokines, adipokines and myokines, which influence biological functions in both local and peripheral tissues resulting in inter-tissue crosstalk[15,16]. One such hepatokine[17,18], previously regarded as an adipokine[19,20], is dipeptidyl peptidase-4

(DPP4). It selectively cleaves N-terminal dipeptides from substrates, the most well-characterized being the incretin hormones glucagon-like peptide-1 (GLP-1) and glucose-dependent insulinotropic polypeptide (GIP), which are quickly inactivated preventing postprandial insulin secretion[21-23]. In line with this, we recently revealed increased active GLP-1 in the portal vein and reduced hepatic glucose production with genetic elimination of hepatocyte-derived *Dpp4* (*Dpp4*$^{hep-/-}$) in mice[24].

Through hepatocyte-targeted siRNA, Ghorpade *et. al*.[18] silenced hepatocyte *Dpp4* and demonstrated reduced adipose tissue inflammation and insulin resistance in obese mice. Consistent with these findings, in *Dpp4*$^{hep-/-}$ mice, Varin *et. al.*[17] showed decreased inflammation in liver and adipose tissue but had no effect on glucose tolerance. Conversely, Baumeier *et. al.*[25] overexpressed hepatic *Dpp4* which resulted in adipose tissue inflammation, hypercholesteremia, hepatic steatosis and insulin resistance which was linked to reduced levels of active vena cava GLP-1 compared to portal vein GLP-1, suggesting inactivation by hepatocyte-derived DPP4. In the context of fatty liver disease, Gorgens *et. al.*[26] revealed that hepatocyte specific siRNA mediated *Dpp4* knockout reduced hepatic steatosis with no change in glucose metabolism in *db/db* mice. We have also recently shown reduced hepatic fibrosis and mRNA expression of immunological pathways in *Dpp4*$^{hep-/-}$ mice[24].

However, despite consistent evidence for reducing inflammation in liver and adipose tissue, the impact of hepatocyte-derived DPP4 in cardiovascular disease progression remains to be evaluated. Here, we investigate the role of hepatic DPP4 in ventricular function and preventing cardiac inflammation and fibrosis in a diet-induced model of hepatic steatosis.

3.4 Methods

3.4.1 Animals

Animals were cared for in accordance with the Canadian Guide for the Care and Use of Laboratory animals (CCAC). All experimental procedures were approved under AUP#2909 and AUP#2029 by the University of Ottawa Animal Care. Male mice were housed under a 12-h light/dark cycle and maintained on high fat, high cholesterol (HFHC; 42% kcal from fat, 42.7% kcal from carbohydrates, 15.2% kcal from protein, 0.2% weight from cholesterol: TD88137, Envigo) diet. Male, whole body *Dpp4*$^{-/-}$ mice, on a C57BL6 background, have been described[27,28]. To generate *Dpp4*$^{hep-/-}$ mice, male *Dpp4*$^{flox/flox}$ adult mice were *i.v.* injected with 1.5x10^{11} GC per mouse of AAV8.TBG.pi.egfp.wpre.bgh (AAV-GFP; control virus, #105535-AAV8) or AAV8.TBG.PI.CRE.rBG (AAV-Cre; #107787-AAV8) prior to the onset of HFHC diet feeding. AAV constructs were obtained from the University of Pennsylvania Vector Core Lab (gift from James M. Wilson, Perelman School of Medicine, University of Pennsylvania, Philadelphia, PA). B6.Cg-Tg(Tek-cre) 1Ywa/J mice were obtained from The Jackson Laboratory (Strain #: 008863, RRID: IMSR_JAX:008863) and bred with *Dpp4*$^{flox/flox}$ *to* generate *Dpp4*$^{EC-/-}$ mice. To assess cardiac dysfunction, experiments were performed in 16–28-week-old mice fed a HFHC diet for 24 weeks sacrifice where tissue collection was performed at 40-52 weeks of age, as previously described[29].

3.4.2 NanoString mRNA Analysis

NanoString (NanoString Technologies, Inc., Seattle WA) nCounter® Mouse Immunology Panel (catalog# XT-CSO-MIM1-12), were used where 100ng RNA was incubated with reporter and capture probes, consisting of 547 immunology-related mouse genes and 14 internal reference controls, for 16h at 65°C as described[24].

Raw gene expression data were analyzed using NanoString's software, nSolver v4.0.70, with the Advanced Analysis Module v2.0.115 with background subtraction. Genes with counts below a threshold of 20 were excluded from subsequent analysis. Data normalization was completed on background-subtracted samples using both the internal positive controls and selected consistent housekeeping genes used across all analyses in ventricular tissue: *Rpl19, Ppia, Eef1g, Oaz1, Gusb, Tbp, G6pdx, Tubb5, Polr2a, Sdha,* Gapdh and *Polr1b*. Significant differential gene expression was determined through analyses using nSolver, which employs multivariate linear regression models to identify significant genes (mixture negative binomial, simplified negative binomial, or log-linear model). Raw mRNA counts were log2 transformed and significance was determined using a T-test. Statistically significant, differentially expressed genes were identified as those with a p-value <0.05. Ratios of $\log_2$ normalized transcript count data were generated for ventricular tissue from HFHC-fed *Dpp4*$^{-/-}$ mice vs baseline HFHC-fed WT mice and HFHC-fed *Dpp4*$^{hep-/-}$ mice vs baseline HFHC-fed *Dpp4*^{GFP} mice.

Pathway scores generated from nSolver Advanced Analysis were standardized by Z-scaling. ClustVis[30] was used to perform supervised hierarchical clustering analysis and principal components analysis of $\log_2$ transformed transcript count data and Z-scaled pathway scores.

3.4.3 Plasma analysis

Analysis for plasma ALT, AST, ALP, TG, cholesterol, LDL and HDL were performed by the Pathology Core at Toronto Centre for Phenogenomics. The Beckman Coulter AU480 clinical chemistry analyzer was used in combination with appropriate reagents (ALT, AST, TG, cholesterol, LDL, and HDL), calibrators

(Beckman Coulter Lyophilized Chemistry Calibrator Levels 1 and 2), and quality control materials (Bio-Rad Liquid Assayed Multiqual 1 and 3).

3.4.4 RNA isolation, cDNA and qRT-PCR

Flash-frozen mouse hearts, without atria, were powdered and homogenized with TriReagent (Sigma Aldrich, St. Louis, MO) using a TissueLyser II system (Qiagen), and total RNA was extracted using manufacturer's protocol. Reverse transcription was performed with the Applied Biosystems™ High-Capacity cDNA Reverse Transcription Kit. cDNA was subsequently used to assess mRNA expression by qRT-PCR (QuantStudio 5 System, Thermo Fisher Scientific) with TaqMan Fast Advanced Master Mix (Thermo Fisher Scientific, 4444557) and TaqMan Gene Expression Assays (Thermo Fisher Scientific). The specific gene expression assays used are listed (**Supplemental Table 3.1**). Quantification of transcript levels was performed by the standard curve method, and expression levels for each gene were normalized to *Gapdh*.

3.4.5 Echocardiography: Image Acquisition

Echocardiographic images were acquired with the Vevo 3100 high frequency small animal ultrasound system (FUIJIFILM VisualSonics, Toronto, Canada), using either the MX400 or MX550D linear array transducers. Mice were anesthetized with 1-2% isoflurane in 2 L/min oxygen and positioned supine on a heated physiological monitoring platform, to collect respiration and ECG traces. Body temperature was monitored using a rectal thermometer and maintained between 36°C and 38°C. Images of the left ventricle were taken at 16 weeks and 24 weeks after HFHC-feeding, using parasternal long axis view in 2D brightness mode (B-mode). To further assess

diastolic function of the left ventricle, pulsed wave and tissue doppler were used to measure mitral valve inflow and mitral annulus velocity, respectively, in an apical four-chamber view of the heart. E and A peaks were measured from 1-3 consecutive heart beats between breaths.

3.4.6 Strain Analysis

Echocardiographic images in long-axis view were analyzed for longitudinal and radial strain and strain rate using Vevo Strain software (Visualsonics). Three consecutive cardiac cycles free of respiratory artifacts were analyzed. Epi- and endocardium of the heart were manually traced at the time of end-diastole in the first cycle and adjusted to ensure accurate tracking of the epi- and endocardial borders throughout the three cycles. The software determined an average time course of strain and strain rate at 49 evenly spaced points along the perimeter of epi- and endocardium. Since it is difficult for technical reasons to detect strains accurately in the apical region, the apex was excluded from the analysis, leaving 34 points along the anterior and posterior myocardium, as previously described[31]. The average strain and strain rate time course was calculated from these points in each of the directions (longitudinal and radial) and the appropriate maxima/minima chosen to represent systolic and diastolic strain and strain rate, respectively.

3.4.7 Statistics

All data were plotted and statistical analysis were performed using GraphPad Prism (version 9.5.1). Data are presented as the means ± SEM, analyzed by unpaired students t-test with Welch's correction, between genetic knockouts and respective controls (*Dpp4*$^{+/+}$ vs *Dpp4*$^{-/-}$ mice, and *Dpp4*^{GFP} vs *Dpp4*$^{hep-/-}$ mice). Statistical differences between groups were evaluated by $P<0.05$ was considered statistically

significant.

3.5 Results

3.5.1 In ventricular tissue, immune-related genes and pathways are largely downregulated in HFHC-fed *Dpp4*$^{hep-/-}$ mice

Plasma biochemical analysis revealed no significant changes between *Dpp4*^{GFP} and *Dpp4*$^{hep-/-}$ mice, however, triglycerides and glucose were significantly decreased in *Dpp4*$^{-/-}$ mice compared to *Dpp4*$^{+/+}$ mice (**Table 3.1**)[29]. Further, $\log_2$ normalized mRNA counts, and plasma and liver DPP4 activity were significantly decreased in *Dpp4*$^{-/-}$ mice, while only plasma DPP4 activity was significantly decreased in *Dpp4*$^{hep-/-}$ mice (**Table 3.1**)[24]. Pathway analysis conducted on gene expression in ventricular tissue collected from *Dpp4*$^{+/+}$ mice (wild-type, WT), *Dpp4*$^{-/-}$ mice (global *Dpp4* deletion), hepatocyte-specific *Dpp4* knockout mice (*Dpp4*$^{hep-/-}$) and their respective controls, *Dpp4*^{GFP} mice fed a high-fat high-cholesterol (HFHC) diet for 24 weeks, revealed distinct and opposing patterns. Only two pathways were significantly upregulated in *Dpp4*$^{-/-}$ mice compared to *Dpp4*$^{+/+}$ controls: lymphocyte activation and MHC class II antigen presentation (**Figure 3.1A**). In contrast, 12 pathways were significantly downregulated in *Dpp4*$^{hep-/-}$ mice compared to their respective controls, *Dpp4*^{GFP} mice (**Figure 3.1B**). This includes chemokine and cytokine signaling, apoptosis and NF-κB signaling. In addition, adaptive immune system, immunometabolism, oxidative stress and Th2 differentiation pathways were all trending downwards in *Dpp4*$^{hep-/-}$ mice compared to their respective controls, *Dpp4*^{GFP} mice (**Figure 3.1B**). Further, individual apoptosis related genes were either unchanged or upregulated in *Dpp4*$^{-/-}$ mice compared to *Dpp4*$^{+/+}$ controls, including

Ly96 (**Figure 3.1C**). In *Dpp4*$^{hep-/-}$ mice compared to *Dpp4*^{GFP} mice, almost all genes were significantly downregulated including *Cd14* and *Tnf* (**Figure 3.1C**). This pattern was maintained when we looked at chemokine and cytokine signaling (**Figure 3.1D**). Most genes were significantly differentially downregulated in *Dpp4*$^{hep-/-}$ mice compared to their respective controls, *Dpp4*^{GFP} mice, and these same genes were either unchanged or upregulated in *Dpp4*$^{-/-}$ mice compared to *Dpp4*$^{+/+}$ controls.

Table 3.1: Biochemical analysis of liver tissue and plasma of aged HFHC-fed *Dpp4*$^{+/+}$, *Dpp4*$^{-/-}$, *Dpp4*^{GFP} and *Dpp4*$^{hep-/-}$ mice. Data are presented as the means ± SEM, analyzed by unpaired students t-test with Welch's correction, between genetic knockouts and respective controls (*Dpp4*$^{+/+}$ vs *Dpp4*$^{-/-}$ and *Dpp4*^{GFP} vs *Dpp4*$^{hep-/-}$), ns p>0.05, *p=0.01-0.05, **p=0.001-0.01, ***p=0.0001-0.001 and ****p<0.0001.

	***Dpp4*$^{+/+}$**	***Dpp4*$^{-/-}$**	***Dpp4*^{GFP}**	***Dpp4*$^{hep-/-}$**
ALT (IU/L)	244.66 ± 95.2	128.26 ± 38.6	194.125 ± 58.6	325.85 ± 66.4
AST (IU/L)	202.21 ± 46.5	180.40 ± 15.3	224.675 ± 62.6	273.13 ± 26.4
ALP (IU/L)	26.95 ± 7.7	31.35 ± 17.7	41.15 ± 27.7	27.64 ± 6.3
Cholesterol (mg/dL)	293.60 ± 30.2	249.66 ± 44.8	261.35 ± 48.7	320.01 ± 17.7
HDL (mg/dL)	113.52 ± 8.0	102.71 ± 11.9	109.20 ± 15.6	126.55 ± 7.6
TG (mg/dL)	82.82 ± 7.4	56.95 ± 0.8 ✱✱	64.87±1.6	66.32 ± 3.0
LDL (mg/dL)	34.71 ± 5.1	21.64 ± 4.6	23.26 ± 5.1	29.23 ± 3.2
Glucose (mg/dL)	373.88 ± 17.4	314.58 ± 35.4 ✱	290.45 ± 14.3	335.35 ± 33.2
Body weight (g)	49.07 ± 2.9	52.71 ± 4.6	49.49 ± 3.2	54.39 ± 2.1
Plasma DPP4 Activity (nmol/min/ml)	6.60 ± 1.20	0.00 ± 0.00 ✱✱✱	7.67 ± 1.21	2.63 ± 0.14 ✱
Liver DPP4 Activity (nmol/min/mg protein)	0.73 ± 0.23	0.00 ± 0.00 ✱✱	0.47 ± 0.15	0.08 ± 0.04

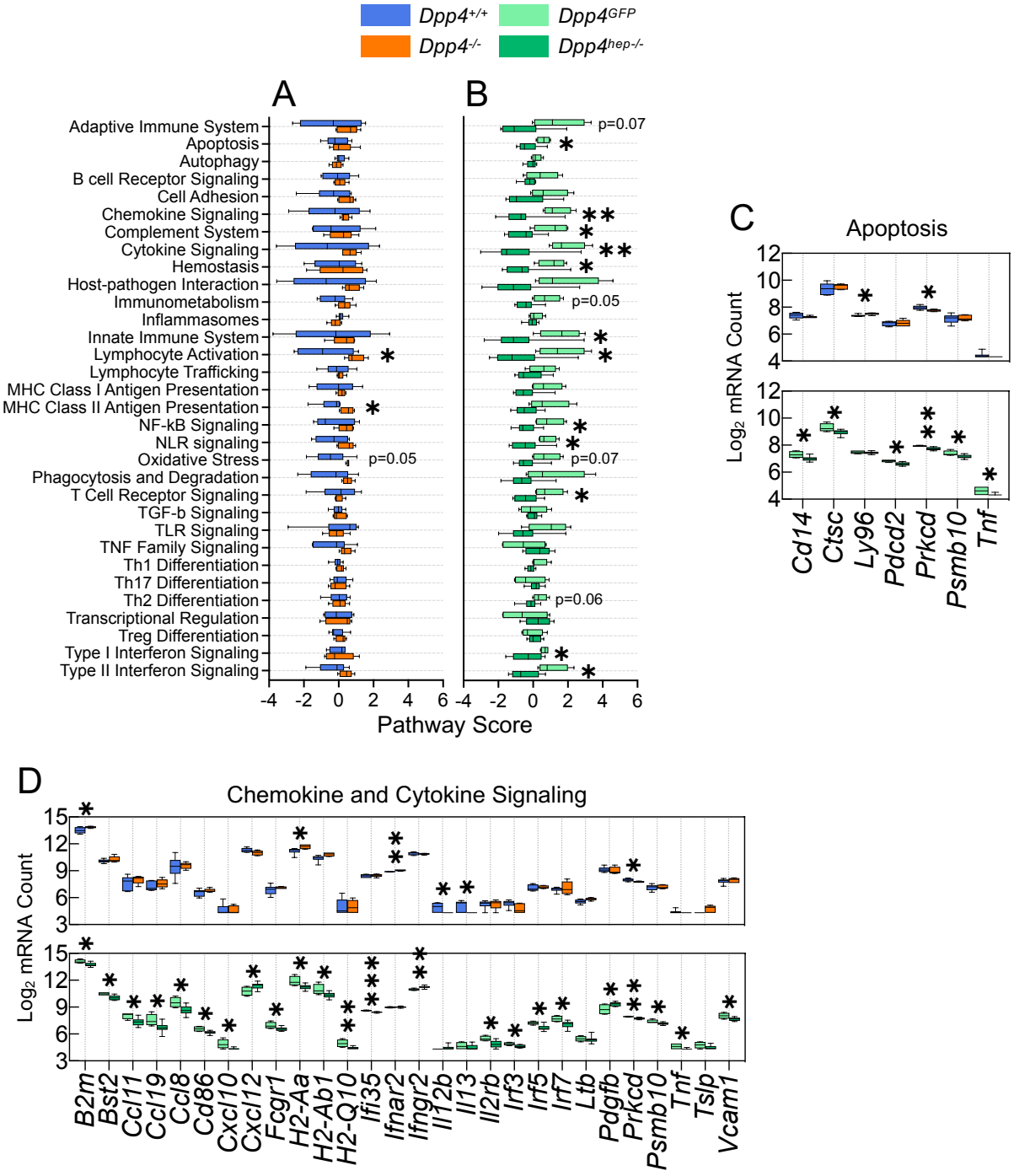

Figure 3.1: In *Dpp4*$^{hep-/-}$ mice, immune-related genes and pathways are downregulated compared to controls, but relatively unchanged in *Dpp4*$^{-/-}$ mice. Scores of immunological pathways in ventricular tissue of (**A**) HFHC-fed *Dpp4*$^{+/+}$ and *Dpp4*$^{-/-}$ mice and (**B**) HFHC-fed *Dpp4*^{GFP} and *Dpp4*$^{hep-/-}$ mice. Log_2 normalized mRNA counts of genes associated with (**C**) apoptosis and (**D**) chemokine and cytokine signaling. Box and whisker plots: box extends from the 25th to 75th percentiles, the whiskers go down to the smallest value and up to the largest. Data are presented as the means ± SEM, analyzed by unpaired students t-test with Welch's correction, ns $p<0.05$, *$p=0.01$-0.05, **$p=0.001$-0.01, ***$p=0.0001$-0.001.

3.5.2 Fibrosis related genes, but not hypertrophy or metabolism related genes, are upregulated in *Dpp4*$^{-/-}$ mice and unchanged in *Dpp4*$^{hep-/-}$ mice

Since immunological pathways and genes were downregulated in *Dpp4*$^{hep-/-}$ mice, we evaluated hypertrophy, fibrosis and metabolism related genes using qRT-PCR in ventricular tissue to determine if there were additional molecular changes. Interestingly, pro-fibrotic genes *Col1a1* (**Figure 3.2A**), *Col3a1* (**Figure 3.2B**), *Ctgf* (**Figure 3.2C**) and *Myh7* (**Figure 3.2D**) were all significantly upregulated in *Dpp4*$^{-/-}$ mice compared to *Dpp4*$^{+/+}$ controls, however, unchanged in *Dpp4*$^{hep-/-}$ mice. Interestingly, additional hypertrophy and fibrosis related genes, including *Nppa* (**Figure 3.2E**), *Nppb* (**Figure 3.2F**), *Mmp2* (**Figure 3.2G**), *Mmp9* (**Figure 3.2H**), *Ddr2* (**Figure 3.2I**) and *Vim* (**Figure 3.2J**) were all unchanged between groups. Similarly, senescence and cell cycle genes *Ankrd1* (**Figure 3.2K**) and *Cdkn1a* (**Figure 3.2L**) were also unchanged. Following these trends, all metabolism related genes involved in fatty acid oxidation and glucose metabolism were unchanged between genotypes, including *Pnpla2* (**Figure 3.2M**), *Acadm* (**Figure 3.2N**), *Cd36* (**Figure 3.2O**), *Pgc1a* (**Figure 3.2P**), *Dgat1* (**Figure 3.2Q**), *Pdk4* (**Figure 3.2R**), *Cpt1b* (**Figure 3.2S**) and *Slc27a1* (**Figure 3.2T**).

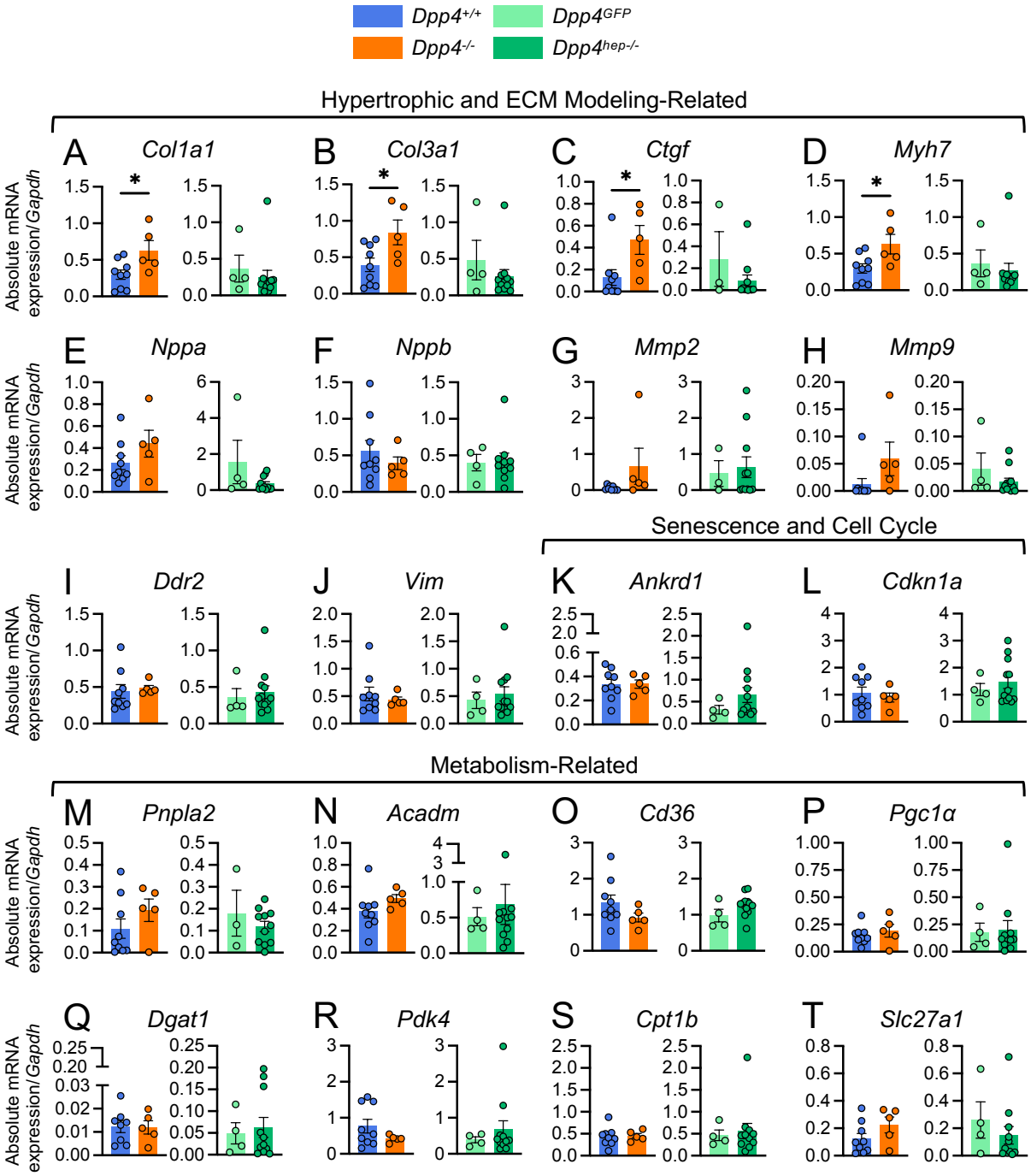

Figure 3.2: Fibrosis-related genes are upregulated in *Dpp4*$^{-/-}$ mice and unchanged in *Dpp4*$^{hep-/-}$ mice, but no differences were detected in senescence and metabolism-related genes. Ventricular mRNA abundance (relative to *Gapdh*) of hypertrophic and ECM modeling-related genes (**A**) *Col1a1*, (**B**) *Col3a1*, (**C**) *Ctgf*, (**D**) *Myh7*, (**E**) *Nppa*, (**F**) *Nppb*, (**G**) *Mmp2* (**H**) *Mmp9*, (**I**) *Ddr2* and (**J**) *Vim*. Senescence and cell cycle genes (**K**) *Ankrd1* and (**L**) *Cdkn1a*. Metabolism-related genes (**M**) *Pnpla2*, (**N**) *Acadm*, (**O**) *Cd36*, (**P**) *Pgc1α*, (**Q**) *Dgat1*, (**R**) *Pdk4*, (**S**) *Cpt1b* and (**T**) *Slc27a1*. Data are presented as the means ± SEM, analyzed by unpaired students t-test with Welch's correction, ns p<0.05, *p=0.01-0.05, **p=0.001-0.01.

3.5.3 Ventricular remodelling and systolic function are unchanged in *Dpp4*$^{-/-}$ and *Dpp4*$^{hep-/-}$ mice compared to respective controls

Immune and inflammation-related genes and associated pathway analysis were significantly reduced in ventricular tissue from *Dpp4*$^{hep-/-}$ mice. Additionally, *Col1a1* and *Col3a1* were also induced in *Dpp4*$^{-/-}$ mice, prompting us to perform echocardiography to assess gross remodeling and assess if molecular changes translated to a functional cardiac phenotype. Heart weight normalized to both total body weight, and tibia length were unchanged between groups. Similarly end diastolic and end systolic left ventricular mass were unchanged (**Table 3.2**). Interventricular septal thickness at diastole was trending downwards in *Dpp4*$^{hep-/-}$ mice and unchanged in *Dpp4*$^{-/-}$ mice, however at systole, there was no change. The left ventricular internal diameter was unchanged between genotypes at both diastole and systole, and the left ventricular posterior wall (LVPW) thickness was unchanged at diastole in both genotypes (**Table 3.2**). Interestingly, however, at systole, LVPW thickness significantly increased in *Dpp4*$^{-/-}$ mice, along with overall thickness, which were both unchanged in *Dpp4*$^{hep-/-}$ mice. These structural changes and altered immune and fibrosis molecular signatures, however, did not translate to altered systolic function, as left ventricular ejection fraction (LVEF), stroke volume (SV) and cardiac output (CO) were all unchanged (**Table 3.2**).

Table 3.2: Physiological and systolic echocardiographic analyses reveal no differences between genotypes and their controls. HW = heart weight, BW = body weight, TL = tibia length, EDLVM = end diastolic left ventricular mass, ESLVM = end systolic left ventricular mass, IVS = interventricular septal thickness, LVID = left ventricular internal diameter, LVPW = left ventricular posterior wall thickness, HR = heart rate, LVEF = ejection fraction, SV = stroke volume, CO = cardiac output, d = diastole, s = systole and bpm = beats per minute. Data are presented as the means ± SEM, analyzed by unpaired students t-test with Welch's correction, between genetic knockouts and respective controls (*Dpp4*$^{+/+}$ vs *Dpp4*$^{-/-}$ and *Dpp4*^{GFP} vs *Dpp4*$^{hep-/-}$), ns $p<0.05$, *$p=0.01-0.05$.

		***Dpp4*$^{+/+}$**	***Dpp4*$^{-/-}$**	***Dpp4*^{GFP}**	***Dpp4*$^{hep-/-}$**
HW/BW	mg/g	3.69 ± 0.21	3.9 ± 0.46	3.86 ± 0.23	3.44 ± 0.18
HW/TL	mg/mm	7.88 ± 0.55	9.16 ± 0.7	7.78 ± 0.47	8.29 ± 0.28
EDLVM	mg	111 ± 7.06	106.4 ± 10.74	105.33 ± 11.09	92.77 ± 3.14
ESLVM	mg	106 ± 7.29	104 ± 12	102 ± 11.37	94.44 ± 4.69
IVS,d	mm	1.08 ± 0.04	1.18 ± 0.06	1.09 ± 0.1	0.93 ± 0.03
IVS,s	mm	1.53 ± 0.05	1.64 ± 0.07	1.54 ± 0.16	1.35 ± 0.05
LVID,d	mm	4.21 ± 0.14	4.01 ± 0.32	4.07 ± 0.16	4.24 ± 0.1
LVID,s	mm	2.92 ± 0.18	2.54 ± 0.31	2.84 ± 0.13	2.91 ± 0.12
LVPW,d	mm	0.92 ± 0.04	0.98 ± 0.07	0.92 ± 0.06	0.87 ± 0.03
LVPW,s	mm	1.24 ± 0.06	1.46 ± 0.07 *	1.27 ± 0.09	1.17 ± 0.04
Thickening	mm	0.31 ± 0.04	0.47 ± 0.02 *	0.35 ± 0.03	0.29 ± 0.02
HR	bpm	481.61 ± 17.14	482.14 ± 12.8	516.83 ± 16.62	456.81 ± 20.63
LVEF	%	56.32 ± 4.12	58.21 ± 4.49	49.41 ± 4.08	50.61 ± 2.68
SV	uL	36.7 ± 2.32	37.12 ± 4.23	33.8 ± 4.87	33.81 ± 1.71
CO	mL/min	17.43 ± 1.17	17.61 ± 1.83	17.53 ± 2.35	15.2 ± 0.78

3.5.4 Strain and strain rate are unaltered between genotypes

We used 2D strain analysis, a more sensitive measure of systolic function[32], to identify sub-clinical left ventricular dysfunction. Endocardial global longitudinal strain (GLS) was unchanged between genotypes, however, at aortic valve closure (AVC) radial strain (RS) was significantly increased in *Dpp4*$^{-/-}$ mice, while longitudinal strain (LS) was significantly decreased in *Dpp4*$^{hep-/-}$ mice (**Table 3.3**). Consistently, radial strain rate at peak ejection (RSR at PE) was significantly increased in *Dpp4*$^{-/-}$ mice unchanged in *Dpp4*$^{hep-/-}$ mice, and no further changes were observed in longitudinal strain rate at peak ejection (LSR at PE) in either group. At systole, time-to-peak (TTP) RS was trending upwards in *Dpp4*$^{hep-/-}$ mice but unchanged in *Dpp4*$^{-/-}$ mice (**Table 3.3**). Additional systolic measurements, including RS, TTP RSR, RSR and TTP LS were all unchanged. LS however, was trending downwards in *Dpp4*$^{hep-/-}$ mice and unchanged in *Dpp4*$^{-/-}$ mice, but TTP LSR and LSR were unchanged in both genotypes. When averaged across 34 segments along the myocardium of the left ventricle, average diastolic radial strain (aDRS) was significantly decreased in *Dpp4*$^{hep-/-}$ mice and unchanged in *Dpp4*$^{-/-}$ mice, however, average diastolic longitudinal strain (aDLS), average diastolic radial and longitudinal strain rate were unchanged between genotypes (**Table 3.3**).

Table 3.3: Echocardiographic strain analysis in mice after 6-months of HFHC feeding, reveals no differences between genotypes. GLS = global longitudinal strain, RS = radial strain, LS = longitudinal strain, AVC = aortic valve closure, RSR = radial strain rate, LSR = longitudinal strain rate, PE = peak ejection, TTP = time-to-peak, a = average, DRS = diastolic radial strain, DLS = diastolic longitudinal strain, DRSR = diastolic radial strain rate, DLSR = diastolic longitudinal strain rate and n/a = not applicable. Data are presented as the means ± SEM, analyzed by unpaired students t-test with Welch's correction, between genetic knockouts and respective controls (*Dpp4*$^{+/+}$ vs *Dpp4*$^{-/-}$ and *Dpp4*^{GFP} vs *Dpp4*$^{hep-/-}$), ns p<0.05, *p=0.01-0.05, **p=0.001-0.01.

		***Dpp4*$^{+/+}$**	***Dpp4*$^{-/-}$**	***Dpp4*^{GFP}**	***Dpp4*$^{hep-/-}$**
GLS	%	-17.06 ± 1.8	-19.45 ± 1.4	-12.32 ± 3.25	-15.13 ± 1.12
RS at AVC	%	27.13 ± 2.95	38.38 ± 4.24 *	25.56 ± 2.84	25.71 ± 1.25
LS at AVC	%	-13.16 ± 2.46	-12.4 ± 3.77	-6.65 ± 3.42	-13.83 ± 1.38 *
RSR at PE	1/sec	5.88 ± 0.43	8.83 ± 1.08 *	6.84 ± 0.55	5.69 ± 0.47
LSR at PE	1/sec	-4.31 ± 0.79	-3.88 ± 0.91	-2.91 ± 0.53	-5.35 ± 0.77
TTP RS	ms	54.03 ± 1.9	57.2 ± 4.43	52.33 ± 2.2	60.83 ± 2.06
RS	%	31.77 ± 3.79	39.1 ± 4.15	27 ± 2.72	28.73 ± 1.65
TTP RSR	ms	24.62 ± 1.94	26 ± 2.84	29 ± 1.28	28.52 ± 2.54
RSR	1/sec	8.43 ± 0.83	9.6 ± 1.09	7.83 ± 0.08	7.53 ± 0.36
TTP LS	ms	55.09 ± 3.47	62.35 ± 9.88	61.04 ± 3.77	65.29 ± 4.3
LS	%	-14.58 ± 1.19	-14.06 ± 1.23	-11.05 ± 1.15	-14.36 ± 0.77
TTP LSR	ms	40.68 ± 3.46	50.72 ± 7.55	47.41 ± 1.95	57.25 ± 5.07
LSR	1/sec	-8.93 ± 0.68	-8.41 ± 0.89	-7.95 ± 0.32	-8.14 ± 0.52
aDRS	n/a	-0.8 ± 0.2	-0.71 ± 0.43	-0.29 ± 0.15	-1.6 ± 0.29 **
aDLS	n/a	1.1 ± 0.38	0.96 ± 0.8	0.64 ± 0.41	1.35 ± 0.3
aDRSR	1/sec	-10.27 ± 1.06	-12.99 ± 1.58	-9.08 ± 0.49	-10.58 ± 0.61
aDLSR	1/sec	4.81 ± 0.56	4.75 ± 1	3.92 ± 1.07	5.31 ± 0.83

3.5.5 Pulsed wave and tissue doppler echocardiography revealed no differences in *Dpp4*$^{-/-}$ and *Dpp4*$^{hep-/-}$ mice

In addition to strain analysis, we used pulsed wave and tissue doppler echocardiography to assess diastolic function further. Isovolumetric contraction and relaxation time were unchanged between genotypes. In line with this, mitral valve atrial contraction (A) and rapid filling (E) velocities were unchanged between genotypes. Similarly, mitral annular velocity during atrial contraction (A') and rapid filling (E') were also unchanged between genotypes. Further, the resulting ratios were all unchanged between genotypes, including E'/A', E/A and E/E'. However, there is a trend towards mild diastolic dysfunction in *Dpp4*$^{hep-/-}$ mice indicated by reduced E'/A' and E/A ratios compared to *Dpp4*^{GFP} control mice[33] (**Table 3.4**).

Table 3.4: Echocardiographic pulsed wave doppler and tissue doppler analysis reveals no differences between genotypes after 6-months of HFHC-feeding. A' = Tissue doppler mitral valve A' wave, E' = Tissue doppler mitral valve E' wave, IVCT = isovolumetric contraction time, IVRT = isovolumetric relaxation time, MV A = mitral valve A wave, MV E = mitral valve E wave, HR = heart rate, BPM = beats per minute and n/a = not applicable. Data are presented as the means ± SEM, analyzed by unpaired students t-test with Welch's correction, between genetic knockouts and respective controls (*Dpp4*$^{+/+}$ vs *Dpp4*$^{-/-}$ and *Dpp4*^{GFP} vs *Dpp4*$^{hep-/-}$), ns p<0.05.

		***Dpp4*$^{+/+}$**	***Dpp4*$^{-/-}$**	***Dpp4*^{GFP}**	***Dpp4*$^{hep-/-}$**
A'	mm/s	-24.93 ± 2.25	-26.19 ± 2.84	-25.74 ± 3.3	-32.91 ± 2.49
E'	mm/s	-33.36 ± 4.05	-37.42 ± 4.07	-39.44 ± 8.08	-40.12 ± 4.09
IVCT	ms	13.97 ± 0.93	14.24 ± 1.42	13.77 ± 0.58	15.87 ± 1.05
IVRT	ms	13.42 ± 0.88	15.31 ± 1.23	11.89 ± 0.69	13.84 ± 0.8
MV A	mm/s	609.12 ± 33.89	692.14 ± 96.9	617.59 ± 84.55	645.53 ± 27.56
MV E	mm/s	781.97 ± 16.35	874.03 ± 58.22	811.13 ± 45.03	777.54 ± 30.76
E'/A'		1.35 ± 0.11	1.43 ± 0.08	1.52 ± 0.17	1.24 ± 0.09
MV E/A		1.31 ± 0.07	1.25 ± 0.12	1.38 ± 0.19	1.21 ± 0.04
MV E/E'		25.86 ± 2.44	24.19 ± 2.62	22.62 ± 3.44	21.09 ± 2.11
HR	bpm	519.1 ± 16.95	517.2 ± 16.7	574.75 ± 12.37	499.72 ± 14.87

3.6 Discussion

Altered levels of several hepatokines like adropin[34], fetuin-A, fibroblast (FGF-21)[35], alpha-1-microglobulin[36] and selenoprotein P[37] have been implicated in CVD progression via disturbances in inflammation, fibrosis and adverse LV remodeling. DPP4 has been previously established as a hepatokine [18,25], however, its role in CVD progression remains elusive. Circulating DPP4 levels are significantly increased in mice and in humans in metabolic disease and obesity[17-19,38]. Importantly, hepatocyte-derived DPP4 has been identified as a pro-inflammatory peptide, while regulation of GLP-1 bioactivity and regulation of glucose has been ascribed to endothelial cell-derived DPP4[17]. Chronic inflammation and systemic disruption of metabolic homeostasis such as that observed in obesity and MASLD are established precursors to diastolic HF[39]. The present data demonstrate that elimination of *Dpp4* specifically in hepatocytes in aged, HFHC-fed mice significantly reduces immune-related genes (i.e. *Tnf*, *Il12b* and *Mcp-2* (*Ccl8*)) and associated pathways in ventricular tissue compared to their controls, $Dpp4^{GFP}$. This is not observed in $Dpp4^{-/-}$ mice compared to $Dpp4^{+/+}$ mice, which is consistent with previous reports in euglycemic $Dpp4^{-/-}$ mice after trans-aortic constriction (TAC) surgery, where markers of inflammation were significantly increased[40]. Similar to our findings, silencing hepatocyte specific *Dpp4* in diet induced obese (DIO) mice effectively suppressed visceral adipose tissue (VAT) inflammation identified by decreased *Il6*, *Mcp-1*/*Ccl2*, *Tnfa* and *Il1b* mRNA expression[18]. Our results are additionally supported by Varin *et. al.*[17] where mRNA expression of inflammatory cytokines (*Il1b*, *Il2*, *Il12b* and *Mcp-1*/*Ccl2*) was decreased in epididymal white adipose tissue in HFHC-fed $Dpp4^{hep-/-}$ mice. These results, collectively with our data, reveal a significant inflammatory role of hepatocyte derived

DPP4 in peripheral tissue, namely ventricular tissue.

Myocardial fibrosis and stiffening in diastolic HF are linked to increased mortality in clinical studies, making it an important therapeutic target[41]. We recently revealed increased hepatic fibrosis in aged, HFHC-fed *Dpp4*$^{-/-}$ mice, which was not observed in *Dpp4*$^{hep-/-}$ mice, suggesting an anti-fibrotic role for DPP4, but not that derived from hepatocytes[29]. Consistently, we report that hypertrophic and modeling-related genes, *Col1a1*, *Col3a1*, *Ctgf* and *Myh7* were significantly increased in *Dpp4*$^{-/-}$ mice compared to *Dpp4*$^{+/+}$, however there was no change in *Dpp4*$^{hep-/-}$ mice compared to *Dpp4*^{GFP} mice. Our findings are supported by others who use DPP4 inhibitors and systemic genetic elimination. Mulvihill *et. al.*[40] found that fibrosis was decreased in euglycemic *Dpp4*$^{-/-}$ mice, however, inducers and markers of fibrosis were elevated in aged, diabetic, HFD-fed DPP4 inhibitor (MK-0626) treated mice after TAC surgery. In contrast, Shigeta *et. al.*[42] demonstrated that both systemic genetic elimination and inhibition with vildagliptin reversed interstitial fibrosis and decreased connective tissue growth factor levels induced by streptozotocin induced diabetes after TAC surgery in male Fischer 344 rats. Our results are further contested by studies which use pharmacological inhibition rather than genetic elimination, generally in younger, euglycemic rodents. In 4-week-old C57BL6/J mice fed a high-fat/high-fructose western diet treated with MK-0626 for 16 weeks, inhibition ameliorated diet induced cardiac fibrosis and oxidant stress[43]. Vildagliptin exerted a similar cardioprotective phenotype in C57BL6/J mice after TAC surgery, both myocardial apoptosis and fibrosis were attenuated[44]. This improvement in fibrosis, or lack thereof, with pharmacological inhibition versus genetic elimination of *Dpp4* may be a result of its enzymatic and non-enzymatic capacity. DPP4 is reported to cleave collagen[45],

however, it has also been shown to bind to extracellular matrix (ECM) components, like fibronectin, and form complexes with fibroblast activation protein to degrade ECM[46-48]. Interestingly, linagliptin can block DPP4 and ECM component interactions, preventing signal transduction[49] and prevent fibroblast activation[50]. Systemic genetic elimination of *Dpp4* is hypothesized to prevent fibroblast activation and ECM degradation as previously described[40,42], this was not directly assessed in this study, however, we saw no changes in ECM remodelling-related genes (*Mmp2*, *Mmp9*, *Ddr2* and *Vim*). We also see no change in fibrosis in our $Dpp4^{hep-/-}$ mice, this may suggest that DPP4 from the liver, in aged, HFHC-fed mice, may be pro-fibrotic, and its genetic elimination is cardioprotective. Therefore, further investigation to elucidate organ and tissue specific DPP4 function are warranted.

Molecular changes like inflammation and fibrosis prevent the myocardium from relaxing properly, leading to concentric hypertrophy, inadequate ventricular filling, and less blood perfusion to the periphery[51]. In our study, we see only modest hypertrophy in our $Dpp4^{-/-}$ mice compared to $Dpp4^{+/+}$ mice, where both left ventricular posterior wall thickness, and overall thickening, are significantly increased with no differences in cardiac function like LVEF. This is not observed in our $Dpp4^{hep-/-}$ mice, however. Consistent with our findings, Shigeta *et. al.*[42] reported significantly increased LV hypertrophy via posterior wall thickness in $Dpp4^{-/-}$ mice after TAC surgery compared to controls, while cardiac function was unchanged. Similarly, Mulvihill *et. al.*[40] revealed that in aged, diabetic mice treated with MK-0626 possessed modest cardiac hypertrophy and impaired cardiac function.

3.7 Limitations

Left ventricular stiffness and inflexibility, preventing adequate relaxation during diastole is prevalent in patients with T2D and typically precedes systolic dysfunction[52]. We observed no improvements in diastolic function with systemic or hepatocyte specific *Dpp4* genetic elimination. The present study used HFHC feeding and age to facilitate cardiac dysfunction. However, this was not sufficient to induce a measurable phenotype, similar to previous studies that illustrate resilience among C57BL/6J mice[53]; the background genotype of the mice used in this study which develop liver disease rapidly on this diet[54,55]. Despite extensive lard-based HFD-feeding and saturated fat-rich diet feeding cardiac dysfunction was not observed. Further, high-fat feeding did result in cardiac hypertrophy, however, fibrosis and diastolic dysfunction were unchanged[53].

The use of diet-induced HF does not indicate whether *Dpp4* genetic elimination could preserve cardiac function. Future studies could use a surgical intervention, such as trans-aortic constriction, to induce pressure overload and uncover subtle functional changes otherwise not revealed in our less invasive protocol. Further, this study was not designed to completely illuminate the non-enzymatic role that DPP4 may have in diastolic HF. Future studies could employ *in vitro* binding assays with primary isolated cardiomyocytes and inflammatory and fibrotic binding partners like adenosine deaminase (ADA), caveolin-1 and fibrinogen.

Considering the lack of systolic and diastolic changes in our study, we could additionally employ stress echocardiography by administering dobutamine to mice. This has previously been identified as a technique in clinical and pre-clinical research that can reveal subtle changes in cardiac function which may otherwise remain

hidden[56]. Interestingly, in patients with ischemic CVD and preserved LV function, a single dose of sitagliptin (100 mg) significantly improved LVEF during a stress echo with dobutamine at rest, at peak stress and 30 minutes afterwards[57].

3.8 Conclusion

In summary, we have demonstrated that eliminating hepatocyte-derived *Dpp4* decreases immunological pathway expression in cardiac tissue, however, systemic elimination does not. Hypertrophy and modeling-related gene expression are significantly increased in *Dpp4*$^{-/-}$ mice, however, this is not observed in *Dpp4*$^{hep-/-}$ mice, compared to controls. Metabolism and senescence-related genes are unchanged in both genotypes, compared to their respective controls. Despite changes in inflammation and fibrosis, there were no changes in cardiac hypertrophy, systolic and diastolic function.

3.9 Acknowledgements

We would like to thank the Toronto Centre for Phenogenomics for plasma analysis. EEM is the guarantor of this work and, as such, had full access to all the data in the study and takes responsibility for the data's integrity and the data analysis's accuracy. The Canadian Institutes of Health Research (CIHR) supported this work (ARJ-162628, Project Grant 156136 and a Heart and Stroke National New Investigator award to EEM). NAT was supported by a UOHI endowment scholarship. BV was supported by a CIHR postdoctoral fellowship.

Supplemental Table 3.1: List of qRT-PCR primers, from Applied Biosystems.

Oligonucleotides	Identifier
Collagen, type I, alpha 1 (*Col1a1*)	Mm00801666_g1
Collagen, type I3 alpha 1 (*Col1a1*)	Mm00802331_m1
Connective tissue growth factor (*Ctgf*)	Mm01192931_g1
Myosin, heavy polypeptide 7, cardiac muscle, beta (*Myh7*)	Mm00600555_m1
Natriuretic peptide type A (*Nppa*)	Mm01255747_g1
Natriuretic peptide type B (*Nppb*)	Mm01255770_g1
Matrix metallopeptidase 2 (Mmp2)	Mm00439498_m1
Matrix metallopeptidase 9 (*Mmp9*)	Mm01240562_g1
Discoidin domain receptor family, member 2 (*Ddr2*)	Mm00445614_m1
Vimentin (*Vim*)	Mm01333430_m1
Ankyrin repeat domain 1 (cardiac muscle) (*Ankrd1*)	Mm00496512_m1
Cyclin-dependent kinase inhibitor 1A (P21) (Cdkn1a)	Mm00432448_m1
Patatin-like phospholipase domain containing 2 (*Pnpla2*)	Mm00503040_m1
Acyl-Coenzyme A dehydrogenase, medium chain (*Acadm*)	Mm01323360_g1
CD36 antigen (*Cd36*)	Mm00432403_m1
Peroxisome proliferative activated receptor, gamma, coactivator 1 alpha (*Pgc1*α)	Mm01208835_m1
Diacylglycerol O-acyltransferase 1 (*Dgat1*)	Mm00515643_m1
Pyruvate dehydrogenase kinase, isoenzyme 4 (*Pdk4*)	Mm01166879_m1
Carnitine palmitoyltransferase 1b, muscle (*Cpt1b*)	Mm00487191_g1
Solute carrier family 27 (fatty acid transporter), member 1 (*Slc27a1*)	Mm00449511_m1

3.10 References

1. Sarafidis PA, Nilsson PM. The metabolic syndrome: a glance at its history. *J Hypertens.* 2006;24(4):621-626.
2. Rinella ME, Lazarus JV, Ratziu V, et al. A multisociety Delphi consensus statement on new fatty liver disease nomenclature. *J Hepatol.* 2023;79(6):1542-1556.
3. VanWagner LB, Wilcox JE, Colangelo LA, et al. Association of nonalcoholic fatty liver disease with subclinical myocardial remodeling and dysfunction: A population-based study. *Hepatology.* 2015;62(3):773-783.
4. Bonci E, Chiesa C, Versacci P, Anania C, Silvestri L, Pacifico L. Association of Nonalcoholic Fatty Liver Disease with Subclinical Cardiovascular Changes: A Systematic Review and Meta-Analysis. *Biomed Res Int.* 2015;2015:213737.
5. Targher G, Day CP, Bonora E. Risk of cardiovascular disease in patients with nonalcoholic fatty liver disease. *N Engl J Med.* 2010;363(14):1341-1350.
6. Sinn DH, Kang D, Chang Y, et al. Non-alcoholic fatty liver disease and progression of coronary artery calcium score: a retrospective cohort study. *Gut.* 2017;66(2):323-329.
7. Cakir E, Ozbek M, Colak N, Cakal E, Delibasi T. Is NAFLD an independent risk factor for increased IMT in T2DM? *Minerva Endocrinol.* 2012;37(2):187-193.
8. Anstee QM, Mantovani A, Tilg H, Targher G. Risk of cardiomyopathy and cardiac arrhythmias in patients with nonalcoholic fatty liver disease. *Nat Rev Gastroenterol Hepatol.* 2018;15(7):425-439.
9. Francque S. The Liver and the Cardiovascular System: Two of a Kind? *J Am Heart Assoc.* 2021;10(8):e020286.
10. Francque SM, van der Graaff D, Kwanten WJ. Non-alcoholic fatty liver disease and cardiovascular risk: Pathophysiological mechanisms and implications. *J Hepatol.* 2016;65(2):425-443.
11. Dusi V, Ghidoni A, Ravera A, De Ferrari GM, Calvillo L. Chemokines and Heart Disease: A Network Connecting Cardiovascular Biology to Immune and Autonomic Nervous Systems. *Mediators Inflamm.* 2016;2016:5902947.
12. Harrison SA, Bedossa P, Guy CD, et al. A Phase 3, Randomized, Controlled Trial of Resmetirom in NASH with Liver Fibrosis. *N Engl J Med.* 2024;390(6):497-509.
13. Fabbrini E, Sullivan S, Klein S. Obesity and nonalcoholic fatty liver disease: biochemical, metabolic, and clinical implications. *Hepatology.* 2010;51(2):679-689.
14. Perry RJ, Samuel VT, Petersen KF, Shulman GI. The role of hepatic lipids in hepatic insulin resistance and type 2 diabetes. *Nature.* 2014;510(7503):84-91.
15. Ren Y, Zhao H, Yin C, et al. Adipokines, Hepatokines and Myokines: Focus on Their Role and Molecular Mechanisms in Adipose Tissue Inflammation. *Front Endocrinol (Lausanne).* 2022;13:873699.
16. Priest C, Tontonoz P. Inter-organ cross-talk in metabolic syndrome. *Nat Metab.* 2019;1(12):1177-1188.
17. Varin EM, Mulvihill EE, Beaudry JL, et al. Circulating Levels of Soluble Dipeptidyl Peptidase-4 Are Dissociated from Inflammation and Induced by Enzymatic DPP4 Inhibition. *Cell Metab.* 2019;29(2):320-334 e325.

18. Ghorpade DS, Ozcan L, Zheng Z, et al. Hepatocyte-secreted DPP4 in obesity promotes adipose inflammation and insulin resistance. *Nature.* 2018;555(7698):673-677.
19. Lamers D, Famulla S, Wronkowitz N, et al. Dipeptidyl peptidase 4 is a novel adipokine potentially linking obesity to the metabolic syndrome. *Diabetes.* 2011;60(7):1917-1925.
20. Rohrborn D, Eckel J, Sell H. Shedding of dipeptidyl peptidase 4 is mediated by metalloproteases and up-regulated by hypoxia in human adipocytes and smooth muscle cells. *FEBS Lett.* 2014;588(21):3870-3877.
21. Mentlein R, Gallwitz B, Schmidt WE. Dipeptidyl-peptidase IV hydrolyses gastric inhibitory polypeptide, glucagon-like peptide-1(7-36)amide, peptide histidine methionine and is responsible for their degradation in human serum. *Eur J Biochem.* 1993;214(3):829-835.
22. Mentlein R. Dipeptidyl-peptidase IV (CD26)--role in the inactivation of regulatory peptides. *Regul Pept.* 1999;85(1):9-24.
23. Lambeir AM, Durinx C, Scharpe S, De Meester I. Dipeptidyl-peptidase IV from bench to bedside: an update on structural properties, functions, and clinical aspects of the enzyme DPP IV. *Crit Rev Clin Lab Sci.* 2003;40(3):209-294.
24. Trzaskalski NA, Vulesevic B, Nguyen MA, et al. Hepatocyte-derived DPP4 regulates portal GLP-1 bioactivity, glucose production, and its absence alters liver disease progression. *JCI Insight.* 2022.
25. Baumeier C, Schluter L, Saussenthaler S, et al. Elevated hepatic DPP4 activity promotes insulin resistance and non-alcoholic fatty liver disease. *Mol Metab.* 2017;6(10):1254-1263.
26. Gorgens SW, Jahn-Hofmann K, Bangari D, et al. A siRNA mediated hepatic dpp4 knockdown affects lipid, but not glucose metabolism in diabetic mice. *PLoS One.* 2019;14(12):e0225835.
27. Marguet D, Baggio L, Kobayashi T, et al. Enhanced insulin secretion and improved glucose tolerance in mice lacking CD26. *Proc Natl Acad Sci U S A.* 2000;97(12):6874-6879.
28. Mulvihill EE, Varin EM, Gladanac B, et al. Cellular Sites and Mechanisms Linking Reduction of Dipeptidyl Peptidase-4 Activity to Control of Incretin Hormone Action and Glucose Homeostasis. *Cell Metab.* 2017;25(1):152-165.
29. Trzaskalski NA, Vulesevic B, Nguyen MA, et al. Hepatocyte-derived DPP4 regulates portal GLP-1 bioactivity, modulates glucose production, and when absent influences NAFLD progression. *JCI Insight.* 2023;8(2).
30. Metsalu T, Vilo J. ClustVis: a web tool for visualizing clustering of multivariate data using Principal Component Analysis and heatmap. *Nucleic Acids Res.* 2015;43(W1):W566-570.
31. Tanacli R, Hashemi D, Lapinskas T, et al. Range Variability in CMR Feature Tracking Multilayer Strain across Different Stages of Heart Failure. *Sci Rep.* 2019;9(1):16478.
32. Kalam K, Otahal P, Marwick TH. Prognostic implications of global LV dysfunction: a systematic review and meta-analysis of global longitudinal strain and ejection fraction. *Heart.* 2014;100(21):1673-1680.

33. Gopal K, Al Batran R, Altamimi TR, et al. FoxO1 inhibition alleviates type 2 diabetes-related diastolic dysfunction by increasing myocardial pyruvate dehydrogenase activity. *Cell Rep.* 2021;35(1):108935.
34. Wu L, Fang J, Chen L, et al. Low serum adropin is associated with coronary atherosclerosis in type 2 diabetic and non-diabetic patients. *Clin Chem Lab Med.* 2014;52(5):751-758.
35. Chou RH, Huang PH, Hsu CY, et al. Circulating Fibroblast Growth Factor 21 is Associated with Diastolic Dysfunction in Heart Failure Patients with Preserved Ejection Fraction. *Sci Rep.* 2016;6:33953.
36. Hakuno D, Kimura M, Ito S, et al. Hepatokine alpha1-Microglobulin Signaling Exacerbates Inflammation and Disturbs Fibrotic Repair in Mouse Myocardial Infarction. *Sci Rep.* 2018;8(1):16749.
37. Takeishi R, Misaka T, Ichijo Y, et al. Increases in Hepatokine Selenoprotein P Levels Are Associated With Hepatic Hypoperfusion and Predict Adverse Prognosis in Patients With Heart Failure. *J Am Heart Assoc.* 2022;11(11):e024901.
38. Sell H, Bluher M, Kloting N, et al. Adipose dipeptidyl peptidase-4 and obesity: correlation with insulin resistance and depot-specific release from adipose tissue in vivo and in vitro. *Diabetes Care.* 2013;36(12):4083-4090.
39. Shulman GI. Ectopic fat in insulin resistance, dyslipidemia, and cardiometabolic disease. *N Engl J Med.* 2014;371(23):2237-2238.
40. Mulvihill EE, Varin EM, Ussher JR, et al. Inhibition of Dipeptidyl Peptidase-4 Impairs Ventricular Function and Promotes Cardiac Fibrosis in High Fat-Fed Diabetic Mice. *Diabetes.* 2016;65(3):742-754.
41. Garg P, Assadi H, Jones R, et al. Left ventricular fibrosis and hypertrophy are associated with mortality in heart failure with preserved ejection fraction. *Sci Rep.* 2021;11(1):617.
42. Shigeta T, Aoyama M, Bando YK, et al. Dipeptidyl peptidase-4 modulates left ventricular dysfunction in chronic heart failure via angiogenesis-dependent and -independent actions. *Circulation.* 2012;126(15):1838-1851.
43. Bostick B, Habibi J, Ma L, et al. Dipeptidyl peptidase inhibition prevents diastolic dysfunction and reduces myocardial fibrosis in a mouse model of Western diet induced obesity. *Metabolism.* 2014;63(8):1000-1011.
44. Takahashi A, Asakura M, Ito S, et al. Dipeptidyl-peptidase IV inhibition improves pathophysiology of heart failure and increases survival rate in pressure-overloaded mice. *Am J Physiol Heart Circ Physiol.* 2013;304(10):H1361-1369.
45. Bermpohl F, Loster K, Reutter W, Baum O. Rat dipeptidyl peptidase IV (DPP IV) exhibits endopeptidase activity with specificity for denatured fibrillar collagens. *FEBS Lett.* 1998;428(3):152-156.
46. Ghersi G, Zhao Q, Salamone M, Yeh Y, Zucker S, Chen WT. The protease complex consisting of dipeptidyl peptidase IV and seprase plays a role in the migration and invasion of human endothelial cells in collagenous matrices. *Cancer Res.* 2006;66(9):4652-4661.
47. Ghersi G, Dong H, Goldstein LA, et al. Regulation of fibroblast migration on collagenous matrix by a cell surface peptidase complex. *J Biol Chem.* 2002;277(32):29231-29241.

48. Ohm B, Moneke I, Jungraithmayr W. Targeting cluster of differentiation 26 / dipeptidyl peptidase 4 (CD26/DPP4) in organ fibrosis. *Br J Pharmacol.* 2022.
49. Hasan AA, Hocher B. Role of soluble and membrane-bound dipeptidyl peptidase-4 in diabetic nephropathy. *J Mol Endocrinol.* 2017;59(1):R1-R10.
50. Lee SY, Wu ST, Liang YJ, et al. Soluble Dipeptidyl Peptidase-4 Induces Fibroblast Activation Through Proteinase-Activated Receptor-2. *Front Pharmacol.* 2020;11:552818.
51. Phan TT, Shivu GN, Abozguia K, Sanderson JE, Frenneaux M. The pathophysiology of heart failure with preserved ejection fraction: from molecular mechanisms to exercise haemodynamics. *Int J Cardiol.* 2012;158(3):337-343.
52. van Heerebeek L, Hamdani N, Handoko ML, et al. Diastolic stiffness of the failing diabetic heart: importance of fibrosis, advanced glycation end products, and myocyte resting tension. *Circulation.* 2008;117(1):43-51.
53. Tadinada SM, Weatherford ET, Collins GV, et al. Functional resilience of C57BL/6J mouse heart to dietary fat overload. *Am J Physiol Heart Circ Physiol.* 2021;321(5):H850-H864.
54. Eccleston HB, Andringa KK, Betancourt AM, et al. Chronic exposure to a high-fat diet induces hepatic steatosis, impairs nitric oxide bioavailability, and modifies the mitochondrial proteome in mice. *Antioxid Redox Signal.* 2011;15(2):447-459.
55. Savard C, Tartaglione EV, Kuver R, et al. Synergistic interaction of dietary cholesterol and dietary fat in inducing experimental steatohepatitis. *Hepatology.* 2013;57(1):81-92.
56. Settelmeier S, Rassaf T, Hendgen-Cotta UB. Revealing Subtle Changes in Cardiac Function using Transthoracic Dobutamine Stress Echocardiography in Mice. *J Vis Exp.* 2021(168).
57. Read PA, Khan FZ, Heck PM, Hoole SP, Dutka DP. DPP-4 inhibition by sitagliptin improves the myocardial response to dobutamine stress and mitigates stunning in a pilot study of patients with coronary artery disease. *Circ Cardiovasc Imaging.* 2010;3(2):195-201.

4 Reduced DPP4 activity in combination metformin and sitagliptin treated *Dpp4*$^{hep-/-}$ mice improves left ventricular ejection fraction after LAD-ligation

Authors: **Natasha A. Trzaskalski**, Jessica Hursti, Natasha Jeraj, Branka Vulesevic & Erin E. Mulvihill

4.1 Author Contributions

Conceptualization: EEM; Methodology: EEM; Formal Analysis: NAT, JH; Investigation: NAT, JH, NJ, BV, EEM; Resources: EEM; Writing – Original Draft: NAT, EEM; Writing – Review and Editing: NAT, EEM; Supervision: EEM; Project Administration: EEM; Funding Acquisition: EEM.

4.2 Abstract

Background: Currently, there are 11.7 million Canadians living with diabetes or prediabetes, and cardiovascular events, including ischemic heart disease, are a major cause of death. Dipeptidyl peptidase-4 (DPP4) inhibitors (DPP4i's) are a safe and effective therapy for the treatment of type 2 diabetes (T2D) which inhibit the enzymatic action of DPP4 to prevent degradation of the incretin hormones. Meta-regression analysis of DPP4 inhibitor cardiovascular endpoint trials demonstrated combination therapy with metformin was cardioprotective. Interestingly, DPP4i treatment increases circulating levels of DPP4 protein. Preclinical studies suggest metformin reduces DPP4 shedding from organ depots into circulation, while concomitantly increasing levels of active glucagon-like peptide-1 (GLP-1). These data collectively demonstrate a role for enzymatic and non-enzymatic DPP4 in cardiovascular disease progression, however, how this happens, remains to be revealed.

Hypothesis: Metformin reduces DPP4i-induced increases in circulating DPP4 protein which effectively reduces inflammation and ischemic heart disease progression. Further, metformin will reduce circulating DPP4 protein to a greater extent in *Dpp4*$^{hep-/-}$ mice, compared to *Dpp4*$^{EC-/-}$, as previous literature revealed endothelial cells as the main cellular target of metformin.

Methods and Results: Twenty-five week old wildtype (*Dpp4*$^{+/+}$), whole-body DPP4 knockout (*Dpp4*$^{-/-}$), mice containing LoxP sites in *Dpp4* injected with AAV8 containing a hepatocyte-specific promoter driving Cre (*Dpp4*$^{hep-/-}$ mice) or control (*Dpp4*^{GFP} mice), and endothelial cell-specific knockout (*Dpp4*$^{EC-/-}$) and control (*Dpp4*$^{EC+/+}$) mice were fed a high-fat high-cholesterol diet and treated with sitagliptin (DPP4 inhibitor; 5mg/kg/day), metformin (200 mg/kg/day), or combination therapy. Mice were then

subjected to left anterior descending ligation surgery to induce a permanent ischemic injury. Prior to, and after surgery, we performed echocardiography to assess cardiac function and myocardial kinesis. Both before and after LAD-ligation, LVEF was improved in *Dpp4*$^{hep-/-}$ mice with DT treatment, while myocardial kinesis was maintained in *Dpp4*$^{EC-/-}$ mice, compared to respective controls. Interestingly, DPP4 activity and soluble protein levels were dissociated; DPP4 activity dropped 1-week after surgery and rose again at endpoint, while protein levels continued to increase throughout the experiment. Further, our results revealed that DPP4 is dynamically regulated; hepatocytes contribute to the active circulating DPP4 pool, while endothelial cells contribute to overall protein levels.

Conclusions: With DT treatment, *Dpp4*$^{hep-/-}$ mice experienced improved cardiac function before and after LAD-ligation compared to *Dpp4*^{GFP} mice. Further, myocardial kinesis was improved in *Dpp4*$^{EC-/-}$ mice. These data suggest that metformin and DPP4 inhibitors are cardioprotective in the absence of hepatocyte-derived DPP4. Future studies will investigate the molecular basis of this functional improvement, primarily focusing on the cardioprotective actions of active GLP-1.

4.3 Introduction

Given the dramatic increase in cardiovascular disease (CVD) risk in patients with type 2 diabetes (T2D), drugs developed to treat hyperglycemia must be proven to have cardiovascular safety[1]. The Food and Drug Administration (FDA) has therefore imposed recommendations that all drug therapies for the treatment of T2D approved after 2008 undergo extensive cardiovascular characterization evaluating major cardiovascular endpoints[2]. Metformin is the first-line glucose-lowering therapy prescribed, which reduces hepatic glucose production[3], increases insulin sensitivity[4] and potentiates glucagon-like polypeptide 1 (GLP-1) secretion[5-7]. Dipeptidyl peptidase-4 (DPP4) inhibitors (DPP4i's) are a typical second-line therapy[8] that effectively prevent cleavage and inactivation of the incretin hormones GLP-1 and glucose-dependent insulinotropic polypeptide (GIP) so they may interact with their respective receptors in the pancreas to regulate post-prandial insulin secretion and glucagon secretion[9,10]. However, DPP4 is multifaceted; endothelial cell-derived DPP4 is implicated in glucose regulation while hepatocyte-derived DPP4 appears to be pro-inflammatory affecting both local and peripheral tissue[11-13]. To date, only systemic genetic elimination has been investigated in CVD, which reveals cardioprotection with genetic ablation of *Dpp4* in mice and rats[14-17]. Further, pharmaceutical DPP4 inhibition has also demonstrated cardioprotection in preclinical studies in young mice, however this is not sustained in aged mice[14-16,18].

Cardiovascular outcome trials (CVOT) of DPP4i's have reported neutral effect, in major adverse cardiovascular events (MACE)[19]. However, a meta-analysis of three DPP4i CVOT's revealed prevalent metformin use was associated with a favorable trend towards cardioprotection, or a reduction in MACE when treated in combination

with a DPP4i (HR 0.92)[20]. Notably, circulating, soluble DPP4 (sDPP4) and DPP4 activity is significantly increased in individuals with T2D and reduced with metformin use[21,22]. Since metformin does not directly inhibit enzymatic DPP4 activity, metformin associated reductions have instead been credited to reduced total sDPP4 levels[21,23,24].

Baggio *et. al.*[25] determined metformin reduces circulating levels of DPP4 in combination with DPP4i's in mice. However, this was not recapitulated in humans, where despite significant DPP4 inhibition, protein levels were unchanged. Dual therapy (DT) with sitagliptin reduced circulating DPP4 levels significantly compared to sitagliptin alone, specifically bone marrow-derived DPP4, suggesting this compartment is dynamically regulated by DPP4i's[25]. Further, when *Dpp4* was selectively genetically eliminated in hematopoietic and endothelial cells (*Dpp4*$^{EC-/-}$), treatment with sitagliptin reduced basal DPP4 activity and protein levels compared to wildtype (WT) controls[25]. After *Dpp4*$^{EC-/-}$ mice received a bone marrow transplant from WT mice, this decrease was attenuated[25]. In addition, recent data shows upregulation of circulating levels of sDPP4 after administration of a DPP4i. Namely, endothelial cells are the main contributor of sDPP4, as *Dpp4*$^{EC-/-}$ mice experience a significant decrease in enzyme concentration which is not increased with DPP4i's[11]. These studies collectively demonstrate a complex relationship between sDPP4, DPP4 activity and concomitant DPP4i and metformin use. However, the molecular target of these pharmaceuticals and their CV benefit, namely in *Dpp4* genetic knockout models, has yet to be fully elucidated.

4.4 Methods

4.4.1 Animals

Studies were performed according to protocols approved by the University of Ottawa Animal Care Committee and in accordance with guidelines of the Canadian Council on Animal Care. Animals were cared for in accordance with the Canadian Guide for the Care and Use of Laboratory animals (CCAC). All experimental procedures were approved under AUP# 2909 and AUP# 2029 by the University of Ottawa Animal Care and Veterinary Service. Male mice were housed under a 12-h light/dark cycle and maintained on standard laboratory diet (SLD, 22% kcal from fat, 55% kcal from carbohydrates, 23% kcal from protein, 0% cholesterol; 2019, Envigo) until experimental use. Whole body *Dpp4*$^{-/-}$ mice, on a C57BL6 background, have been described[26,27]. To generate *Dpp4*$^{hep-/-}$ *mice*, 21-week-old *Dpp4*$^{flox/flox}$ mice were *i.v.* injected with 1.5x10^{11}GC/mouse of AAV8.TBG.pi.egfp.wpre.bgh (AAV-GFP; control virus, #105535-AAV8) or AAV8.TBG.PI.CRE.rBG (AAV-Cre; #107787-AAV8) prior to the onset of HFHC diet feeding. AAV constructs were obtained from the University of Pennsylvania Vector Core Lab as a generous gift from James M. Wilson (Perelman School of Medicine, University of Pennsylvania, Philadelphia, PA). B6.Cg-Tg(Tek-cre) 1Ywa/J mice were obtained from The Jackson Laboratory (Strain #: 008863, RRID: IMSR_JAX:008863) and bred with *Dpp4*$^{flox/flox}$ to generate *Dpp4*$^{EC-/-}$ mice.

4.4.2 Pig Heart Resection and *Ex Vivo* Processing

The pigs in this study were large domestic animals (Yorkshire/Landrace/Duroc crossbreed) acquired from Panmure Farms at approximately 3 months of age. Pigs were intubated under general anesthesia and maintained on a ventilator. An incision

was made at the third and fourth intercostal space and the ribs were retracted to reveal the heart. The pericardium was dissected, and the aorta and pulmonary vein were cross clamped. The heart was excised and perfused with a peristaltic pump using cold 1X PBS, *ex vivo*, for approximately 10 minutes. The heart was subsequently dissected, and tissue was flash frozen with liquid nitrogen and stored at -80°C.

4.4.3 Mouse Diets and Drug Treatments

At 25 weeks of age, mice started on a high fat, high cholesterol (HFHC; 42% kcal from fat, 42.7% kcal from carbohydrates, 15.2% kcal from protein, 0.2% weight from cholesterol; TD.88137, Envigo) diet ad libitum. After 6 weeks, at 31 weeks of age, mice were stratified and weight matched into one of four treatment groups; water as the control, sitagliptin (5 mg/kg/day; Abcam, Biovision, ab142101), metformin (hydrochloride) (200 mg/kg/day; Cayman Chemical, 13118) and DT (sitagliptin 5 mg/kg/day + metformin 200 mg/kg/day). Drugs were administered via drinking water in opaque water bottles and changed twice a week. Mice were weighed every week and dosages were adjusted as necessary based on weight gain.

4.4.4 Left Anterior Descending (LAD)-Ligation Surgery

LAD-ligation was performed as previously described[28]. Briefly, slow-release buprenorphine (1.2 mg/kg) was administered prior to surgery. Mice (35 weeks old) were anesthetized with 2-3% isoflurane and intubated with an endotracheal tube and ventilation was maintained at 200 breaths/min using a small animal ventilator and pure oxygen. At the level of the third and fourth intercostal space, an incision was made, and the ribs are retracted, at which point the pericardium is dissected and the left ventricle (LV) is exposed. An 8-0 nylon suture was passed under the LAD coronary

artery mid-way down the LV and tied off to produce an infarct. The chest was closed with a 6-0 visorb suture using a purse-string suture. During recovery mice were provided with supplemental heat and allowed to self-extubate. Further, mice received supplemental oxygen and postoperative analgesia (buprenorphine, 0.5 mg/kg/ip). Successful LAD-ligation was determined via echocardiography where mice were excluded from further analysis if the difference from baseline to post-MI was <10%.

4.4.5 Echocardiography Image Acquisition

Echocardiographic images were acquired as previously described[28] using the Vevo3100 high-frequency small animal ultrasound system using the MX400 linear array transducer (FUJIFILM VisualSonics, Toronto, Canada). Images were taken at baseline prior to LAD-ligation and 4 weeks post-surgery using a parasternal long axis (PSLAX) 2D B-mode approach. Mice were maintained on isoflurane (3-4%) for the duration of the imaging, body temperature was monitored via rectal probe and ECG was obtained via 4-lead ECG needle electrodes (Scintica Instrumentation Inc., 380-0002-02).

4.4.6 Echocardiographic Functional Analysis and Infarct Size Quantification

Manual LV contours were completed by tracing the endocardium at end-systole and end-diastole using the Vevo Lab LV trace function as previously described[28]. Infarct size quantification was completed using the manual distance function. At end-diastole, the endocardium was traced starting and ending at the aortic root and ventricle junction and defined as the Total Endocardial Segment. Tracing was repeated on the portion of the endocardium without movement or contractility (akinetic length), or with reduced movement or contractility (hypokinetic length). The akinetic and hypokinetic length was presented as a percentage, calculated as:

$$\text{Akinetic or Hypokinetic Length (\%)} = \frac{\text{Akinetic/Hypokinetic Segment (mm)}}{\text{Total Endocardial Length (mm)}} \times 100$$

4.4.7 Blood and Tissue Collection

Pre- and post- surgical tail vein blood samples were collected in EDTA-coated capillary microvette tubes. Terminal blood samples were obtained via cardiac puncture after sacrifice with CO_2 inhalation and collected in 1.5 mL micro-centrifuge tubes with 25 mM EDTA. DPP4 activity was assessed using fluorometric assay (substrate: 10mM H-Gly-Pro-AMC HBr, Bachem cat. #I-1225, standard: AMC, Bachem cat. #Q-1025). DPP4 protein (sDPP4) level was measured using DPPIV/CD26 DuoSet ELISA kit (DY954; R&D System) following the manufacturer's instructions. Plasma GDF-15 was assessed to evaluate metformin action using GDF-15 DuoSet ELISA kit (DY6385; R&D Systems) following the manufacturer's instructions. Chemokines and cytokines were also assessed using Mesoscale kit V-Plex® Proinflammatory Panel 1 (K15048D).

4.4.8 RNA isolation, cDNA and qRT-PCR

Frozen mouse liver, ventricular tissue and pig heart tissue were homogenized with TriReagent (Sigma Aldrich, cat# T9424) using a TissueLyser II system (Qiagen). Total RNA was extracted using manufacturer's protocol and reverse transcription was performed with the Applied Biosystems™ High-Capacity cDNA Reverse Transcription kit (cat# 4368813). cDNA was then used to assess mRNA expression by qRT-PCR (QuantStudio 5 System, Thermo Fisher Scientific) with TaqMan Fast Advanced Master Mix (Thermo Fisher Scientific, 4444557) and TaqMan Gene Expression Assays (Thermo Fisher Scientific). The specific gene expression assays used are listed (**Supplemental Table 4.1**). Quantification of transcript levels was performed by

the standard curve method, and expression levels for each gene were normalized to *Actb* (β-actin).

4.4.9 Statistical Analysis

All data were plotted and statistically analyzed using GraphPad Prism (version 10.1.1). Data are expressed as mean ± standard error of the mean (SEM). Statistical significance is defined as $P<0.05$ between groups.

4.5 Results

4.5.1 DPP4 in porcine hearts is associated with endothelial cells and increases in the infarct in murine hearts

We, and others, have previously reported that hepatocyte-derived DPP4 is a pro-inflammatory hepatokine while endothelial cell-derived DPP4 is glucoregulatory[11-13,29]. We explored DPP4 activity and mRNA expression in individual parts of a pig heart and found that DPP4 activity (**Figure 4.1A**) associated with *Pecam-1* mRNA expression, a marker of endothelial cells (**Figure 4.1B**), suggesting endothelial cell derived DPP4 may be directly present in the heart, as expression in cardiomyocytes is very low or absent. We also confirmed this finding by probing the single cell transcriptomics of the heart via the Tabula Muris[30], which showed increased *Dpp4* expression in endocardial cells, specialized endothelial cells of the heart[31]. Additionally, we evaluated regulation in response to injury and found increased DPP4 activity in the infarcted and peri-infarcted region in murine hearts post-MI up to 7 days. DPP4 activity was increased significantly from 1 to 3 days post-MI in the infarct region, however, at 3 days was significantly higher than activity in the peri-infarcted region (**Figure 4.1C**). The infarcted region upon tissue collection was defined as the

myocardium that was thin and white, while the peri-infarct was approximately 2-3 mm in thickness, incorporating the transition of the infarct. Interestingly there was a modest trend for increased liver DPP4 activity 1 to 7 days post-MI (**Figure 4.1D**). Additionally, we assessed mRNA expression of *Dpp4* and its CV-related substrates prior to, and after MI surgery. *Dpp4* expression decreased from baseline to 3 days post-MI, in the peri-infarct region (**Figure 4.2A**). In contrast, *Ccl2* (*Mcp-1*; **Figure 4.2B**)[16,32] and *Cxcl10* (*Ip-10*; **Figure 4.2C**)[33] mRNA expression increased from baseline to 3 days post-MI in the infarct and peri-infarct regions, and decreased again after 7 days, especially *Cxcl10* expression. However, *Ccl5* (*RANTES*; **Figure 4.2D**)[34] and *Ccl11* (*Eotaxin;* **Figure 4.2E**)[35] expression followed a similar trend to *Dpp4*, decreasing 3 days post-MI compared to baseline, while *Cxcl12* (*Sdf-1*)[15,36,37] expression, increased in the infarcted region 7 days post-MI (**Figure 4.2F**). Collectively, these data ultimately prompted us to further our investigation of the cardioprotective effects of DT in mice post-MI, however, with hepatocyte- and endothelial cell-specific *Dpp4* genetic ablation.

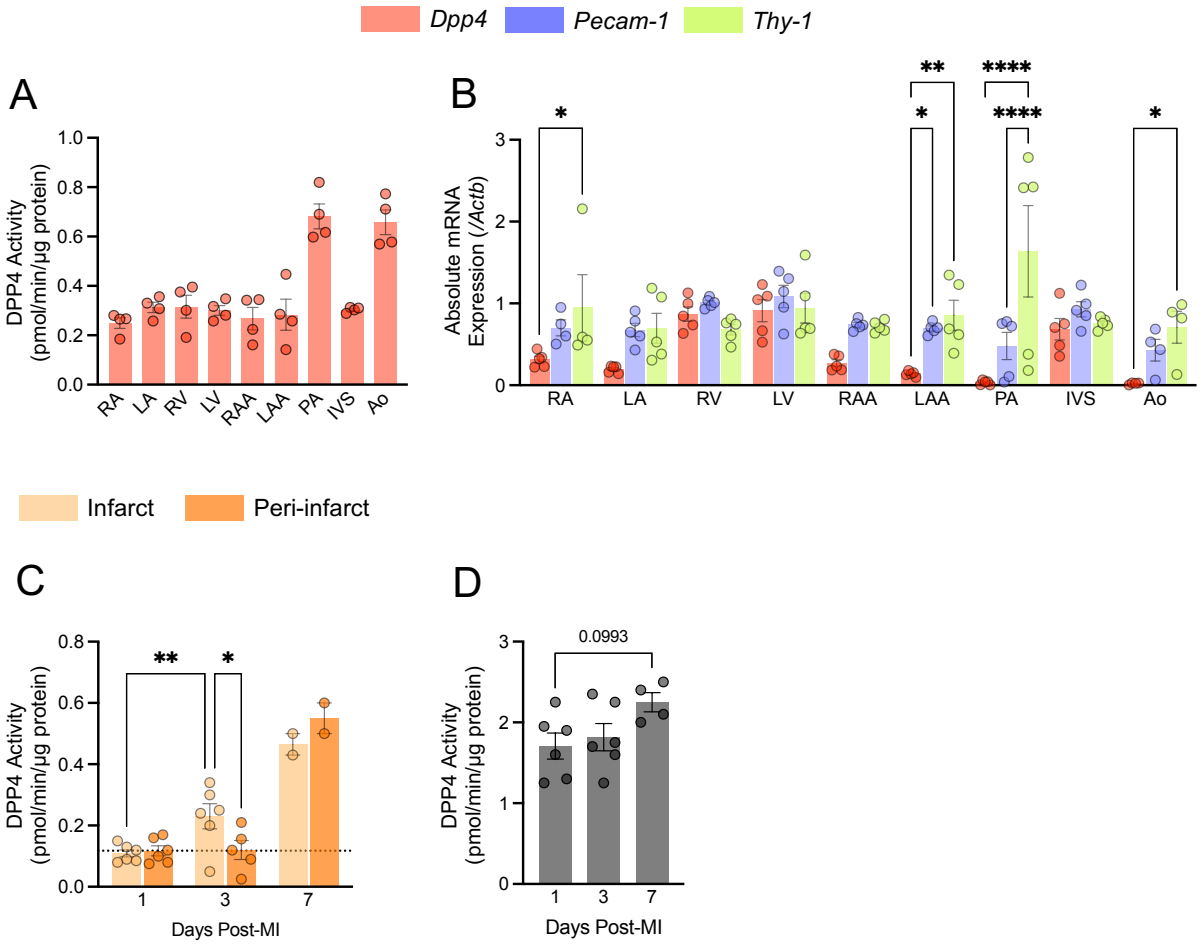

Figure 4.1: DPP4 is increased in endothelial cell associated cardiac structures in porcine hearts and post-MI in murine hearts. (**A**) DPP4 activity and (**B**) *Dpp4*, *Pecam-1* and *Thy-1* absolute mRNA expression in dissected parts of porcine heart. RA = right atrium, LA = left atrium, RV = right ventricle, LV = left ventricle, RAA = right atrial appendage, LAA = left atrial appendage, PA = pulmonary artery, IVS = interventricular septum and Ao = aorta. DPP4 activity in the (**C**) infarct, peri-infarct (dotted line represents baseline ventricular DPP4 activity) and (**D**) liver tissue at the times indicated post-MI in *Dpp4*$^{+/+}$ mice. Data are presented as means ± SEM analyzed by a two-way ANOVA, and a one-day ANOVA in (D), with a Tukey post-hoc multiple comparisons correction reported as adjusted p value, *p=0.01-0.05, **p=0.001-0.01, ***p=0.0001-0.001 and ****p<0.0001.

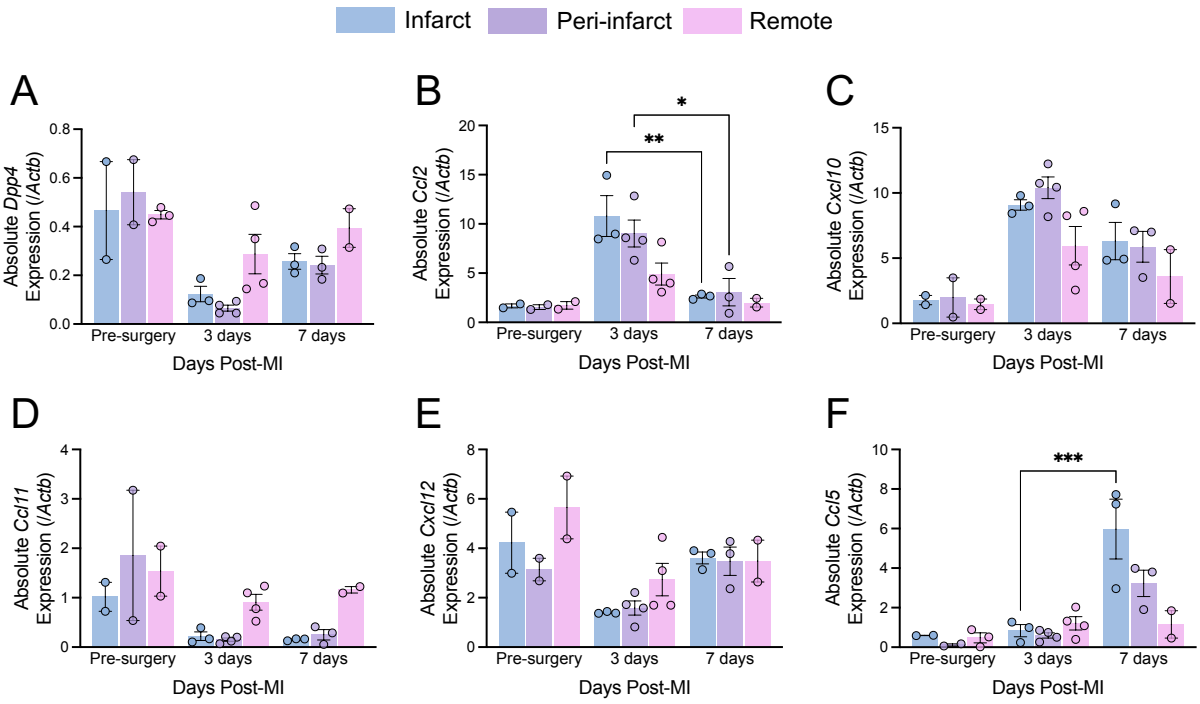

Figure 4.2: *Dpp4* and DPP4 substrate mRNA expression fluctuate acutely post-MI. mRNA expression of (**A**) *Dpp4*, (**B**) *Ccl2*, (**C**) *Cxcl10*, (**D**) *Ccl11*, (**E**) *Cxcl12* and (**F**) *Ccl5* in the infarct, peri-infarct, remote or representative section, in hearts harvested prior to, 3-days and 7-days after LAD-ligation in WT mice. Data are presented as means ± SEM analyzed by a two-way ANOVA with a Tukey post-hoc multiple comparisons correction reported as adjusted p value, *p=0.01-0.05, **p=0.001-0.01, ***p=0.0001-0.001.

4.5.2 DPP4 activity and protein are significantly reduced in *Dpp4*$^{hep-/-}$ and *Dpp4*$^{EC-/-}$ mice, respectively, prior to LAD-ligation

Previous studies report that metformin reduces DPP4 activity via protein reduction in mice, and DT with DPP4i's has a cardioprotective effect clinically[20,21,23,25]. Further, as previously described, DPP4 possessed different capabilities depending on its cellular origin, therefore, in addition to pharmaceutical treatment we incorporated systemic genetic *Dpp4* elimination (*Dpp4*$^{-/-}$), hepatocyte-specific elimination (*Dpp4*$^{hep-/-}$) and endothelial cell-specific elimination (*Dpp4*$^{EC-/-}$), in mice. These mice were aged, fed a HFHC-diet then treated with either sitagliptin, metformin or DT in their drinking water, with water as the control. We confirmed metformin bioactivity by evaluating GDF-15 protein levels, which increased by 29% in circulation with metformin use, as previously described (**Supplemental Figure 4.1**)[38]. Echocardiography was performed before and 4 weeks after LAD-ligation, while tail vein blood was collected prior to surgery, as well as 1, 4, 24 hours and 7 days post-MI, and finally at sacrifice (**Figure 4.3A**).

When we assessed DPP4 activity and sDPP4 levels at baseline, prior to LAD-ligation but after 4 weeks of drug treatment, we found a dissociation between these measurements within *Dpp4*$^{hep-/-}$ and *Dpp4*$^{EC-/-}$ mice and their respective controls. As anticipated, plasma DPP4 activity and sDPP4 levels were not detected in our *Dpp4*$^{-/-}$ model, confirming the genotype (**Figure 4.3B, E**). Interestingly, DPP4 activity was significantly reduced in control treated *Dpp4*$^{hep-/-}$ mice compared to *Dpp4*^{GFP} mice (**Figure 4.3C**), however sDPP4 levels were unchanged (**Figure 4.3F**). In contrast, the opposite was evident in *Dpp4*$^{EC-/-}$ mice compared to *Dpp4*$^{EC+/+}$ mice with control treatment; there was no change in DPP4 activity (**Figure 4.3D**) while sDPP4 levels

were significantly reduced (**Figure 4.3G**). DPP4 activity and sDPP4 levels changed further with the introduction of DT, sitagliptin and metformin pharmaceutical treatments. DPP4 activity was significantly reduced by 68% in DT treated *Dpp4*$^{+/+}$ mice compared to metformin treated mice as anticipated (**Figure 4.3B**), however, the opposite was observed with protein levels, where DT significantly increased sDPP4 by 41% compared to control treatment (**Figure 4.3E**). sDPP4 levels in *Dpp4*$^{+/+}$ mice were similar to those reported previously in humans with sitagliptin and metformin treatment[25]. DPP4 activity was significantly reduced in control-treated (by 70%) *Dpp4*$^{hep-/-}$ mice compared to *Dpp4*^{GFP} mice (**Figure 4.3C**). Interestingly, only metformin treatment in *Dpp4*$^{hep-/-}$ mice significantly reduced sDPP4 by half compared to *Dpp4*^{GFP} mice (**Figure 4.3F**). DPP4 protein was also significantly reduced in metformin treated *Dpp4*$^{hep-/-}$ mice compared to those treated with sitagliptin (by 57%) and DT (by 65%), and protein was reduced in control-treated mice compared to DT-treated mice (**Figure 4.3F**). In contrast, DPP4 activity was unchanged between *Dpp4*$^{EC-/-}$ mice and *Dpp4*$^{EC+/+}$ mice with all drug treatments (**Figure 4.3D**). Interestingly however, sDPP4 was significantly reduced with all drug treatments between *Dpp4*$^{EC-/-}$ mice and *Dpp4*$^{EC+/+}$ mice (**Figure 4.3G**). *Dpp4*$^{EC+/+}$ mice treated with DT and sitagliptin had significantly higher plasma DPP4 protein by 31% and 42%, respectively, compared to controls. Further, sitagliptin treated *Dpp4*$^{EC+/+}$ mice had 35% higher sDPP4 compared to those treated with metformin (**Figure 4.3G**).

Additionally, to further evaluate if upregulation of DPP4 substrates *Ccl2*, *Cxcl10* and *Ccl5* had an impact on inflammatory cytokine levels with pharmaceutical treatment, we treated a separate cohort of *Dpp4*$^{+/+}$ mice with sitagliptin, metformin and DT with water as the control. There were no significant differences in plasma

concentrations of Il-1β (**Figure 4.4A**) and TNF-α (**Figure 4.4B**), between drug treatments or between timepoints. However, IL-6 was significantly increased 4-hours post-MI, with no differences between treatment groups (**Figure 4.4C**). Here we show that hepatocyte-derived DPP4 drives DPP4 activity, while endothelial cell-derived DPP4 contributes to sDPP4 levels.

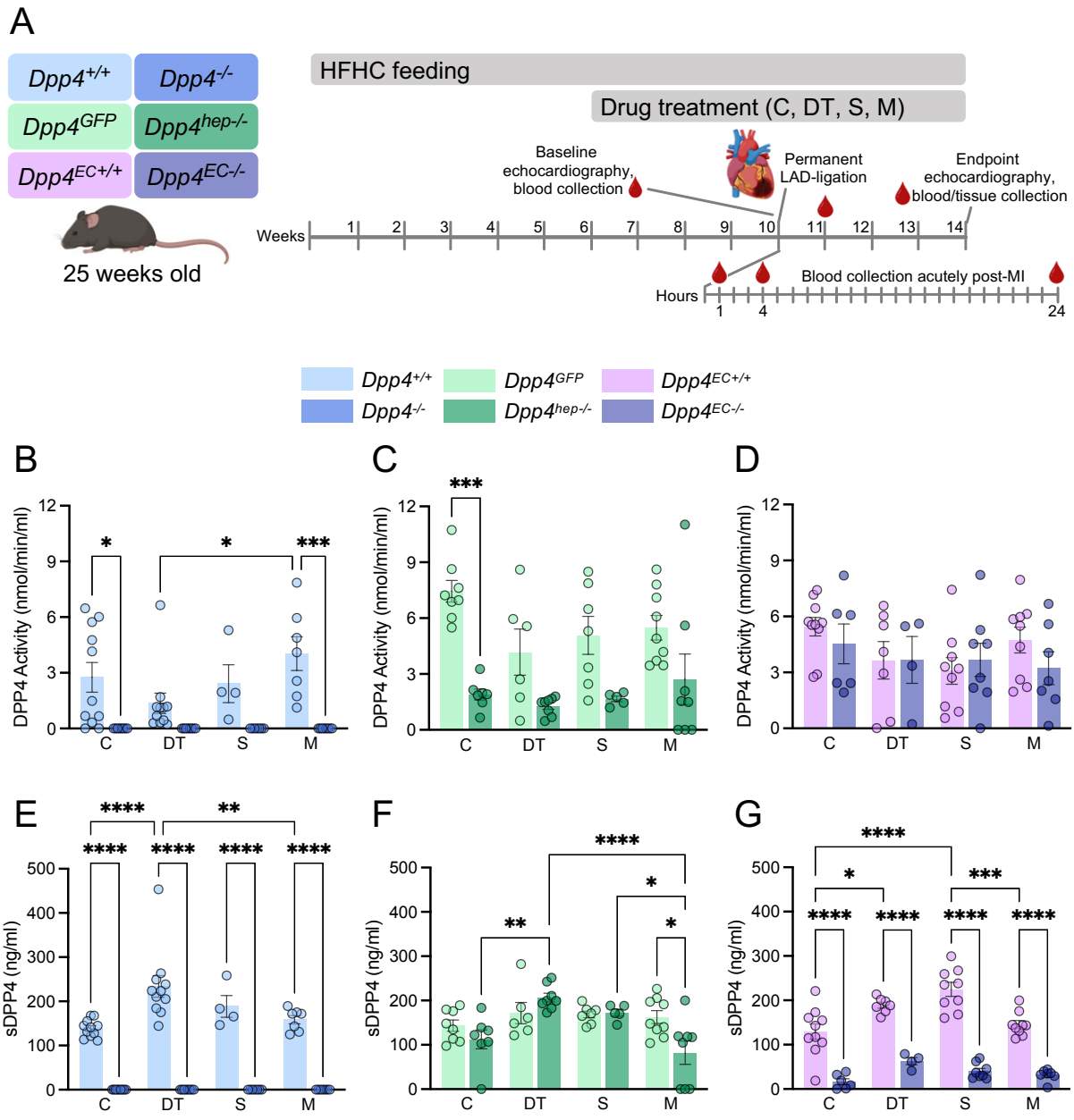

Figure 4.3: Baseline plasma DPP4 activity and sDPP4 are dynamically regulated in *Dpp4*$^{hep-/-}$ and *Dpp4*$^{EC-/-}$ mice. Experimental timeline, highlighting drug treatment LAD-ligation echocardiography and blood collection timepoints. Plasma DPP4 activity in (**B**) *Dpp4*$^{+/+}$ and *Dpp4*$^{-/-}$, (**C**) *Dpp4*^{GFP} and *Dpp4*$^{hep-/-}$ and (**D**) *Dpp4*$^{EC+/+}$ and *Dpp4*$^{EC-/-}$ mice, and DPP4 protein concentration in (**E**) *Dpp4*$^{+/+}$ and *Dpp4*$^{-/-}$, (**F**) *Dpp4*^{GFP} and *Dpp4*$^{hep-/-}$ and (**G**) *Dpp4*$^{EC+/+}$ and *Dpp4*$^{EC-/-}$ mice, after 10 weeks of HFHC feeding, 4 weeks of drug treatment and prior to LAD-ligation. Drug treatments: C = control (water), DT = dual therapy (sitagliptin and metformin combination), S = Sitagliptin, M = Metformin. Data are presented as means ± SEM analyzed by a two-way ANOVA with a Tukey post-hoc multiple comparisons correction reported as adjusted p value, *p=0.01-0.05, **p=0.001-0.01, ***p=0.0001-0.001 and ****p<0.0001.

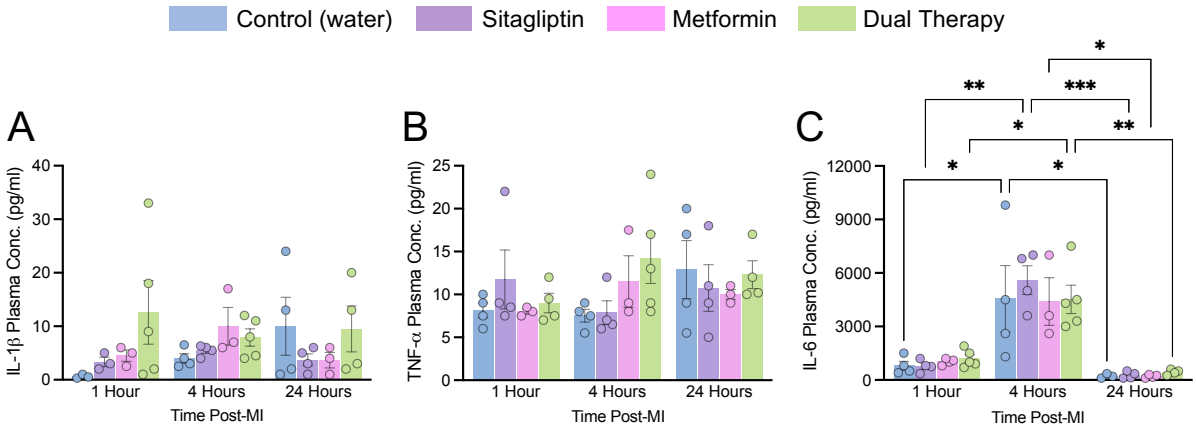

Figure 4.4: Plasma Il-1β, TNF-α and IL-6 are unaltered with drug treatment in *Dpp4*$^{+/+}$ mice post-MI.(**A**) Il-1β, (**B**) TNF-α and (**C**) IL-6 in WT mice, 1-, 4- and 24-hours after LAD-ligation after treatment with control (water), sitagliptin, metformin and DT (sitagliptin and metformin). Data are presented as means ± SEM analyzed by a two-way ANOVA with a Tukey post-hoc multiple comparisons correction reported as adjusted p value, *p=0.01-0.05, **p=0.001-0.01, ***p=0.0001-0.001 and ****p<0.0001.

4.5.3 With DT treatment, LVEF is improved in *Dpp4*$^{hep-/-}$ mice prior to MI, and ESV and EDV are reduced post-MI

Considering the changes in DPP4 activity and sDPP4 between genotypes and pharmaceutical treatment, we continued with our evaluation of cardiac function, prior to and after LAD-ligation. Interestingly, no changes in LVEF, stroke volume (SV), cardiac output (CO), end systolic volume (ESV) and end diastolic volume (EDV) were detected between *Dpp4*$^{+/+}$ and *Dpp4*$^{-/-}$ mice at baseline or endpoint with all drug treatments, with the exception of reduced heart rate (HR) in *Dpp4*$^{-/-}$ compared to *Dpp4*$^{+/+}$ mice at baseline. However, with DT treatment, HR was reduced in *Dpp4*$^{hep-/-}$ mice compared to controls pre- and post-MI, and in turn, this translated to a decrease in CO post-MI. In addition, LVEF was significantly increased in *Dpp4*$^{hep-/-}$ mice at baseline alongside reduced ESV and EDV. At baseline with DT treatment, *Dpp4*$^{EC-/-}$ mice had higher SV and CO compared to controls, with no improvement in LVEF, interestingly. Sitagliptin treatment only resulted in reduced baseline CO in *Dpp4*$^{EC-/-}$ mice compared to controls. HR at baseline and LVEF post-MI were significantly increased with metformin treatment in *Dpp4*$^{hep-/-}$ mice compared to *Dpp4*^{GFP} mice, while ESV was significantly reduced post-MI. Lastly, metformin treatment in *Dpp4*$^{EC-/-}$ mice reduced baseline SV and CO compared to *Dpp4*$^{EC+/+}$ mice. Together, these results reveal modest improvements in cardiac function with DT even at baseline, exemplified by increased LVEF in *Dpp4*$^{hep-/-}$ compared to *Dpp4*^{GFP} mice, and increased SV and CO in *Dpp4*$^{EC-/-}$ compared to *Dpp4*$^{EC+/+}$ mice. Interestingly, this was not evident with the no treatment control, or sitagliptin and metformin monotherapy only improved post-MI LVEF in *Dpp4*$^{hep-/-}$ mice compared to *Dpp4*^{GFP} mice (**Table 4.1**).

Table 4.1: Ventricle dimensions are improved in *Dpp4*$^{hep-/-}$ with DT after LAD-ligation. LV cardiac hypertrophy and function *in vivo* assessed using 2D echocardiography prior to LAD-ligation, after 10-weeks of HFHC-feeding and 4-weeks of pharmacological treatment (referred to as baseline) and 4-weeks after LAD-ligation, 14-weeks of HFHC-feeding and 8-weeks of pharmacological treatment (referred to as post-MI), in *Dpp4*$^{+/+}$, *Dpp4*$^{-/-}$, *Dpp4*^{GFP}, *Dpp4*$^{hep-/-}$, *Dpp4*$^{EC+/+}$ and *Dpp4*$^{EC-/-}$ male mice. Data are presented as means ± SEM, within treatment groups between genetic knockouts and their respective controls, data were analyzed by student's t test, *p=0.01-0.05. BPM = beats per minute.

		Heart Rate (BPM)		Ejection Fraction (%)		Stroke Volume (µL)		Cardiac Output (mL/min)		End Systolic Volume (µL)		End Diastolic Volume (µL)	
		Baseline	Post-MI	Baseline	Post-MI	Baseline	Post-MI	Baseline	Post-MI	Baseline	Post-MI	Baseline	Post-MI
Control (water)	*Dpp4*$^{+/+}$	570.82 ± 24.14	549.68 ± 15.34	55.69 ± 1.84	28.77 ± 3.71	37.06 ± 2.61	26.49 ± 2.66	21.47 ± 2.35	14.57 ± 1.61	29.07 ± 1.54	84.31 ± 17.51	66.13 ± 3.25	110.81 ± 15.86
	Dpp4$^{-/-}$	551.22 ± 21.21	515.32 ± 19.83	54.75 ± 3.6	37.03 ± 5.71	34.1 ± 1.76	23.11 ± 2.18	18.62 ± 0.78	11.7 ± 0.9	29.39 ± 3.83	48.11 ± 9.31	63.5 ± 2.97	71.23 ± 8.48
	Dpp4^{GFP}	457.83 ± 42.9	527.82 ± 28.01	58.08 ± 3.45	25.25 ± 3.08	47.06 ± 3.75	32.83 ± 3.7	21.48 ± 2.72	17.14 ± 1.99	34.6 ± 3.93	110.91 ± 22.53	81.67 ± 5.44	143.75 ± 24.27
	Dpp4$^{hep-/-}$	451.94 ± 38.3	484.64 ± 16.94	57.12 ± 1.9	32.81 ± 3.4	43.26 ± 4.74	30.25 ± 2.26	19.72 ± 2.74	14.79 ± 1.53	33.02 ± 4.23	67.1 ± 9.18	76.29 ± 8.41	97.36 ± 10.23
	Dpp4$^{EC+/+}$	505.19 ± 23.21	542.79 ± 13.87	55.24 ± 1.41	26.73 ± 4.56	36.57 ± 3.03	26.9 ± 1.55	18.45 ± 1.66	14.71 ± 1.07	29.4 ± 2.16	110.95 ± 27.91	65.97 ± 4.78	137.85 ± 28.24
	Dpp4$^{EC-/-}$	523.95 ± 10.93	568.37 ± 20.57	52.87 ± 2.59	26.45 ± 2.97	36.76 ± 2.37	31.63 ± 3.31	19.2 ± 1.12	17.76 ± 1.6	32.82 ± 2.44	90.8 ± 9.43	69.58 ± 3.31	122.43 ± 9.49
Dual Therapy (Metformin+Sitagliptin)	*Dpp4*$^{+/+}$	571.44 ± 10.45	569.91 ± 8.9	53.56 ± 2.06	26.24 ± 3.24	32.05 ± 1.8	22.59 ± 2.34	18.31 ± 1.1	12.94 ± 1.4	28.77 ± 2.95	72.46 ± 11.8	60.82 ± 4.36	95.06 ± 11.92
	Dpp4$^{-/-}$	557.63 ± 11.77	554.85 ± 15.67	55.41 ± 1.89	25.88 ± 3.75	33.01 ± 3.72	23.21 ± 2.69	18.38 ± 2.13	12.78 ± 1.33	25.74 ± 1.51	80.43 ± 19.69	58.76 ± 4.72	103.64 ± 20.61
	Dpp4^{GFP}	555.15 ± 13.11	550.27 ± 8.42	50.41 ± 4.22	24.24 ± 3.53	41.31 ± 6.3	33.88 ± 1.63	22.65 ± 2.98	18.6 ± 0.73	39.41 ± 4.02	123.38 ± 25.5	80.73 ± 7.22	157.27 ± 26.06
	Dpp4$^{hep-/-}$	470.26 ± 13.46 ***	482.64 ± 18.12 *	64.42 ± 2.02 **	35.94 ± 5.19	50.9 ± 3.64	29.77 ± 3.34	23.9 ± 1.83	14.21 ± 1.49 *	28.76 ± 3.51	60.02 ± 10.55 *	79.67 ± 6.49	89.79 ± 9.28 *
	Dpp4$^{EC+/+}$	530.56 ± 24.33	582.31 ± 23.09	51.06 ± 5.78	23.22 ± 3.06	26.92 ± 3.84	25.91 ± 4.2	14.17 ± 2.13	15.5 ± 2.91	27.76 ± 5.4	87.03 ± 10.04	54.69 ± 6.5	112.95 ± 11.56
	Dpp4$^{EC-/-}$	555.91 ± 9.5	571.64 ± 20.74	57.89 ± 2.28	29.86 ± 5.41	42.05 ± 3.43 *	24.6 ± 3.9	23.49 ± 2.28 *	14.11 ± 2.39	30.86 ± 3.36	63.42 ± 12.28	72.92 ± 6.26	88.02 ± 10.48
Sitagliptin	*Dpp4*$^{+/+}$	570.82 ± 16.98	549.68 ± 12.78	55.69 ± 0.86	28.77 ± 4.57	37.06 ± 1.82	26.49 ± 2.26	21.47 ± 0.9	14.57 ± 1.06	29.07 ± 1.61	84.31 ± 17.5	66.13 ± 3.27	110.81 ± 16.49
	Dpp4$^{-/-}$	551.22 ± 6.28 *	515.32 ± 22.76	54.75 ± 3.52	37.03 ± 3.55	34.1 ± 3.33	23.11 ± 2.07	18.62 ± 1.88	11.7 ± 1.07	29.39 ± 3.4	48.11 ± 20.19	63.5 ± 4.72	71.23 ± 19.98
	Dpp4^{GFP}	457.83 ± 19.69	527.82 ± 55.98	58.08 ± 4.52	25.25 ± 5.5	47.06 ± 3.88	32.83 ± 4.08	21.48 ± 2.54	17.14 ± 2.68	34.6 ± 4.87	110.91 ± 13.76	81.67 ± 6.72	143.75 ± 13.31
	Dpp4$^{hep-/-}$	451.94 ± 17.59	484.64 ± 22.43	57.12 ± 6.09	32.81 ± 2.88	43.26 ± 4.71	30.25 ± 1.95	19.72 ± 2.59	14.79 ± 1.02	33.02 ± 5.76	67.1 ± 12.47	76.29 ± 7.26	97.36 ± 13.94
	Dpp4$^{EC+/+}$	555.77 ± 15	544.95 ± 15.35	53.58 ± 1.98	26.3 ± 3.04	40.59 ± 3.23	26.67 ± 3.57	22.28 ± 1.4	14.42 ± 1.92	35.79 ± 3.99	77.35 ± 9.31	76.39 ± 6.85	104.03 ± 10.53
	Dpp4$^{EC-/-}$	534.38 ± 20.67	561.04 ± 12.56	53.21 ± 2.64	21.41 ± 2.36	32.16 ± 2.66	23.51 ± 2.45	16.99 ± 1.22 *	13.31 ± 1.67	30.55 ± 5.15	92.2 ± 11.36	62.72 ± 7.56	115.71 ± 11.64
Metformin	*Dpp4*$^{+/+}$	539.14 ± 24.25	532.18 ± 21.55	58.63 ± 3.11	28.02 ± 5.2	34.96 ± 2.7	25.89 ± 3.4	18.72 ± 1.41	13.65 ± 1.87	24.86 ± 2.81	80.08 ± 16.46	59.83 ± 4.05	105.98 ± 15.04
	Dpp4$^{-/-}$	560.31 ± 14.89	542.99 ± 22.35	53.88 ± 6.17	21.78 ± 5.68	37.36 ± 3.68	22.98 ± 2.26	20.78 ± 1.81	12.43 ± 1.24	34.3 ± 6.07	125.61 ± 31.04	71.67 ± 5.89	148.6 ± 29.77
	Dpp4^{GFP}	454.8 ± 26.1	566.88 ± 34.84	55.94 ± 4.65	22.6 ± 2.09	33.09 ± 2.37	23.69 ± 2.03	15.04 ± 1.36	13.25 ± 1.14	27.82 ± 5.14	84.03 ± 7.04	60.91 ± 4.56	107.72 ± 7.46
	Dpp4$^{hep-/-}$	541.15 ± 21.38 *	553.8 ± 35.52	61.91 ± 2.99	35.51 ± 2.96 **	33.63 ± 2.34	27.44 ± 2.21	18.01 ± 1.02	14.78 ± 0.69	20.88 ± 2.33	52.02 ± 5.71 **	54.52 ± 3.3	79.47 ± 6.59
	Dpp4$^{EC+/+}$	513.79 ± 23.68	528.58 ± 12.07	55.34 ± 2.66	32.89 ± 4.77	40.83 ± 2.88	33.77 ± 3.73	20.9 ± 1.63	17.71 ± 1.87	35.15 ± 5.64	77.48 ± 11.84	75.98 ± 8.05	111.26 ± 10.32
	Dpp4$^{EC-/-}$	517.26 ± 13.3	539.58 ± 22.75	61.89 ± 4.33	25.13 ± 2.99	36.14 ± 3.12 *	26.27 ± 2.32	18.63 ± 1.53 *	14.23 ± 1.56	22.96 ± 3.5	89.09 ± 17.86	59.11 ± 4.37	115.37 ± 18.01

4.5.4 Cardiac function is rescued with DT treatment pre- and post-MI in *Dpp4$^{hep-/-}$* mice, without altering myocardial kinesis

Across all genotypes and treatments, LVEF was largely decreased (approximately 40-50%) as a result of the LAD-ligation surgery, as expected (**Figure 4.5A-C, Supplemental Figure 4.2A-C**). This decrease was modestly, but not significantly, attenuated in control treated *Dpp4$^{-/-}$* mice compared to *Dpp4$^{+/+}$* mice post-MI as previously reported by Sauvé *et. al.*[14] (**Figure 4.5A**). Interestingly, LVEF did not differ between DT treated *Dpp4$^{+/+}$* and *Dpp4$^{-/-}$* mice, however function decreased by 30% with DT compared to control treatment in *Dpp4$^{-/-}$* mice, which is not consistent with human studies[20] (**Figure 4.5A)**. There were no differences detected between *Dpp4^{GFP}* and *Dpp4$^{hep-/-}$* mice with control treatment. Most notably however, DT treatment in *Dpp4$^{hep-/-}$* mice resulted in higher LVEF compared to *Dpp4^{GFP}* mice, at baseline and post-MI, suggesting that eliminating *Dpp4* peripherally from the liver and modulating endothelial cell-derived *Dpp4* effectively rescues function (**Figure 4.5B**). Similar to *Dpp4$^{+/+}$* and *Dpp4$^{-/-}$* mice, no significant differences were detected between *Dpp4$^{EC+/+}$* and *Dpp4$^{EC-/-}$* mice with both control and DT treatment (**Figure 4.5C**). When we assessed the effects of sitagliptin and metformin monotherapy on LVEF, we detected no changed between *Dpp4$^{+/+}$* and *Dpp4$^{-/-}$* mice with drug treatment at baseline or endpoint (**Supplemental Figure 4.2A**). However, at endpoint, we did observe a significant increase in LVEF with metformin treatment in *Dpp4$^{hep-/-}$* mice compared to *Dpp4^{GFP}* mice, suggesting a cardioprotective mechanism independent of hepatocyte-specific DPP4 (**Supplemental Figure 4.2B**). This was confirmed as we saw no change between *Dpp4$^{EC-/-}$* and *Dpp4$^{EC+/+}$* mice with sitagliptin and metformin treatment (**Supplemental Figure 4.2C**).

Our group has previously described *in vivo* infarct measurement; it is comparable to the gold standard histological analysis, with the added benefit that tissue may be instead used for molecular analyses[28]. We employed this strategy and evaluated the prevalence of fully kinetic myocardia with full movement, hypokinetic myocardia with decreased movement, and akinetic myocardia with infarcts that do not move. Approximately 20% of control treated *Dpp4*$^{-/-}$ mice had fully kinetic myocardia, while 18% of *Dpp4*$^{+/+}$ mice had hypokinetic hearts (**Figure 4.5D**). DT treatment resulted in 10% and 25% prevalence of hypokinetic myocardia in *Dpp4*$^{+/+}$ and *Dpp4*$^{-/-}$ mice, respectively, however the majority were akinetic (**Figure 4.5D**). Control and DT treated *Dpp4*$^{hep-/-}$ mice had more hypokinetic hearts compared to *Dpp4*^{GFP} mice, but the majority again were akinetic (**Figure 4.5E**). This is in contrast to DT treated *Dpp4*$^{EC-/-}$ mice where almost 60% of hearts are fully kinetic (**Figure 4.5F**), and interestingly not associated with rescued LVEF. Further, all DT treated *Dpp4*$^{EC+/+}$ mice had akinetic hearts, however 30% of these mice had hypokinetic myocardia with control treatment (**Figure 4.5F**). With sitagliptin monotherapy, 50% of *Dpp4*$^{+/+}$ mice had hypokinetic hearts and the remainder were akinetic, while metformin monotherapy treatment was beneficial in *Dpp4*$^{-/-}$ mice resulting in approximately 40% hypokinetic hearts (**Supplemental Figure 4.2D**). Interestingly, sitagliptin and metformin monotherapy resulted in an even distribution of *Dpp4*$^{hep-/-}$ mice with hypokinetic and akinetic hearts, making both treatments superior in these mice compared to control *Dpp4*^{GFP} mice (**Supplemental Figure 4.2E**). Metformin-treated *Dpp4*$^{EC-/-}$ mice all had akinetic hearts, while sitagliptin treatment resulted in approximately 30% hypokinetic hearts, however, both sitagliptin and metformin treatment were beneficial to *Dpp4*$^{EC+/+}$ mice, resulting in 35-55% hypokinetic hearts

(**Supplemental Figure 4.2F**). Interestingly, we did not observe significant differences between genotypes within treatment groups when we assessed total endocardial left ventricular length (**Figure 4.5G-I, Supplemental Figure 4.2G-I**). Additionally, we did not detect significant differences in infarct sizes between genotypes with all drug treatments, despite improved function in DT treated *Dpp4*$^{hep-/-}$ mice pre- and post-MI, and metformin treated *Dpp4*$^{hep-/-}$ mice, post-MI (**Figure 4.5G-I, Supplemental Figure 4.2G-I**). With DT treatment, more *Dpp4*$^{hep-/-}$ mice had hypokinetic hearts while no mice with metformin treatment did; all hearts were akinetic. Therefore, we may deduce that the cardioprotective phenotype with DT treatment is partially due to rescued myocardial kinesis, however, in both cases, metformin treatment with or without the addition of sitagliptin is targeting endothelial cell-specific DPP4 and modulating local effects in the heart.

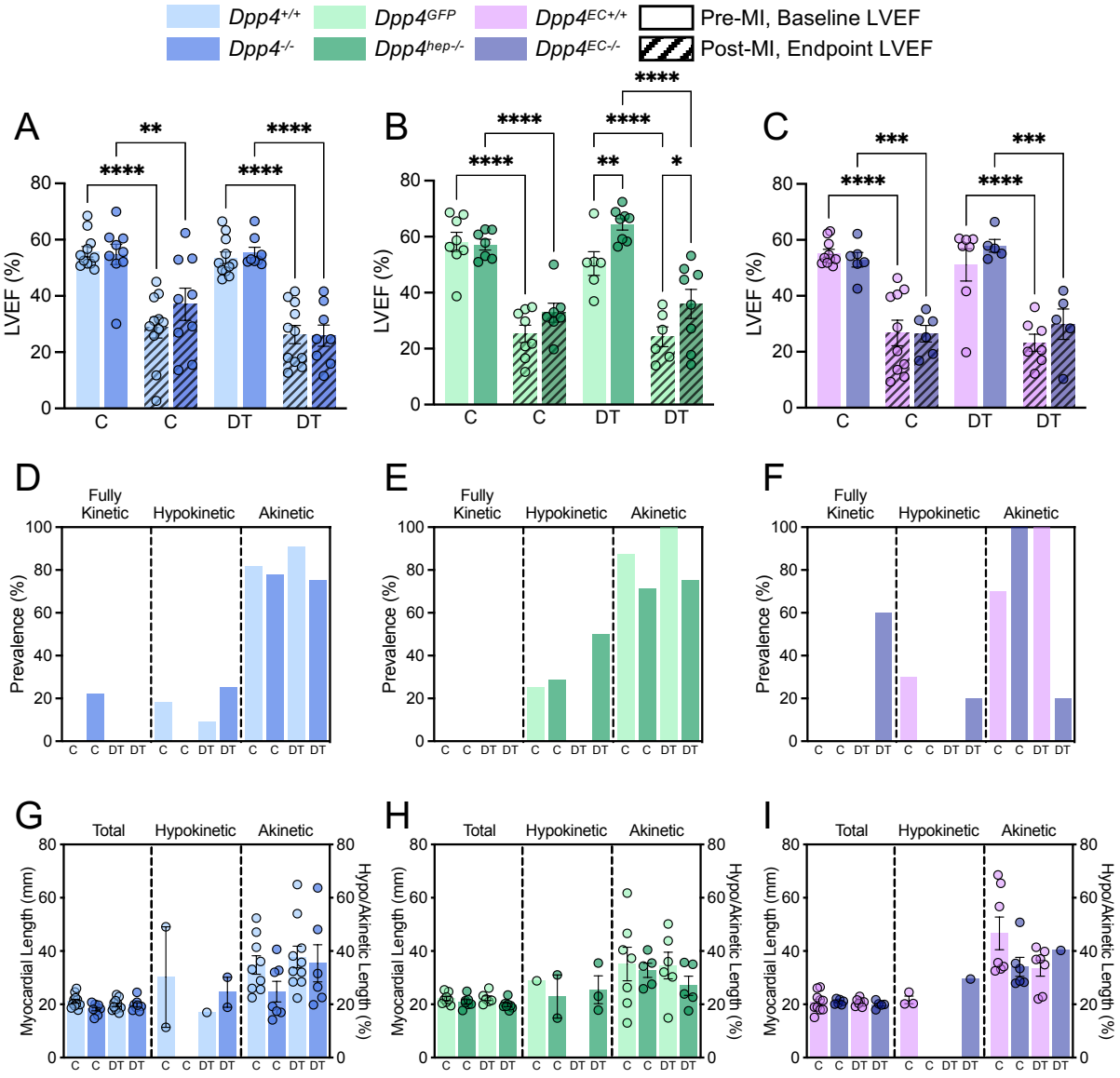

Figure 4.5: DT treatment improved ejection fraction, but did not improve myocardial kinesis or change average infarct size in *Dpp4*$^{hep-/-}$ mice. LVEF at baseline (plain bars) after 10-weeks of HFHC-feeding and 4 weeks of pharmacological treatment and at endpoint (patterned bars), 4-weeks after LAD-ligation, and after 14-weeks of HFHC-feeding and 8-weeks of pharmacological treatment, in (**A**) *Dpp4*$^{+/+}$ and *Dpp4*$^{-/-}$, (**B**) *Dpp4*^{GFP} and *Dpp4*$^{hep-/-}$ and (**C**) *Dpp4*$^{EC+/+}$ and *Dpp4*$^{EC-/-}$ male mice. Prevalence of fully kinetic, hypokinetic and akinetic myocardium after LAD-ligation in (**D**) *Dpp4*$^{+/+}$ and *Dpp4*$^{-/-}$, (**E**) *Dpp4*^{GFP} and *Dpp4*$^{hep-/-}$ and (**F**) *Dpp4*$^{EC+/+}$ and *Dpp4*$^{EC-/-}$ male mice. Total endocardial left ventricle length (left Y-axis), and hypokinetic and akinetic proportion (right y-axis) in (**G**) *Dpp4*$^{+/+}$ and *Dpp4*$^{-/-}$, (**H**) *Dpp4*^{GFP} and *Dpp4*$^{hep-/-}$ and (**I**) *Dpp4*$^{EC+/+}$ and *Dpp4*$^{EC-/-}$ male mice. Data are presented as means ± SEM analyzed by a two-way ANOVA with a Tukey's post-hoc test, *p=0.01-0.05.

4.5.5 DPP4 activity is dissociated from sDPP4 levels over time

We next evaluated changes in DPP4 activity and sDPP4 levels from baseline prior to MI (10 weeks), to 1-week post-MI (11 weeks) until endpoint (14 weeks). Interestingly, we found a consistent trend where DPP4 activity decreased 1-week post-MI from baseline but increased at endpoint. These fluctuations were not significant between timepoints in control treated *Dpp4*$^{+/+}$ mice (**Figure 4.6A**) and *Dpp4*^{GFP} and *Dpp4*$^{hep-/-}$ mice (**Figure 4.6B**), however, these trends were significant in *Dpp4*$^{EC+/+}$ mice (**Figure 4.6C**). DT treatment in *Dpp4*$^{+/+}$ resulted in significant increases at endpoint compared to baseline and 1-week post-MI (**Figure 4.6D**). Similar trends were observed in *Dpp4*$^{hep-/-}$ mice with DT treatment, as well as a significant decrease between baseline and 1-week post-MI (**Figure 4.6E**). In *Dpp4*^{GFP} mice however, a significant change was only observed between 11 and 14 weeks (**Figure 4.6E**). DT treatment significantly increased DPP4 activity after surgery to endpoint in *Dpp4*$^{EC+/+}$ mice, while a trend was observed in *Dpp4*$^{EC-/-}$ mice (**Figure 4.6F**). With sitagliptin treatment, DPP4 activity increased after surgery up to endpoint in *Dpp4*$^{+/+}$ mice (**Supplemental Figure 4.3A**). Activity was significantly reduced in *Dpp4*$^{hep-/-}$ mice from before to after surgery, and to endpoint (**Supplemental Figure 4.3B**). Similarly, a decrease was also observed in *Dpp4*^{GFP} mice from before to after surgery, and there was a trend for increase from the 1-week post-MI timepoint to endpoint (**Supplemental Figure 4.3B**). This was also observed in *Dpp4*$^{EC-/-}$ mice, albeit the change from 11 to 14 weeks was significant (**Supplemental Figure 4.3C**). Interestingly however, there were no significant differences between timepoints in any genotypes with metformin treatment, with only a trend observed in *Dpp4*^{GFP} mice from 1-week post-MI to endpoint for increased activity (**Supplemental Figure 4.3D-F**).

In our evaluation of plasma sDPP4 levels, the majority of control and treated mice experienced a similar trend to varying degrees; sDPP4 increased from before surgery (10 weeks) to 1-week after (11 weeks), and further from 1-week post MI to endpoint (14 weeks). This was significantly evident in *Dpp4*$^{+/+}$ mice where sDPP4 was increased from 10 to 14 weeks and from 11 to 14 weeks (**Figure 4.6G**). From 10 to 14 weeks, there was a significant increase in sDPP4 in *Dpp4*^{GFP} mice. *Dpp4*$^{hep-/-}$ mice, however, experienced a significant increase from 10 to 11 weeks (**Figure 4.6H**). Interestingly, sDPP4 levels were significantly increased from 10 to 11 weeks and from 10 to 14 weeks in *Dpp4*^{GFP} mice, while a significant increase was observed in *Dpp4*$^{EC-/-}$ mice only from baseline to endpoint (**Figure 4.6I**). In contrast to DPP4 activity analysis and control treatment sDPP4 measurements, DT treatment did not significantly alter sDPP4 levels in *Dpp4*$^{+/+}$ mice (**Figure 4.6J**) or *Dpp4*^{GFP} and *Dpp4*$^{hep-/-}$ mice, however there was a trend for increase from 10 to 14 weeks in *Dpp4*^{GFP} mice (**Figure 4.6K**). In comparison, DT treated *Dpp4*$^{EC+/+}$ and *Dpp4*$^{EC-/-}$ mice saw a trend for increase in sDPP4 levels from baseline (10 weeks) to endpoint (14 weeks) (**Figure 4.6L**). Comparable to DT treatment, sitagliptin treatment did not result in any major fluctuations in *Dpp4*$^{+/+}$ mice (**Supplemental Figure 4.3G**), however sDPP4 levels increased from 10 weeks and 11 weeks to endpoint in *Dpp4*$^{hep-/-}$ mice, and was trending up in *Dpp4*^{GFP} mice from before to after MI (**Supplemental Figure 4.3H**). In all three comparisons between timepoints, 10 to 11, 10 to 14 and 11 to 14 weeks, *Dpp4*$^{EC-/-}$ mice saw increased sDPP4 levels with sitagliptin treatment (**Supplemental Figure 4.3I**). Compared to sitagliptin treated *Dpp4*$^{+/+}$ mice, those treated with metformin did in fact experience a significant increase in sDPP4 levels from prior to surgery to endpoint (**Supplemental Figure 4.3J**). Similarly, sDPP4 levels

were increased in *Dpp4*^{GFP} mice from before MI to endpoint, and there was a trend for increase from before to after surgery in *Dpp4*$^{hep-/-}$ mice (**Supplemental Figure 4.3K**). Lastly, in *Dpp4*$^{EC-/-}$ mice, sDPP4 increased from before to 1-week after surgery with metformin treatment (**Supplemental Figure 4.3L**). sDPP4 levels increased and were statistically higher in *Dpp4*$^{EC+/+}$ mice from 1-week post MI to endpoint, and from before surgery to endpoint as well (**Supplemental Figure 4.3L**). These data illustrate a dissociation between DPP4 activity and sDPP4 protein over the timeline of the experiment. DPP4 activity appears to be affected heavily by surgery, however it is restored before the end of the experiment. In contrast sDPP4 levels continue to rise from baseline at 10 weeks, through 11 weeks (1-week post- MI), and up until endpoint, signifying that sDPP4 is not affected by surgery, rather increases with continued HFHC-feeding instead.

We then evaluated DPP4 activity and sDPP4 levels between genotypes at 1-week post-MI (11 weeks) and endpoint 4 weeks post-MI (14 weeks). DPP4 activity was significantly reduced in *Dpp4*$^{-/-}$ mice versus *Dpp4*$^{+/+}$ mice with control and metformin treatment, while DT and sitagliptin treatment reduced activity in *Dpp4*$^{+/+}$ mice thereby no significant differences were observed (**Supplemental Figure 4.4A**). Additionally, consistent with a model of genetic elimination, 7 days after LAD-ligation, DPP4 activity and protein was undetectable in *Dpp4*$^{-/-}$ (**Supplemental Figure 4.4A**). DPP4 activity was significantly lower in sitagliptin, and DT treated *Dpp4*^{GFP} mice compared to control treated mice (**Supplemental Figure 4.4B**). Further, *Dpp4*$^{hep-/-}$ mice had lower DPP4 activity than *Dpp4*^{GFP} mice treated with water and metformin, however no significant changes were detected between sitagliptin, and DT treated mice (**Supplemental Figure 4.4B**). DPP4 activity was significantly reduced in

Dpp4$^{EC+/+}$ mice with DT treatment compared to water, sitagliptin and metformin, however no significant changes were observed between controls and *Dpp4*$^{EC-/-}$ mice (**Supplemental Figure 4.4C**). This did not associate with circulating DPP4 protein, which was significantly increased in DT treated *Dpp4*$^{+/+}$ mice compared to all other drug treatments by 27-44% (**Supplemental Figure 4.4D**). Interestingly, no significant changes were found between *Dpp4*$^{hep-/-}$ and *Dpp4*^{GFP} mice, or between treatment groups, when we assessed sDPP4 (**Supplemental Figure 4.4E**). Lastly, sDPP4 was significantly reduced between *Dpp4*$^{EC+/+}$ and *Dpp4*$^{EC-/-}$ mice treated with water and sitagliptin (**Supplemental Figure 4.4F**).

At endpoint, *Dpp4*$^{-/-}$ mice had no detectable levels of DPP4 activity and soluble protein (**Supplemental Figure 4.5A, D**). Metformin treatment significantly increased DPP4 activity in *Dpp4*$^{+/+}$ mice compared to those treated with DT (**Supplemental Figure 4.5A**). Activity was also significantly reduced between *Dpp4*$^{hep-/-}$ and *Dpp4*^{GFP} mice with all treatments, but no differences were detected between treatments (**Supplemental Figure 4.5B**). In contrast, no significant changes were noted between *Dpp4*$^{EC-/-}$ and *Dpp4*$^{EC+/+}$ mice with respect to plasma DPP4 activity (**Supplemental Figure 4.5C**). sDPP4 levels did not fluctuate with drug treatments in *Dpp4*$^{+/+}$ mice (**Supplemental Figure 4.5D**), or in *Dpp4*^{GFP} and *Dpp4*$^{hep-/-}$ mice (**Supplemental Figure 4.5E**). DPP4 protein levels were significantly reduced in control treated *Dpp4*$^{EC-/-}$ mice compared to controls, while all other drug treatment groups were trending down (**Supplemental Figure 4.5F**). While the same general trend exits in DPP4 activity and sDPP4 levels from baseline to post-MI at 11 and 14 weeks, there are subtle differences between drug treatment groups at 11 weeks, 1 week-post MI. Namely, DT treatment appears to reduce DPP4 activity among all genotype control

mice (*Dpp4*$^{+/+}$, *Dpp4*^{GFP} and *Dpp4*$^{EC+/+}$ mice). Further, the same trend exists at these timepoints and at baseline; DPP4 activity and protein are differentially regulated by *Dpp4* genetic elimination from hepatocytes and endothelial cells, respectively.

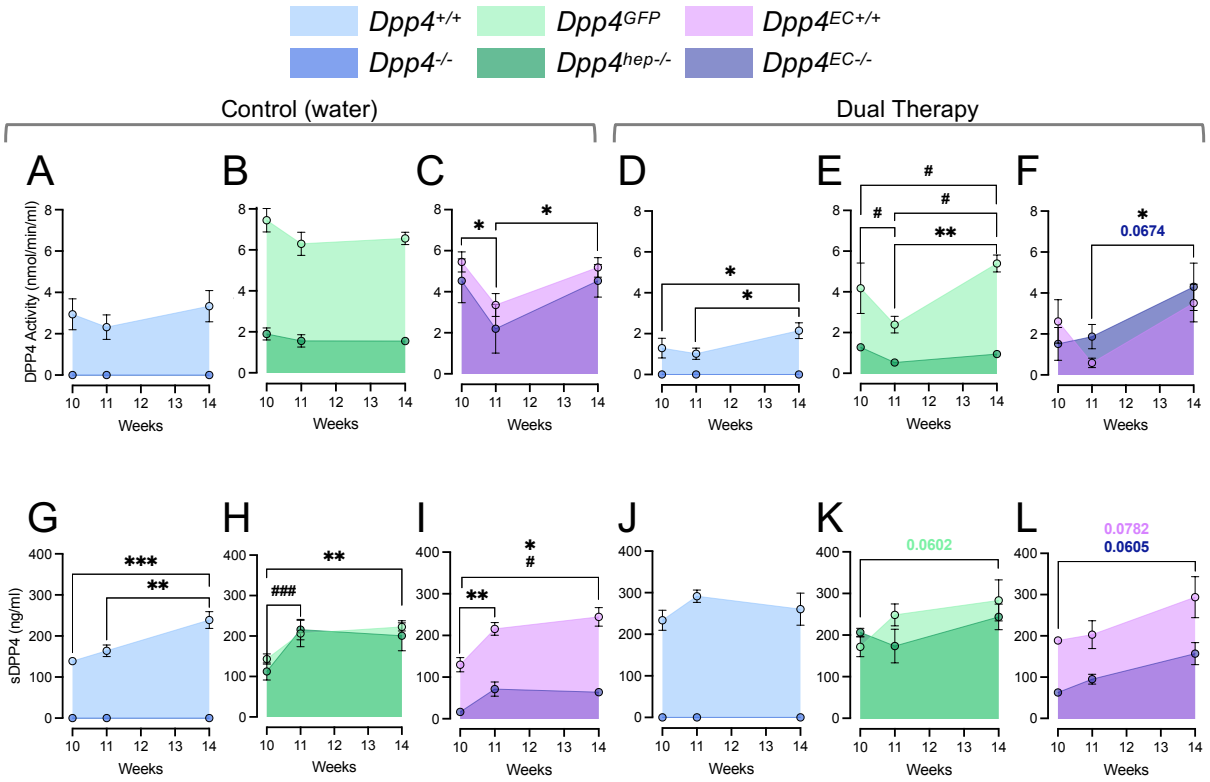

Figure 4.6: DPP4 activity and sDPP4 levels increase at endpoint after MI surgery. Plasma DPP4 activity in (**A**) *Dpp4*$^{+/+}$ and *Dpp4*$^{-/-}$, (**B**) *Dpp4*^{GFP} and *Dpp4*$^{hep-/-}$ and (**C**) *Dpp4*$^{EC+/+}$ and *Dpp4*$^{EC-/-}$ mice, and DPP4 protein concentration in (**G**) *Dpp4*$^{+/+}$ and *Dpp4*$^{-/-}$, (**H**) *Dpp4*^{GFP} and *Dpp4*$^{hep-/-}$ and (**I**) *Dpp4*$^{EC+/+}$ and *Dpp4*$^{EC-/-}$ mice with control (water) treatment. Plasma DPP4 activity in (**D**) *Dpp4*$^{+/+}$ and *Dpp4*$^{-/-}$, (**E**) *Dpp4*^{GFP} and *Dpp4*$^{hep-/-}$ and (**F**) *Dpp4*$^{EC+/+}$ and *Dpp4*$^{EC-/-}$ mice, and DPP4 protein concentration in (**J**) *Dpp4*$^{+/+}$ and *Dpp4*$^{-/-}$, (**K**) *Dpp4*^{GFP} and *Dpp4*$^{hep-/-}$ and (**L**) *Dpp4*$^{EC+/+}$ and *Dpp4*$^{EC-/-}$ mice with DT treatment. The 10-week time point includes 10 weeks of HFHC-feeding and 4 weeks of treatment. The 11-week time point includes 11 weeks of HFHC-feeding and 5 weeks of treatment and is 1 week after LAD-ligation. The 14-week time point includes 14 weeks of HFHC-feeding and 8 weeks of treatment and is 4 weeks after LAD-ligation. Data are presented as means ± SEM analyzed by a two-way ANOVA with repeated measures and a Tukey post-hoc multiple comparisons correction reported as adjusted p value. Significant differences in *Dpp4*$^{+/+}$, *Dpp4*^{GFP} and *Dpp4*$^{EC+/+}$, *p=0.01-0.05, **p=0.001-0.01, ***p=0.0001-0.001 and ****p<0.0001. Significant differences in *Dpp4*$^{-/-}$, *Dpp4*$^{hep-/-}$ and *Dpp4*$^{EC-/-}$, #p=0.01-0.05, ##p=0.001-0.01 and ###p=0.0001-0.001. Trends are reported as adjusted p values in the colour of their respective genotype.

4.6 Discussion

DT treatment with DPP4i's and metformin has demonstrated cardiovascular superiority compared to DPP4i monotherapy, which have shown neutral effects in CVOTs[20]. The mechanism has been explored[25,39], however, how DPP4 reductions in enzymatic activity and sDPP4 levels affect post-MI healing have not been investigated. Firstly, the present data reveal a complex relationship between DPP4 source and enzymatic activity or sDPP4 fluctuations as previously described by Varin *et. al.*[11]. In our study at baseline, DPP4 activity was reduced by 71% in *Dpp4*$^{hep-/-}$ mice compared to *Dpp4*^{GFP} mice, while sDPP4 levels were reduced by 88% in *Dpp4*$^{EC-/-}$ mice versus *Dpp4*$^{EC+/+}$ mice. DPP4i bioavailability varies wildly between drugs, ranging from 30-85%[40-44]. This in turn translates to incomplete DPP4 inhibition, resulting in 50-85% inhibition in the few studies that evaluate this; typically DPP4 inhibition is evaluated via reductions in fasting glucose or increases in active GLP-1 in clinical studies, even at low concentrations[44-47]. Most pre-clinical studies evaluate DPP4i mechanisms and effects by complete inhibition, here, we model clinical studies instead for more translational findings.

We cannot overlook partial inhibition of DPP4 as a mechanism to cardioprotection, as intestinal specific inhibitory concentrations of DPP4i's improved glucose tolerance and increased insulin secretion even though plasma DPP4 activity was not affected[48]. Interestingly, these results were still GLP-1 dependent, exemplified via genetic deletion of the GLP-1 receptor which prevented the glycemic benefit of sitagliptin[48]. Gut-derived DPP4, which is localized to capillaries near the enteroendocrine cells that give rise to GLP-1 and glucagon-dependent insulinotropic polypeptide (GIP), can inactivate these hormones immediately after release[49]. With

inhibition at low doses, intestinal DPP4 is enzymatically inactivated thereby preserving GLP-1 and GIP activity[48]. Additionally, beyond reducing sDPP4, metformin can increase GLP-1 secretion[24,50,51], which is already increased with inflammation after MI as well[52,53]. Of importance, endothelial cell-derived DPP4 is implicated in glucoregulation and genetic elimination results in significantly increased levels of intact GLP-1[11]. There is substantial evidence to show cardiovascular benefit of intact GLP-1, via reduced inflammation and ischemic injury, as well as improved endothelial function[54]. Further, reduced GIP levels have been revealed as a predictor of poor outcome in high-risk patients with acute MI[55]. Therefore, we will assess active and total levels of GLP-1 and GIP in our study to determine if our findings are dependent on their cardioprotective actions.

Our preliminary studies did not reveal a precise mechanism behind our positive findings in LVEF improvement in *Dpp4*$^{hep-/-}$ mice, and an increased number of *Dpp4*$^{EC-/-}$ mice with fully kinetic hearts. Interestingly, we observed no significant functional improvement in *Dpp4*$^{-/-}$ mice compared to *Dpp4*$^{+/+}$ mice, which contrasts previous reports[14,16]. We did observe a trend for maintained function from baseline to endpoint in *Dpp4*$^{-/-}$ mice compared to *Dpp4*$^{+/+}$ mice with control treatment, however. Overall, this data suggests that reductions in DPP4 activity and protein can improve function and reduce infarcts sizes to varying degrees, respectively. Our findings in *Dpp4*$^{-/-}$ mice is in line with studies that report lack of improvement in high-fat diet-fed, diabetic mice treated with MK-0626 after trans-aortic constriction surgery to induce pressure overload[16]. In contrast to the study conducted by Sauve *et. al.*[14], our mice were aged and treated with lower concentrations of drugs, which may account for discrepancies, however a true mechanism was not uncovered in the current study.

Most notably, we saw a significant improvement in LVEF in DT treated *Dpp4*$^{hep-/-}$ mice, both pre- and post-MI. This group was more responsive to treatment compared to both *Dpp4*$^{-/-}$ mice and *Dpp4*$^{EC-/-}$ mice, suggesting endothelial cell-derived DPP4 is the target of metformin action potentially. Additionally, metformin targets the liver via its organ specific organ cation transporter 1 (OCT1). We have previously shown that the liver is central to obesity where *Pemt*$^{-/-}$ mice do not gain weight but do have steatotic livers, and in this case DPP4 activity was increased 4-fold[29]. It is possible that metformin improved liver lipid metabolism[56] in our study, to impact endothelial cell-derived DPP4, or hepatocyte-derived DPP4 in *Dpp4*$^{EC-/-}$ mice to improve myocardial kinesis. Future experiments will investigate lipid metabolism pathways and myocardial fuel metabolism to determine how this affected ventricular function.

Additionally, we observed a relationship between DPP4 activity and protein which was not completely linear. DPP4 activity was reduced 1-week post-MI and increased thereafter, while DPP4 protein levels steadily rose from prior to surgery, to endpoint 4 weeks after LAD-ligation. This data may suggest a role for active DPP4 after infarction at which point cytokines and chemokines also fluctuate, as we have also shown.

4.7 Limitations

This study does not fully investigate the contribution of DPP4 expression on immune cells not targeted by Tie2-Cre which may be acutely increased after MI. Future studies could employ flow-cytometry to investigate how systemic or organ and cell specific genetic ablation as well as pharmaceutical treatment, affect DPP4 expression on immune cells, and further investigate inflammation and resolution.

4.8 Conclusion

In summary, we have demonstrated that prior to MI, *Dpp4*$^{hep-/-}$ and *Dpp4*$^{EC-/-}$ mice have moderately superior cardiac dimensions and function, respectively, compared to their controls, after HFHC-feeding and metformin or DT, respectively. Post-MI, similar trends persist, illustrating CV improvement in *Dpp4*$^{hep-/-}$ and *Dpp4*$^{EC-/-}$ mice, however, only *Dpp4*$^{EC-/-}$ mice have significantly smaller akinetic lengths. Future studies will elaborate on the mechanisms behind these improvements, focusing on GLP-1 and acute post-infarct inflammation characterization. Future studies will evaluate the infarct, peri-infarct and remote parts of the ventricle for changes in remodelling and fibrosis associated genes, as well as protein levels of cytokines and chemokines. In circulation, we will evaluate active and total GLP-1 as well as GIP and pro-inflammatory and pro-resolving DPP4 substrates.

4.9 Acknowledgements

We would like to thank the Animal Care and Veterinary Services Staff at UOHI for their animal husbandry and post-surgical support. Further, we would like to thank fellow members of the Mulvihill lab, Nadya M. Morrow, Andrew C. Clement, My-Anh Nguyen, Antonio A. Hanson and Evgenia Fadzeyeva for their assistance throughout the study with animal sacrifice. EEM is the guarantor of this work and, as such, had full access to all the data in the study and take responsibility for the integrity of the data and the accuracy of the data analysis. The Canadian Institutes of Health Research (CIHR) supported this work (ARJ-162628, Project Grant 156136 and a Heart and Stroke National New Investigator award to EEM). NAT is supported by a UOHI endowment scholarship. NMM is supported by a CIHR doctoral award. AMC is

supported by a CIHR masters award. BV was supported by a CIHR postdoctoral fellowship.

Supplemental Table 4.1: List of qRT-PCR primers, from Applied Biosystems.

Oligonucleotides	**Identifier**
Swine dipeptidyl peptidase-4 (*Dpp4*)	Ss03383683_u1
Swine platelet endothelial cell adhesion molecule-1 (*Pecam1*)	Ss03392600_u1
Swine *Thy1*	Ss03376963_u1
Murine chemokine (C-C motif) ligand 2 (*Ccl2*)	Mm00441242_m1
Murine chemokine (C-X-C motif) ligand 10 (*Cxcl10*)	Mm00445235_m1
Murine chemokine (C-C motif) ligand 11 (*Ccl11*)	Mm00441238_m1
Murine chemokine (C-X-C motif) ligand 12 (*Cxcl12*)	Mm00445553_m1
Murine chemokine (C-C motif) ligand 5 (*Ccl5*)	Mm01302427_m1

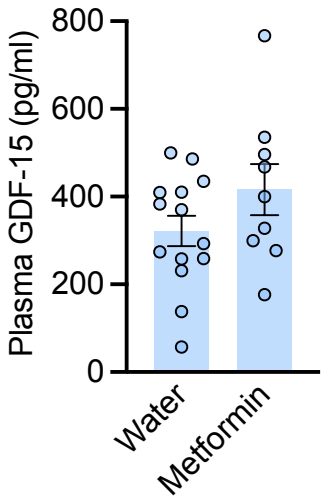

Supplemental Figure 4.1: Plasma GDF-15 is increased with metformin treatment. Plasma GDF-15 levels in control (water) or metformin treated *Dpp4*$^{+/+}$ mice

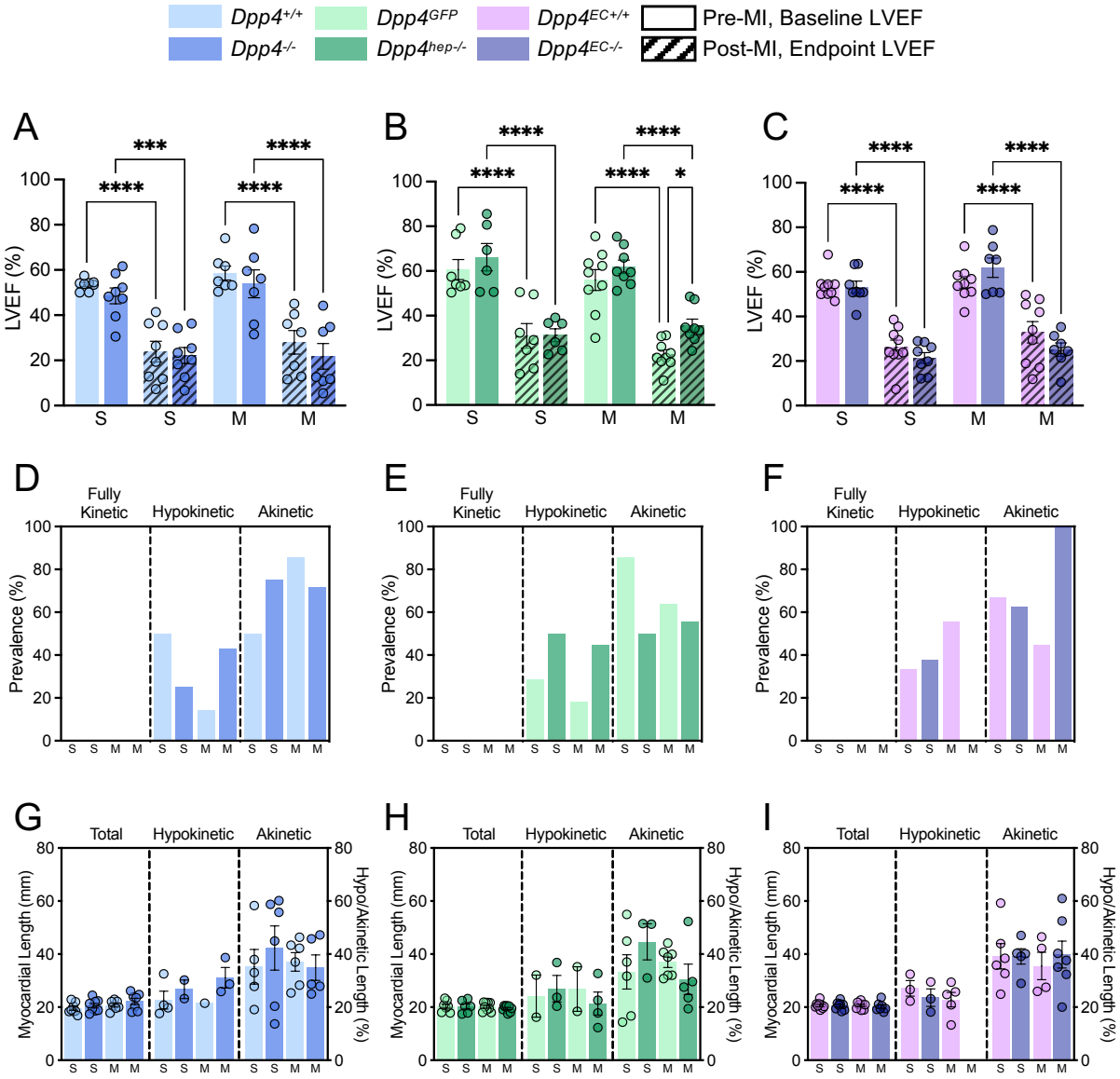

Supplemental Figure 4.2: Metformin treatment in *Dpp4*$^{EC-/-}$ and *Dpp4*$^{hep-/-}$ mice does not rescue myocardial kinesis, or reduce infarct size. LVEF at baseline (plain bars) after 10-weeks of HFHC-feeding and 4 weeks of pharmacological treatment and at endpoint (patterned bars) after 4-weeks after LAD-ligation, 14-weeks of HFHC-feeding and 8-weeks of pharmacological treatment, in (**A**) *Dpp4*$^{+/+}$ and *Dpp4*$^{-/-}$, (**B**) *Dpp4*^{GFP} and *Dpp4*$^{hep-/-}$ and (**C**) *Dpp4*$^{EC+/+}$ and *Dpp4*$^{EC-/-}$ male mice. Prevalence of fully kinetic, hypokinetic and akinetic myocardium after LAD-ligation in (**D**) *Dpp4*$^{+/+}$ and *Dpp4*$^{-/-}$, (**E**) *Dpp4*^{GFP} and *Dpp4*$^{hep-/-}$ and (**F**) *Dpp4*$^{EC+/+}$ and *Dpp4*$^{EC-/-}$ male mice. Total endocardial left ventricle length (left Y-axis), and hypokinetic and akinetic proportion (right y-axis) in (**G**) *Dpp4*$^{+/+}$ and *Dpp4*$^{-/-}$, (**H**) *Dpp4*^{GFP} and *Dpp4*$^{hep-/-}$ and (**I**) *Dpp4*$^{EC+/+}$ and *Dpp4*$^{EC-/-}$ male mice. Data are presented as means ± SEM analyzed by a two-way ANOVA with a Tukey's post-hoc test, *p=0.01-0.05.

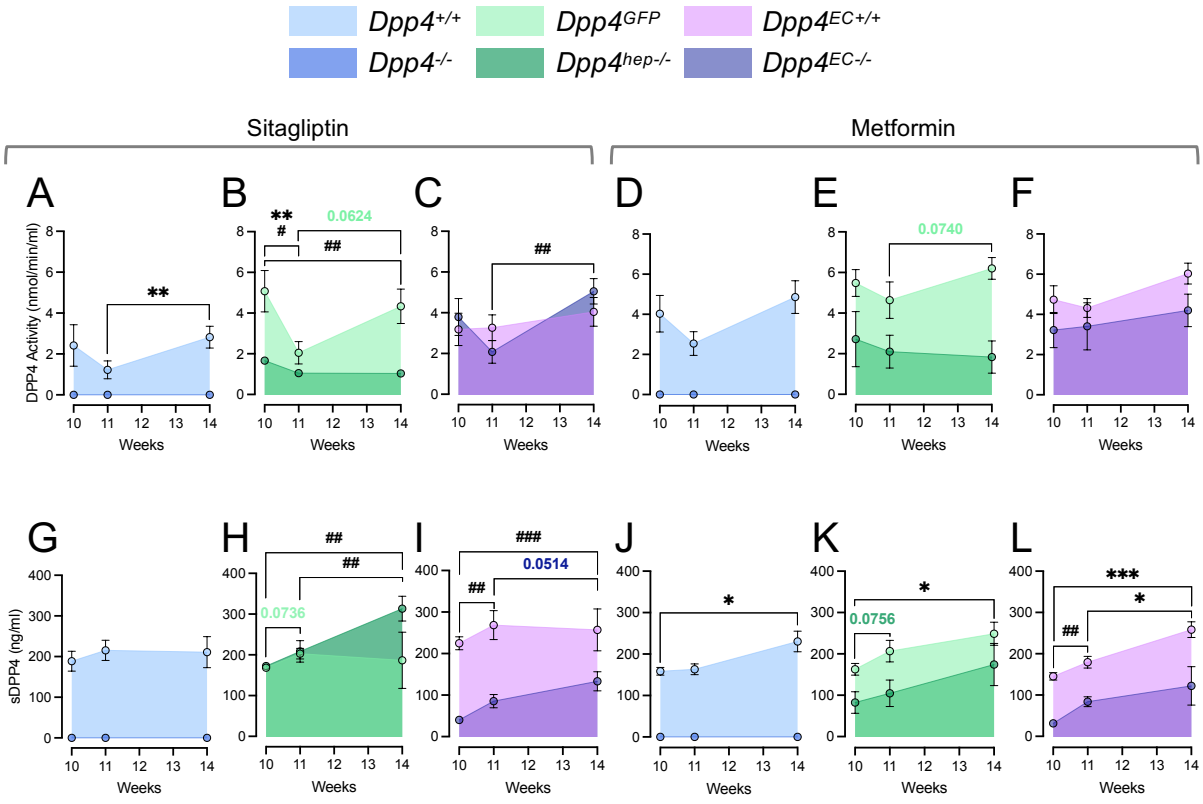

Supplemental Figure 4.3: DPP4 activity and sDPP4 over time in sitagliptin and metformin treated mice. Plasma DPP4 activity in (**A**) *Dpp4*$^{+/+}$ and *Dpp4*$^{-/-}$, (**B**) *Dpp4*^{GFP} and *Dpp4*$^{hep-/-}$ and (**C**) *Dpp4*$^{EC+/+}$ and *Dpp4*$^{EC-/-}$ mice, and DPP4 protein concentration in (**G**) *Dpp4*$^{+/+}$ and *Dpp4*$^{-/-}$, (**H**) *Dpp4*^{GFP} and *Dpp4*$^{hep-/-}$ and (**I**) *Dpp4*$^{EC+/+}$ and *Dpp4*$^{EC-/-}$ mice with sitagliptin treatment. Plasma DPP4 activity in (**D**) *Dpp4*$^{+/+}$ and *Dpp4*$^{-/-}$, (**E**) *Dpp4*^{GFP} and *Dpp4*$^{hep-/-}$ and (**F**) *Dpp4*$^{EC+/+}$ and *Dpp4*$^{EC-/-}$ mice, and DPP4 protein concentration in (**J**) *Dpp4*$^{+/+}$ and *Dpp4*$^{-/-}$, (**K**) *Dpp4*^{GFP} and *Dpp4*$^{hep-/-}$ and (**L**) *Dpp4*$^{EC+/+}$ and *Dpp4*$^{EC-/-}$ mice with metformin treatment. The 10-week time point includes 10 weeks of HFHC-feeding and 4 weeks of treatment. The 11-week time point includes 11 weeks of HFHC-feeding and 5 weeks of treatment and is 1 week after LAD-ligation. The 14-week time point includes 14 weeks of HFHC-feeding and 8 weeks of treatment and is 4 weeks after LAD-ligation. Data are presented as means ± SEM analyzed by a two-way ANOVA with repeated measures and a Tukey post-hoc multiple comparisons correction reported as adjusted p value. Significant differences in *Dpp4*$^{+/+}$, *Dpp4*^{GFP} and *Dpp4*$^{EC+/+}$, *p=0.01-0.05, **p=0.001-0.01, ***p=0.0001-0.001 and ****p<0.0001. Significant differences in *Dpp4*$^{-/-}$, *Dpp4*$^{hep-/-}$ and *Dpp4*$^{EC-/-}$, #p=0.01-0.05, ##p=0.001-0.01 and ###p=0.0001-0.001. Trends are reported as adjusted p values in the colour of their respective genotype.

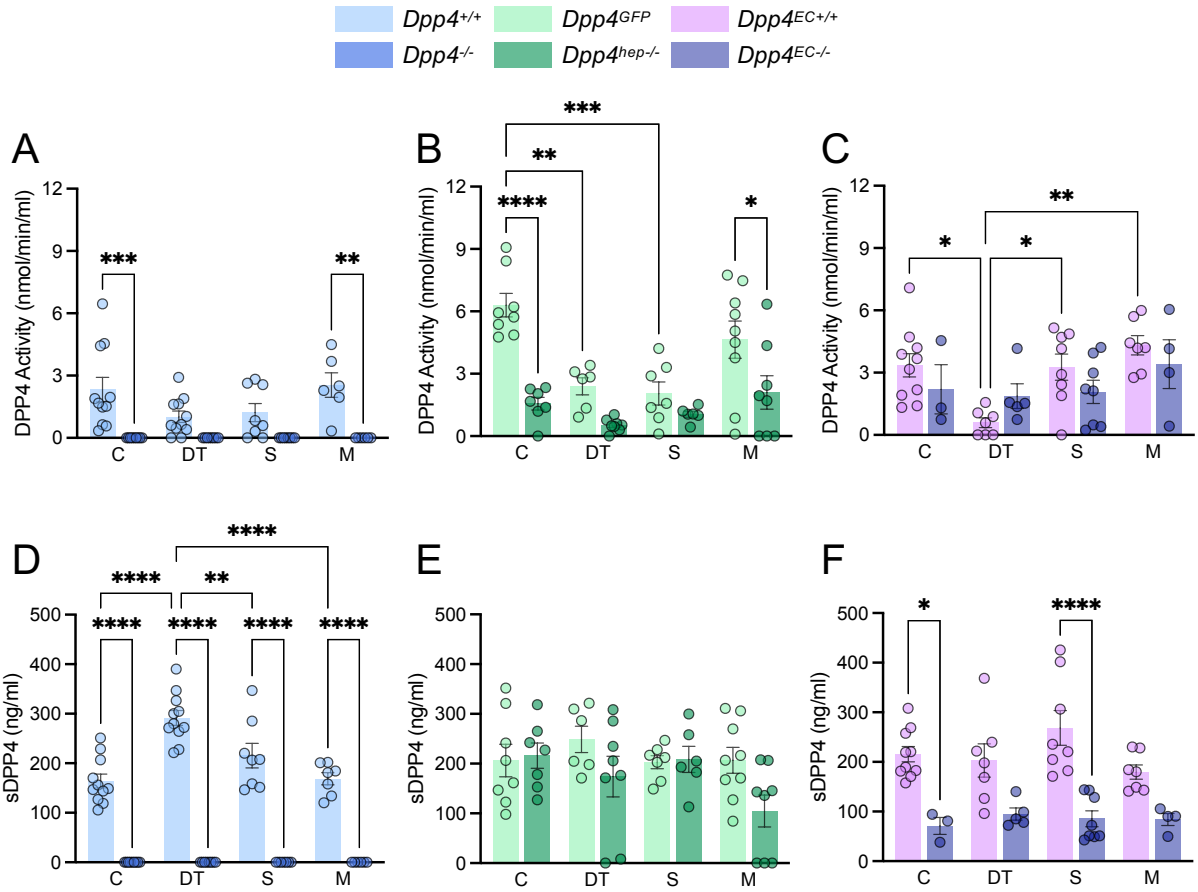

Supplemental Figure 4.4: Seven days post-MI, DPP4 activity is reduced, but sDPP4 levels are maintained. Plasma DPP4 activity in (A) *Dpp4*$^{+/+}$ and *Dpp4*$^{-/-}$, (B) *Dpp4*^{GFP} and *Dpp4*$^{hep-/-}$ and (C) *Dpp4*$^{EC+/+}$ and *Dpp4*$^{EC-/-}$ mice, and DPP4 protein concentration in (D) *Dpp4*$^{+/+}$ and *Dpp4*$^{-/-}$, (E) *Dpp4*^{GFP} and *Dpp4*$^{hep-/-}$ and (F) *Dpp4*$^{EC+/+}$ and *Dpp4*$^{EC-/-}$ mice, after 14 weeks of HFHC feeding, 8 weeks of drug treatment and 4 weeks following LAD-ligation. Drug treatments: C = control (water), S = Sitagliptin, M = Metformin and DT = dual therapy (Sitagliptin and Metformin combination). Data are presented as means ± SEM analyzed by a two-way ANOVA with a Tukey post-hoc multiple comparisons correction reported as adjusted p value, *p=0.01-0.05, **p=0.001-0.01, ***p=0.0001-0.001 and ****p<0.0001.

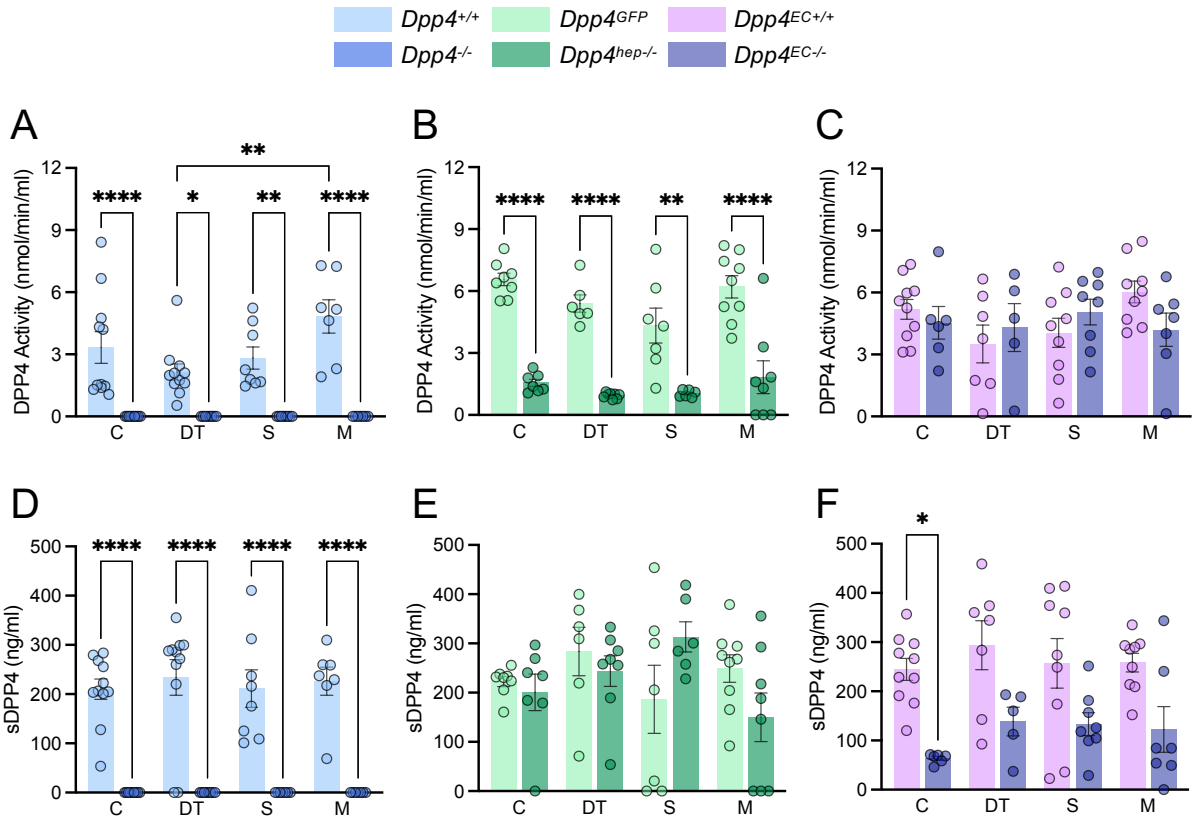

Supplemental Figure 4.5: Four weeks post-MI, DPP4 activity and sDPP4 levels resemble baseline trends. Plasma DPP4 activity in (A) *Dpp4*$^{+/+}$ and *Dpp4*$^{-/-}$, (B) *Dpp4*^{GFP} and *Dpp4*$^{hep-/-}$ and (C) *Dpp4*$^{EC+/+}$ and *Dpp4*$^{EC-/-}$ mice, and DPP4 protein concentration in (D) *Dpp4*$^{+/+}$ and *Dpp4*$^{-/-}$, (E) *Dpp4*^{GFP} and *Dpp4*$^{hep-/-}$ and (F) *Dpp4*$^{EC+/+}$ and *Dpp4*$^{EC-/-}$ mice, after 14 weeks of HFHC feeding, 8 weeks of drug treatment and 4 weeks following LAD-ligation. Drug treatments: C = control (water), S = Sitagliptin, M = Metformin and DT = dual therapy (Sitagliptin and Metformin combination). Data are presented as means ± SEM analyzed by a two-way ANOVA with a Tukey post-hoc multiple comparisons correction reported as adjusted p value, *p=0.01-0.05, **p=0.001-0.01, ***p=0.0001-0.001 and ****p<0.0001.

4.10 References

1. Guide for Industry. Diabetes Mellitus: Evaluating Cardiovascular Risk in New Antidiabetic Therapies To Treat Type 2 Diabetes.Silver Spring, MD: Food and Drug Administration; 2008. http://www.fda.gov/downloads/Drugs/guidanceComplianceRegulatoryInformation/guidances/ucm071627.pdf. Accessed December 15, 2023.
2. Cefalu WT, Kaul S, Gerstein HC, et al. Cardiovascular Outcomes Trials in Type 2 Diabetes: Where Do We Go From Here? Reflections From a Diabetes Care Editors' Expert Forum. *Diabetes Care.* 2018;41(1):14-31.
3. Miller RA, Chu Q, Xie J, Foretz M, Viollet B, Birnbaum MJ. Biguanides suppress hepatic glucagon signalling by decreasing production of cyclic AMP. *Nature.* 2013;494(7436):256-260.
4. Chacra AR. Evolving metformin treatment strategies in type-2 diabetes: from immediate-release metformin monotherapy to extended-release combination therapy. *Am J Ther.* 2014;21(3):198-210.
5. DeFronzo RA, Buse JB, Kim T, et al. Once-daily delayed-release metformin lowers plasma glucose and enhances fasting and postprandial GLP-1 and PYY: results from two randomised trials. *Diabetologia.* 2016;59(8):1645-1654.
6. Mannucci E, Tesi F, Bardini G, et al. Effects of metformin on glucagon-like peptide-1 levels in obese patients with and without Type 2 diabetes. *Diabetes Nutr Metab.* 2004;17(6):336-342.
7. Wu T, Thazhath SS, Bound MJ, Jones KL, Horowitz M, Rayner CK. Mechanism of increase in plasma intact GLP-1 by metformin in type 2 diabetes: stimulation of GLP-1 secretion or reduction in plasma DPP-4 activity? *Diabetes Res Clin Pract.* 2014;106(1):e3-6.
8. Inzucchi SE, Bergenstal RM, Buse JB, et al. Management of hyperglycemia in type 2 diabetes: a patient-centered approach: position statement of the American Diabetes Association (ADA) and the European Association for the Study of Diabetes (EASD). *Diabetes Care.* 2012;35(6):1364-1379.
9. Deacon CF. Circulation and degradation of GIP and GLP-1. *Horm Metab Res.* 2004;36(11-12):761-765.
10. Deacon CF, Danielsen P, Klarskov L, Olesen M, Holst JJ. Dipeptidyl peptidase IV inhibition reduces the degradation and clearance of GIP and potentiates its insulinotropic and antihyperglycemic effects in anesthetized pigs. *Diabetes.* 2001;50(7):1588-1597.
11. Varin EM, Mulvihill EE, Beaudry JL, et al. Circulating Levels of Soluble Dipeptidyl Peptidase-4 Are Dissociated from Inflammation and Induced by Enzymatic DPP4 Inhibition. *Cell Metab.* 2019;29(2):320-334 e325.
12. Ghorpade DS, Ozcan L, Zheng Z, et al. Hepatocyte-secreted DPP4 in obesity promotes adipose inflammation and insulin resistance. *Nature.* 2018;555(7698):673-677.
13. Baumeier C, Schluter L, Saussenthaler S, et al. Elevated hepatic DPP4 activity promotes insulin resistance and non-alcoholic fatty liver disease. *Mol Metab.* 2017;6(10):1254-1263.

14. Sauve M, Ban K, Momen MA, et al. Genetic deletion or pharmacological inhibition of dipeptidyl peptidase-4 improves cardiovascular outcomes after myocardial infarction in mice. *Diabetes.* 2010;59(4):1063-1073.
15. Shigeta T, Aoyama M, Bando YK, et al. Dipeptidyl peptidase-4 modulates left ventricular dysfunction in chronic heart failure via angiogenesis-dependent and -independent actions. *Circulation.* 2012;126(15):1838-1851.
16. Mulvihill EE, Varin EM, Ussher JR, et al. Inhibition of Dipeptidyl Peptidase-4 Impairs Ventricular Function and Promotes Cardiac Fibrosis in High Fat-Fed Diabetic Mice. *Diabetes.* 2016;65(3):742-754.
17. Ku HC, Chen WP, Su MJ. DPP4 deficiency preserves cardiac function via GLP-1 signaling in rats subjected to myocardial ischemia/reperfusion. *Naunyn Schmiedebergs Arch Pharmacol.* 2011;384(2):197-207.
18. Chang G, Zhang P, Ye L, et al. Protective effects of sitagliptin on myocardial injury and cardiac function in an ischemia/reperfusion rat model. *Eur J Pharmacol.* 2013;718(1-3):105-113.
19. Cefalu WT, Kaul S, Gerstein HC, et al. Cardiovascular outcomes trials in type 2 diabetes: where do we go from here? Reflections from a diabetes care editors' expert forum. *Diabetes care.* 2018;41(1):14-31.
20. Crowley MJ, Williams JW, Jr., Kosinski AS, D'Alessio DA, Buse JB. Metformin Use May Moderate the Effect of DPP-4 Inhibitors on Cardiovascular Outcomes. *Diabetes Care.* 2017;40(12):1787-1789.
21. Ahmed RH, Huri HZ, Al-Hamodi Z, Salem SD, Muniandy S. Serum Levels of Soluble CD26/Dipeptidyl Peptidase-IV in Type 2 Diabetes Mellitus and Its Association with Metabolic Syndrome and Therapy with Antidiabetic Agents in Malaysian Subjects. *PLoS One.* 2015;10(10):e0140618.
22. Lee SA, Kim YR, Yang EJ, et al. CD26/DPP4 levels in peripheral blood and T cells in patients with type 2 diabetes mellitus. *J Clin Endocrinol Metab.* 2013;98(6):2553-2561.
23. Lenhard JM, Croom DK, Minnick DT. Reduced serum dipeptidyl peptidase-IV after metformin and pioglitazone treatments. *Biochem Biophys Res Commun.* 2004;324(1):92-97.
24. Migoya EM, Bergeron R, Miller JL, et al. Dipeptidyl peptidase-4 inhibitors administered in combination with metformin result in an additive increase in the plasma concentration of active GLP-1. *Clin Pharmacol Ther.* 2010;88(6):801-808.
25. Baggio LL, Varin EM, Koehler JA, et al. Plasma levels of DPP4 activity and sDPP4 are dissociated from inflammation in mice and humans. *Nat Commun.* 2020;11(1):3766.
26. Mulvihill EE, Varin EM, Gladanac B, et al. Cellular Sites and Mechanisms Linking Reduction of Dipeptidyl Peptidase-4 Activity to Control of Incretin Hormone Action and Glucose Homeostasis. *Cell Metab.* 2017;25(1):152-165.
27. Marguet D, Baggio L, Kobayashi T, et al. Enhanced insulin secretion and improved glucose tolerance in mice lacking CD26. *Proc Natl Acad Sci U S A.* 2000;97(12):6874-6879.
28. Dann MM, Clark SQ, Trzaskalski NA, et al. Quantification of murine myocardial infarct size using 2-D and 4-D high-frequency ultrasound. *Am J Physiol Heart Circ Physiol.* 2022;322(3):H359-H372.

29. Trzaskalski NA, Vulesevic B, Nguyen MA, et al. Hepatocyte-derived DPP4 regulates portal GLP-1 bioactivity, modulates glucose production, and when absent influences NAFLD progression. *JCI Insight.* 2023;8(2).
30. Tabula Muris C, Overall c, Logistical c, et al. Single-cell transcriptomics of 20 mouse organs creates a Tabula Muris. *Nature.* 2018;562(7727):367-372.
31. Zhang H, Lui KO, Zhou B. Endocardial Cell Plasticity in Cardiac Development, Diseases and Regeneration. *Circ Res.* 2018;122(5):774-789.
32. Zeng Y, Li C, Guan M, et al. The DPP-4 inhibitor sitagliptin attenuates the progress of atherosclerosis in apolipoprotein-E-knockout mice via AMPK- and MAPK-dependent mechanisms. *Cardiovasc Diabetol.* 2014;13:32.
33. Metzemaekers M, Van Damme J, Mortier A, Proost P. Regulation of Chemokine Activity - A Focus on the Role of Dipeptidyl Peptidase IV/CD26. *Front Immunol.* 2016;7:483.
34. von Hundelshausen P, Weber KS, Huo Y, et al. RANTES deposition by platelets triggers monocyte arrest on inflamed and atherosclerotic endothelium. *Circulation.* 2001;103(13):1772-1777.
35. Haley KJ, Lilly CM, Yang JH, et al. Overexpression of eotaxin and the CCR3 receptor in human atherosclerosis: using genomic technology to identify a potential novel pathway of vascular inflammation. *Circulation.* 2000;102(18):2185-2189.
36. Huang CY, Shih CM, Tsao NW, et al. Dipeptidyl peptidase-4 inhibitor improves neovascularization by increasing circulating endothelial progenitor cells. *Br J Pharmacol.* 2012;167(7):1506-1519.
37. Kanki S, Segers VF, Wu W, et al. Stromal cell-derived factor-1 retention and cardioprotection for ischemic myocardium. *Circ Heart Fail.* 2011;4(4):509-518.
38. Gerstein HC, Pare G, Hess S, et al. Growth Differentiation Factor 15 as a Novel Biomarker for Metformin. *Diabetes Care.* 2017;40(2):280-283.
39. Packer M. Worsening Heart Failure During the Use of DPP-4 Inhibitors: Pathophysiological Mechanisms, Clinical Risks, and Potential Influence of Concomitant Antidiabetic Medications. *JACC Heart Fail.* 2018;6(6):445-451.
40. Deacon CF. Dipeptidyl peptidase-4 inhibitors in the treatment of type 2 diabetes: a comparative review. *Diabetes Obes Metab.* 2011;13(1):7-18.
41. Munir KM, Lamos EM. Diabetes type 2 management: what are the differences between DPP-4 inhibitors and how do you choose? *Expert Opin Pharmacother.* 2017;18(9):839-841.
42. Fura A, Khanna A, Vyas V, et al. Pharmacokinetics of the dipeptidyl peptidase 4 inhibitor saxagliptin in rats, dogs, and monkeys and clinical projections. *Drug Metab Dispos.* 2009;37(6):1164-1171.
43. Herman GA, Stein PP, Thornberry NA, Wagner JA. Dipeptidyl peptidase-4 inhibitors for the treatment of type 2 diabetes: focus on sitagliptin. *Clin Pharmacol Ther.* 2007;81(5):761-767.
44. He YL, Sadler BM, Sabo R, et al. The absolute oral bioavailability and population-based pharmacokinetic modelling of a novel dipeptidylpeptidase-IV inhibitor, vildagliptin, in healthy volunteers. *Clin Pharmacokinet.* 2007;46(9):787-802.
45. Chacra AR. Saxagliptin for type 2 diabetes. *Diabetes Metab Syndr Obes.* 2010;3:325-335.

46. Herman GA, Bergman A, Stevens C, et al. Effect of single oral doses of sitagliptin, a dipeptidyl peptidase-4 inhibitor, on incretin and plasma glucose levels after an oral glucose tolerance test in patients with type 2 diabetes. *J Clin Endocrinol Metab.* 2006;91(11):4612-4619.
47. Saini K, Sharma S, Khan Y. DPP-4 inhibitors for treating T2DM - hype or hope? an analysis based on the current literature. *Front Mol Biosci.* 2023;10:1130625.
48. Waget A, Cabou C, Masseboeuf M, et al. Physiological and pharmacological mechanisms through which the DPP-4 inhibitor sitagliptin regulates glycemia in mice. *Endocrinology.* 2011;152(8):3018-3029.
49. Hansen L, Deacon CF, Orskov C, Holst JJ. Glucagon-like peptide-1-(7-36)amide is transformed to glucagon-like peptide-1-(9-36)amide by dipeptidyl peptidase IV in the capillaries supplying the L cells of the porcine intestine. *Endocrinology.* 1999;140(11):5356-5363.
50. Mulherin AJ, Oh AH, Kim H, Grieco A, Lauffer LM, Brubaker PL. Mechanisms underlying metformin-induced secretion of glucagon-like peptide-1 from the intestinal L cell. *Endocrinology.* 2011;152(12):4610-4619.
51. Kappe C, Patrone C, Holst JJ, Zhang Q, Sjoholm A. Metformin protects against lipoapoptosis and enhances GLP-1 secretion from GLP-1-producing cells. *J Gastroenterol.* 2013;48(3):322-332.
52. Diebold S, Moellmann J, Kahles F, et al. Myocardial infarction is sufficient to increase GLP-1 secretion, leading to improved left ventricular contractility and mitochondrial respiratory capacity. *Diabetes Obes Metab.* 2018;20(12):2911-2918.
53. Kahles F, Meyer C, Mollmann J, et al. GLP-1 secretion is increased by inflammatory stimuli in an IL-6-dependent manner, leading to hyperinsulinemia and blood glucose lowering. *Diabetes.* 2014;63(10):3221-3229.
54. Ussher JR, Drucker DJ. Cardiovascular actions of incretin-based therapies. *Circ Res.* 2014;114(11):1788-1803.
55. Kahles F, Rau M, Reugels M, et al. The gut hormone glucose-dependent insulinotropic polypeptide is downregulated in response to myocardial injury. *Cardiovasc Diabetol.* 2022;21(1):18.
56. Viollet B, Guigas B, Sanz Garcia N, Leclerc J, Foretz M, Andreelli F. Cellular and molecular mechanisms of metformin: an overview. *Clin Sci (Lond).* 2012;122(6):253-270.

5 General Discussion

In tandem with the rise in obesity and an aging population, the prevalence of metabolic disease has been climbing steadily[1]. As of 2023, 30% of Canadians live with diabetes or prediabetes, costing individuals with T2D up to $10,000 a year in direct pharmaceutical, medical and hospital visit associated costs[2]. Complications of metabolic syndrome and T2D include NAFLD or MAFLD/MASLD, which is present in up to 70% of individuals with T2D[3]. Most importantly, these individuals are also over three times more likely to be hospitalized with CVD, which is a major cause of death as well[4]. Bearing in mind the considerable overlap between these diseases, identifying common disturbed pathways is of significant interest. Most notably, DPP4 is a pharmacological target to treat T2D[5], however, its involvement in metabolic and CVD is still emerging. For example, DPP4 is a Middle East respiratory syndrome coronavirus receptor, which made it a point of investigation at the height of the COVID-19 pandemic[6-8]. In addition, DPP4 enzymatic activity positively correlates with hyperglycemia in patients with T2D[9], and hepatic expression is increased in patients with MASLD[10] and HCV[11] and remodelling and inflammation in CVD[12]. However, DPP4 involvement in metabolic disease progression, namely in molecular processes such as inflammation, fibrosis and lipid metabolism are incompletely understood.

Consistent with numerous studies, this thesis highlights the complexity of DPP4 biology in disease. In Chapter 2, we reveal that hepatocyte-derived DPP4 is directly involved in regulating HGP via regulation of GLP-1 bioactivity. Further, consistent with previous reports[13] we determined that DPP4 cleavage of incretin hormones in the portal vein versus systemic circulation, represents a reservoir of DPP4 that could be targeted for more efficient HGP reduction and preservation of intact incretin

hormones. The GLP-1 receptor is expressed in the portal vein[14,15] which stimulates vagal afferent nerve activity to mediate glucose tolerance in rats[16]. In addition, direct GLP-1 portal vein infusion decreases the size of ongoing meals in rats, evidently independent of the vagus nerve[17]. Other gut-derived peptides like cholecystokinin octapeptide[18] and DPP4 substrate PYY[19,20], are also implicated in inducing satiety via the portal vein, identified with direct infusion[21]. Our results in tandem with these studies reveal a regulatory role for DPP4 of gut-derived peptides in the portal vein to regulate glucose.

In addition, previous reports illustrate reduced plasma triglyceride levels in patients with T2D with DPP4 inhibition with sitagliptin[22], which was replicated in obese *Dpp4*$^{-/-}$ mice. Further, we were also the first to show a significant 4-fold increase in plasma DPP4 activity concurrent with lipid pathway dysregulation but independent of obesity, in a lean MASLD model using *Pemt*$^{-/-}$ mice. Previous reports consistently show a direct correlation between obesity and increased DPP4 activity[23], but here we reveal that hepatomegaly and hepatic steatosis due to *de novo* choline synthesis may be another factor in DPP4 enzyme activity regulation. DPP4 has been previously described as an adipokine[24], however, this data reveal that it is most likely related to hepatic accumulation of FAs and not addition of adipose tissue. Similarly, in patients with HCV treated with ribavirin, DPP4 activity and protein decreased with reduced viral load, but metabolic parameters like fasting glucose, insulin and HOMA-IR were unchanged[25]. DPP4 activity is increased in metabolic disease and decreases with resolution or improvement[24]. Considering individuals with HCV experience increased lipogenesis, and impaired lipid degradation and export[26], our data further infer a relationship between DPP4 and hepatic lipid metabolism. However, our findings

highlight a disconnect between infection resolution, metabolism and DPP4 activity and protein levels. Instead, our data emphasize that inflammation may be an additional driver of DPP4 versus metabolic factors alone in individuals with HCV. Even in the absence of obesity, our *Pemt*$^{-/-}$ mice also experienced an increase in DPP4 activity, and previous reports show increased hepatic inflammation in this mouse model[27]. Therefore, the inflammatory aspects of metabolic disease may be driving DPP4 expression, increased enzymatic activity and sDPP4 levels.

DPP4 has been a previously recognized as a regulator of immune cells, notably as a costimulatory molecule of T cell signal transduction[28], and associated with inflammation[29,30]. We show that systemic *Dpp4* elimination increases expression of immune-related pathways, which was unchanged in *Dpp4*$^{hep-/-}$ mice, compared to controls. Previous studies support our findings that with HFHC-feeding, systemic *Dpp4* elimination does not result in reduced cytokine and chemokine mRNA expression. However, multiple reports contrast our findings in *Dpp4*$^{hep-/-}$ mice, which typically show reduced inflammation[13,31,32], however, this discrepancy could be explained by the use of aged mice in our case, versus young mice used in previous literature. Our mice were approximately 1-year-old at time of sacrifice which may have affected DPP4 activity. This has been previously described in *Dpp4*$^{EC-/-}$ mice; in 8-20 week old mice, with regular chow and HFD-feeding, DPP4 activity was significantly reduced compared to controls, however in 25-30 week old mice, this reduction was not maintained[31]. These results, in concert with ours, underline a dynamic relationship between increased age and DPP4 activity which has been previously described[31], but has yet to be thoroughly explored as an age-related factor in disease progression. Throughout this thesis we modelled human disease by using aged mice, rather than

younger, relatively healthy mice. Chapter 2 illustrated the role of hepatocyte-derived DPP4 in HGP and showed a clear disconnect between DPP4 in lipid metabolism, fibrosis and inflammation.

It has been well documented that hepatocyte-derived DPP4 exerts local and peripheral actions, including reducing hepatic steatosis and inflammation, and AT inflammation and insulin resistance in its absence[13,31,32]. However, despite the strong incidence of CVD in individuals with T2D, the potential implications of hepatocyte-derived DPP4 in the heart have not been evaluated. In our second study in Chapter 3, we revealed that mRNA expression of immune-related pathways and protein levels were reduced in *Dpp4*$^{hep-/-}$ mice, while *Col1a1* and *Col3a1* mRNA expression was increased in *Dpp4*$^{-/-}$ mice, and trending down in *Dpp4*$^{hep-/-}$ mice, compared to controls. Interestingly regardless of molecular changes, systolic and diastolic function were unchanged in both genotypes compared to controls. We were the first to illustrate that hepatocyte-derived DPP4 can influence ventricular molecular pathways in inflammation. However, fibrosis-related gene expression was only increased by systemic *Dpp4* genetic elimination, suggesting that DPP4 originating from other places besides hepatocytes is involved in this process, and that DPP4 is indispensable in regulating pathophysiological fibrosis. Further, we observed no differences in cardiac function. This may be due to the fact we relied on high-fat, high-cholesterol diet-induced cardiac dysfunction rather than a surgical insult, such as TAC surgery. Mice with a C57BL/6J background, such as in our studies, are protected from diet-induced cardiac functional impairment even when cardiac hypertrophy and FA metabolism are increased[33]. Further, in previous studies, euglycemic *Dpp4*$^{-/-}$ mice exhibited reduced fibrosis and cardioprotection, despite increased mRNA expression

of inflammation-related genes, however, this was not recapitulated in older, diabetic mice, underscoring the effect of age and suggesting that differences in cardiac function may have been evident at earlier timepoints[34]. Nonetheless, the studies described in Chapter 2 and 3, together solidify the complicated and incompletely explored field of DPP4 biology in cardiometabolic disease. We reveal more evidence that suggests DPP4 action is dynamic depending on its site of origin; whereby inflammation and immune-related genes and pathways were reduced in *Dpp4*$^{hep-/-}$ mouse hearts.

Given the progressive nature of T2D, medications are typically added in sequence to effectively manage hyperglycemia[35]. However, the molecular impact of concomitant pharmaceutical therapy use has not been evaluated in preclinical models. Recent studies have shown that sDPP4 levels are increased with DPP4i use in mice[31]. Conversely, metformin appears to reduce DPP4 shedding into circulation[36]. Interestingly this is not recapitulated in human samples where despite 50-85% reduction in DPP4 activity in a subset of patients prescribed 100 mg/day (the typical dose), sDPP4 levels do not change, even with metformin[36]. In our case, we had range of inhibition from 15-56% inhibition, depending on genotype, and despite this we still had modest increases in sDPP4 levels with administration of sitagliptin. Among the SAVOR TIMI-53[37], TECOS[38] and EXAMINE[39] DPP4i CVOTs, there was a range of DPP4i dosage, from below, and up to, the average dose. DPP4 activity is not reported in large CVOTs, but based on other smaller clinical studies[40-42] we can deduce that DPP4 activity is not reduced to zero as typically seen in many mouse studies. Therefore, our lower dose of DPP4i, sitagliptin, in our mouse studies better recapitulates what is seen in the CVOTs and what would be expected with DPP4

inhibition and DT treatment with metformin in terms of sDPP4 levels. Further, DT treatment with DPP4i's and metformin is cardioprotective, as described in a meta-regression analysis that compared prevalent metformin users to DPP4i monotherapy[43]. In addition, there is evidence to suggest that DPP4 in bone marrow (Tie2+ cells) is the depot which is affected by metformin[36], however, how this translates into a cardioprotective phenotype still has not been investigated. In Chapter 4, we showed that with DT treatment (metformin and sitagliptin), LVEF was rescued prior to and after LAD-ligation in *Dpp4*$^{hep-/-}$ mice, compared to control, while *Dpp4*$^{EC-/-}$ mice had a greater number of mice with fully kinetic hearts. Additionally, we observed a dissociated relationship between DPP4 activity and sDPP4 proteins, where activity decreases after surgery and goes back to baseline levels, at endpoint, while sDPP4 levels continue to increase from baseline, through to endpoint even after surgery. Thus far however, we have not investigated further to identify the mechanism behind this phenotype. We predict that it is due to GLP-1 action in the heart that is moderated via both pharmacological and genetic reduction in DPP4 that effectively decreases both activity and protein levels. Several studies have revealed a significant cardioprotective phenotype with GLP-1RA's, namely by increasing myocardial glucose uptake and use, reducing oxidative stress, cardiomyocyte apoptosis, inflammation and fibrosis[44-47]. GLP-1 is increased with inflammation and after MI[48,49], and considering the cardioprotective phenotype of GLP-1RA's, we believe this is the most likely mechanism leading to the modest protection observed. We plan to explore these mechanisms in our study and evaluate active and total GLP-1, GIP and other substrate levels, acutely post-MI, at 1-, 4-, 24 hours and 7 days after surgery. These timepoints should capture the acute sterile inflammation phase and resolution/repair

phase[50]. This study is novel as it attempts to determine which cellular depot of DPP4 is implicated in the cardioprotection observed with DT treatment, via murine genetic models.

5.1 The Future of DPP4 Research

5.1.1 DPP4 Substrates: Tip of the Iceberg

Our studies coupled with previous literature clearly revealed the complexity of DPP4 biology, including its activity throughout the circulatory system, i.e. portal vs. systemic circulation, and between organ systems. Therefore, further exploration of these reservoirs and other potential DPP4 targets is necessary. The majority of DPP4 substrates have been characterized as pharmacological substrates, while only a handful have been confirmed as physiological substrates. Considering DPP4 substrates have illustrated utility as pharmacological agents, such as in the case of GLP-1RA's, identifying additional substrates is of great interest. Further, as acknowledged in this thesis and by others, DPP4 plays a role in disease pathophysiology beyond T2D, revealing a gap in therapeutic potential. As previously mentioned, DPP4 cleaves only two amino acids from the N-terminal, making identification of cleaved and intact proteins difficult due to the lack of sensitivity of current approaches. Therefore, in collaboration with Dr. Anne-Claude Gingras' lab (Lunenfeld-Tanenbaum Research Institute, Toronto, ON), we tested and compared Hydrophobic Tagging-Assisted N-termini Enrichment (HYTANE)[51] (**Figure 5.1**) and Terminal Amine Isotopic Labelling of Substrates (TAILS)[52,53] coupled with analysis by liquid chromatography with tandem mass spectrometry (LC-MS/MS) to enrich, identify and distinguish DPP4-generated neo-N-termini from other peptides in complex biological samples, including intestinal tissue (detailed methods in Appendix 2). After

testing, HYTANE proved to be superior, yielding fewer total peptides, the majority of which were N-termini (**Figure 5.2A**). After applying this method to ventricular tissue from dysglycemic mice after TAC surgery, we revealed 5 putative substrates: apolipoprotein C1 (ApoC1) (**Figure 5.2B, C**), growth hormone binding protein (GHBP) (**Figure 5.4A, B**), ependymin related 1 (EPDR1) (**Figure 5.5A**), insulin-like growth factor-binding protein 1 (IGFBF) (**Figure 5.6A**) and transforming growth factor β induced (TGFBI) (**Figure 5.7A**).

We then validated these as pharmacological substrates by incubating each peptide with recombinant DPP4 and analyzing samples using mass spectrometry to identify cleavage (**Figure 5.3A, 5.3B, 5.4C, 5.4D, 5.7B and 5.7C**). Interestingly, we identified sequential DPP4 dipeptide cleavage of EPDR1 (**Figure 5.5B, C**) and IGFBP1 (**Figure 5.6B, C**), determining these peptides lose 4 amino acids from their N-terminus.

Further, we revealed that truncated ApoC1 does not inhibit cholesterol ester transfer protein (CETP) as efficiently as full length ApoC1 or torcetrapib, a pharmaceutical CETP inhibitor (**Figure 5.8**) suggesting a biological function to DPP4 cleavage. Further experiments have been designed to complete the biological validation for the remaining putative substrates. Ultimately, we aim to inject mice with recombinant protein resistant to DPP4 cleavage after HF or MI to determine the cardioprotective capacity, in a similar manner to GLP-1RA's. Literature investigating DPP4 substrates in CVD suggests that many, including GLP-1[54], SDF-1[55,56] and HMGB1[57], are cardioprotective when infused as a cleavage resistant peptide or with DPP4i treatment. Conversely, other substrates lose their cardioprotective phenotype

with cleavage, like brain natriuretic peptide (BNP). BNP [1-32] is cleaved by DPP4 to BNP [3-32] leading to reduced vasodilatory activity[58]. Therefore, future studies will evaluate if these putative substrates are also cardioprotective at suprapharmacological levels or detrimental to CV health when cleaved.

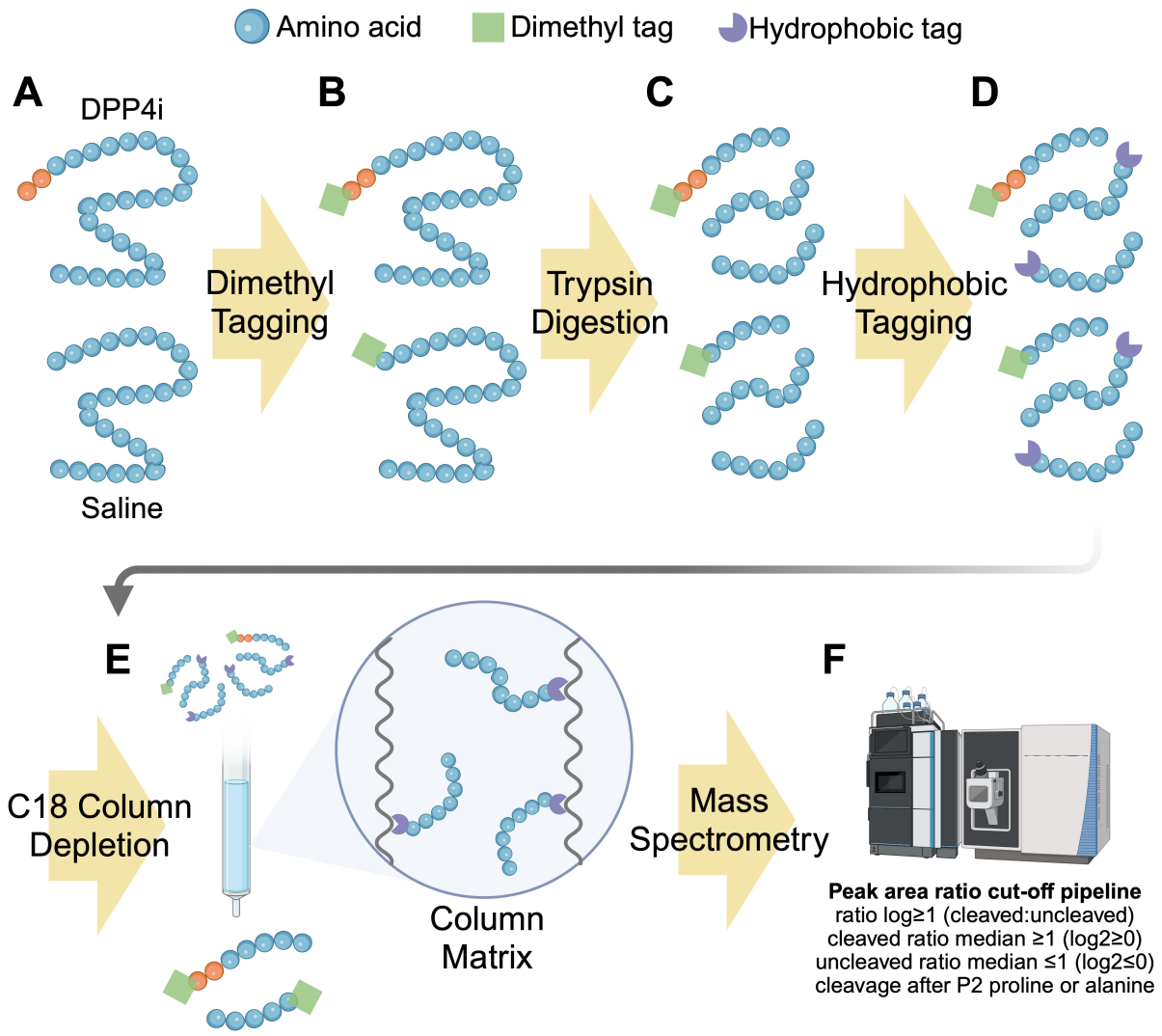

Figure 5.1: DPP4 substrate discovery can be improved via hydrophobic tagging-assisted N-termini enrichment. Mice were fed a high-fat diet for 3 months and injected with streptozotocin to induce dysglycemia. Subsequently, mice were treated with either saline or MK0626, a DPP4 inhibitor, and subjected to TAC surgery to induce pressure overload. (**A**) 10 weeks later mice were sacrificed, and plasma was collected for HYTANE analysis. (**B**) Samples are separately isotopically labeled with either light or heavy dimethyl tags. (**C**) Plasma samples were pooled together, and trypsin digested. (**D**) Neo-N-termini generated after trypsin digestion were hydrophobically tagged. (**E**) Original N-termini were negatively selected via C18 column depletion. Peptide fragments with a hydrophobic tag will bind to the column matrix, while dimethyl tagged peptides pass through. (**F**) Dimethyl tagged peptides were then fractionated, identified and quantified using high-pH and analyzed by nano-LC-MS/MS data with an Eksigent 425 HPLC and a Thermo Scientific™ Orbitrap Fusion™ Lumos™ Mass Spectrometer. Using a strict cut-off pipeline, 5 putative substrates were identified.

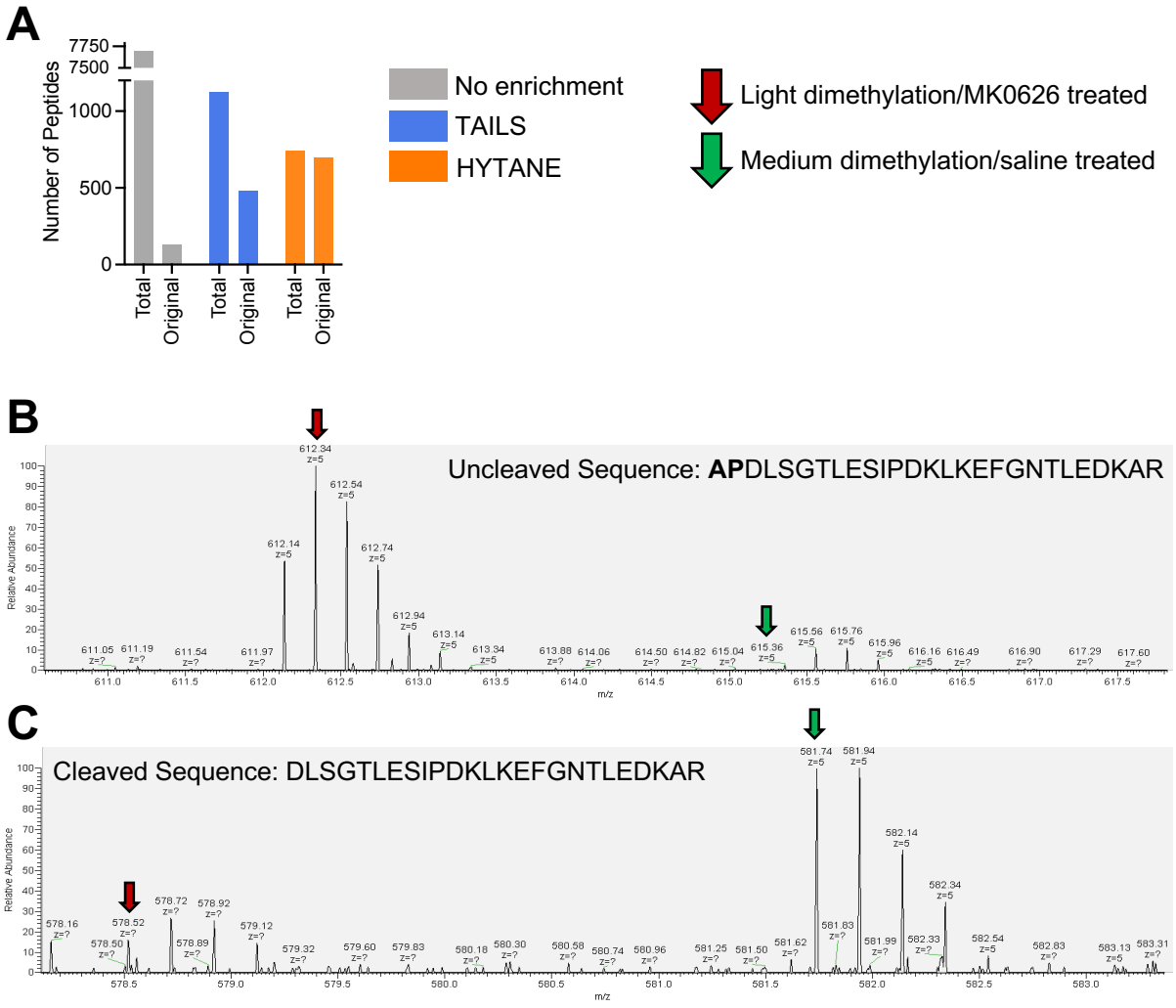

Figure 5.2: HYTANE is a superior method for DPP4 substrate discovery. (**A**) peptide yield of total (neo- and original peptides) and only original peptides with no enrichment, TAILS and HYTANE n-terminal enrichment strategies in gut tissue. Mass spectrum of ApoC1 (**B**) uncleaved and (**C**) cleaved sequence, depicting light (red arrow) and medium (green arrow) dimethylation of peptides from ventricular tissue of MK0626 (DPP4i) and saline treated mice. Samples were collected from mice that were fed a HFD for 3 months and injected with streptozotocin to induce dysglycemia and subjected to TAC surgery to induce pressure overload.

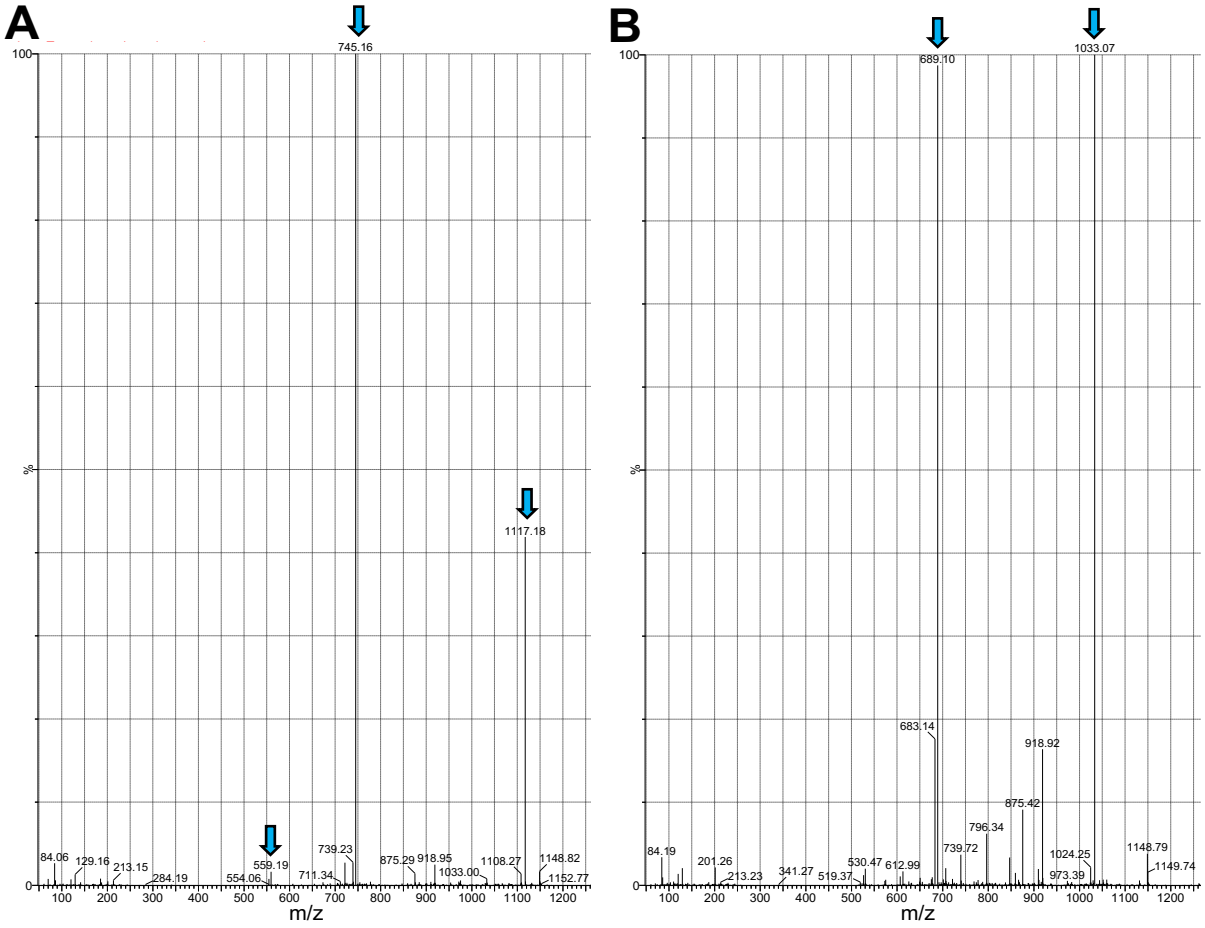

Figure 5.3: DPP4 cleaves ApoC1 *in vitro*. Mass spectrum of (**A**) full length and (**B**) DPP4-cleaved ApoC1 after *in vitro* incubation.

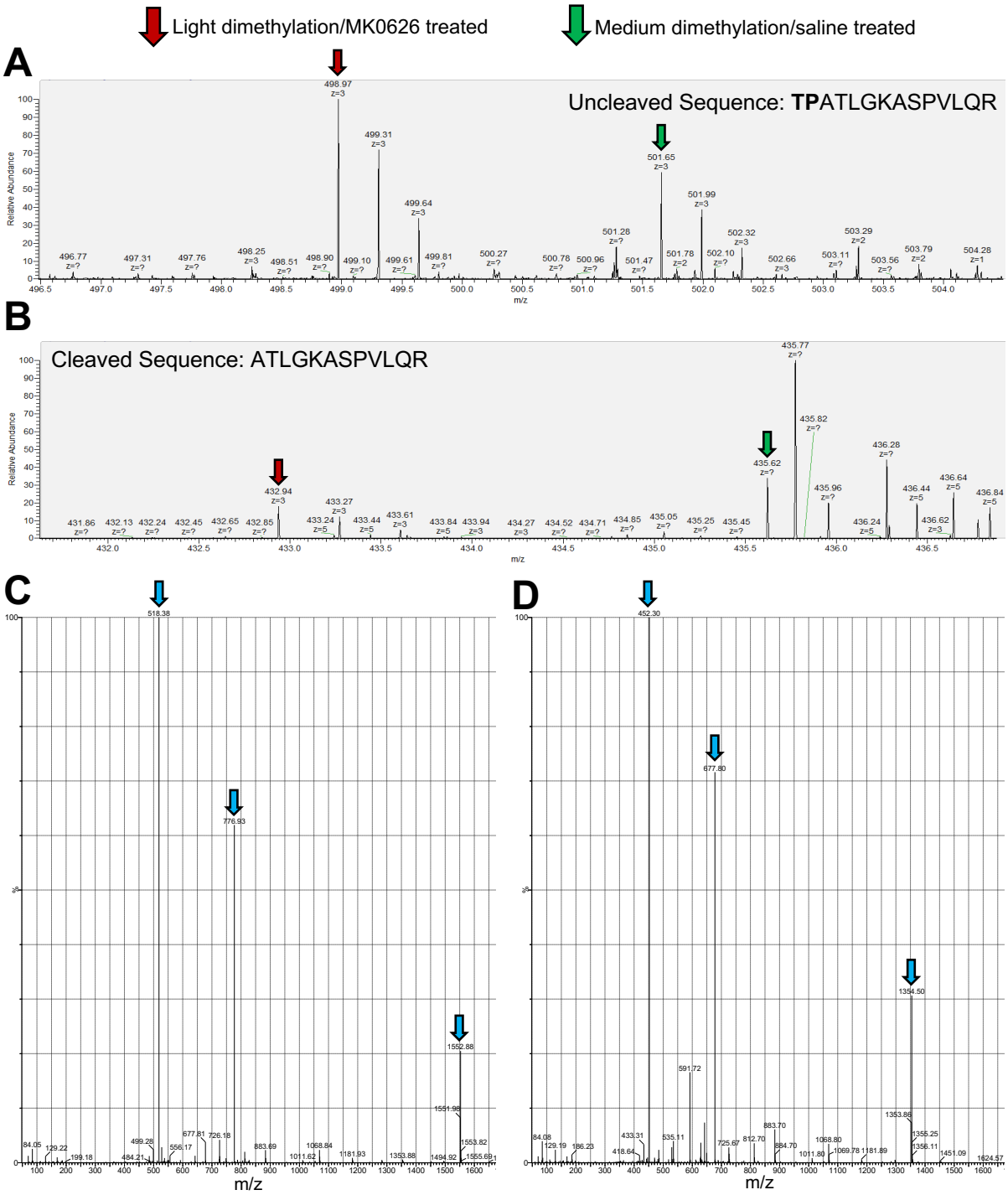

Figure 5.4: DPP4 cleaves GHBP, identified by HYTANE. Mass spectrum of GHBP (**A**) uncleaved and (**B**) cleaved sequence, depicting light (red arrow) and medium (green arrow) dimethylation of peptides from ventricular tissue of MK0626 (DPP4i) and saline treated mice. Samples were collected from mice that were fed a HFD for 3 months and injected with streptozotocin to induce dysglycemia and subjected to TAC surgery to induce pressure overload. Mass spectrum of (**C**) full length and (**D**) DPP4-cleaved ApoC1 after *in vitro* incubation.

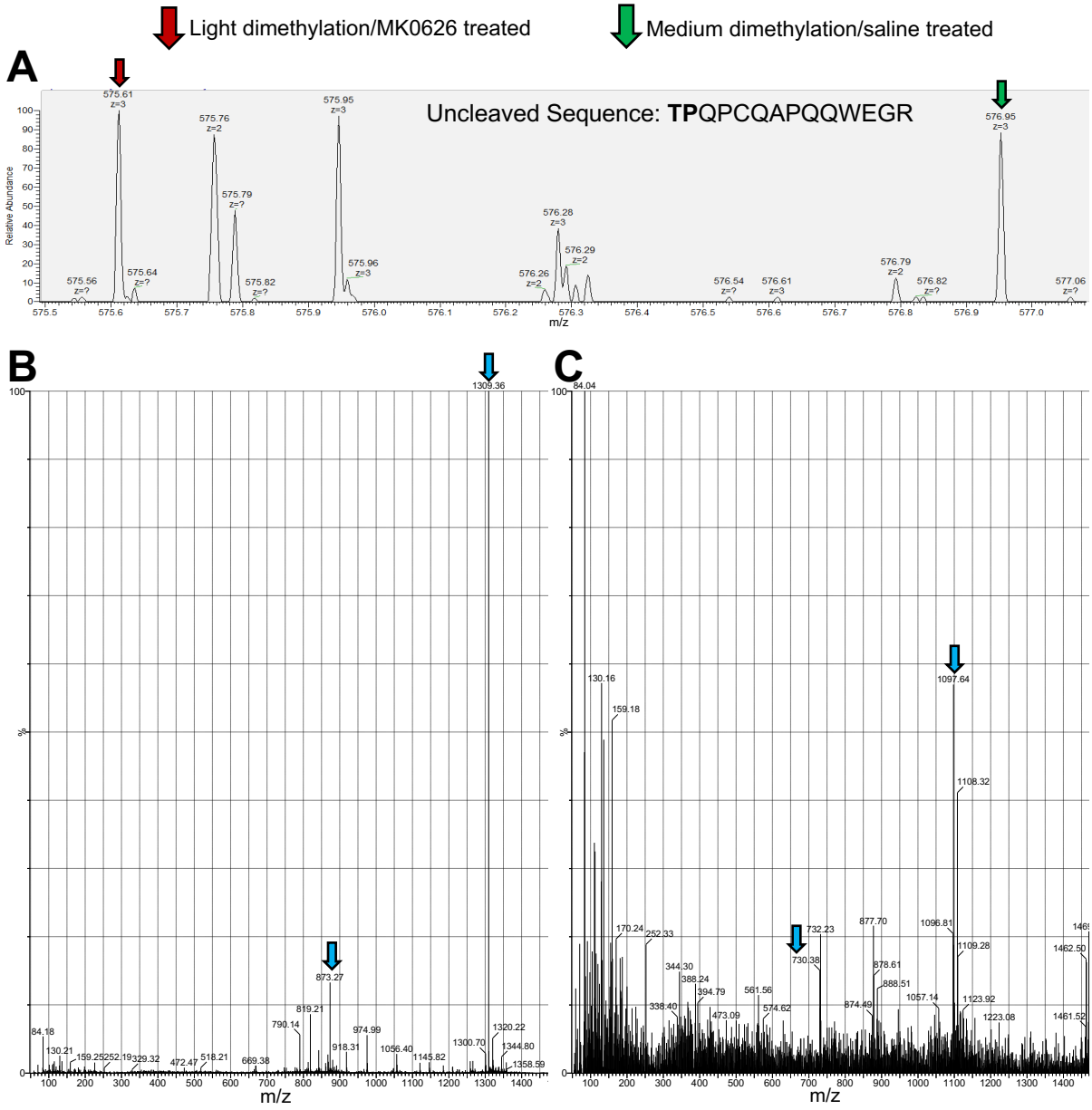

Figure 5.5: DPP4 cleaves EDPR1, sequential cleavage was identified during validation. Mass spectrum of EPDR1 (**A**) uncleaved sequence, depicting light (red arrow) and medium (green arrow) dimethylation of peptides from ventricular tissue of MK0626 (DPP4i) and saline treated mice. Samples were collected from mice that were fed a HFD for 3 months and injected with streptozotocin to induce dysglycemia, and subjected to TAC surgery to induce pressure overload. Mass spectrum of (**B**) full length and (**C**) DPP4-cleaved EPDR1 after *in vitro* incubation.

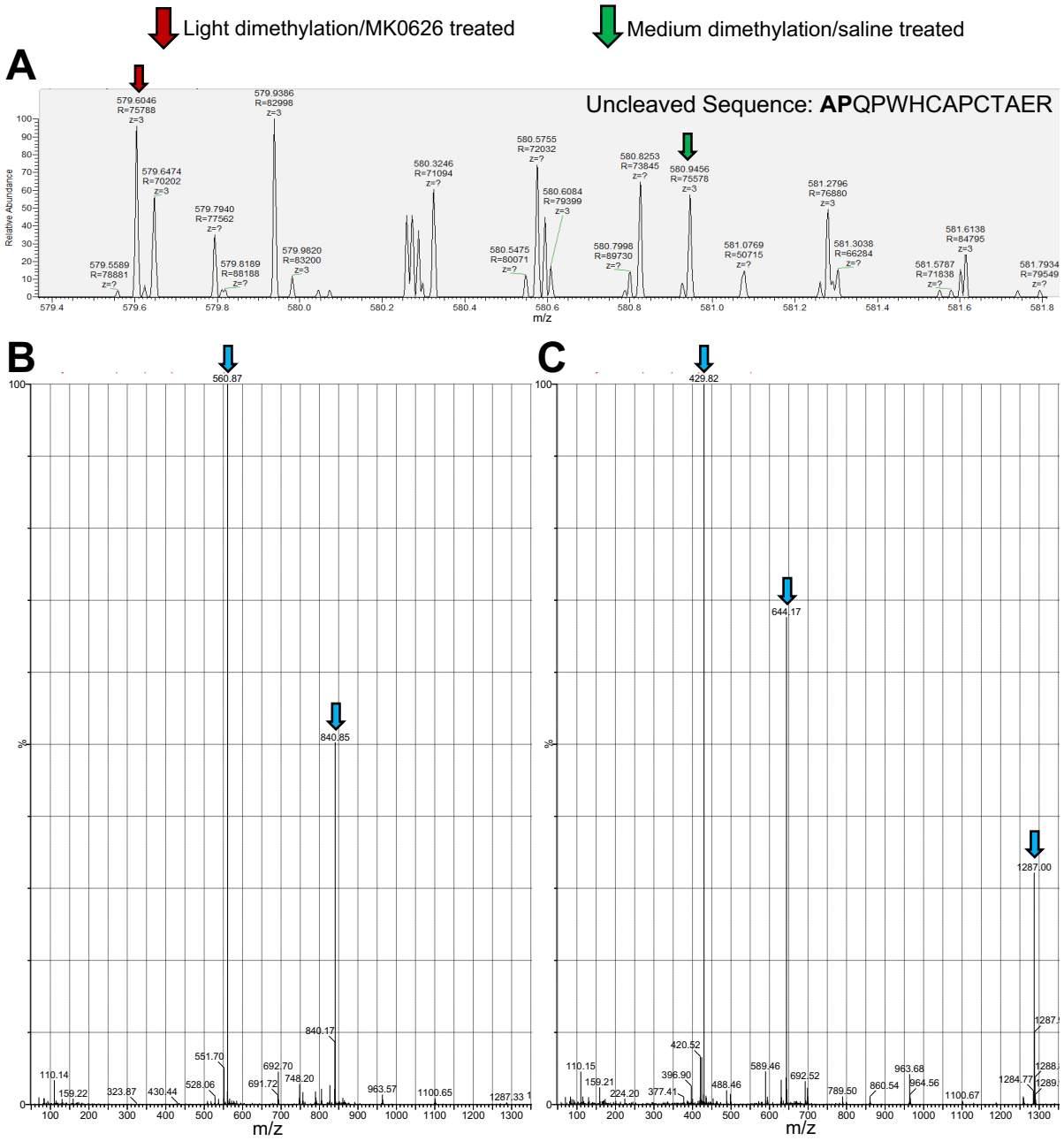

Figure 5.6: DPP4 cleaves IGFBP1, sequential cleavage was identified during validation. Mass spectrum of IGFBP1 (**A**) uncleaved sequence, depicting light (red arrow) and medium (green arrow) dimethylation of peptides from ventricular tissue of MK0626 (DPP4i) and saline treated mice. Samples were collected from mice that were fed a HFD for 3 months and injected with streptozotocin to induce dysglycemia, and subjected to TAC surgery to induce pressure overload. Mass spectrum of (**B**) full length and (**C**) DPP4-cleaved IGFBP1 after *in vitro* incubation.

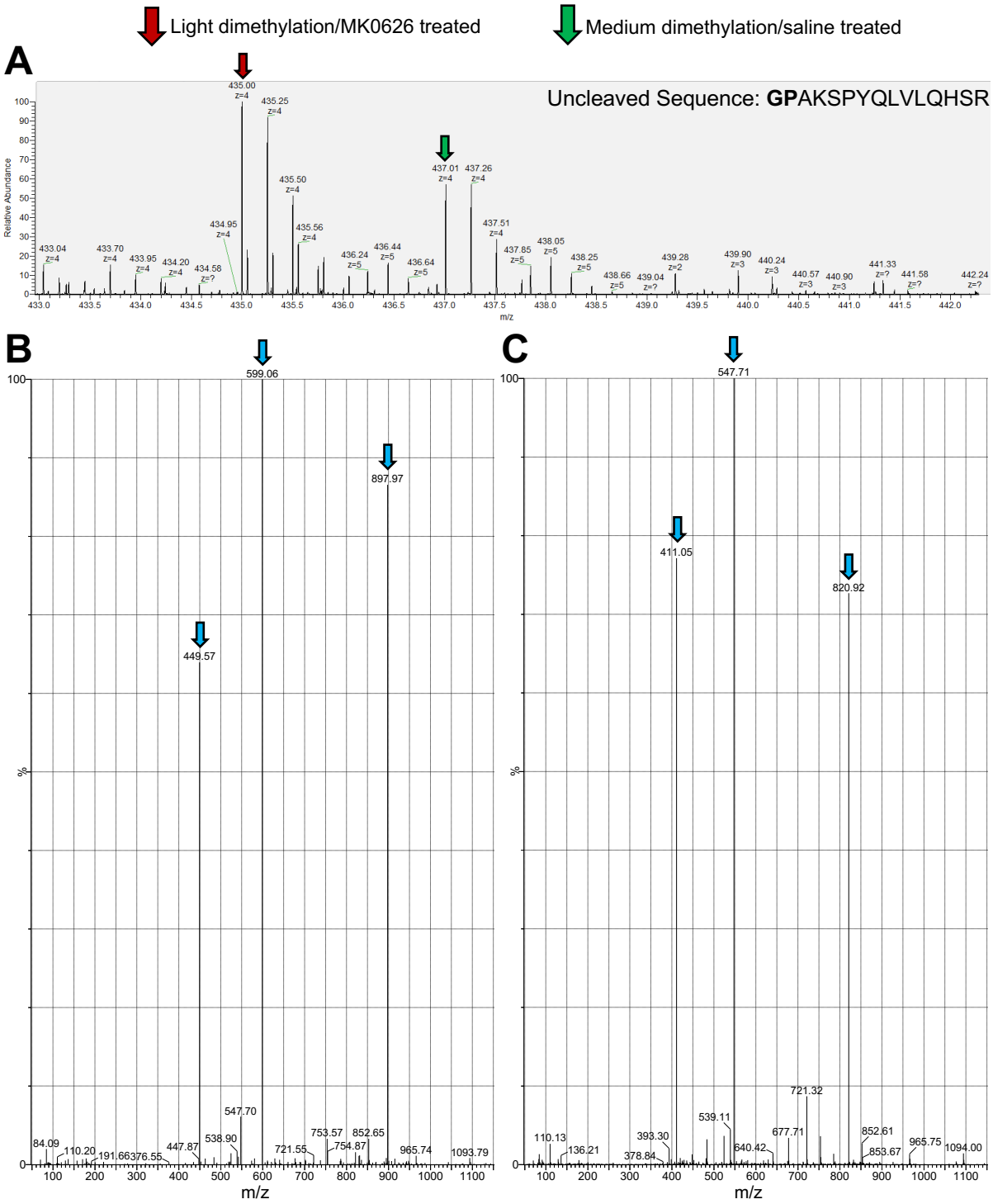

Figure 5.7: DPP4 cleaves TGFBI *in vivo*. Mass spectrum of TGFBI (**A**) uncleaved sequence, depicting light (red arrow) and medium (green arrow) dimethylation of peptides from ventricular tissue of MK0626 (DPP4i) and saline treated mice. Samples were collected from mice that were fed a HFD for 3 months and injected with streptozotocin to induce dysglycemia and subjected to trans-aortic constriction surgery to induce pressure overload. Mass spectrum of (**B**) full length and (**C**) DPP4-cleaved TGFBI after *in vitro* incubation.

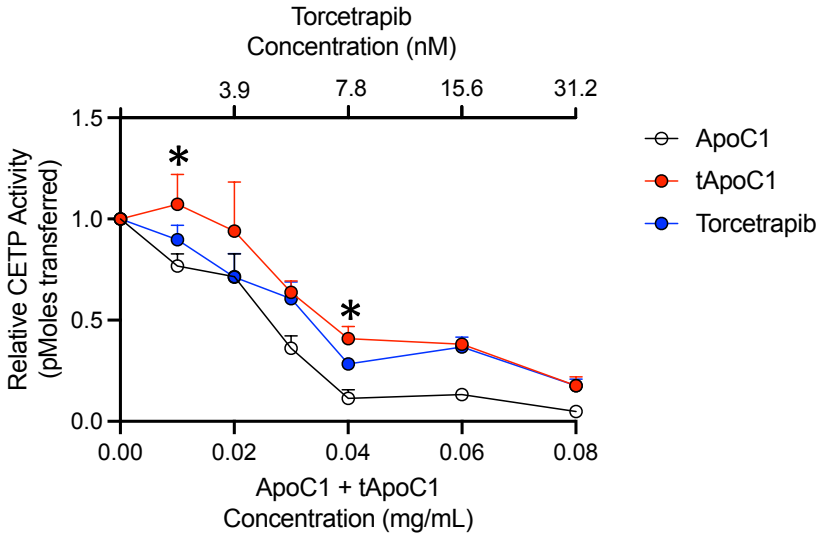

Figure 5.8: DPP4 cleavage of ApoC1 reduces its CETP inhibition capacity. Total CETP activity in healthy human plasma with ApoC1, truncated ApoC1 (tApoC1) and CETP inhibitor Torcetrapib. Data are presented as means ± SEM analyzed with two-way ANOVA and Tukey post-hoc multiple comparisons correction reported as adjusted p value, for ApoC1 vs tApoC1, *p=0.01-0.05, **p=0.001-0.01, ***p=0.0001-0.001 and ****p<0.0001, Torcetrapib vs tApoC1, #p=0.01-0.05, # #p=0.001-0.01, # # #p=0.0001-0.001 and # # # #p<0.0001.

5.1.2 DPP4 Enzymatic Activity is Altered by Post-Translational Modifications

The studies presented in this thesis and others have demonstrated that DPP4 enzymatic activity and protein levels are susceptible to pharmaceutical and genetic-induced variations. For example, we and Varin *et. al.*[31] show that activity is significantly reduced in *Dpp4*$^{hep-/-}$ mice, while protein levels are significantly reduced in *Dpp4*$^{EC-/-}$ mice. There are multiple PTMs, such as glycosylation[59-61], sialylation[62] and oxidation[63], that could affect activity, and we believe this is the mechanism that ultimately affects organ and tissue specific variations. To confirm this hypothesis, future studies will employ mass spectrometry (immunoprecipitation coupled with Orbitrap mass spectrometry) to evaluate how PTMs vary between genotypes, namely in *Dpp4*$^{hep-/-}$ and *Dpp4*$^{EC-/-}$ mice versus their respective controls. This information could be exploited for diagnostic purposes as described by Noels *et. al.*[63], where oxidation on DPP4 was evident in plasma samples from patients will poor outcomes or longer stays in the intensive care unit after coronary surgery with coronary bypass.

5.1.3 The Sheddases Responsible for Liberating Membrane-Bound DPP4 are Incompletely Understood

Thus far, DPP4 shedding has been proposed to be released by metalloproteinases (MMP1, MMP2, MMP14)[64] or KLK5[65]. However, these studies use *ex vivo*, *in vitro* and *in silico* methods to evaluate surface expression and there is a disconnect between cells which express these metalloproteinases and which release DPP4. Further, we[25] and others[13,31,32] have identified hepatocyte-derived DPP4 as the main depot responsible for excess circulating DPP4 in metabolic disease. The aforementioned studies evaluated DPP4 shedding in adipocytes, smooth muscle cells

and in circulatory CD4+ T cells[65]. Future studies should explore DPP4 shedding in the liver and evaluate this in a metabolic dysfunction setting as well.

5.2 Unexplored Sex-Based Differences: Exclusion of Female Mice

Throughout this thesis, and in much of the works cited, male mice are exclusively used for experimental MASLD and CVD investigations. Female mice exhibit potential variability due to the estrous cycle and other reproductive hormones[66-69], however, several studies have revealed no significant difference between males and females regarding this type of variability[70,71]. Metabolism varies significantly between the sexes; male mice exhibit more pronounced phenotypes in disease models, namely in obesity, T2D and CVD studies[72]. It is well documented that premenopausal women have less CVD and CV-related morbidity and mortality compared to men of the same age[73]; however, this cardioprotective phenotype is lost after menopause[74,75] suggesting it is related to gonadal sex hormones however this simplistic association has not held up with estrogen replacement therapy[76]. This is recapitulated in female mice, seemingly via reduced inflammation and preserved cardiac function overall[77,78]. Future studies should replicate our experiments with the addition of female mice to ensure that both sexes are included. Further, we could incorporate ovariectomized female mice to compare our findings in male mice, independent of female reproductive hormones.

5.3 Conclusions

DPP4 has consistently been implicated in numerous diseases including T2D, MASLD, CVD and cancer. Its biology is complex as exemplified by tissue specific variations in enzymatic activity and protein expression that can fluctuate with pharmaceutical therapies like DPP4i's and metformin. DPP4 inhibition is mainly

exploited for treatment of T2D, however, as DPP4 biology is unravelled, it has the potential to be used to treat other diseases.

Our future experiments will allow us to influence the field of DPP4 biology. By unraveling the biochemical processes that are responsible for the cardioprotective phenotype with dual therapy treatment, we can finally determine how metformin regulates DPP4. Investigating how GLP-1, GIP and other DPP4 substrates fluctuate after MI, we can illuminate how DPP4 cleavage is implicated in inflammation, resolution and remodelling. We can exploit these findings to guide prescriptive clinical decisions to ensure individuals with CV risk factors are treated appropriately. Lastly, novel substrate discovery using HYTANE could reveal proteins which are involved in cardiometabolic disease, and lead to the development of new peptide therapies.

5.4 References

1. Rao DP, Dai S, Lagace C, Krewski D. Metabolic syndrome and chronic disease. *Chronic Dis Inj Can.* 2014;34(1):36-45.
2. Ottawa: Diabetes Canada. Canadian Diabetes Cost Model. 2016.
3. Huang DQ, Wilson LA, Behling C, et al. Fibrosis Progression Rate in Biopsy-Proven Nonalcoholic Fatty Liver Disease Among People With Diabetes Versus People Without Diabetes: A Multicenter Study. *Gastroenterology.* 2023;165(2):463-472 e465.
4. Pelletier C, Dai S, Roberts KC, Bienek A, Onysko J, Pelletier L. Report summary. Diabetes in Canada: facts and figures from a public health perspective. *Chronic Dis Inj Can.* 2012;33(1):53-54.
5. Hansen L, Deacon CF, Orskov C, Holst JJ. Glucagon-like peptide-1-(7-36)amide is transformed to glucagon-like peptide-1-(9-36)amide by dipeptidyl peptidase IV in the capillaries supplying the L cells of the porcine intestine. *Endocrinology.* 1999;140(11):5356-5363.
6. Gao Q, Zhang W, Li T, et al. Interrelationship between 2019-nCov receptor DPP4 and diabetes mellitus targets based on protein interaction network. *Sci Rep.* 2022;12(1):188.
7. Li Y, Zhang Z, Yang L, et al. The MERS-CoV Receptor DPP4 as a Candidate Binding Target of the SARS-CoV-2 Spike. *iScience.* 2020;23(6):101160.
8. Chitadze G, Wehkamp U, Janssen O, Bruggemann M, Lettau M. The Serine Protease CD26/DPP4 in Non-Transformed and Malignant T Cells. *Cancers (Basel).* 2021;13(23).
9. Mannucci E, Pala L, Ciani S, et al. Hyperglycaemia increases dipeptidyl peptidase IV activity in diabetes mellitus. *Diabetologia.* 2005;48(6):1168-1172.
10. Miyazaki M, Kato M, Tanaka K, et al. Increased hepatic expression of dipeptidyl peptidase-4 in non-alcoholic fatty liver disease and its association with insulin resistance and glucose metabolism. *Mol Med Rep.* 2012;5(3):729-733.
11. Itou M, Kawaguchi T, Taniguchi E, et al. Altered expression of glucagon-like peptide-1 and dipeptidyl peptidase IV in patients with HCV-related glucose intolerance. *J Gastroenterol Hepatol.* 2008;23(2):244-251.
12. Zhong J, Maiseyeu A, Davis SN, Rajagopalan S. DPP4 in cardiometabolic disease: recent insights from the laboratory and clinical trials of DPP4 inhibition. *Circulation research.* 2015;116(8):1491-1504.
13. Baumeier C, Schluter L, Saussenthaler S, et al. Elevated hepatic DPP4 activity promotes insulin resistance and non-alcoholic fatty liver disease. *Mol Metab.* 2017;6(10):1254-1263.
14. Aulinger BA, Perabo M, Seeley RJ, Parhofer KG, D'Alessio DA. Rapid hepatic metabolism blunts the endocrine action of portally infused GLP-1 in male rats. *Am J Physiol Endocrinol Metab.* 2020;318(2):E189-E197.
15. Andersen DB, Grunddal KV, Pedersen J, et al. Using a Reporter Mouse to Map Known and Novel Sites of GLP-1 Receptor Expression in Peripheral Tissues of Male Mice. *Endocrinology.* 2021;162(3).
16. Vahl TP, Tauchi M, Durler TS, et al. Glucagon-like peptide-1 (GLP-1) receptors expressed on nerve terminals in the portal vein mediate the effects of

endogenous GLP-1 on glucose tolerance in rats. *Endocrinology.* 2007;148(10):4965-4973.
17. Ruttimann EB, Arnold M, Hillebrand JJ, Geary N, Langhans W. Intrameal hepatic portal and intraperitoneal infusions of glucagon-like peptide-1 reduce spontaneous meal size in the rat via different mechanisms. *Endocrinology.* 2009;150(3):1174-1181.
18. Qian M, Wu GS, Adem A, Johnson AE, Sodersten P. CCK-8 can inhibit ingestive behavior by acting on the liver. *Neuroreport.* 1999;10(2):359-362.
19. Stadlbauer U, Arnold M, Weber E, Langhans W. Possible mechanisms of circulating PYY-induced satiation in male rats. *Endocrinology.* 2013;154(1):193-204.
20. Mentlein R, Dahms P, Grandt D, Kruger R. Proteolytic processing of neuropeptide Y and peptide YY by dipeptidyl peptidase IV. *Regul Pept.* 1993;49(2):133-144.
21. Bacharach SZ, Tordoff MG, Alhadeff AL. Glucose Sensing in the Hepatic Portal Vein and Its Role in Food Intake and Reward. *Cell Mol Gastroenterol Hepatol.* 2023;16(2):189-199.
22. Tremblay AJ, Lamarche B, Deacon CF, Weisnagel SJ, Couture P. Effect of sitagliptin therapy on postprandial lipoprotein levels in patients with type 2 diabetes. *Diabetes Obes Metab.* 2011;13(4):366-373.
23. Ahmed RH, Huri HZ, Muniandy S, et al. Altered circulating concentrations of active glucagon-like peptide (GLP-1) and dipeptidyl peptidase 4 (DPP4) in obese subjects and their association with insulin resistance. *Clin Biochem.* 2017;50(13-14):746-749.
24. Lamers D, Famulla S, Wronkowitz N, et al. Dipeptidyl peptidase 4 is a novel adipokine potentially linking obesity to the metabolic syndrome. *Diabetes.* 2011;60(7):1917-1925.
25. Trzaskalski NA, Vulesevic B, Nguyen MA, et al. Hepatocyte-derived DPP4 regulates portal GLP-1 bioactivity, modulates glucose production, and when absent influences NAFLD progression. *JCI Insight.* 2023;8(2).
26. Negro F, Sanyal AJ. Hepatitis C virus, steatosis and lipid abnormalities: clinical and pathogenic data. *Liver Int.* 2009;29 Suppl 2:26-37.
27. Wan S, van der Veen JN, Bakala N'Goma JC, Nelson RC, Vance DE, Jacobs RL. Hepatic PEMT activity mediates liver health, weight gain, and insulin resistance. *FASEB J.* 2019;33(10):10986-10995.
28. Ohnuma K, Dang NH, Morimoto C. Revisiting an old acquaintance: CD26 and its molecular mechanisms in T cell function. *Trends Immunol.* 2008;29(6):295-301.
29. Broxmeyer HE, Hoggatt J, O'Leary HA, et al. Dipeptidylpeptidase 4 negatively regulates colony-stimulating factor activity and stress hematopoiesis. *Nat Med.* 2012;18(12):1786-1796.
30. Proost P, Struyf S, Schols D, et al. Truncation of macrophage-derived chemokine by CD26/ dipeptidyl-peptidase IV beyond its predicted cleavage site affects chemotactic activity and CC chemokine receptor 4 interaction. *The Journal of biological chemistry.* 1999;274(7):3988-3993.

31. Varin EM, Mulvihill EE, Beaudry JL, et al. Circulating Levels of Soluble Dipeptidyl Peptidase-4 Are Dissociated from Inflammation and Induced by Enzymatic DPP4 Inhibition. *Cell Metab.* 2019;29(2):320-334 e325.
32. Ghorpade DS, Ozcan L, Zheng Z, et al. Hepatocyte-secreted DPP4 in obesity promotes adipose inflammation and insulin resistance. *Nature.* 2018;555(7698):673-677.
33. Tadinada SM, Weatherford ET, Collins GV, et al. Functional resilience of C57BL/6J mouse heart to dietary fat overload. *Am J Physiol Heart Circ Physiol.* 2021;321(5):H850-H864.
34. Mulvihill EE, Varin EM, Ussher JR, et al. Inhibition of Dipeptidyl Peptidase-4 Impairs Ventricular Function and Promotes Cardiac Fibrosis in High Fat-Fed Diabetic Mice. *Diabetes.* 2016;65(3):742-754.
35. Diabetes Canada Clinical Practice Guidelines Expert C, Lipscombe L, Butalia S, et al. Pharmacologic Glycemic Management of Type 2 Diabetes in Adults: 2020 Update. *Can J Diabetes.* 2020;44(7):575-591.
36. Baggio LL, Varin EM, Koehler JA, et al. Plasma levels of DPP4 activity and sDPP4 are dissociated from inflammation in mice and humans. *Nat Commun.* 2020;11(1):3766.
37. Scirica BM, Bhatt DL, Braunwald E, et al. Saxagliptin and cardiovascular outcomes in patients with type 2 diabetes mellitus. *N Engl J Med.* 2013;369(14):1317-1326.
38. Green JB, Bethel MA, Armstrong PW, et al. Effect of Sitagliptin on Cardiovascular Outcomes in Type 2 Diabetes. *N Engl J Med.* 2015;373(3):232-242.
39. White WB, Cannon CP, Heller SR, et al. Alogliptin after acute coronary syndrome in patients with type 2 diabetes. *N Engl J Med.* 2013;369(14):1327-1335.
40. Price JD, Linder G, Li WP, et al. Effects of short-term sitagliptin treatment on immune parameters in healthy individuals, a randomized placebo-controlled study. *Clin Exp Immunol.* 2013;174(1):120-128.
41. Decalf J, Tarbell KV, Casrouge A, et al. Inhibition of DPP4 activity in humans establishes its in vivo role in CXCL10 post-translational modification: prospective placebo-controlled clinical studies. *EMBO Mol Med.* 2016;8(6):679-683.
42. Tatosian DA, Guo Y, Schaeffer AK, et al. Dipeptidyl peptidase-4 inhibition in patients with type 2 diabetes treated with saxagliptin, sitagliptin, or vildagliptin. *Diabetes Ther.* 2013;4(2):431-442.
43. Crowley MJ, Williams JW, Jr., Kosinski AS, D'Alessio DA, Buse JB. Metformin Use May Moderate the Effect of DPP-4 Inhibitors on Cardiovascular Outcomes. *Diabetes Care.* 2017;40(12):1787-1789.
44. Rakipovski G, Rolin B, Nohr J, et al. The GLP-1 Analogs Liraglutide and Semaglutide Reduce Atherosclerosis in ApoE(-/-) and LDLr(-/-) Mice by a Mechanism That Includes Inflammatory Pathways. *JACC Basic Transl Sci.* 2018;3(6):844-857.
45. Gopal K, Chahade JJ, Kim R, Ussher JR. The Impact of Antidiabetic Therapies on Diastolic Dysfunction and Diabetic Cardiomyopathy. *Front Physiol.* 2020;11:603247.

46. Ban K, Noyan-Ashraf MH, Hoefer J, Bolz SS, Drucker DJ, Husain M. Cardioprotective and vasodilatory actions of glucagon-like peptide 1 receptor are mediated through both glucagon-like peptide 1 receptor-dependent and -independent pathways. *Circulation.* 2008;117(18):2340-2350.
47. Ussher JR, Drucker DJ. Glucagon-like peptide 1 receptor agonists: cardiovascular benefits and mechanisms of action. *Nat Rev Cardiol.* 2023;20(7):463-474.
48. Kahles F, Meyer C, Mollmann J, et al. GLP-1 secretion is increased by inflammatory stimuli in an IL-6-dependent manner, leading to hyperinsulinemia and blood glucose lowering. *Diabetes.* 2014;63(10):3221-3229.
49. Diebold S, Moellmann J, Kahles F, et al. Myocardial infarction is sufficient to increase GLP-1 secretion, leading to improved left ventricular contractility and mitochondrial respiratory capacity. *Diabetes Obes Metab.* 2018;20(12):2911-2918.
50. Prabhu SD, Frangogiannis NG. The Biological Basis for Cardiac Repair After Myocardial Infarction: From Inflammation to Fibrosis. *Circ Res.* 2016;119(1):91-112.
51. Chen L, Shan Y, Weng Y, et al. Hydrophobic tagging-assisted N-termini enrichment for in-depth N-terminome analysis. *Analytical chemistry.* 2016;88(17):8390-8395.
52. Kleifeld O, Doucet A, Prudova A, et al. Identifying and quantifying proteolytic events and the natural N terminome by terminal amine isotopic labeling of substrates. *Nat Protoc.* 2011;6(10):1578-1611.
53. Kleifeld O, Doucet A, auf dem Keller U, et al. Isotopic labeling of terminal amines in complex samples identifies protein N-termini and protease cleavage products. *Nat Biotechnol.* 2010;28(3):281-288.
54. Ussher JR, Greenwell AA, Nguyen MA, Mulvihill EE. Cardiovascular Effects of Incretin-Based Therapies: Integrating Mechanisms With Cardiovascular Outcome Trials. *Diabetes.* 2022;71(2):173-183.
55. Penn MS, Pastore J, Miller T, Aras R. SDF-1 in myocardial repair. *Gene Ther.* 2012;19(6):583-587.
56. Yamaguchi J, Kusano KF, Masuo O, et al. Stromal cell-derived factor-1 effects on ex vivo expanded endothelial progenitor cell recruitment for ischemic neovascularization. *Circulation.* 2003;107(9):1322-1328.
57. Sato A, Suzuki S, Watanabe S, et al. DPP4 Inhibition Ameliorates Cardiac Function by Blocking the Cleavage of HMGB1 in Diabetic Mice After Myocardial Infarction. *Int Heart J.* 2017;58(5):778-786.
58. Boerrigter G, Costello-Boerrigter LC, Harty GJ, Lapp H, Burnett JC, Jr. Des-serine-proline brain natriuretic peptide 3-32 in cardiorenal regulation. *Am J Physiol Regul Integr Comp Physiol.* 2007;292(2):R897-901.
59. Aertgeerts K, Ye S, Shi L, et al. N-linked glycosylation of dipeptidyl peptidase IV (CD26): effects on enzyme activity, homodimer formation, and adenosine deaminase binding. *Protein Sci.* 2004;13(1):145-154.
60. Abbott CA, McCaughan GW, Gorrell MD. Two highly conserved glutamic acid residues in the predicted beta propeller domain of dipeptidyl peptidase IV are required for its enzyme activity. *FEBS Lett.* 1999;458(3):278-284.

61. Fan H, Meng W, Kilian C, Grams S, Reutter W. Domain-specific N-glycosylation of the membrane glycoprotein dipeptidylpeptidase IV (CD26) influences its subcellular trafficking, biological stability, enzyme activity and protein folding. *Eur J Biochem.* 1997;246(1):243-251.
62. Smith RE, Talhouk JW, Brown EE, Edgar SE. The significance of hypersialylation of dipeptidyl peptidase IV (CD26) in the inhibition of its activity by Tat and other cationic peptides. CD26: a subverted adhesion molecule for HIV peptide binding. *AIDS Res Hum Retroviruses.* 1998;14(10):851-868.
63. Noels H, Theelen W, Sternkopf M, et al. Reduced post-operative DPP4 activity associated with worse patient outcome after cardiac surgery. *Sci Rep.* 2018;8(1):11820.
64. Rohrborn D, Eckel J, Sell H. Shedding of dipeptidyl peptidase 4 is mediated by metalloproteases and up-regulated by hypoxia in human adipocytes and smooth muscle cells. *FEBS Lett.* 2014;588(21):3870-3877.
65. Nargis T, Kumar K, Ghosh AR, et al. KLK5 induces shedding of DPP4 from circulatory Th17 cells in type 2 diabetes. *Mol Metab.* 2017;6(11):1529-1539.
66. Mauvais-Jarvis F, Arnold AP, Reue K. A Guide for the Design of Pre-clinical Studies on Sex Differences in Metabolism. *Cell Metab.* 2017;25(6):1216-1230.
67. Beery AK, Zucker I. Sex bias in neuroscience and biomedical research. *Neurosci Biobehav Rev.* 2011;35(3):565-572.
68. Mogil JS, Chanda ML. The case for the inclusion of female subjects in basic science studies of pain. *Pain.* 2005;117(1-2):1-5.
69. Shansky RM. Are hormones a "female problem" for animal research? *Science.* 2019;364(6443):825-826.
70. Becker JB, Prendergast BJ, Liang JW. Female rats are not more variable than male rats: a meta-analysis of neuroscience studies. *Biol Sex Differ.* 2016;7:34.
71. Itoh Y, Arnold AP. Are females more variable than males in gene expression? Meta-analysis of microarray datasets. *Biol Sex Differ.* 2015;6:18.
72. Mauvais-Jarvis F. Sex differences in metabolic homeostasis, diabetes, and obesity. *Biol Sex Differ.* 2015;6:14.
73. Wake R, Yoshiyama M. Gender differences in ischemic heart disease. *Recent Pat Cardiovasc Drug Discov.* 2009;4(3):234-240.
74. Aggarwal NR, Patel HN, Mehta LS, et al. Sex Differences in Ischemic Heart Disease: Advances, Obstacles, and Next Steps. *Circ Cardiovasc Qual Outcomes.* 2018;11(2):e004437.
75. Kannel WB, Hjortland MC, McNamara PM, Gordon T. Menopause and risk of cardiovascular disease: the Framingham study. *Ann Intern Med.* 1976;85(4):447-452.
76. Manson JE, Crandall CJ, Rossouw JE, et al. The Women's Health Initiative Randomized Trials and Clinical Practice: A Review. *JAMA.* 2024;331(20):1748-1760.
77. Pullen AB, Kain V, Serhan CN, Halade GV. Molecular and Cellular Differences in Cardiac Repair of Male and Female Mice. *J Am Heart Assoc.* 2020;9(8):e015672.
78. Wang F, Keimig T, He Q, et al. Augmented healing process in female mice with acute myocardial infarction. *Gend Med.* 2007;4(3):230-247.

6 Appendix 1

Table 6.1: DPP4i CVOTs. CI: confidence interval, hHF, hospitalization for heart failure, HR: hazard ratio, CAD: coronary artery disease, UACR: urine albumin-creatinine ratio.

Trial Name, Drug Name, Clinical Trial ID	Trial Design	Primary Endpoint	Results	CVD Findings
SAVOR-TIMI 53[1] (Saxagliptin, Onglyza) Saxaglipton Assessment of Vascular Outcomes Recorded in patients with diabetes mellitus NTC01107886	Assigned 16,492 patients with T2D who had a history of, or were at risk for, CV events to receive 2.5/5mg/day of saxagliptin or placebo and followed them for a median of 2.1 years	Time to first confirmed CV event (nonfatal MI, nonfatal ischaemic stroke or cardiovascular death)	Did not affect the risk of ischemic cardiovascular events, reduced progressive albuminuria, irrespective of baseline renal function	No overall risk for cardiovascular events, but there was a 27% increase (3.5% vs 2.8%) in the rate of the first event of hHF and a potential increased risk for all-cause mortality
EXAMINE[2] (Alopliptin, Nesina) Examination of Cardiovascular Outcomes with Alogliptin versus Standard of Care NTC00968708	5,380 patients with T2D and either an acute MI or unstable angina requiring hospitalization within the previous 15–90 days were randomized to alogliptin (6.25, 12.25, or 25 mg/day depending on estimated glomerular filtration rate) or placebo and followed for a median of 18 months	Percentage of participants with primary major adverse cardiac events: Composite defined as CV-related death, nonfatal MI, or nonfatal stroke	Modest reductions in HbA1C were noted (by 36%), with no increase in hypoglycemia events. No increase in pancreatitis or pancreatic cancer was noted	3.9% vs 3.3% placebo were hospitalized for HF, but not statistically significant (HR, 1.19), HF was not an end point of the study. CV death and hHF: 7.4% vs. 7.5%, p = 0.98. Did not increase risk of new HF re-hospitalizations, but slight increase in patients without prior history
TECOS[3] (Sitaglipton, Januvia)	14,671 patients with T2D and prevalent	Time to first confirmed CV event: Composite	Small difference in HbA1C levels (least-	hHF occurred in 3.1% vs 3.1% (unadjusted HR,

Trial Evaluating Cardiovascular Outcomes with Sitagliptin NCT00790205	atherosclerotic vascular disease were randomized to sitaglipton (50mg/day if baseline estimated glomerular filtration rate was between 30 and <50 mL/min/1.73m^2) or matching placebo and followed for a median of 2.9 years	defined as CV-related death, nonfatal MI, nonfatal stroke, or unstable angina requiring hospitalization	squares mean difference for sitagliptin vs. placebo, −0.29 percentage points; 95% confidence interval [CI], −0.32 to −0.27). No significant between-group differences in rates of acute pancreatitis (P=0.07) or pancreatic cancer (P=0.32)	1.00; 95% CI, 0.83-1.19). No difference in total hHF events between the sitagliptin and placebo groups (unadjusted hazard ratio, 1.00; 95% CI, 0.80-1.25). Post-hHF all-cause death was similar in the sitagliptin and placebo groups (29.8% vs 28.8%, respectively), as was CV death (22.4% vs 23.1%, respectively)
OPTIMUS Study[4] (Gemiglipton, Gemiglo/Zemiglo), LG Life Sciences NCT02290301	5,180 (Korean) patients with T2D with no recent (3 months prior) history of acute coronary syndrome or ischemic stroke, patients followed for 4 years until MACE, completion or drop out. Patients received gemigliptin mono-therapy, or gemigliptin with the addition of metformin, sulfonylurea, insulin, some combination of these or 'other' drugs	Primary composite MACE: time to first confirmed CV event (nonfatal MI, nonfatal ischaemic stroke or cardiovascular death)	HbA1C levels were reduced by 0.94% in the monotherapy group compared to baseline after 6 months. Incidence of overall adverse events was 28.70%, most frequently reported was hyperlipidemia (2.25%). No cases of pancreatitis, increased blood amylase, lipase of bacteriuria were reported.	Primary composite MACE occurred in 26 patients within 12 months (estimated incidence 0.49%, 95% CI 0.29–0.69%) and in 54 patients within 54 months (estimated incidence 1.35%, 95% CI: 0.92–1.77%). In a subset analyses, MACE was lowest in the monotherapy group and highest in the gemigliptin+sulfonylurea group
CAROLINA[5,6] (Linagliptin, Tradjenta) CARdiovascular Outcome Trial of LINAgliptin Versus	6,033 patients with T2D at elevated cardiovascular risk (pre-existing CVD, diabetes organ damage) receiving	Time to first occurrence of the primary composite endpoint; CV death (including fatal stroke and fatal MI), non-fatal MI	Adjusted mean change in HbA1C favoured glimepiride over linagliptin, but overall there was no significant difference between the	Primary outcome occurred in 11.8% of the linagliptin group compared with 12.0% of the glimepiride group (p for noninferiority < 0.001, p for superiority =

Glimepiride in Type 2 Diabetes NCT01243424	usual care, compared to outcome against Glimepride. randomized to 5mg/day linaglipton vs 1-4mg/day glimepiride, followed for 6.3 years	(excluding silent MI) or non-fatal stroke	groups. Modest weight gain was reported with glimepiride, incidence of hypoglycemic events was lower in the linagliptin group	0.76), meeting the noninferiority criterion but not superiority
OMNEON 018[7] (Omarigliptin, MK-3102) NCT01703208 Terminated early on December 12, 2017 (for business reasons not due to safety or efficacy)	4,202 patients with T2D and pre-existing vascular disease (CAD, ischemic cerebrovascular disease, atherosclerotic peripheral artery disease), randomized to omarigliptin (MK-3102) 25mg/week or matching placebo	Time to first confirmed CV event: Composite defined as CV-related death, fatal or nonfatal MI, fatal or nonfatal stroke, all-cause mortality, confirmed hHF or CV death	After 142 weeks, the least-squares mean difference (omarigliptin vs. placebo) in HbA1C was −0.3% (95% CI −0.46, −0.14). The number of patients who experienced adverse or serious adverse effects, or discontinued treatment, was similar between groups	At follow-up (median 96 weeks), the primary MACE outcome occurred in 5.45% vs 5.43% of patients in the omarigliptin and placebo group, respectively, with a hazard ratio of 1.00 (95% CI, 0.77-1.29) hHF occurred in 0.95% and 1.57% of patients in the omarigliptin vs placebo group, respectively
CARMELINA[8,9] (Linagliptin) Cardiovascular and Renal Microvascular Outcome Study With Linagliptin NCT01897532	7,003 patients with T2DM and elevated CV events, defined by albuminuria and previous macrovascular disease and/or impaired renal function with predefined UACR, randomized to 5mg/day or matching placebo on a background standard of care, with a median follow-up of 2.2 years	Time to first confirmed CV event: composite defined as CV-related death, nonfatal MI, nonfatal stroke, or unstable angina requiring hospitalization	Overall difference over the full study duration in HbA1C between linatgliptin and placebo was −0.36% (95% CI, −0.42% to −0.29% based on least-square means), fewer patients treated with linagliptin had to increase or introduce insulin therapy, no notable differences in weight	The primary outcome occurred in 12.4% vs 12.1% of patients in the linagliptin and placebo groups, respectively (HR 1.02, 95% CI, 0.89-1.17). hHF occurred in 6% vs 6.5% of patients in the linagliptin or placebo group, respectively (HR 0.90, 95% CI, 0.74-1.08, *P*=0.26)

Table 6.2: Rodent research diet composition. SLD: standard laboratory diet, HFHC; high-fat, high-cholesterol, kcal; kilocalorie.

	SLD (2019, Inotiv)	HFHC (TD.88137, Inotiv)
Macronutrients (%)		
Protein	19.2	17.3
Carbohydrate	44.9	48.5
Fat	9.0	21.2
Macronutrients (% kcal)		
Protein	23	15.2
Carbohydrate	55	42.7
Fat	22	42
Fatty acids (%)		
Saturated fat	1.2	12.8
Monounsaturated fat	1.7	5.6
Polyunsaturated fat	4.4	1.0
4:0 (Butyric)	–	2.1
6:0 (Caproic)	–	1.5
8:0 (Caprylic)	–	1.1
10:0 (Capric)	–	2.6
12:0 (Lauric)	–	3.3
14:0 (Myristic)	–	10.6
16:0 (Palmitic)	0.9	28.9
16:1(Palmitoleic)	–	1.5
18:0 (Stearic)	0.2	12.5
18:1 (Oleic)	1.7	20.9
18:2 (Linoleic)	3.9	2.3
18:3 (Linolenic)	0.4	0.7
Other (%)		
Cholesterol	–	0.2

6.1 References

1. Scirica BM, Bhatt DL, Braunwald E, et al. Saxagliptin and cardiovascular outcomes in patients with type 2 diabetes mellitus. *N Engl J Med.* 2013;369(14):1317-1326.
2. White WB, Cannon CP, Heller SR, et al. Alogliptin after acute coronary syndrome in patients with type 2 diabetes. *N Engl J Med.* 2013;369(14):1327-1335.
3. Green JB, Bethel MA, Armstrong PW, et al. Effect of Sitagliptin on Cardiovascular Outcomes in Type 2 Diabetes. *N Engl J Med.* 2015;373(3):232-242.
4. Kim EH, Kim SS, Kim DJ, et al. A prospective cohort study on effects of gemigliptin on cardiovascular outcomes in patients with type 2 diabetes (OPTIMUS study). *Sci Rep.* 2020;10(1):19033.
5. Rosenstock J, Kahn SE, Johansen OE, et al. Effect of Linagliptin vs Glimepiride on Major Adverse Cardiovascular Outcomes in Patients With Type 2 Diabetes: The CAROLINA Randomized Clinical Trial. *JAMA.* 2019;322(12):1155-1166.
6. Rosenstock J, Marx N, Kahn SE, et al. Cardiovascular outcome trials in type 2 diabetes and the sulphonylurea controversy: rationale for the active-comparator CAROLINA trial. *Diab Vasc Dis Res.* 2013;10(4):289-301.
7. Gantz I, Chen M, Suryawanshi S, et al. A randomized, placebo-controlled study of the cardiovascular safety of the once-weekly DPP-4 inhibitor omarigliptin in patients with type 2 diabetes mellitus. *Cardiovasc Diabetol.* 2017;16(1):112.
8. Rosenstock J, Perkovic V, Alexander JH, et al. Rationale, design, and baseline characteristics of the CArdiovascular safety and Renal Microvascular outcomE study with LINAgliptin (CARMELINA((R))): a randomized, double-blind, placebo-controlled clinical trial in patients with type 2 diabetes and high cardio-renal risk. *Cardiovasc Diabetol.* 2018;17(1):39.
9. Rosenstock J, Perkovic V, Johansen OE, et al. Effect of Linagliptin vs Placebo on Major Cardiovascular Events in Adults With Type 2 Diabetes and High Cardiovascular and Renal Risk: The CARMELINA Randomized Clinical Trial. *JAMA.* 2019;321(1):69-79.

7 Appendix 2: HYTANE Methods

7.1 Blood and Tissue Collection

Different biological replicate of heart and gut samples from WT and DPP4i treated mice were dissolved in 2 mL 6M guanidine hydrochloride with 4 µL of 500 × stock of protease inhibitor cocktail (Cat #P8340, Sigma-Aldrich). The samples were sonicated at 4°C using three 10 second bursts with 10 s pauses at 35% amplitude and then centrifuged at 20,000 g at 4°C for 50 min. Protein concentration was determined by a BCA assay (Cat #500-0119, Bio-Rad). The supernatants were stored at -80°C. Different biological replicate of plasma samples from WT and DPP4i treated mice were diluted by 10 times in 2 mL 6M guanidine hydrochloride with 4 µL of 500 × stock of protease inhibitor cocktail (Cat #P8340, Sigma-Aldrich). Protein concentration was determined by a BCA assay (Cat #500-0119, Bio-Rad).

7.2 Dimethylation of Primary Amines on Proteins

Protein extracted from gut, heart and plasma of WT and DPP4i-treated mice was isotopically labeled at the N-termini and lysine residues by incorporating heavy and light dimethylation reagents as previously described but with minor modifications. 200 µg proteins from WT and DPP4i treated samples dissolved in 6 M guanidine hydrochloride containing 100 mM TEAB (pH 8.2) were reduced by 10 mM DTT for 1 h at 56 °C, followed by alkylation of thiol group with 30 mM acrylamide for 1 h at room temperature. The excess acrylamide was extinguished with an additional 10mM DTT. After that, formaldehyde and sodium cyanoborohydride were added to a final concentration of 100 mM and 60 mM respectively for demethylation of free amines to DPP4i treated samples while deuterated formaldehyde and sodium cyanoborohydride were added to WT samples. The reaction was allowed to proceed overnight at 37 °C

before the addition of 10-fold excess of glycine to quench excess formaldehyde/deuterated formaldehyde and sodium cyanoborohydride.

7.3 Proteolytic Digestion

The residual reagents were removed using FASP method according to previous report but with minor changes. Following dimethylation, the protein samples from WT and DPP4i treated samples were combined and transferred to centrifugal filters with 10K molecular weight cut off and washed four times with 6 M guanidine hydrochloride containing 1 M glycine and 50mM ammonium bicarbonate to remove residual reagents. Afterward, background solution was exchanged to 50 mM HEPES (pH 9) by centrifugation and the sample solution was subjected to proteolytic digestion with a substrate/trypsin ratio of 50:1 (m/m) for 12 h at 37 °C. After digestion, the filters were centrifuged at 15,000 g for 15 min, and the flow-through containing the peptides was collected. To increase peptide recovery from the membrane, the membrane was further washed with 100uL 50 mM HEPES (pH 9) and the flow-through from those two steps was then combined.

7.4 Hydrophobic Tagging of Internal Peptides

The free amines of the internal peptides generated from trypsin digestion were further derivatized with hexadecanal to incorporate two long alkyl chains. 100 µL pure water, 40 µL 600 mM $NaBH_3CN$ (dissolved in normal propyl alcohol) and 1mL 10 mg/mL hexadecanal (dissolved in normal propyl alcohol) were added to the sample solution in sequence. The solution was incubated overnight at 50°C.

7.5 C18 Material Assisted-Depletion

20 µL of freshly prepared NaBH3CN (600 mM) was added to the solution, and the solution was then dried in a Speed Vac Concentrator. The dried sample was

redissolved in 2% ACN containing 5% FA. The precipitated hexadecanal was removed by centrifugation at 14000 g for 15min. The supernatant was collected and loaded onto C18 trap column, followed by washing with 2% ACN containing 5% FA, after that, C18 trap column was washed with 60% ACN containing 5% FA to elute the N-terminal peptides. The eluate was collected and dried for further use.

7.6 High pH Fractionation

The HYTANE enriched peptides were fractionated using the Pierce TM High pH Reversed-Phase Peptide Fractionation Kit (Cat #84868). Eight fractions were collected using: 10, 12.5, 15, 17.5, 20, 22.5, 25 and 50% acetonitrile. Those fractions were subsequently vacuum-centrifuged to dryness, resuspended in 10 µL of 5% formic acid and half of it was analyzed by LC-MS/MS.

7.7 LC-ESI-MS/MS Analysis

LC-MS/MS was performed using an Eksigent 425 nano Ultra HPLC system and a Thermo Scientific Orbitrap Fusion Lumos mass spectrometer. Samples were loaded using an autosampler directly onto a home-made 75 µm ID × 15 cm packed tip column filled with C 18 particles (3 µm, Reprosil). Digested peptides were separated with a 60 min or 90 min linear gradient from 4% solvent B (0.1% formic acid in acetonitrile) to 30% solvent B (0.1% formic acid in acetonitrile), at a flow rate of 200 nL/min. The run time was 120 minutes or 150 minutes for each fraction, including sample loading and column reconditioning. Data-dependent acquisition was performed using the Xcalibur 4.0 software in positive ion mode at a spray voltage of 2.5 kV. Survey spectra were acquired in the Orbitrap with a resolution of 120,000 and a mass range from 350 to 1500 m/z. For HCD scans, the collision energy was set at 35, maximum inject time was 50 ms and the AGC target was 1.0e5. We used an isolation window of 0.7 m/z.

Ions from charge state +1 to +6 selected for MS/MS were dynamically excluded for 15 s after fragmentation.

7.8 Database Searching

The Proteome Discoverer 2.1.0.81 software (Thermo Fisher Scientific) was used for analyses of RAW files. Searching was performed using The SEQUEST HT database search engine and the mouse proteome database (SwissProt TaxID=10090, 2016-05-11) downloaded from ProteinCenter supplemented with a list of common contaminants derived from ProteinCenter (PD_Contaminants_2015_5). Both the forward and reversed databases were used for database search in order to evaluate the false discovery rates (FDRs); 50346 total entries were searched. Mass tolerances were set as 10 ppm for parent ions and 0.6Da for fragments. Propionamidation (71.037Da) on cysteine, light dimethylation (+28.031Da) or heavy demethylation (+32.056Da) on lysine were set as fixed modifications. Acetylation (+42.011Da) on peptide N-terminus, oxidation (+15.9949Da) on methionine, pyroglutamate on Glutamic acid (-17.027Da) and Glutamine (-18.011Da), light dimethylation (+28.031Da) or heavy demethylation (+32.056Da) on peptide N-terminus were set as variable modifications. To identify the neo-N-termini, semi-style Arg-C cleavage searches were applied with up to two missed cleavages. The results were filtered by the incorporated percolator in ProteomeDiscoverer to control the false discovery rate (FDR) less than 1%.

7.9 Bioinformatics Filtering

As DPP4 is a classic serine protease which recognizes and cleaves the 2 N-terminal amino acid residues with the consensus sequence X-Pro, X-Ala or X-Ser, in the search results we defined the peptides with prior amino acid as Proline, Alanine

or Serine as “cleaved peptide” (eg. P.XXXXXX.X) while defined the peptides with second amino acid as Pro, Ala or Ser as “uncleaved peptide” (eg. X.XPXXXX.X). Then we classified these peptides into three categories: 1. “Cleaved/Uncleaved matched pair”: in this category, both cleaved sequence and its corresponding uncleaved sequence were identified; 2. “Cleaved only”: in this category, only cleaved sequence was identified; 3. ”Uncleaved only”: only uncleaved sequence was identified. The peptides in these three categories were further filtered according to the following ratio criteria: 1. For “Cleaved/Uncleaved matched pair”:, the log2 ratio between cleaved and uncleaved should be larger or equal to 1, meanwhile, the Cleaved ratio should larger than 1 and uncleaved ratio should smaller than 1; 2. For “Cleaved only”, the log2 cleaved ratio must be larger than 1 and there must be two ratio values among three biological replicates; 3. For “Uncleaved only”, the log2 cleaved ratio must be smaller than 1 and there must be two ratio values among three biological replicates. After ratio cutoff, two criteria were finally applied: 1. the start position of the peptide sequence should be within 20 amino acids after signal peptide cleavage; 2. the peptide corresponding protein subcellular location should be secreted.

7.10 *In vitro* Peptide Cleavage Validation

Custom peptides were purchased from Peptide 2.0 Inc., or synthesized by the BEaTS Peptide Synthesis Core (University of Ottawa Heart Institute, Ottawa, Canada). Full length or truncated versions of each peptide (0.1 mg/mL, diluted in sterile PBS) were incubated with recombinant human DPP4 (1 mU; Sigma-Aldrich, cat# D4943) for 25 hours at 37°C. Cleavage was identified via precursor and product ions.

7.11 Select Reaction Monitoring (SRM) Validation

Qualitative analysis was accomplished on a Waters TQD UPLC-MS/MS equipped with electrospray ionization (ESI) operated in the positive ionization mode. Chromatographic separation was carried out using UPLC system; composed of Accela 1250 quaternary pump and Accela open autosampler. Software version was used to control all parameters of UPLC, MS and analysis of obtained data. Positive-ion mass spectrometric detection method with ESI and SRM mode was used. The optimized parameters were: turbo ion spray temperature of 400°C, capillary temperature of 270°C, auxiliary gas of 2 psi, sheath gas of 20 psi, ion spray voltage of 3500 V, and capillary offset of 35. The quadrupole mass spectrometer operated at the SRM mode was used for the monitoring of the transitions of molecular ions to the product ions, using the collision energies of 12-18 eV.

7.12 Cholesterol Ester Transfer Protein (CETP) Activity Assay

ApoC1 is an effective endogenous inhibitor of CETP in healthy, normolipidemic patients[1]. Biological function of full length and cleaved ApoC1 was tested using a CETP activity assay kit (Sigma-Aldrich, Roar Biomedical, cat# MAK106), with human plasma as the CETP source. Inhibition was compared to Torcetrapib (Sigma-Aldrich, cat# PZ0170), a drug developed to treat hypercholesterolemia by inhibiting CETP.

7.13 References

1. Pillois X, Gautier T, Bouillet B, et al. Constitutive inhibition of plasma CETP by apolipoprotein C1 is blunted in dyslipidemic patients with coronary artery disease. *J Lipid Res.* 2012;53(6):1200-1209.

8 Appendix 3: Review Article – Dipeptidyl Peptidase-4 at the Interface Between Inflammation and Metabolism

Authors: **Natasha A. Trzaskalski**, Evgenia Fadzeyeva and Erin E. Mulvihill

Published: Clinical Medicine Insights: Endocrinology and Diabetes
Trzaskalski, N. A., Fadzeyeva, E., & Mulvihill, E. E. (2020). Dipeptidyl peptidase-4 at the interface between inflammation and metabolism. Clinical Medicine Insights: Endocrinology and Diabetes, 13, 1179551420912972.

8.1 Author Contributions

The manuscript and figures were conceptualized and written by NAT, EF and EEM.

8.2 Abstract

Dipeptidyl peptidase-4 (DPP4) is a serine protease that rapidly inactivates the incretin peptides, glucagon-like peptide-1, and glucose-dependent insulinotropic polypeptide to modulate postprandial islet hormone secretion and glycemia. Dipeptidyl peptidase-4 also has nonglycemic effects by controlling the progression of inflammation, which may be mediated more through direct protein-protein interactions than catalytic activity in the context of nonalcoholic fatty liver disease (NAFLD), obesity, and type 2 diabetes (T2D). Failure to resolve inflammation resulting in chronic subclinical activation of the immune system may influence the development of metabolic dysregulation. Thus, through both its cleavage and regulation of the bioactivity of peptide hormones and its influence on inflammation, DPP4 exhibits a diverse array of effects that can influence the progression of metabolic disease. Here, we highlight our current understanding of the complex biology of DPP4 at the inter- section of inflammation, obesity, T2D, and NAFLD. We compare and review new mechanisms identified in basic laboratory and clinical studies, which may have therapeutic application and relevance to the pathogenesis of obesity and T2D.

Keywords: Dipeptidyl peptidase-4, incretin hormones, inflammation, glycemia, insulin resistance, type 2 diabetes, nonalcoholic fatty liver disease

8.3 Introduction

Dipeptidyl peptidase-4 (DPP4) is a protease with a well-characterized role in regulating the bioactivity of gastrointestinal-derived peptide hormones, leading to significant implications for endocrine pathways[1,2]. Inhibition of DPP4-mediated degradation of gut hormones potentiates islet hormone secretion and enhances postprandial metabolism to successfully treat hyperglycemia in patients with type 2 diabetes (T2D)[3]. Dipeptidyl peptidase-4 has also cleaves and inactivates several chemokines and cytokines with a significant impact on inflammation and immune function[4]. Dipeptidyl peptidase-4 can also directly cleave the extracellular matrix and influence cell migration[5,6].

Interestingly, both activation of intracellular signaling cascades regulating immune cell activation and its interaction within a complex to influence extracellular matrix proteolysis can occur independently of catalytic activity[5,7]. Therefore, dissection of the actions mediated by the catalytic activity and posttranslational regulation of its host of substrates versus those mediated by cleavage-independent or direct protein interactions with cell surface receptors, extracellular matrix, and cell signaling cascades is currently important given its emerging role as a biomarker of metabolic disease[8]. Recent research has placed these distinct functions at a direct intersection, where regulation of inflammation may influence the progression of dysglycemia, insulin resistance, obesity, and nonalcoholic fatty liver disease (NAFLD) (**Figure 1**). Here, we discuss and contrast the potential substrates identified with those experimental observations which appear to be independent of catalytic activity and high- light relevance for human disease.

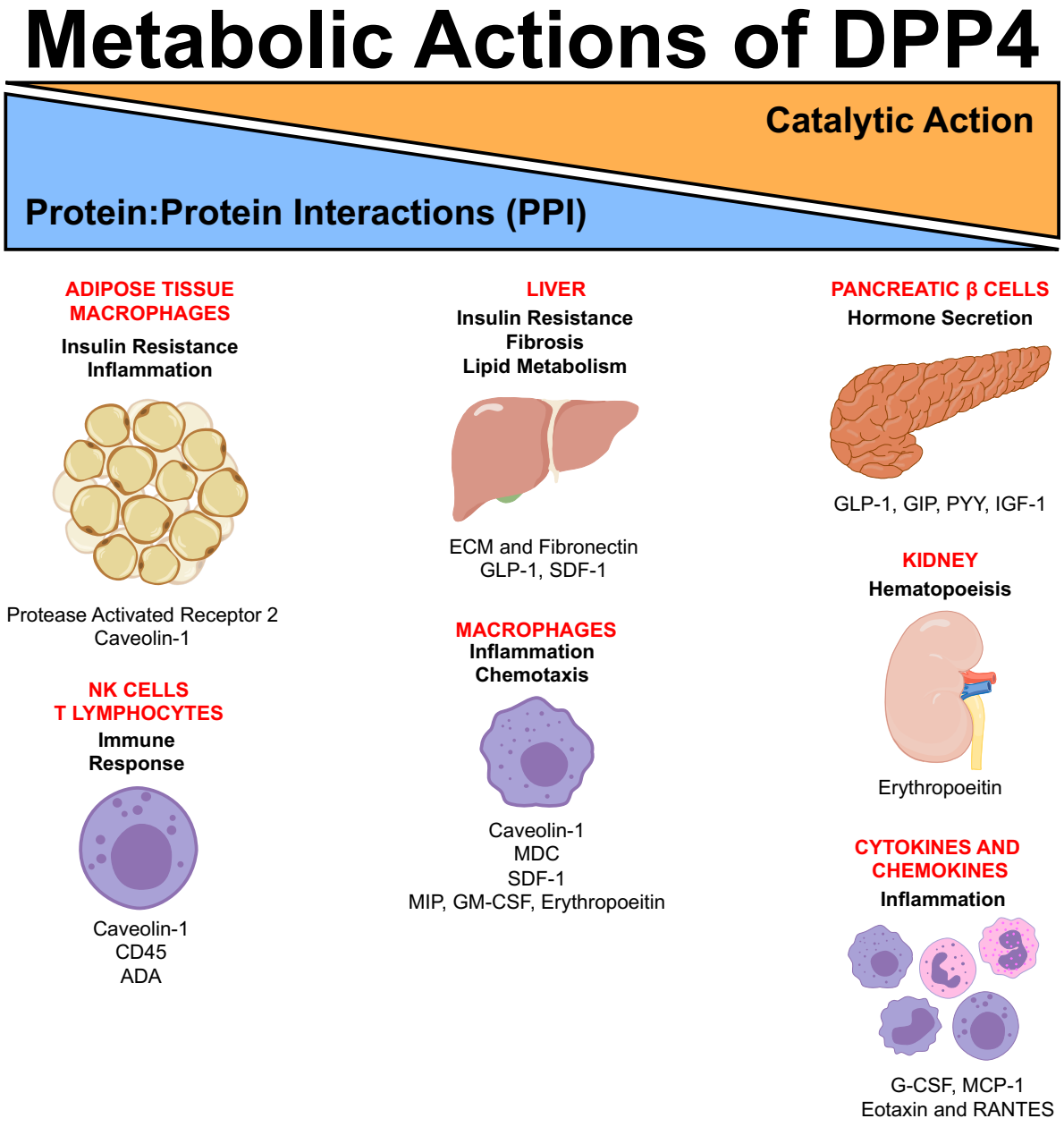

Figure 8.1: Schematic illustrating the metabolic consequences and cellular specificity of dipeptidyl peptidase-4 regarding glucose tolerance and inflammation and the evidence indicated to date on substrate cleavage and regulation vs noncatalytic/direct protein-protein interactions as the mechanisms underlying these effects. ADA indicates adenosine deaminase; G-CSF, granulocyte colony-stimulating factor; GIP, glucose-dependent insulinotropic polypeptide; GLP-1, glucagon-like peptide 1; GM-CSF, granulocyte macrophage colony-stimulating factor; IGF-1, insulin growth factor; MDC, macrophage-derived cytokine; MIP-1, macrophage inflammatory protein 1; PYY, peptide tyrosine tyrosine; SDF-1, stromal-derived factor 1.

8.4 DPP4 Structure and Catalytic Activity

Dipeptidyl peptidase-4 is a type II cell surface exopeptidase with a classic serine triad defining the C-terminal catalytic active site and a single hydrophobic sequence anchoring the mostly extracellular protein (only 6 amino acids extend into the cytoplasm in the membrane)[9]. Dipeptidyl peptidase-4 belongs to the prolyl endopeptidase family, a group of atypical serine proteases with an active site consisting of the catalytic residues Ser630, Asp708, and His740, which hydrolyze a prolyl bond in substrate proteins[2,9-13].

8.5 Transcriptional Control of DPP4

Dipeptidyl peptidase-4 contains a GC-rich sequence[14,15]. This region contains several consensus binding sites for transcriptional factors, including hepatocyte nuclear factor-1-beta (HNF1B)[16], cut-like homeobox 1 (CUX1)[17] glucocorticoid receptor[6], and specificity protein 1 (SP1)[18], as well as several cytokines, such as interferon-γ and tumor necrosis factor α (TNF-α), which regulate *Dpp4* messenger RNA (mRNA) expression in a cell type–specific manner[18]. Promoter analysis has also identified consensus sites for nuclear factor kappa- light-chain-enhancer of activated B cells (NF-κB) and epidermal growth factor activating protein 1[19]. In HepG2 cells, incubation with high concentrations of glucose increases the expression of *Dpp4*[20] and has been confirmed by luciferase assays[21,22]. Positive correlations have been established with plasma DPP4 activity and fasting plasma glucose[23] and HbA1c[24] However, this regulation may be more complicated in vivo as patients with improved glycemic control do not consistently experience a reduction in circulating DPP4[25], and short-term treatment of mice with the glucose-lowering agent Exendin-4 does not reduce circulating DPP4 activity[26]. Incubation of HepG2 cells with insulin, palmitate,

oleate, or cholesterol did not result in increased DPP4 mRNA expression. In THP-1 macrophages, dexamethasone treatment significantly induced transcriptional upregulation of DPP4 due to the presence of two glucocorticoid responsive elements within the promoter[9].

8.6 Posttranscriptional Regulation of DPP4

Dipeptidyl peptidase-4 exerts enzymatic activity in both the membrane-anchored and circulating soluble form[2,9,12], and it requires heterodimerization or homodimerization for catalytic function[13]. As a dimer, DPP4 selectively and preferentially cleaves a dipeptide from the N-terminus with a position 2 proline or alanine and a protonated amino terminus[11]. Dipeptidyl peptidase-4 can be post-translationally modified, including glycosylation (sialylation) at several sites responsible for targeting DPP4 to the apical membrane.[27] Particularly noteworthy is the N-glycosylation at the Asn319 site, which when mutated significantly reduces dimerization and catalytic activity[28]. In addition, DPP4 can also be oxidized, which reduces its activity[29].

Dipeptidyl peptidase-4 is present on the membrane of parenchymal cells within metabolic organs, including hepatocytes, enterocytes, islets cell, and within endothelial cells and immune populations[26,30]. The level of expression depends on the cell type, differentiation state, and/or the activation state[4,31,32]. Dipeptidyl peptidase-4 can also be shed from the membrane and circulates throughout many bodily fluids[33]. Sheddases are a class of membrane-bound enzymes that can cleave transmembrane proteins and have been proposed for the release of DPP4 from the cell membrane into circulation as classic endothelial reticulum/Golgi secretion pathways are not involved[34]. Matrix metalloproteinases (MMP) 1, 2, 14, and 9 and Kallikrein-related

peptidase 5 (KLK5) have all been identified to have a role in shedding[33]. However, the contribution, regulation, and cell-type specificity of these sheddases to the regulation of soluble DPP4 and disease progression are currently unknown.

8.7 Direct Protein-Protein Interactions with DPP4

In addition to its well-described peptidase activity, DPP4 also possesses noncatalytic functions through its interaction with ligands, including adenosine deaminase (ADA), caveolin-1[35], extracellular matrix (collagen and fibronectin), and C-X-C chemokine receptor 4 (CXCR4)[19]. Dipeptidyl peptidase-4 is a co-stimulator for T-cell activation by interaction and activation of ADA. As adenosine is a potent suppressor of T-cell proliferation, inducing its degradation through increased ADA activity induces T-cell proliferation. However, studies using DPP4 with a mutation within the active site rendering it catalytically inactive or a mutant DPP4 unable to bind ADA, demonstrated that DPP4 induces T-cell proliferation through pathways independent of ADA and substrate degradation[36]. Dipeptidyl peptidase-4 has also been proposed to bind directly to CD45 to induce T-cell receptor signaling[37]. However, given that mice with genetic elimination of *Dpp4* or treatment with a highly selective DPP4 inhibitor (DPP4i) had comparable and robust primary and secondary antibody responses to T-dependent antigens provides compelling evidence that although DPP4 has a role in mediating T-cell activation, it is not absolutely required for T-cell–directed immune responses[38]. Evidence also exists that DPP4 physically interacts with caveolin-1 on antigen-presenting cells to induce aggregation and phosphorylation, which activates NF-κB[39]. In addition, DPP4 has been demonstrated to activate signaling on endothelial cells through direct interaction with the mannose 6 phosphate/ insulin-like growth factor 2 receptor[40,41].

8.7.1 DPP4 and regulation of the bioactivity of incretin hormones

The best-characterized substrates regulated by DPP4 catalytic activity are glucagon-like peptide-1 (GLP-1) and glucose- dependent insulinotropic polypeptide (GIP), which are responsible for the incretin effect or 60% of insulin secreted in response to nutrients[42]. Both the GLP-1 receptor (GLP-1R) and GIP receptor (GIPR) belong to the G-protein–coupled receptor B1 superfamily, which activates Gαs proteins and stimulates cyclic adenosine monophosphate (cAMP) production upon ligand binding[43]. Both GLP-1 and GIP in circulation are degraded by DPP4 cleavage of the N-terminal two amino acids very efficiently, eliminating their glucoregulatory action due to a decrease in their respective receptor's affinity[1]. Meal-induced spikes in circulating concentrations sufficient to reach the islet last only minutes[44]. Most degradation occurs within the vessels draining the mesentery and within the portal circulation and hepatic bed[30,45-48]. However, the ablation of osteoclasts through treatment with denosumab has been reported to reduce circulating DPP4 levels and raise GLP-1, suggesting many metabolic circumstances may influence DPP4 levels and incretin cleavage[49]. Inhibition of degradation of GLP-1 and GIP by pharmacological inhibitors preserves the bioactivity of active incretins, allowing direct activation of incretin receptors on the β cell to augment meal-stimulated insulin secretion. In addition, GLP-1 inhibits glucagon secretion through activation of GLP-1 receptors on δ cells to stimulate somatostatin secretion[50].

8.7.2 DPP4 inhibitors for the treatment of hyperglycemia in patients with T2D

Dipeptidyl peptidase-4 inhibitors (DPP4i) are approved for the treatment of hyperglycemia in patients with T2D. They are highly selective for and lead to significant inhibition of the catalytic activity of DPP4, ultimately functioning by

preventing the degradation of the incretin hormones, stimulating post- prandial insulin secretion[2,8], and reducing hepatic glucose production through lowered glucagon secretion[51]. Generally, the structures of DPP4i fall within 3 broad categories: (1) a substrate-like electrophilic group that can interact either covalently or noncovalently with the active binding site of DPP4, (2) non–substrate-like inhibitors, or (3) xanthine-based compounds[52]. DPP4i are relatively well tolerated as the risk of hypoglycemia is low, given the glucose dependence of incretin- mediated insulin release. Overall, DPP4i do not have any reported impact on body weight, blood pressure, or heart rate, and treatment results in small improvements in the aberrant lipid profile associated with T2D, including reduced triglycerides (TG) and increased high-density lipoprotein cholesterol[53]. All the cardiovascular outcome trials of DPP4i have reported significantly improved glycemic control and met the safety requirements of a neutral effect on major adverse cardiovascular events[54-57], despite being powered to demonstrate the expected benefit on cardiovascular disease inferred from ample preclinical data (as reviewed elsewhere)[58-62]. In addition to glycemic control, DPP4i have also demonstrated to be effective erythropoiesis-stimulating agents for renal anemia through the preservation of active erythropoietin[63,64]. Also, although B-type natriuretic or brain peptide is a substrate for DPP4 cleavage, inhibition of DPP4 with linagliptin did not affect N-terminal pro–brain natriuretic peptide (BNP) levels or BNP in patients with T2D[65]. It has also demonstrated that sitagliptin treatment of healthy subjects does not potentiate vasodilation in response to BNP injection[66].

8.8 DPP4 Inhibitors in Combination with Metformin

DPP4i are often prescribed together or provided as a dual therapy when metformin is not sufficient to maintain euglycemia[67-73]. Patients who receive dual

therapy experience additive glucose-lowering and superior improvements in HbA1c[74]. Metformin has been demonstrated to mediate significant metabolic effects through its action within the gastrointestinal tract[75,76]. Preproglucagon (*Gcg*) is expressed in enteroendocrine L cells, which are dispersed throughout the duodenum but more concentrated toward the distal colon[77,78]. Glucagon-like peptide-1 is processed from the preproglucagon polypeptide by prohormone convertase 1/3 (PC1/3), and its secretion is stimulated by ingested nutrients[44,79,80].

One proposed gut-based mechanism of action for metformin is to stimulate GLP-1 secretion directly from the L cell[81]. In addition, metformin may also enhance GLP-1R and GIPR expression within the β cell[82,83]. Consistent with increased secretion, nondiabetic, obese patients who received metformin monotherapy experience an increase in active GLP- 1, and metformin did not alter the kinetics of GLP-1 degradation by DPP4[84,85]. Metformin is, therefore, an effective partner for additive therapy with a DPP4i. In addition to the superior lowering of HbA1c, dual therapy is a promising course of treatment for reducing adverse cardiovascular events. A recent post hoc subgroup analysis of the three cardiovascular outcome trials for DPP4i suggests that patients treated at baseline with metformin may derive cardiovascular benefit from DPP4i compared with metformin nonusers[86,87].

8.8.1 Role of endothelial cell–derived DPP4 in glycemic regulation

Both *Dpp4*$^{-/-}$ mice and F-344/DuCrj rats (deficient in DPP4 catalytic activity) demonstrate increased GLP-1 concentrations, higher insulin secretion, and improved postprandial glucose control[88-90]. Activation of the GLP-1R present on β cells regulates not only hormone secretion from endocrine cells potentiating glucose-stimulated insulin secretion and reducing glucagon secretion through stimulation of

somatostatin but also increases insulin synthesis, β-cell neogenesis, islet mass, and β-cell survival[91-93]. Dipeptidyl peptidase-4 is present on endothelial cells throughout the body, including those adjacent to the enteroendocrine L cells which produce GLP-1[94]. Consistent with these observations, enteric targeting of DPP4 by genetic elimination of *Dpp4* from endothelial cells or low pharmacological concentrations of DPP4 inhibitors can significantly increase circulating, active GLP-1 concentrations and improve glycemia[8,30,95]. The portal circulation and hepatic bed have also been identified as DPP4+ sites for GLP-1 degradation[30,45-48,96]. However, it is most likely endothelial cells within the portal system which regulate the cleavage as elimination of *Dpp4* specifically from hepatocytes or administration of a small interfering RNA (siRNA) to target *Dpp4* within hepatocytes failed to augment circulating incretin levels and improve glucose tolerance[26,97].

The proGIP gene encodes the incretin hormone GIP, which is mainly expressed in the intestinal K cells.44 Similar to GLP- 1, PC1/3 converts a proGIP prohormone precursor into active GIP. In addition to being an incretin hormone, GIP signaling and GIPR have been shown to play a role in diet-induced obesity[98], adipokine secretion[99], lipoprotein lipase activity, and TG accumulation[100]. Degradation of significant amounts of GIP by DPP4 occurs within in the gut by both endothelial and immune cell populations[30].

8.8.2 Role of islet-derived DPP4 in glycemic regulation

Recent evidence in mice genetically engineered to re-express *Gcg* has suggested that bioactive and glucoregulatory GLP-1 may be produced in the pancreas[101]. Dipeptidyl peptidase-4 protein expression has been observed in isolated human islets[102], and GLP-1R antagonism blunts the DPP4i (linagliptin) improvement

in mice with *Gcg* expression restricted to the pancreas[103], suggesting a potential pancreatic, paracrine circuit to control glycemia. However, further use of these models to re-express *Gcg* in the proximal and distal gut demonstrates gut-derived GLP-1 is indeed the dominant site of GLP-1, and pancreas perfusion studies with a DPP4i have demonstrated no impact on glycemia[104]. However, recently, *Dpp4* mRNA and DPP4 protein have been proposed to be expressed dynamically in late fetal stages of β-cell development, which coincide with the expression of GLP-1R and may regulate GLP-1–mediated signaling responses important for β-cell maturation[105]. The importance of preproglucagon-derived peptides in the control of islet cell communication through cAMP has been recently demonstrated[106,107], and the addition of sitagliptin to metformin is associated with a lower rate of diabetes progression[108]. These data suggest that although an islet-DPP4-GLP-1 axis may not regulate whole-body glucose metabolism, it may regulate necessary islet-specific signaling important in β-cell function and survival.

Both the mRNA of proGIP and a biologically active, truncated form of GIP(1-30) have been localized to alpha cells of both mouse and human islets, which is stimulated and secreted in response to arginine[109]. The DPP4-mediated degradation product GIP(3-42) has also been demonstrated to act as a GIPR antagonist[43]. However, the importance of DPP4-mediated regulation of GIP within the islet is complicated by observations that in states of T2D, the GIPR undergoes desensitization and degradation[110-113].

Peptide tyrosine tyrosine (PYY) is another DPP4 substrate secreted by endocrine L cells and pancreatic α cells in response to glucose and is associated with insulin secretion[114]. Cleavage of PYY(1-36) by DPP4 leads to the creation of truncated

peptide, PYY(3-36), which exhibits altered receptor selectivity. Unlike PYY(1-36) that binds to all NPY receptor subtypes with equal affinity, the truncated PYY(3-36) exhibits high-affinity binding to the NPY2 receptor[115]. PYY(1-36) was shown to inhibit glucose-stimulated insulin secretion in isolated islets, whereas PYY(3-36) had no effect[116]. Also, administration of exogenous PYY(3-36) during an intraperitoneal glucose tolerance test has been shown to lower glycemia through GLP-1–mediated improvements in insulin secretion, whereas PYY(1-36) did not[116-118]. Further studies using native PYY (1-36) have demonstrated β-cell proliferation and protection from cytokine-induced apoptosis in BRIN BD11 and 1.1B4 cells[119]. As levels of intact and DPP4 cleavage products of PYY have been difficult to measure, the biological relevance of islet cleavage in the regulation of glucose is uncertain.

8.9 DPP4 as a Regulator of Immune Cells

Consistent with the promoter analysis, altered expression of DPP4 in autoimmune and infectious diseases, hematological cancers, and tumors has been reviewed in detail elsewhere[4,7,11,120]. There are several significant differences between mice and humans in this regard, as DPP4 expression in the hematopoietic compartment differs between them. In human subjects, DPP4 is expressed predominantly by T cells, whereas in mice, dendritic cells, B cells, and natural killer cells also express significant levels of DPP4[121]. Lipopolysaccharide treatment of mice increases expression of DPP4 on macrophages 5- to 10-fold, suggesting acute activators of inflammation are associated with significantly increased DPP4 expression in circulating immune cells.[22] Consistent with this, the release of DPP4 is induced by treatment with TNF-α and with insulin[122]. The effects of low-grade, often subclinical inflammation observed in patients with metabolic disease offers less clarity

in the form of DPP4 expression on immune cell populations. Assessment of 14 controls versus 27 patients with confirmed atherosclerotic plaque identified that DPP4 is elevated on CD11b+ monocytes, and it correlates with plasma TG and cholesterol, but not with glucose or insulin concentrations[123].

Peripheral blood mononuclear cells isolated from patients with T2D demonstrated no difference in DPP4 activity or gene expression[124]. It has been reproducibly demonstrated that a significant portion of circulating DPP4 originates from bone marrow–derived cells[30,121,125,126], suggesting they are an essential reservoir of soluble DPP4. In patients with severe combined immunodeficiency, as well as studies in irradiated mice, the number of lymphocytes in circulation correlated with levels of circulating DPP4[121]. Additional evidence suggests DPP4 can derive from osteoclasts and signal through receptor activator of nuclear factor-kappa B ligand (RANKL) under circumstances of bone remodeling[49]. RNA-seq data have identified DPP4 as one of the factors produced by adipogenic marrow cells that negatively influence bone healing in response to age and high-fat diet feeding[127]. Nine-day treatment with sitagliptin increased the shift toward osteogenic progenitors in the tibia, suggestive of enzymatic activity regulating differentiation[127].

8.10 DPP4 Expression in Mature Adipocytes and Adipocyte Progenitors

Increased DPP4 expression and activity have been consistently associated with obesity (increased body mass index and excess adipose tissue in humans)[26,35,96,122,128]. In addition, leptin concentrations and the size of adipocytes in both visceral and subcutaneous depots positively associate with DPP4, whereas adiponectin levels negatively correlate with circulating DPP4[128]. Given its strong correlation with increased adipose tissue accumulation, the origin of obesity-induced

circulating DPP4 was originally proposed to be the mature adipocyte[122,128,129]. Consistent with this idea, the genetic elimination of adipose tissue DPP4 triggers beneficial adipose tissue remodeling and improved hepatic insulin sensitivity in diet-induced obesity[130]. In addition, in 1-year-old obese mice fed a high-fat, high-cholesterol diet (HFHC), it was determined that a small portion of circulating DPP4 originates from adiponectin + cells[26].

Recent single-cell RNA sequencing combined with elegant microscopy evidence suggests that DPP4 expression is limited in adipose tissue to multipotent progenitors, which exist within the reticular interstitium and give rise to intercellular adhesion molecule 1 (ICAM)+ and CD142+ preadipocytes[131]. Previous studies are consistent with *Dpp4* expression on progenitor populations as decreased DPP4 expression is associated with early steps in adipocyte differentiation, including adipocyte maturation[132]. However, it is possible that in states of obesity DPP4+, mesenchymal progenitor cells are depleted, which reduces the population of preadipocytes disrupting the required adipose tissue hyperplasia, shifting to maladaptive hypertrophy within visceral depots[131]. This concept requires further investigation.

8.11 DPP4 Within the Adipose Tissue Stromal Vascular Fraction

Dipeptidyl peptidase-4 expression in adipose tissue is much more prevalent in the stromal vascular fraction than in the adipocyte fraction, particularly under conditions of high-fat feeding[26] Increased DPP4 expression in obese humans and *ob/ob* mice is observed in populations of dendritic cells and macrophages isolated from visceral adipose tissue[22]. However, the increase in circulating DPP4 observed with increased adipose tissue accumulation is entirely unaffected in mice lacking DPP4 in CD45+ immune cell populations[30], suggesting that the majority of

dysregulated circulating DPP4 due to obesity was not originating from CD45+ immune cells.

8.12 DPP4 as a Biomarker of Metabolic Liver Disease

The liver has been proposed as a primary source of circulating DPP4[133]. Within the liver, DPP4 is expressed in both hepatocytes and nonparenchymal cells, yet obesity only increases *Dpp4* expression in hepatocytes[134]. Analysis by Baumeier *et. al*.[135] calculated by total weight predicted that in mice, the majority of DPP4 protein release came from the liver. Several groups have identified that circulating DPP4 levels are also positively associated with NAFLD[20,136]. In humans, plasma DPP4 expression and activity are increased in patients with NAFLD and have a strong correlation with liver fat content[135]. Higher hepatic DPP4 expression and elevated plasma levels are observed in patients with NAFLD compared with healthy subjects[20]. Nonbiased, discovery-based proteome profiling in the plasma from patients with T2D, NAFLD, and cirrhosis demonstrated that DPP4 protein levels significantly correlated with concentrations of liver enzymes used currently as markers of liver damage, including alanine aminotransferase (ALT), aspartate transaminase (AST), alkaline phosphatase, and gamma-glutamyl transferase[137]. Indeed, methylation at CpG sites in the *Dpp4* southern shore has been reported to regulate the expression of *Dpp4* in the liver[138], but not in adipose[135], kidneys, or brain[138] of mice, suggesting liver-specific transcriptional regulation in disease states.

8.13 DPP4 as a Hepatokine

Consistent with the role of hepatocyte-derived DPP4 in metabolic disease, Ghorpade *et. al.*[35] identified DPP4 as a circulating casual factor downstream of hepatic CAMKII signaling, which promoted macrophage chemoattractant protein

(*Mcp-1*), interleukin 6 (*Il6*), *Tnf α*, and *Il-1β* expression and crown-like structures within visceral, but not inguinal or brown adipose tissue. Varin *et. al.*[26] a confirmed these findings in *Dpp4*$^{Hep-/-}$ mice, which confirmed that the 40% increase in circulating DPP4 under high-fat diet feeding or obesity is hepatocyte-derived. Similarly, in the absence of hepatic *Dpp4*, reduced levels of F4/80 (Adgre1), Il2, C-C chemokine ligand 2 (Ccl2), and Tnf-α were observed in both the livers and gonadal adipose tissue of HFHC-fed *Dpp4*$^{Hep-/-}$ mice[26]. In both models, reductions in hepatic DPP4 resulted in improvements in whole-body insulin sensitivity, and the effects could not be replicated by treatment with a DPP4i[26,35]. The HFHC-fed mice treated with the DPP4i MK-0626 demonstrated no changes in cytokine expression in the liver, epididymal fat, or plasma. Also, patients with T2D treated for 4 weeks with the DPP4i sitagliptin failed to demonstrate any significant changes in circulating concentrations of inflammatory cytokines, chemokines, or growth factors[139]. Conversely, the gonadal white adipose tissue isolated from mice with a hepatocyte-specific overexpression of *Dpp4* (1.6-fold increase in hepatic protein and a 2-fold increase in circulating) demonstrated increased markers of macrophage infiltration (F4/80) and inflammatory cytokines (TNF-α and MCP-1) and increased leptin:adiponectin ratios[135]. Consistent with a direct effect on insulin sensitivity, insulin treatment of HepG2 hepatoma cells and primary mouse hepatocytes infected with adenovirus to overexpress DPP4 demonstrated a reduction in insulin-stimulated Akt phosphorylation[135]. Incubation of adipocytes, skeletal muscle cells, and smooth muscle cells with DPP4 reduced Akt phosphorylation induced by insulin in a dose-responsive manner, suggesting these signaling effects are direct[122].

Hypoxia-inducible factor-1 α (*Hif1α*) is also elevated in obesity, and hepatocyte-specific elimination of *Hif1a*, but not *Hif2α*, decreased the upregulation of hepatic *Dpp4* observed with an excess of adipose tissue[96]. These data suggest that hypoxia may be an initiating factor for the shedding of DPP4 and are consistent with the model proposed by Chowdhury *et. al.*[140]. Deletion of hepatocyte *Hif1α*, which prevents obesity-induced increases in hepatic DPP4, demonstrated increased active portal GLP-1 and improved glucose tolerance[96]. The lack of upregulation of *Dpp4* within the liver in *Hif1α*$^{-/-}$ mice was associated with a decrease in phosphorylated p65 NF-κB levels[96], confirming that elimination of the obesity-induced increase in hepatic DPP4 is linked to reduced inflammation. It has been difficult to dissect the temporal relationship between lipid accumulation, inflammation, and insulin resistance, as mice with hepatic overexpression of DPP4 exhibited increased liver TG accumulation and adipose tissue accumulation beginning at 20 weeks and persisting throughout the 30-week study. They also exhibited increases in fatty acid transporter CD36[135]. Elimination of Dpp4 from hepatocytes with siRNA from mice with diet-induced obesity or *ob/ob* mice reduced circulating nonesterified fatty acids (NEFA), effects not replicated with sitagliptin treatment. However, both lipogenesis and oleic acid uptake were similar in both control and DPP4 over-expressing hepatocytes[135], and genetic elimination of *Dpp4* specifically from hepatocytes did not lead to any changes in NEFA, TG, or liver lipid accumulation[26]. These data suggest aberrant communication between adipose tissue and the liver can be the main driver of DPP4's role in insulin resistance and inflammation. The main cell type identified to respond to liver-derived DPP4 is the adipose tissue macrophage (ATM). In vitro studies have also identified protease-activated receptor 2 (PAR2) as a potential target of soluble DPP4 action in

smooth muscle cells[141] and in cultured human coronary artery endothelial cells[129]. Ghorpade *et. al.*[35] demonstrated that both PAR2 and caveolin-1 signaling were instrumental in stimulating inflammation in ATM by using an intraperitoneal injection of siRNA encapsulated in micrometer-sized glucan shells to specifically target signaling in ATMs. In addition, they propose that activated factor X may signal synergistically with DPP4 and activate extracellular signal-regulated kinase (ERK1/2) and NF-κB to increase downstream expression mediators of inflammation, including MCP-1, IL-6, and TNF-α[35]. Indeed, disrupting protein-protein interactions with DPP4, but not DPP4 inhibitor treatment, reduced adipose tissue inflammation[22], consistent with a noncatalytic mechanism of action.

8.14 DPP4 Inhibitors and Metabolic Liver Disease

Both diet-induced obese mice and *ob/ob* mice treated with the DPP4i linagliptin improved glycemic parameters and reduced the liver fat content and markers of inflammation, suggesting potentiation of DPP4 substrates may have short-term benefit on liver metabolism[142]. More recently, Kawakubo *et. al.*[143] treated a genetically obese melanocortin 4 receptor-deficient mouse (model of insulin resistance, hepatic steatosis, nonalcoholic steatosis hepatitis [NASH], and hepatocellular carcinoma) with a DPP4i which prevented the progression of simple steatosis to NASH, and decreased hepatic crown-like structures and expression of inflammatory and fibrosis-related genes. Also, in randomized control trials with patients treated with sitagliptin (100mg) for 1year, biopsy demonstrated reduced steatosis and ballooning[144]. In addition, in further studies, sitagliptin (100mg) decreased ALT and AST and improved histological scoring[145]. However, adding to the complexity of interpretation, randomized controlled trials of patients with liver disease where patients treated with alogliptin (25 mg/day

for 12 months)[146], vildagliptin (50 mg, twice a day for 6 months)[146], or sitagliptin (100 mg for 12 months)[147] reports confirm failure to provide any clear benefit.

8.15 DPP4 and Fibrosis

Shigeta *et.al.*[148] discovered that the activity of the membrane-bound form of DPP4 is elevated in a diabetic rat model but reduced in their normoglycemic counterparts. As a result, circulating stromal-derived factor 1 (SDF-1), angiogenesis, and the number of CXC chemokine receptor–positive/vascular endothelial growth factor receptor–positive (CXCR+KDR+) endothelial progenitor cells were decreased, while there was an increase in fibrosis. The opposite was observed in *Dpp4*$^{-/-}$ and normoglycemic control rats[148]. CXCL12 signaling has been proposed to promote liver fibrosis by recruiting immune cell populations and has also been linked to the development of hepatocellular carcinoma[149], although it is unclear to date whether DPP4i can potentiate this process. Dipeptidyl peptidase-4 has been demonstrated to define fibroblast populations within human skin biopsies[150], and DPP4+ fibroblasts have been shown to express higher levels of myofibroblast markers[151] and collagen, but whether these pathways are relevant in liver disease remains to be determined. Treatment of mice predisposed to fibrosis by treatment with bleomycin or chronic graft versus host disease with DPP4i has resulted in reduced fibrosis and inflammation, and DPP4i have also been found to promote the migration of keratinocytes, and reduce collagen synthesis and deposition, limiting scar formation[152].

8.16 Future Directions

The substantial body of preclinical evidence in genetic mouse models linking cell-specific actions of DPP4 with insulin resistance, obesity, and NAFLD requires further confirmation and mechanistic studies in patient populations and human model

systems to confirm its role as a biomarker or causal agent in disease progression. The novel discovery of the fate of several DPP4+ progenitor cell populations illustrates additional metabolic pathways that may also contribute to the regulation of glucose, insulin sensitivity, and metabolic disease. These observations solidify the need for further elucidation of how DPP4 regulates these pathways—through catalytic activity and cleavage of substrate peptides or direct protein-protein interactions.

8.17 References

1. Deacon CF. Physiology and Pharmacology of DPP-4 in Glucose Homeostasis and the Treatment of Type 2 Diabetes. *Front Endocrinol (Lausanne).* 2019;10:80.
2. Mulvihill EE, Drucker DJ. Pharmacology, Physiology and Mechanisms of Action of Dipeptidyl Peptidase-4 Inhibitors. *Endocr Rev.* 2014:er20141035.
3. Nauck MA, Meier JJ. GIP and GLP-1: Stepsiblings Rather Than Monozygotic Twins Within the Incretin Family. *Diabetes.* 2019;68(5):897-900.
4. Klemann C, Wagner L, Stephan M, von Horsten S. Cut to the chase: a review of CD26/dipeptidyl peptidase-4's (DPP4) entanglement in the immune system. *Clin Exp Immunol.* 2016;185(1):1-21.
5. Ghersi G, Zhao Q, Salamone M, Yeh Y, Zucker S, Chen WT. The protease complex consisting of dipeptidyl peptidase IV and seprase plays a role in the migration and invasion of human endothelial cells in collagenous matrices. *Cancer Res.* 2006;66(9):4652-4661.
6. Diaz-Jimenez D, Petrillo MG, Busada JT, Hermoso MA, Cidlowski JA. Glucocorticoids mobilize macrophages by transcriptionally up-regulating the exopeptidase DPP4. *The Journal of biological chemistry.* 2020;295(10):3213-3227.
7. Wagner L, Klemann C, Stephan M, von Horsten S. Unravelling the immunological roles of dipeptidyl peptidase 4 (DPP4) activity and/or structure homologue (DASH) proteins. *Clin Exp Immunol.* 2016;184(3):265-283.
8. Mulvihill EE. Dipeptidyl peptidase inhibitor therapy in type 2 diabetes: Control of the incretin axis and regulation of postprandial glucose and lipid metabolism. *Peptides.* 2018;100:158-164.
9. Ogata S, Misumi Y, Ikehara Y. Primary structure of rat liver dipeptidyl peptidase IV deduced from its cDNA and identification of the NH2-terminal signal sequence as the membrane-anchoring domain. *The Journal of biological chemistry.* 1989;264(6):3596-3601.
10. Thoma R, Loffler B, Stihle M, Huber W, Ruf A, Hennig M. Structural basis of proline-specific exopeptidase activity as observed in human dipeptidyl peptidase-IV. *Structure.* 2003;11(8):947-959.
11. Lambeir AM, Durinx C, Scharpe S, De Meester I. Dipeptidyl-peptidase IV from bench to bedside: an update on structural properties, functions, and clinical aspects of the enzyme DPP IV. *Crit Rev Clin Lab Sci.* 2003;40(3):209-294.
12. Ogata S, Misumi Y, Tsuji E, Takami N, Oda K, Ikehara Y. Identification of the active site residues in dipeptidyl peptidase IV by affinity labeling and site-directed mutagenesis. *Biochemistry.* 1992;31(9):2582-2587.
13. Chien CH, Tsai CH, Lin CH, Chou CY, Chen X. Identification of hydrophobic residues critical for DPP-IV dimerization. *Biochemistry.* 2006;45(23):7006-7012.
14. Qvist H, Sjostrom H, Noren O. The TATA-less, GC-rich porcine dipeptidylpeptidase IV (DPPIV) promoter shows bidirectional activity. *Biol Chem.* 1998;379(1):75-81.
15. Bohm SK, Gum JR, Jr., Erickson RH, Hicks JW, Kim YS. Human dipeptidyl peptidase IV gene promoter: tissue-specific regulation from a TATA-less GC-

rich sequence characteristic of a housekeeping gene promoter. *Biochem J.* 1995;311 (Pt 3)(Pt 3):835-843.
16. Senkel S, Lucas B, Klein-Hitpass L, Ryffel GU. Identification of target genes of the transcription factor HNF1beta and HNF1alpha in a human embryonic kidney cell line. *Biochim Biophys Acta.* 2005;1731(3):179-190.
17. Rohrborn D, Wronkowitz N, Eckel J. DPP4 in Diabetes. *Front Immunol.* 2015;6:386.
18. Silva AP, Cavadas C, Baisse-Agushi B, Spertini O, Brunner HR, Grouzmann E. NPY, NPY receptors, and DPP IV activity are modulated by LPS, TNF-alpha and IFN-gamma in HUVEC. *Regul Pept.* 2003;116(1-3):71-79.
19. Zhong J, Maiseyeu A, Davis SN, Rajagopalan S. DPP4 in cardiometabolic disease: recent insights from the laboratory and clinical trials of DPP4 inhibition. *Circ Res.* 2015;116(8):1491-1504.
20. Miyazaki M, Kato M, Tanaka K, et al. Increased hepatic expression of dipeptidyl peptidase-4 in non-alcoholic fatty liver disease and its association with insulin resistance and glucose metabolism. *Mol Med Rep.* 2012;5(3):729-733.
21. Baumeier C, Saussenthaler S, Kammel A, et al. Hepatic DPP4 DNA Methylation Associates With Fatty Liver. *Diabetes.* 2017;66(1):25-35.
22. Zhong J, Rao X, Deiuliis J, et al. A potential role for dendritic cell/macrophage-expressing DPP4 in obesity-induced visceral inflammation. *Diabetes.* 2013;62(1):149-157.
23. Mannucci E, Pala L, Ciani S, et al. Hyperglycaemia increases dipeptidyl peptidase IV activity in diabetes mellitus. *Diabetologia.* 2005;48(6):1168-1172.
24. Ryskjaer J, Deacon CF, Carr RD, et al. Plasma dipeptidyl peptidase-IV activity in patients with type-2 diabetes mellitus correlates positively with HbAlc levels, but is not acutely affected by food intake. *Eur J Endocrinol.* 2006;155(3):485-493.
25. Fadini GP, Albiero M, Menegazzo L, de Kreutzenberg SV, Avogaro A. The increased dipeptidyl peptidase-4 activity is not counteracted by optimized glucose control in type 2 diabetes, but is lower in metformin-treated patients. *Diabetes Obes Metab.* 2012;14(6):518-522.
26. Varin EM, Mulvihill EE, Beaudry JL, et al. Circulating Levels of Soluble Dipeptidyl Peptidase-4 Are Dissociated from Inflammation and Induced by Enzymatic DPP4 Inhibition. *Cell Metab.* 2019;29(2):320-334 e325.
27. Slimane TA, Lenoir C, Sapin C, Maurice M, Trugnan G. Apical secretion and sialylation of soluble dipeptidyl peptidase IV are two related events. *Exp Cell Res.* 2000;258(1):184-194.
28. Fan H, Meng W, Kilian C, Grams S, Reutter W. Domain-specific N-glycosylation of the membrane glycoprotein dipeptidylpeptidase IV (CD26) influences its subcellular trafficking, biological stability, enzyme activity and protein folding. *Eur J Biochem.* 1997;246(1):243-251.
29. Noels H, Theelen W, Sternkopf M, et al. Reduced post-operative DPP4 activity associated with worse patient outcome after cardiac surgery. *Sci Rep.* 2018;8(1):11820.
30. Mulvihill EE, Varin EM, Gladanac B, et al. Cellular Sites and Mechanisms Linking Reduction of Dipeptidyl Peptidase-4 Activity to Control of Incretin Hormone Action and Glucose Homeostasis. *Cell Metab.* 2017;25(1):152-165.

31. Hong WJ, Petell JK, Swank D, Sanford J, Hixson DC, Doyle D. Expression of dipeptidyl peptidase IV in rat tissues is mainly regulated at the mRNA levels. *Exp Cell Res.* 1989;182(1):256-266.
32. Hildebrandt M, Reutter W, Gitlin JD. Tissue-specific regulation of dipeptidyl peptidase IV expression during development. *Biochem J.* 1991;277 (Pt 2)(Pt 2):331-334.
33. Nargis T, Chakrabarti P. Significance of circulatory DPP4 activity in metabolic diseases. *IUBMB Life.* 2018;70(2):112-119.
34. Rohrborn D, Eckel J, Sell H. Shedding of dipeptidyl peptidase 4 is mediated by metalloproteases and up-regulated by hypoxia in human adipocytes and smooth muscle cells. *FEBS Lett.* 2014;588(21):3870-3877.
35. Ghorpade DS, Ozcan L, Zheng Z, et al. Hepatocyte-secreted DPP4 in obesity promotes adipose inflammation and insulin resistance. *Nature.* 2018;555(7698):673-677.
36. Yu DM, Slaitini L, Gysbers V, et al. Soluble CD26 / dipeptidyl peptidase IV enhances human lymphocyte proliferation in vitro independent of dipeptidyl peptidase enzyme activity and adenosine deaminase binding. *Scand J Immunol.* 2011;73(2):102-111.
37. Ishii T, Ohnuma K, Murakami A, et al. CD26-mediated signaling for T cell activation occurs in lipid rafts through its association with CD45RO. *Proc Natl Acad Sci U S A.* 2001;98(21):12138-12143.
38. Vora KA, Porter G, Peng R, et al. Genetic ablation or pharmacological blockade of dipeptidyl peptidase IV does not impact T cell-dependent immune responses. *BMC Immunol.* 2009;10:19.
39. Ohnuma K, Inoue H, Uchiyama M, et al. T-cell activation via CD26 and caveolin-1 in rheumatoid synovium. *Mod Rheumatol.* 2006;16(1):3-13.
40. Ikushima H, Munakata Y, Ishii T, et al. Internalization of CD26 by mannose 6-phosphate/insulin-like growth factor II receptor contributes to T cell activation. *Proc Natl Acad Sci U S A.* 2000;97(15):8439-8444.
41. Ikushima H, Munakata Y, Iwata S, et al. Soluble CD26/dipeptidyl peptidase IV enhances transendothelial migration via its interaction with mannose 6-phosphate/insulin-like growth factor II receptor. *Cell Immunol.* 2002;215(1):106-110.
42. Campbell JE, Drucker DJ. Pharmacology, physiology, and mechanisms of incretin hormone action. *Cell Metab.* 2013;17(6):819-837.
43. Gabe MBN, van der Velden WJC, Smit FX, Gasbjerg LS, Rosenkilde MM. Molecular interactions of full-length and truncated GIP peptides with the GIP receptor - A comprehensive review. *Peptides.* 2020;125:170224.
44. Baggio LL, Drucker DJ. Biology of incretins: GLP-1 and GIP. *Gastroenterology.* 2007;132(6):2131-2157.
45. Deacon CF. What do we know about the secretion and degradation of incretin hormones? *Regul Pept.* 2005;128(2):117-124.
46. Deacon CF, Johnsen AH, Holst JJ. Degradation of glucagon-like peptide-1 by human plasma in vitro yields an N-terminally truncated peptide that is a major endogenous metabolite in vivo. *J Clin Endocrinol Metab.* 1995;80(3):952-957.
47. Deacon CF, Nauck MA, Toft-Nielsen M, Pridal L, Willms B, Holst JJ. Both subcutaneously and intravenously administered glucagon-like peptide I are

rapidly degraded from the NH2-terminus in type II diabetic patients and in healthy subjects. *Diabetes.* 1995;44(9):1126-1131.
48. Deacon CF, Wamberg S, Bie P, Hughes TE, Holst JJ. Preservation of active incretin hormones by inhibition of dipeptidyl peptidase IV suppresses meal-induced incretin secretion in dogs. *J Endocrinol.* 2002;172(2):355-362.
49. Weivoda MM, Chew CK, Monroe DG, et al. Identification of osteoclast-osteoblast coupling factors in humans reveals links between bone and energy metabolism. *Nat Commun.* 2020;11(1):87.
50. Orgaard A, Holst JJ. The role of somatostatin in GLP-1-induced inhibition of glucagon secretion in mice. *Diabetologia.* 2017;60(9):1731-1739.
51. Balas B, Baig MR, Watson C, et al. The dipeptidyl peptidase IV inhibitor vildagliptin suppresses endogenous glucose production and enhances islet function after single-dose administration in type 2 diabetic patients. *J Clin Endocrinol Metab.* 2007;92(4):1249-1255.
52. Shubrook J, Colucci R, Guo A, Schwartz F. Saxagliptin: A Selective DPP-4 Inhibitor for the Treatment of Type 2 Diabetes Mellitus. *Clin Med Insights Endocrinol Diabetes.* 2011;4:1-12.
53. Nauck MA, Meier JJ, Cavender MA, Abd El Aziz M, Drucker DJ. Cardiovascular Actions and Clinical Outcomes With Glucagon-Like Peptide-1 Receptor Agonists and Dipeptidyl Peptidase-4 Inhibitors. *Circulation.* 2017;136(9):849-870.
54. White WB, Cannon CP, Heller SR, et al. Alogliptin after acute coronary syndrome in patients with type 2 diabetes. *N Engl J Med.* 2013;369(14):1327-1335.
55. Scirica BM, Bhatt DL, Braunwald E, et al. Saxagliptin and cardiovascular outcomes in patients with type 2 diabetes mellitus. *N Engl J Med.* 2013;369(14):1317-1326.
56. Rosenstock J, Perkovic V, Johansen OE, et al. Effect of Linagliptin vs Placebo on Major Cardiovascular Events in Adults With Type 2 Diabetes and High Cardiovascular and Renal Risk: The CARMELINA Randomized Clinical Trial. *JAMA.* 2019;321(1):69-79.
57. Green JB, Bethel MA, Armstrong PW, et al. Effect of Sitagliptin on Cardiovascular Outcomes in Type 2 Diabetes. *N Engl J Med.* 2015;373(3):232-242.
58. Ussher JR, Drucker DJ. Cardiovascular biology of the incretin system. *Endocr Rev.* 2012;33(2):187-215.
59. Ussher JR, Drucker DJ. Cardiovascular actions of incretin-based therapies. *Circ Res.* 2014;114(11):1788-1803.
60. Pala L, Rotella CM. The role of DPP4 activity in cardiovascular districts: in vivo and in vitro evidence. *J Diabetes Res.* 2013;2013:590456.
61. Zhong J, Rao X, Rajagopalan S. An emerging role of dipeptidyl peptidase 4 (DPP4) beyond glucose control: potential implications in cardiovascular disease. *Atherosclerosis.* 2013;226(2):305-314.
62. Bistola V, Lambadiari V, Dimitriadis G, et al. Possible mechanisms of direct cardiovascular impact of GLP-1 agonists and DPP4 inhibitors. *Heart Fail Rev.* 2018;23(3):377-388.

63. Broxmeyer HE, Hoggatt J, O'Leary HA, et al. Dipeptidylpeptidase 4 negatively regulates colony-stimulating factor activity and stress hematopoiesis. *Nat Med.* 2012;18(12):1786-1796.
64. Chaykovska L, von Websky K, Rahnenfuhrer J, et al. Effects of DPP-4 inhibitors on the heart in a rat model of uremic cardiomyopathy. *PLoS One.* 2011;6(11):e27861.
65. Fadini GP, Bonora BM, Albiero M, Zaninotto M, Plebani M, Avogaro A. DPP-4 inhibition has no acute effect on BNP and its N-terminal pro-hormone measured by commercial immune-assays. A randomized cross-over trial in patients with type 2 diabetes. *Cardiovasc Diabetol.* 2017;16(1):22.
66. Devin JK, Pretorius M, Nian H, Yu C, Billings FTt, Brown NJ. Dipeptidyl-peptidase 4 inhibition and the vascular effects of glucagon-like peptide-1 and brain natriuretic peptide in the human forearm. *J Am Heart Assoc.* 2014;3(4).
67. Gallwitz B, Rosenstock J, Rauch T, et al. 2-year efficacy and safety of linagliptin compared with glimepiride in patients with type 2 diabetes inadequately controlled on metformin: a randomised, double-blind, non-inferiority trial. *Lancet.* 2012;380(9840):475-483.
68. Kothny W, Foley J, Kozlovski P, Shao Q, Gallwitz B, Lukashevich V. Improved glycaemic control with vildagliptin added to insulin, with or without metformin, in patients with type 2 diabetes mellitus. *Diabetes Obes Metab.* 2013;15(3):252-257.
69. Gallwitz B. [Type 2 diabetes: Metformin: first choice at the start of therapy]. *Dtsch Med Wochenschr.* 2015;140(4):236.
70. Ross SA, Caballero AE, Del Prato S, et al. Initial combination of linagliptin and metformin compared with linagliptin monotherapy in patients with newly diagnosed type 2 diabetes and marked hyperglycaemia: a randomized, double-blind, active-controlled, parallel group, multinational clinical trial. *Diabetes Obes Metab.* 2015;17(2):136-144.
71. Ma RC, Del Prato S, Gallwitz B, et al. Oral glucose lowering with linagliptin and metformin compared with linagliptin alone as initial treatment in Asian patients with newly diagnosed type 2 diabetes and marked hyperglycemia: Subgroup analysis of a randomized clinical trial. *J Diabetes Investig.* 2017;9(3):579-586.
72. Gallwitz B. Clinical Use of DPP-4 Inhibitors. *Front Endocrinol (Lausanne).* 2019;10:389.
73. Landgraf R, Aberle J, Birkenfeld AL, et al. Therapy of Type 2 Diabetes. *Exp Clin Endocrinol Diabetes.* 2019;127(S 01):S73-S92.
74. Ballav C, Gough SC. Safety and efficacy of sitagliptin-metformin in fixed combination for the treatment of type 2 diabetes mellitus. *Clin Med Insights Endocrinol Diabetes.* 2013;6:25-37.
75. Song R. Mechanism of Metformin: A Tale of Two Sites. *Diabetes Care.* 2016;39(2):187-189.
76. Buse JB, DeFronzo RA, Rosenstock J, et al. The Primary Glucose-Lowering Effect of Metformin Resides in the Gut, Not the Circulation: Results From Short-term Pharmacokinetic and 12-Week Dose-Ranging Studies. *Diabetes Care.* 2016;39(2):198-205.
77. Lim GE, Brubaker PL. Glucagon-Like Peptide 1 Secretion by the L-Cell: The View From Within. *Diabetes.* 2006;55(Supplement_2):S70-S77.

78. Brubaker PL. Minireview: update on incretin biology: focus on glucagon-like peptide-1. *Endocrinology.* 2010;151(5):1984-1989.
79. MacDonald PE, El-Kholy W, Riedel MJ, Salapatek AM, Light PE, Wheeler MB. The multiple actions of GLP-1 on the process of glucose-stimulated insulin secretion. *Diabetes.* 2002;51 Suppl 3:S434-442.
80. MacDonald PE, Salapatek AM, Wheeler MB. Glucagon-like peptide-1 receptor activation antagonizes voltage-dependent repolarizing K(+) currents in beta-cells: a possible glucose-dependent insulinotropic mechanism. *Diabetes.* 2002;51 Suppl 3:S443-447.
81. Mulherin AJ, Oh AH, Kim H, Grieco A, Lauffer LM, Brubaker PL. Mechanisms underlying metformin-induced secretion of glucagon-like peptide-1 from the intestinal L cell. *Endocrinology.* 2011;152(12):4610-4619.
82. Maida A, Hansotia T, Longuet C, Seino Y, Drucker DJ. Differential importance of glucose-dependent insulinotropic polypeptide vs glucagon-like peptide 1 receptor signaling for beta cell survival in mice. *Gastroenterology.* 2009;137(6):2146-2157.
83. Maida A, Lamont BJ, Cao X, Drucker DJ. Metformin regulates the incretin receptor axis via a pathway dependent on peroxisome proliferator-activated receptor-alpha in mice. *Diabetologia.* 2011;54(2):339-349.
84. Hinke SA, Kuhn-Wache K, Hoffmann T, Pederson RA, McIntosh CH, Demuth HU. Metformin effects on dipeptidylpeptidase IV degradation of glucagon-like peptide-1. *Biochem Biophys Res Commun.* 2002;291(5):1302-1308.
85. Yasuda N, Inoue T, Nagakura T, et al. Enhanced secretion of glucagon-like peptide 1 by biguanide compounds. *Biochem Biophys Res Commun.* 2002;298(5):779-784.
86. Crowley MJ, Williams JW, Jr., Kosinski AS, D'Alessio DA, Buse JB. Metformin Use May Moderate the Effect of DPP-4 Inhibitors on Cardiovascular Outcomes. *Diabetes Care.* 2017;40(12):1787-1789.
87. Scheen AJ. Diabetes: Metformin - a cardiovascular moderator of DPP4 inhibitors? *Nat Rev Endocrinol.* 2018;14(1):8-9.
88. Marguet D, Baggio L, Kobayashi T, et al. Enhanced insulin secretion and improved glucose tolerance in mice lacking CD26. *Proc Natl Acad Sci U S A.* 2000;97(12):6874-6879.
89. Nagakura T, Yasuda N, Yamazaki K, et al. Improved glucose tolerance via enhanced glucose-dependent insulin secretion in dipeptidyl peptidase IV-deficient Fischer rats. *Biochem Biophys Res Commun.* 2001;284(2):501-506.
90. Pederson RA, Kieffer TJ, Pauly R, Kofod H, Kwong J, McIntosh CH. The enteroinsular axis in dipeptidyl peptidase IV-negative rats. *Metabolism.* 1996;45(11):1335-1341.
91. Lamont BJ, Li Y, Kwan E, Brown TJ, Gaisano H, Drucker DJ. Pancreatic GLP-1 receptor activation is sufficient for incretin control of glucose metabolism in mice. *J Clin Invest.* 2012;122(1):388-402.
92. Fehmann HC, Habener JF. Functional receptors for the insulinotropic hormone glucagon-like peptide-I(7-37) on a somatostatin secreting cell line. *FEBS Lett.* 1991;279(2):335-340.

93. Fehmann HC, Hering BJ, Wolf MJ, et al. The effects of glucagon-like peptide-I (GLP-I) on hormone secretion from isolated human pancreatic islets. *Pancreas.* 1995;11(2):196-200.
94. Hansen L, Deacon CF, Orskov C, Holst JJ. Glucagon-like peptide-1-(7-36)amide is transformed to glucagon-like peptide-1-(9-36)amide by dipeptidyl peptidase IV in the capillaries supplying the L cells of the porcine intestine. *Endocrinology.* 1999;140(11):5356-5363.
95. Waget A, Cabou C, Masseboeuf M, et al. Physiological and pharmacological mechanisms through which the DPP-4 inhibitor sitagliptin regulates glycemia in mice. *Endocrinology.* 2011;152(8):3018-3029.
96. Lee YS, Riopel M, Cabrales P, Bandyopadhyay GK. Hepatocyte-specific HIF-1alpha ablation improves obesity-induced glucose intolerance by reducing first-pass GLP-1 degradation. *Sci Adv.* 2019;5(7):eaaw4176.
97. Gorgens SW, Jahn-Hofmann K, Bangari D, et al. A siRNA mediated hepatic dpp4 knockdown affects lipid, but not glucose metabolism in diabetic mice. *PLoS One.* 2019;14(12):e0225835.
98. Miyawaki K, Yamada Y, Ban N, et al. Inhibition of gastric inhibitory polypeptide signaling prevents obesity. *Nat Med.* 2002;8(7):738-742.
99. Hansotia T, Maida A, Flock G, et al. Extrapancreatic incretin receptors modulate glucose homeostasis, body weight, and energy expenditure. *J Clin Invest.* 2007;117(1):143-152.
100. Kim SJ, Nian C, McIntosh CH. Activation of lipoprotein lipase by glucose-dependent insulinotropic polypeptide in adipocytes. A role for a protein kinase B, LKB1, and AMP-activated protein kinase cascade. *The Journal of biological chemistry.* 2007;282(12):8557-8567.
101. Chambers AP, Sorrell JE, Haller A, et al. The Role of Pancreatic Preproglucagon in Glucose Homeostasis in Mice. *Cell Metab.* 2017;25(4):927-934 e923.
102. Campbell SA, Hubert M, Johnson J, Salamon N, Light PE. The DPP4 Inhibitor Sitagliptin Increases Active GLP-1 Levels from Human Islets and May Increase Islet Cell Survival Prior to Transplantation. *OBM Transplantation.* 2019;03(02):069.
103. Hutch CR, Roelofs K, Haller A, et al. The role of GIP and pancreatic GLP-1 in the glucoregulatory effect of DPP-4 inhibition in mice. *Diabetologia.* 2019;62(10):1928-1937.
104. Andersen ES, Deacon CF, Holst JJ. Do we know the true mechanism of action of the DPP-4 inhibitors? *Diabetes Obes Metab.* 2018;20(1):34-41.
105. Kim S, Whitener RL, Peiris H, et al. Molecular and genetic regulation of pig pancreatic islet cell development. *Development.* 2020;147(6).
106. Capozzi ME, Svendsen B, Encisco SE, et al. beta Cell tone is defined by proglucagon peptides through cAMP signaling. *JCI Insight.* 2019;4(5).
107. Capozzi ME, Wait JB, Koech J, et al. Glucagon lowers glycemia when beta-cells are active. *JCI Insight.* 2019;5(16).
108. Campbell SA, Light PE, Simpson SH. Costarting sitagliptin with metformin is associated with a lower likelihood of disease progression in newly treated people with type 2 diabetes: a cohort study. *Diabet Med.* 2020;37(10):1715-1722.

109. Fujita Y, Wideman RD, Asadi A, et al. Glucose-dependent insulinotropic polypeptide is expressed in pancreatic islet alpha-cells and promotes insulin secretion. *Gastroenterology.* 2010;138(5):1966-1975.
110. Piteau S, Olver A, Kim SJ, et al. Reversal of islet GIP receptor down-regulation and resistance to GIP by reducing hyperglycemia in the Zucker rat. *Biochem Biophys Res Commun.* 2007;362(4):1007-1012.
111. Tseng CC, Zhang XY, Wolfe MM. Effect of GIP and GLP-1 antagonists on insulin release in the rat. *Am J Physiol.* 1999;276(6):E1049-1054.
112. Lynn FC, Pamir N, Ng EH, McIntosh CH, Kieffer TJ, Pederson RA. Defective glucose-dependent insulinotropic polypeptide receptor expression in diabetic fatty Zucker rats. *Diabetes.* 2001;50(5):1004-1011.
113. Lynn FC, Thompson SA, Pospisilik JA, et al. A novel pathway for regulation of glucose-dependent insulinotropic polypeptide (GIP) receptor expression in beta cells. *FASEB J.* 2003;17(1):91-93.
114. Medeiros MD, Turner AJ. Processing and metabolism of peptide-YY: pivotal roles of dipeptidylpeptidase-IV, aminopeptidase-P, and endopeptidase-24.11. *Endocrinology.* 1994;134(5):2088-2094.
115. Batterham RL, Cowley MA, Small CJ, et al. Gut hormone PYY(3-36) physiologically inhibits food intake. *Nature.* 2002;418(6898):650-654.
116. Chandarana K, Gelegen C, Irvine EE, et al. Peripheral activation of the Y2-receptor promotes secretion of GLP-1 and improves glucose tolerance. *Mol Metab.* 2013;2(3):142-152.
117. Guida C, Stephen S, Guitton R, Ramracheya RD. The Role of PYY in Pancreatic Islet Physiology and Surgical Control of Diabetes. *Trends Endocrinol Metab.* 2017;28(8):626-636.
118. Guida C, McCulloch LJ, Godazgar M, et al. Sitagliptin and Roux-en-Y gastric bypass modulate insulin secretion via regulation of intra-islet PYY. *Diabetes Obes Metab.* 2018;20(3):571-581.
119. Lafferty RA, Gault VA, Flatt PR, Irwin N. Effects of 2 Novel PYY(1-36) Analogues, (P(3)L(31)P(34))PYY(1-36) and PYY(1-36)(Lys(12)PAL), on Pancreatic Beta-Cell Function, Growth, and Survival. *Clin Med Insights Endocrinol Diabetes.* 2019;12:1179551419855626.
120. Boonacker E, Van Noorden CJ. The multifunctional or moonlighting protein CD26/DPPIV. *Eur J Cell Biol.* 2003;82(2):53-73.
121. Casrouge A, Sauer AV, Barreira da Silva R, et al. Lymphocytes are a major source of circulating soluble dipeptidyl peptidase 4. *Clin Exp Immunol.* 2018;194(2):166-179.
122. Lamers D, Famulla S, Wronkowitz N, et al. Dipeptidyl peptidase 4 is a novel adipokine potentially linking obesity to the metabolic syndrome. *Diabetes.* 2011;60(7):1917-1925.
123. Rao X, Deiuliis JA, Mihai G, et al. Monocyte DPP4 Expression in Human Atherosclerosis Is Associated With Obesity and Dyslipidemia. *Diabetes Care.* 2018;41(1):e1-e3.
124. Nargis T, Kumar K, Ghosh AR, et al. KLK5 induces shedding of DPP4 from circulatory Th17 cells in type 2 diabetes. *Mol Metab.* 2017;6(11):1529-1539.

125. Gorrell MD, Gysbers V, McCaughan GW. CD26: a multifunctional integral membrane and secreted protein of activated lymphocytes. *Scand J Immunol.* 2001;54(3):249-264.
126. Wang Z, Grigo C, Steinbeck J, von Horsten S, Amann K, Daniel C. Soluble DPP4 originates in part from bone marrow cells and not from the kidney. *Peptides.* 2014;57:109-117.
127. Ambrosi TH, Scialdone A, Graja A, et al. Adipocyte Accumulation in the Bone Marrow during Obesity and Aging Impairs Stem Cell-Based Hematopoietic and Bone Regeneration. *Cell Stem Cell.* 2017;20(6):771-784 e776.
128. Sell H, Bluher M, Kloting N, et al. Adipose dipeptidyl peptidase-4 and obesity: correlation with insulin resistance and depot-specific release from adipose tissue in vivo and in vitro. *Diabetes Care.* 2013;36(12):4083-4090.
129. Romacho T, Vallejo S, Villalobos LA, et al. Soluble dipeptidyl peptidase-4 induces microvascular endothelial dysfunction through proteinase-activated receptor-2 and thromboxane A2 release. *J Hypertens.* 2016;34(5):869-876.
130. Romacho T, Sell H, Indrakusuma I, et al. DPP4 deletion in adipose tissue improves hepatic insulin sensitivity in diet-induced obesity. *Am J Physiol Endocrinol Metab.* 2020;318(5):E590-E599.
131. Merrick D, Sakers A, Irgebay Z, et al. Identification of a mesenchymal progenitor cell hierarchy in adipose tissue. *Science.* 2019;364(6438).
132. Zillessen P, Celner J, Kretschmann A, Pfeifer A, Racke K, Mayer P. Metabolic role of dipeptidyl peptidase 4 (DPP4) in primary human (pre)adipocytes. *Sci Rep.* 2016;6:23074.
133. Gorrell MD. Dipeptidyl peptidase IV and related enzymes in cell biology and liver disorders. *Clin Sci (Lond).* 2005;108(4):277-292.
134. Blatchley MR, Hall F, Wang S, Pruitt HC, Gerecht S. Hypoxia and matrix viscoelasticity sequentially regulate endothelial progenitor cluster-based vasculogenesis. *Sci Adv.* 2019;5(3):eaau7518.
135. Baumeier C, Schluter L, Saussenthaler S, et al. Elevated hepatic DPP4 activity promotes insulin resistance and non-alcoholic fatty liver disease. *Mol Metab.* 2017;6(10):1254-1263.
136. Itou M, Kawaguchi T, Taniguchi E, Sata M. Dipeptidyl peptidase-4: a key player in chronic liver disease. *World J Gastroenterol.* 2013;19(15):2298-2306.
137. Niu L, Geyer PE, Wewer Albrechtsen NJ, et al. Plasma proteome profiling discovers novel proteins associated with non-alcoholic fatty liver disease. *Mol Syst Biol.* 2019;15(3):e8793.
138. Saussenthaler S, Ouni M, Baumeier C, et al. Epigenetic regulation of hepatic Dpp4 expression in response to dietary protein. *J Nutr Biochem.* 2019;63:109-116.
139. Lovshin JA, Rajasekeran H, Lytvyn Y, et al. Dipeptidyl Peptidase 4 Inhibition Stimulates Distal Tubular Natriuresis and Increases in Circulating SDF-1alpha(1-67) in Patients With Type 2 Diabetes. *Diabetes Care.* 2017;40(8):1073-1081.
140. Chowdhury HH, Velebit J, Radic N, Francic V, Kreft M, Zorec R. Hypoxia Alters the Expression of Dipeptidyl Peptidase 4 and Induces Developmental Remodeling of Human Preadipocytes. *J Diabetes Res.* 2016;2016:7481470.

141. Wronkowitz N, Gorgens SW, Romacho T, et al. Soluble DPP4 induces inflammation and proliferation of human smooth muscle cells via protease-activated receptor 2. *Biochim Biophys Acta.* 2014;1842(9):1613-1621.
142. Gallwitz B. Linagliptin-a novel dipeptidyl peptidase inhibitor for type 2 diabetes therapy. *Clin Med Insights Endocrinol Diabetes.* 2012;5:1-11.
143. Kawakubo M, Tanaka M, Ochi K, et al. Dipeptidyl peptidase-4 inhibition prevents nonalcoholic steatohepatitis–associated liver fibrosis and tumor development in mice independently of its anti-diabetic effects. *Scientific Reports.* 2020;10(1):983.
144. Alam S, Ghosh J, Mustafa G, Kamal M, Ahmad N. Effect of sitagliptin on hepatic histological activity and fibrosis of nonalcoholic steatohepatitis patients: a 1-year randomized control trial. *Hepat Med.* 2018;10:23-31.
145. Yilmaz Y, Yonal O, Deyneli O, Celikel CA, Kalayci C, Duman DG. Effects of sitagliptin in diabetic patients with nonalcoholic steatohepatitis. *Acta Gastroenterol Belg.* 2012;75(2):240-244.
146. Mashitani T, Noguchi R, Okura Y, et al. Efficacy of alogliptin in preventing non-alcoholic fatty liver disease progression in patients with type 2 diabetes. *Biomed Rep.* 2016;4(2):183-187.
147. Cui J, Philo L, Nguyen P, et al. Sitagliptin vs. placebo for non-alcoholic fatty liver disease: A randomized controlled trial. *J Hepatol.* 2016;65(2):369-376.
148. Shigeta T, Aoyama M, Bando YK, et al. Dipeptidyl peptidase-4 modulates left ventricular dysfunction in chronic heart failure via angiogenesis-dependent and -independent actions. *Circulation.* 2012;126(15):1838-1851.
149. Liepelt A, Tacke F. Stromal cell-derived factor-1 (SDF-1) as a target in liver diseases. *Am J Physiol Gastrointest Liver Physiol.* 2016;311(2):G203-209.
150. Tabib T, Morse C, Wang T, Chen W, Lafyatis R. SFRP2/DPP4 and FMO1/LSP1 Define Major Fibroblast Populations in Human Skin. *J Invest Dermatol.* 2018;138(4):802-810.
151. Soare A, Gyorfi HA, Matei AE, et al. Dipeptidylpeptidase 4 as a Marker of Activated Fibroblasts and a Potential Target for the Treatment of Fibrosis in Systemic Sclerosis. *Arthritis Rheumatol.* 2020;72(1):137-149.
152. Long M, Cai L, Li W, et al. DPP-4 Inhibitors Improve Diabetic Wound Healing via Direct and Indirect Promotion of Epithelial-Mesenchymal Transition and Reduction of Scarring. *Diabetes.* 2018;67(3):518-531.

9 Rights and Permissions

Figure 1.1, published with CC BY-NC 4.0

This is a License Agreement between Natasha Trzaskalski ("User") and Copyright Clearance Center, Inc. ("CCC") on behalf of the Rightsholder identified in the order details below. The license consists of the order details, the Marketplace Permissions General Terms and Conditions below, and any Rightsholder Terms and Conditions which are included below.

All payments must be made in full to CCC in accordance with the Marketplace Permissions General Terms and Conditions below.

Order Date	10-Apr-2024	Type of Use	Republish in a thesis/dissertation
Order License ID	1472085-1	Publisher	Oxford University Press
ISSN	1365-2249	Portion	Image/photo/illustration

LICENSED CONTENT

Publication Title	Clinical and experimental immunology	Publication Type	e-Journal
Article Title	Cut to the chase: a review of CD26/dipeptidyl peptidase-4's (DPP4) entanglement in the immune system.	Start Page	1
		End Page	21
Author/Editor	British Society for Immunology.	Issue	1
Date	01/01/1966	Volume	185
Language	English	URL	http://onlinelibrary.wiley.com/journal/10....
Country	United Kingdom of Great Britain and Northern Ireland		
Rightsholder	Oxford University Press - Journals		

REQUEST DETAILS

Portion Type	Image/photo/illustration	Distribution	Canada
Number of Images / Photos / Illustrations	1	Translation	Original language of publication
Format (select all that apply)	Electronic	Copies for the Disabled?	No
Who Will Republish the Content?	Academic institution	Minor Editing Privileges?	No
Duration of Use	Life of current edition	Incidental Promotional Use?	No
Lifetime Unit Quantity	Up to 499	Currency	CAD
Rights Requested	Main product		

NEW WORK DETAILS

Title	Dipeptidyl Peptidase-4 in Cardiometabolic Disease	Institution Name	University of Ottawa Heart Institute
		Expected Presentation Date	2024-06-21
Instructor Name	Natasha Trzaskalski		

ADDITIONAL DETAILS

Order Reference Number	N/A	The Requesting Person / Organization to Appear on the License	Natasha Trzaskalski

REQUESTED CONTENT DETAILS

Title, Description or Numeric Reference of the Portion(s)	Dipeptidyl Peptidase-4 in Cardiometabolic Disease	Title of the Article / Chapter the Portion Is From	Cut to the chase: a review of CD26/dipeptidyl peptidase-4's (DPP4) entanglement in the immune system.
Editor of Portion(s)	Klemann, C.; Wagner, L.; Stephan, M.; von Hörsten, S.	Author of Portion(s)	Klemann, C.; Wagner, L.; Stephan, M.; von Hörsten, S.
Volume / Edition	185	Issue, if Republishing an Article From a Serial	1
Page or Page Range of Portion	1-21	Publication Date of Portion	2016-07-01

Chapter 2, primary research article, published with CC BY 4.0 license

Trzaskalski, N. A., Fullerton, M. D., & Mulvihill, E. E. (2022). Hepatocyte-derived DPP4 regulates portal GLP-1 bioactivity, glucose production, and its absence alters liver disease progression. *JCI Insight*, e154314-e154314.

Verbal confirmation from CCC Rightslink for reuse, unresolved issue with acquiring licence for open access article for use in this thesis. Advised to include the Creative

Commons deed information, or information from the respective journals, which state that it may be reused in as an article in a thesis.

License information (obtained from https://insight.jci.org/kiosks/terms)

The American Society for Clinical Investigation (ASCI) publishes JCI Insight. The opinions expressed in the Journal are solely those of the authors and are not necessarily endorsed by the ASCI.

Open access

JCI Insight is a Gold Open Access journal in which all content is freely available without charge to the user or their institution. Effective with the August 20, 2020, issue, all content is published with a Creative Commons Attribution License (CC BY 4.0).

The ASCI retains copyright to many articles published prior to August 20, 2020. While all content is freely available, some use of articles to which the ASCI holds copyright may require permission. (See “Obtaining permission to use JCI Insight content” below.) Copyright or license information is noted on each article.

JCI Insight deposits all content in PubMed and PubMed Central. Authors of articles published in JCI Insight do not need to deposit their articles separately. The Journal meets cOAlition S requirements for authors who receive funding support from Plan S signatories and is fully compliant with Howard Hughes Medical Institute (HHMI), Wellcome, and UK Research and Innovation (UKRI) open access policies; and is indexed in Securing a Hybrid Environment for Research Preservation and Access (Sherpa Romeo) and included in the Directory of Open Access Journals (DOAJ).

Obtaining permission to use JCI Insight content

Articles published on or after August 20, 2020, are published with the CC BY 4.0 license, which allows for reuse without permission as long as the original source is cited. Permission may be required for use of content published prior to August 20, 2020, where the ASCI retains copyright. Permission can be obtained via Copyright Clearance Center. Copyright or license information is noted on each article.

Terms of use

Use of JCI Insight content constitutes an agreement to comply with the terms noted here. Any copies, in whole or in part, must include the associated license information or copyright notice.

In no event shall JCI Insight or the ASCI be liable for any special, incidental, indirect or consequential damages of any kind, or any damages whatsoever resulting from loss of use, data or profits, whether or not advised of the possibility of damage, and on any theory of liability, arising out of or in connection with the use of or reliance on this information. This publication is provided "as is" without warranty of any kind, either expressed or implied, including, but not limited to, the implied warranties of merchantability, fitness for a particular purpose, or non-infringement. Changes in policy or publication may be made at any time. Descriptions of, or references to, products or publications does not imply endorsement of that product or publication.

Chapter 8, Appendix 3, review article, published with CC BY 4.0 license

Verbal confirmation from CCC Rightslink for reuse, unresolved issue with acquiring licence for open access article for use in this thesis. Advised to include the Creative Commons deed information, or information from the respective journals, which state that it may be reused in as an article in a thesis.

10 Curriculum Vitae

Natasha Trzaskalski M.Sc.

PhD Candidate
University of Ottawa

Academic and Training Background

2018 – 2024 **Ph.D. candidate, Faculty of Medicine, University of Ottawa**
Supervisor: Dr. Erin. E. Mulvihill

2015 – 2018 **M.Sc., Environmental and Life Sciences, Trent University**
Supervisor: Dr. R.J. Neil Emery
Thesis Title: The Effect of Carbon Sources on Growth, Hormone Metabolism and Lipid Synthesis in Heterotrophic Cultures of *Euglena gracilis*
Funded by: NSERC CUI2I grant, in association with NobleGen Inc.

2010 – 2015 **B.Sc. (Hons), Biochemistry and Molecular Biology, Trent University**
Supervisor: Dr. R.J. Neil Emery
Thesis Title: Cross-Talk Between Plant Growth Promoting Hormones: Cytokinins and Brassinosteroids

Funding

2021 **University of Ottawa Heart Institute Endowed Award**
$40,000 over 2 years

2018 – 2022 **Doctoral Admission Scholarship**
$60,000 over 4 years
University of Ottawa

2015 – 2017 **NSERC College and Community Innovation Program – College-University Idea to Innovation Grants (CUI2I)**
$40,000 over 2 years
Trent University in collaboration with NobleGen Inc.

Honours and Awards

2023 **Best Oral Presentation**
BMI Seminar Day, University of Ottawa

2022 **Dr. Yves Marcel Award for Best Basic Science Oral Presentation**

Ottawa Cardiovascular Research Day

2021 **Selected BCH student representative**
Honourable mention for National Oral Presentation Award
Canadian Student Health Research Forum 2021

2020 **Best Rapid Oral Presentation**
Canadian Vascular & Lipid Virtual Summit 2020

2019 **Best Oral Presentation (Third Place)**
BMI Seminar Day, University of Ottawa

2019 **Best Oral Presentation**
Ottawa Institute of System Biology (OISB) Retreat, University of Ottawa

2012 – 2015 **Dean's Honour Roll**
Trent University

Abstract Publications

Trzaskalski, N., Vulesevic, B., Nguyen, M.A., Jeraj, N., Fadzeyeva, E., Morrow, N., Hanson, A., Lorenzen-Schmidt, I., & Mulvihill, E.E. (2021). Liver-Specific Depletion of Dpp4 does not Prevent NAFLD Progression via Macrophage Polarization. ***Insulin 100***.

Trzaskalski, N., Vulesevic, B., Nguyen, M.A., Jeraj, N., Fadzeyeva, E., Morrow, N., Hanson, A., Lorenzen-Schmidt, I., & Mulvihill, E.E. (2021). Reduced Hepatic Gluconeogenesis Observed with Inhibition of Dipeptidyl Peptidase 4 (DPP4) Is Mediated by Targeting *Dpp4* Within the Hepatocyte. ***Insulin 100***.

Fadzeyeva, E., Vulesevic, B., **Trzaskalski, N.**, (2021). Regulation of Glucose Metabolism via the Intra-Islet Dpp4/Incretin Axis. **Insulin 100**.

Trzaskalski, N., Vulesevic, B., Fadzeyeva, E., Nguyen, M.A., & Mulvihill, E.E. (2020). Elimination of Hepatocyte Dpp4 Does Not Alter Markers of Liver Disease Progression in Aged, High-Fat, High-Cholesterol-Fed Mice. ***Canadian Journal of Diabetes***, *44*(7), S28.

Fadzeyeva, E., Vulesevic, B., **Trzaskalski, N.**, Capozzi, M. E., Campbell, J.E., & Mulvihill, E.E. (2020). 9-Regulation of Glucose Metabolism via the Intra-Islet DPP4/Incretin Axis. ***Canadian Journal of Diabetes***, *44*(7), S4.

Published Manuscripts

Smith, T. K. T., Ghorbani, P., LeBlond, N. D., Nunes, J. R. C., O'Dwyer, C., Ambursley, Fong-McMaster, C., Minarrieta, L., El Hakim, R., **Trzaskalski, N. A.**, Locatelli, C. A. A., Stotts, C., Pember, C., Rayner, K. J., Kemp, B. E., Loh, K., Harper, M. E., Mulvihill, E. E., St-Pierre, J., Fullerton, M. D. (2024). AMPK-mediated regulation of endogenous cholesterol synthesis does not affect atherosclerosis in a murine Pcsk9-AAV model. Atherosclerosis, 117608.

Ramphal, K., Lewis, A., **Trzaskalski, N. A.**, Kisiala, A., Morrison, E. N., Narine, S. S., & Emery, R. N. (2023). Phytohormonal impacts on fatty acid profiles in Chlorella vulgaris Beijerinck: endogenous identification and exogenous application of cytokinins and abscisic acid. *Journal of Applied Phycology*, *35*(5), 2205-2218.

Fadzeyeva, E.*, Locatelli, C. A.*, **Trzaskalski, N. A.**, Nguyen, M. A., Capozzi, M. E., Vulesevic, B., Morrow, N. M., Ghorbani, P., Hanson, A. A., Lorenzen-Schmidt, I., Doyle, M. A., Seymour, R., Varin, E. M., Fullerton, M. D., Campbell, J. E., Mulvihill, E. E. (2023). Pancreas-derived DPP4 is not essential for glucose homeostasis under metabolic stress. *Iscience*, *26*(5), 106748.
*These authors contributed equally

Nunes, J. R., Smith, T. K., Ghorbani, P., O'Dwyer, C., **Trzaskalski, N. A.**, Dergham, H., Pember, C., Kilgour, M. K., Mulvihill, E. E., Fullerton, M. D. (2023). Thermoneutral housing does not accelerate metabolic dysfunction-associated fatty liver disease in male or female C57Bl/6J mice fed a Western diet. *American Journal of Physiology-Endocrinology and Metabolism*, *325*(1), E10-E20.

Trzaskalski, N. A.*, Vulesevic, B.*, Nguyen, M.A., Jeraj, N., Fadzeyeva, E., Morrow, N. M., Locatelli, C. A. A., Travis, N., Hanson, A. A., Nunes, J. R. C., O'Dwyer, C., van der Veen, J. N., Lorenzen-Schmidt, I., Seymour, R., Pulente, S., Clement, A. C., Crawley, A., Jacobs, R. L., Doyle, M. A., Cooper, C. L., Kim, K. H., Fullerton, M. D., Mulvihill, E. E. (2023). Hepatocyte-derived DPP4 regulates portal GLP-1 bioactivity, modulates glucose production, and when absent influences NAFLD progression. JCI Insight, 8(2).
*These authors contributed equally

Dann, M. M.*, Clark, S. Q.*, **Trzaskalski, N. A.**, Earl, C. C., Schepers, L. E., Pulente, S. M., Lennord, E. N., Annamalai, K., Gruber, J. M., Cox, A. D., Lorenzen-Schmidt, I., Seymour, R., Kim, K. H., Goergen, C. J. & Mulvihill, E. E. (2022). Quantification of Murine Myocardial Infarct Size using 2D and 4D High Frequency Ultrasound. American Journal of Physiology-Heart and Circulatory Physiology.
*These authors contributed equally

Morrow, N. M., **Trzaskalski, N. A.**, Hanson, A. A., Fadzeyeva, E., Telford, D. E., Chhoker, S. S., & Mulvihill, E. E. (2021). Nobiletin Prevents High-Fat Diet-Induced Dysregulation of Intestinal Lipid Metabolism and Attenuates Postprandial Lipemia.

Arteriosclerosis, thrombosis, and vascular biology, ATVBAHA-121.

Trzaskalski, N.A., Fadzeyeva, E., & Mulvihill, E.E. (2020). Dipeptidyl peptidase-4 at the interface between inflammation and metabolism. *Clinical Medicine Insights: Endocrinology and Diabetes*, *13*, 1179551420912972.

LeBlond N.D., Ghorbani P., O'Dwyer C., Ambursley N, Nunes J.R.C., Smith T.K.T., **Trzaskalski N.A.**, Mulvihill E.E., Viollet B., Foretz M., Fullerton M.D. Myeloid deletion and therapeutic activation of AMPK do not alter atherosclerosis in male or female mice. *Journal of Lipid Research*. 2020 Dec; 61(12):1697-1706

Kim, Y.H., Lee, J.H., Yeung, J.L.H., Das, E., Kim, R.Y., Jiang, Y., ... & **Trzaskalski, N.** (2019). Thermogenesis-independent metabolic benefits conferred by isocaloric intermittent fasting in ob/ob mice**.** ***Scientific reports*****,** *9*(1), 2479.

Li, H., **Trzaskalski, N.**, & Neil Emery, R.J. (2017). Analysis of Brassinosteroids in Soybean Seeds and Leaves by Liquid Chromatography-Tandem Mass Spectrometry**.** ***The Open Plant Science Journal*****,** ***10*****(1**).

Podium Presentations

2023 The Liver-Heart Nexus: Targeting the Liver to Spare the Heart
BMI Seminar Day, Ottawa, Canada

2023 DPP4 Depletion from Hepatocytes Downregulates Collagen and Immunological Pathway Expression In The Heart But Does Not Rescue Diastolic Function In An Aged, Obese Mouse Model
UOHI Work-In-Progress, Ottawa, Canada

2022 Combination Metformin and Sitagliptin Therapy Improves Cardiac Function and Conserves Kinesis in Aged, Obese *Dpp4*$^{EC-/-}$ Mice after MI
Canadian Lipid and Vascular Summit, Whistler, Canada

2022 Metabolic Multitool: How Hepatocyte DPP4 Impacts Liver Disease
BMI Symposium, Montebello, Quebec
3 Minute Rapid Fire Oral Presentation

2022 DPP4 Depletion from Hepatocytes Downregulates Collagen and Immunological Pathway Expression In The Heart But Does Not Rescue Diastolic Function In An Aged, Obese Mouse Model
Ottawa Cardiovascular Research Day, Ottawa, Canada

2020 Elimination of Hepatocyte Specific *Dpp4* Does Not Alter Markers of Liver Disease Progression In Aged, High Fat, High Cholesterol-fed Mice

Canadian Vascular & Lipid Virtual Summit 2020

2020 Elimination of Hepatocyte Specific *Dpp4* Does Not Alter Markers of Liver Disease Progression In Aged, High Fat, High Cholesterol-fed Mice
Work in Progress (WIP) Trainee Seminars, Ottawa, Canada

2020 Elimination of Hepatocyte Specific Dpp4 Does Not Alter Markers of Liver Disease Progression in Aged, High Fat, High Cholesterol-fed Mice
Ottawa Cardiovascular Research Day
Selected for oral presentation, cancelled due to COVID-19

2019 Identification of Cardioactive Dipeptidyl Peptidase-4 Substrates
OISB Retreat, Cornwall, Ontario

2018 Cut it out: Cardiovascular Implications of Dipeptidyl Peptidase-4 Cleavage
Work in Progress (WIP) Trainee Seminars, Ottawa, Canada

Poster Presentations

2023 The Liver-Heart Nexus: Targeting the Liver to Spare the Heart
Canadian Lipid and Vascular Summit

2023 It Takes Two: Modulation of Cardiovascular Function with Combination DPP4 Inhibitor and Metformin Treatment
Ottawa Cardiovascular Research Day

2023 The Liver-Heart Nexus: Targeting the Liver to Spare the Heart
Canadian Society for Molecular Biosciences: Metabolic Regulation of Cell Signaling

2022 It Takes Two: Modulation of Cardiovascular Function with Combination DPP4 Inhibitor and Metformin Treatment
The Metabolic Physiology Meeting

2021 Liver-specific depletion of DPP4 reduces hepatic gluconeogenesis but does not improve disease progression or inflammation in a mouse model of NALFD
Canadian Student Health Research Forum

2021 Elimination of hepatocyte specific Dpp4 decreases hepatic gluconeogenesis but does not alter markers of liver disease progression in aged, high fat, high cholesterol-fed mice
Ottawa Cardiovascular Research Day

2021	Liver-specific depletion of DPP4 does not prevent NAFLD progression via macrophage polarization **Insulin 100**
2020	Liver-Specific Depletion of *Dpp4* Reduces Hepatic Gluconeogenesis but does Not Prevent NAFLD Progression **Diabetes Canada Conference**
2020	Elimination of Hepatocyte Specific *Dpp4* Does Not Alter Markers Of Liver Disease Progression In Aged, High Fat, High Cholesterol-fed Mice **Montreal Diabetes Research Centre (MDRC) Conference,** Montreal, Quebec
2019	Poster Presentation: Identification of Novel Natural Substrates of Dipeptidyl Peptidase-4 in Cardiovascular Disease **Canadian Vascular & Lipid Summit 2019**
2019	Identification of Novel Natural Substrates of Dipeptidyl Peptidase-4 in Cardiovascular Disease **BMI Seminar Day**, University of Ottawa, Ottawa
2019	Poster Presentation: Identification of Novel Natural Substrates of Dipeptidyl Peptidase-4 in Cardiovascular Disease **Ottawa Heart Conference 2019: Big Data in Cardiovascular Disease**, Ottawa
2019	Identification of Novel Natural Substrates of Dipeptidyl Peptidase-4 in Cardiovascular Disease **Montreal Diabetes Research Centre (MDRC) Conference**, Montreal, Quebec
2018	N-terminal Enrichment Based Proteomics: Revealing the DPP4 Proteome **Ottawa Heart Conference 2018: Precision Medicine in Cardiovascular Disease**, Ottawa
2018	N-terminal Enrichment Based Proteomics: Revealing the DPP4 Proteome **Ottawa Cardiovascular Research Day 2018**, Ottawa, Canada
2018	N-terminal Enrichment Based Proteomics: Revealing the DPP4 Proteome **Biochemistry, Microbiology and Immunology (BMI) Symposium**, Montebello, Quebec

Mentoring Activities

2024	Invited HOSA Guest Speaker Virtual presentation to high school students regarding a graduate school in STEM
2018 – 2023	TMM Thesis and Rotation Student Mentoring 5 students, 2 which joined the lab as graduate students afterwards
2018 – 2019	Graduate Mentor, DEGREE Mentoring Program University of Ottawa
2018 – 2020	Session Coordinator, Let's Talk Science – Encounters Canada University of Ottawa Heart Institute

Committee and Professional Memberships

2023	Trainee Member, Canadian Society for Molecular Biosciences (CSMB)
2021	Steering Committee, Toronto-Ottawa Heart Summit
2020 – 2021	Chair, UOHI Trainee Committee University of Ottawa Heart Institute
2019 - 2020	Co-Chair, UOHI Trainee Committee University of Ottawa Heart Institute
2019, 2021	Steering Committee, Ottawa Heart Research Day University of Ottawa Heart Institute
2020 – present	Trainee Member, Diabetes Canada
2018 – 2019	Work in Progress Coordinator, UOHI Trainee Committee University of Ottawa Heart Institute